AN EVALUATION OF ADAPTIVE-BEAMFORMING TECHNIQUES APPLIED TO RECORDED SEISMIC DATA

Thomas E. Barnard, et al

Texas Instruments, Incorporated

Prepared for:

Air Force Technical Applications Center
Advanced Research Projects Agency

31 December 1974

ALEX(01)-TR-74-08

AN EVALUATION OF ADAPTIVE-BEAMFORMING TECHNIQUES APPLIED TO RECORDED SEISMIC DATA

TECHNICAL REPORT NO. 8

VELA NETWORK EVALUATION AND AUTOMATIC PROCESSING RESEARCH

Prepared by
Thomas E. Barnard and Leo J. O'Brien

TEXAS INSTRUMENTS INCORPORATED
Equipment Group
Post Office Box 6015
Dallas, Texas 75222

Prepared for

AIR FORCE TECHNICAL APPLICATIONS CENTER

Sponsored by

ADVANCED RESEARCH PROJECTS AGENCY
Nuclear Monitoring Research Office
ARPA Program Code No. 4F10
ARPA Order No. 2551

31 December 1974

Acknowledgment: This research was supported by the Advanced Research Projects Agency, Nuclear Monitoring Research Office, under Project VELA-UNIFORM, and accomplished under the technical direction of the Air Force Technical Applications Center under Contract No. F08606-74-C-0033.

UNCLASSIFIED

SECURITY CLASSIFICATION OF THIS PAGE (When Data Entered)

REPORT DOCUMENTATION PAGE	READ INSTRUCTIONS BEFORE COMPLETING FORM
1. REPORT NUMBER / 2. GOVT ACCESSION NO.	3. RECIPIENT'S CATALOG NUMBER: AD-A011 849
4. TITLE (and Subtitle): AN EVALUATION OF ADAPTIVE-BEAMFORMING TECHNIQUES APPLIED TO RECORDED SEISMIC DATA	5. TYPE OF REPORT & PERIOD COVERED: Technical
	6. PERFORMING ORG. REPORT NUMBER: ALEX(01)-TR-74-08
7. AUTHOR(s): Thomas E. Barnard and Leo J. O'Brien	8. CONTRACT OR GRANT NUMBER(s): F08606-74-C-0033
9. PERFORMING ORGANIZATION NAME AND ADDRESS: Texas Instruments Incorporated, Equipment Group, Dallas, Texas 75222	10. PROGRAM ELEMENT, PROJECT, TASK AREA & WORK UNIT NUMBERS: VELA T/4705/B/ETR
11. CONTROLLING OFFICE NAME AND ADDRESS: Advanced Research Projects Agency, Nuclear Monitoring Research Office, Arlington, Virginia 22209	12. REPORT DATE: 31 December 1974 13. NUMBER OF PAGES: 289
14. MONITORING AGENCY NAME & ADDRESS (if different from Controlling Office): Air Force Technical Applications Center, VELA Seismological Center, Alexandria, Virginia 22314	15. SECURITY CLASS (of this report): UNCLASSIFIED 15a. DECLASSIFICATION DOWNGRADING SCHEDULE

16. DISTRIBUTION STATEMENT (of this Report)

APPROVED FOR PUBLIC RELEASE, DISTRIBUTION UNLIMITED

17. DISTRIBUTION STATEMENT (of the abstract entered in Block 20, if different from Report)

18. SUPPLEMENTARY NOTES

ARPA Order No. 2551

19. KEY WORDS (Continue on reverse side if necessary and identify by block number)

Seismology
Signal Processing
Adaptive Multichannel Filtering
Alaska Long-Period Array

20. ABSTRACT (Continue on reverse side if necessary and identify by block number)

This report presents time-domain maximum likelihood adaptive beamforming results for data from the Alaska Long-Period Array and the Korean Short-Period Array. Adaptive-beamforming detection gain relative to beamsteering is investigated for unmixed long-period seismic events in the presence of background noise and for simulated mixed events where two data samples, each containing a signal, are summed to create a composite sample containing an interfering event.

DD FORM 1 JAN 73 1473 EDITION OF 1 NOV 65 IS OBSOLETE

UNCLASSIFIED

SECURITY CLASSIFICATION OF THIS PAGE (When Data Entered)

20. Continued

In the adaptive beamforming studies for background noise, the performance of two different adaptive algorithms, the effect of using closely-spaced partial arrays instead of the full ALPA array, and the effect of different frequency filters applied to the input channels before array beamforming are examined.

In the interfering-event analysis, the relative on-azimuth to off-azimuth event strength at which an on-azimuth event detection is possible determines the detection gain of adaptive multichannel filtering over time-shift-and-sum beamforming.

ACKNOWLEDGMENTS

Mr. Leo O'Brien wrote the original version of Section III, generated major sections of the new computer program which produced the results of this report, and prepared computer runs for many of the Section II results and for virtually all of the Section III results.

Near the end of the contract, Mr. Wen-Wu Shen began the Korean short-period processing and evaluation.

Mrs. Cherylann Saunders typed all of the text and prepared virtually all of the figures and tables.

Mr. Terence W. Harley took time from his busy schedule for interesting technical discussions which improved the quality of this report.

Thomas E. Barnard

ABSTRACT

This report presents time-domain maximum likelihood adaptive beamforming results for data from the Alaska Long-Period Array and the Korean Short-Period Array. Adaptive-beamforming detection gain relative to beamsteering is investigated for unmixed long-period seismic events in the presence of background noise and for simulated mixed events where two data samples, each containing a signal, are summed to create a composite sample containing an interfering event.

In the adaptive beamforming studies for background noise, the performance of two different adaptive algorithms, the effect of using closely-spaced partial arrays instead of the full ALPA array, and the effect of different frequency filters applied to the input channels before array beamforming are examined.

In the interfering-event analysis, the relative on-azimuth to off-azimuth event strength at which an on-azimuth event detection is possible determines the detection gain of adaptive multichannel filtering over time-shift-and-sum beamforming.

TABLE OF CONTENTS

TABLE OF CONTENTS
(continued)

LIST OF FIGURES

LIST OF FIGURES
(continued)

LIST OF FIGURES
(continued)

LIST OF FIGURES
(continued)

LIST OF FIGURES
(continued)

LIST OF FIGURES
(continued)

LIST OF FIGURES
(continued)

LIST OF FIGURES
(continued)

LIST OF FIGURES
(continued)

LIST OF FIGURES
(continued)

LIST OF FIGURES
(continued)

LIST OF FIGURES
(continued)

LIST OF FIGURES
(continued)

LIST OF FIGURES
(continued)

LIST OF TABLES

LIST OF TABLES
(continued)

LIST OF TABLES
(continued)

LIST OF TABLES
(continued)

LIST OF TABLES
(continued)

LIST OF TABLES
(continued)

LIST OF TABLES
(continued)

SECTION I
INTRODUCTION

A. PURPOSE OF THIS STUDY

The adaptive processing task of the Vela Network Evaluation and Automatic Processing Research Program has as its objectives

- Continued improvement of adaptive-processing gains relative to beamsteering for unmixed long-period seismic events in the presence of background noise.
- Evaluation of potential adaptive-beamforming detection improvement over beamsteering for both long-period and short-period signals buried in off-azimuth interfering events.

This report deals with results obtained from operating a maximum-likelihood adaptive beamforming system on ALPA long-period data and Korean short-period data. To synthesize interfering events by adding and scaling two different recorded data samples, a new computer program employing floating-point arithmetic was developed to achieve the objectives of this study. This program has the capability of processing long-period data from NORSAR and LASA as well as ALPA data and Korean short-period data.

B. DESCRIPTION OF ARRAYS USED

Figure I-1 diagrams the geometrical layout of the Alaska Long-Period Array (ALPA), which is a 19-element hexagonal long-period array with 20-kilometer spacing between sites. Table I-1 gives the ALPA site locations. In this report, the sites at ALPA are referenced in terms of their transmission order. Thus, site 10 refers to site 3-45 in the official nomenclature.

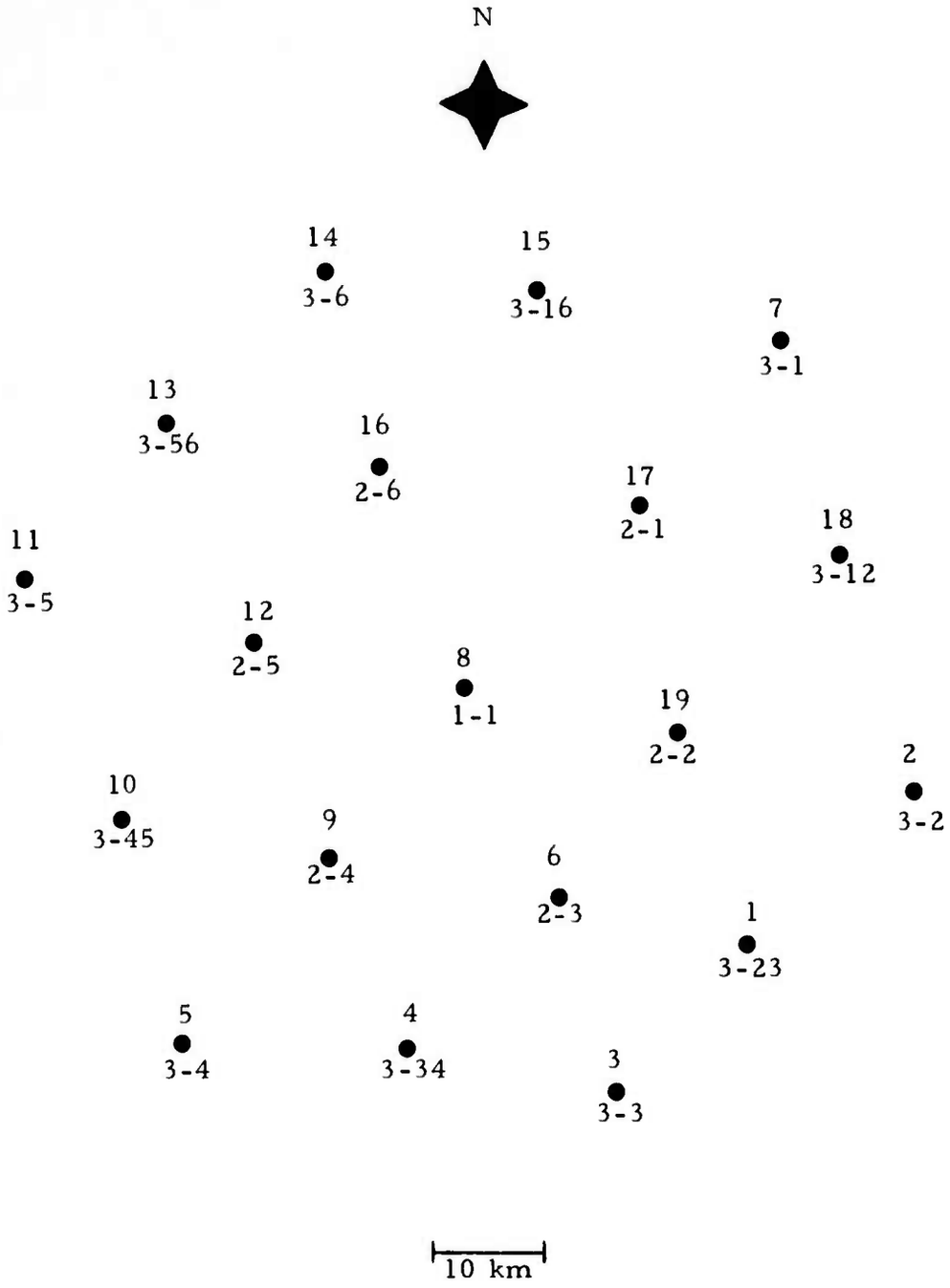

FIGURE I-1

ALPA GEOMETRY

TABLE I-1

ALPA SITE LOCATIONS

Site Number	Transmission Order	N. Lat. ±10 Sec.	W. Long. ± 20 Sec.	X Kilometers	Y Kilometers
1-1	8	65°14'00"	147°44'36"	0.0	0.0
2-1	17	65°22' 25"	147°24'04"	15.941	15.598
2-2	19	65°11'40"	147°18'58"	19.901	-4.324
2-3	6	65°03'55"	147°33'50"	8.359	-18.687
2-4	9	65°05'52"	148°00'05"	-12.021	-15.073
2-5	12	65°16'01"	148°08'11"	-18.309	3.737
2-6	16	65°24'02"	147°53'57"	-7.259	18.594
3-1	7	65°30'10"	147°07'03"	29.153	29.961
3-12	18	65°20'02"	147°00'27"	34.277	11.181
3-2	2	65°08'53"	146°52'45"	40.255	-9.482
3-23	1	65°01'43"	147°11'46"	25.491	-22.764
3-3	3	64°54'36"	147°26'47"	13.832	-35.953
3-34	4	64°56'41"	147°51'34"	-5.409	-32.092
3-4	5	64°57'07"	148°17'03"	-25.193	-31.289
3-45	10	65°07'42"	148°24'05"	-30.654	-11.675
3-5	11	65°18'55"	148°35'10"	-39.259	9.112
3-56	13	65°26'09"	148°18'56"	-26.655	22.517
3-6	14	65°33'24"	148°00'00"	-11.956	35.953
3-16	15	65°32'23"	147°35'31"	7.052	34.069

C. ADAPTIVE MULTICHANNEL FILTERING

Multichannel filtering is a form of array processing in which multiple channel inputs undergo individual frequency-shaping and phase-shift filtering prior to the channel-summation operation which produces the beamformer output. Figure I-2 is a schematic diagram of multichannel filtering. This illustration incorporates the option to preprocess the transducer outputs before they are input to the multichannel beamformer. Examples of preprocessing are frequency filtering (most commonly with identical frequency responses on all channels) and time shifting to align waves emanating from a particular direction. The preprocessed transducer outputs become the input channels to a multichannel filter set, where individual filters (generally different from channel to channel) are applied to the input channels. These filters are implemented as convolution filters in time-domain processing or as complex-valued multiplicative filters in frequency-domain processing. The multichannel filter output is created by summing the individual filtered channel outputs.

In systems where second-order statistics (crosscorrelation functions and crosspower spectra) are used to describe interrelationships among the input channels, there are two basic forms of multichannel filtering. In Wiener-Kolmogorov multichannel filtering, the average squared error between the desired signal and the multichannel filter output is minimized. To minimize the mean square error, the crosscorrelation functions or crosspower spectra between the input channels and the desired signal are required. In maximum likelihood multichannel filtering, the average squared output from the multichannel filter set is minimized subject to signal-preservation constraints which place some suitably-chosen frequency response on the signal. For maximum likelihood multichannel filtering, unlike Wiener-Kolmogorov filtering, only the direction of the signal needs to be specified, but not the signal-to-noise ratio.

Multichannel filtering can be employed with fixed or time-varying filter sets. When the filters are updated as new data inputs enter the multichannel

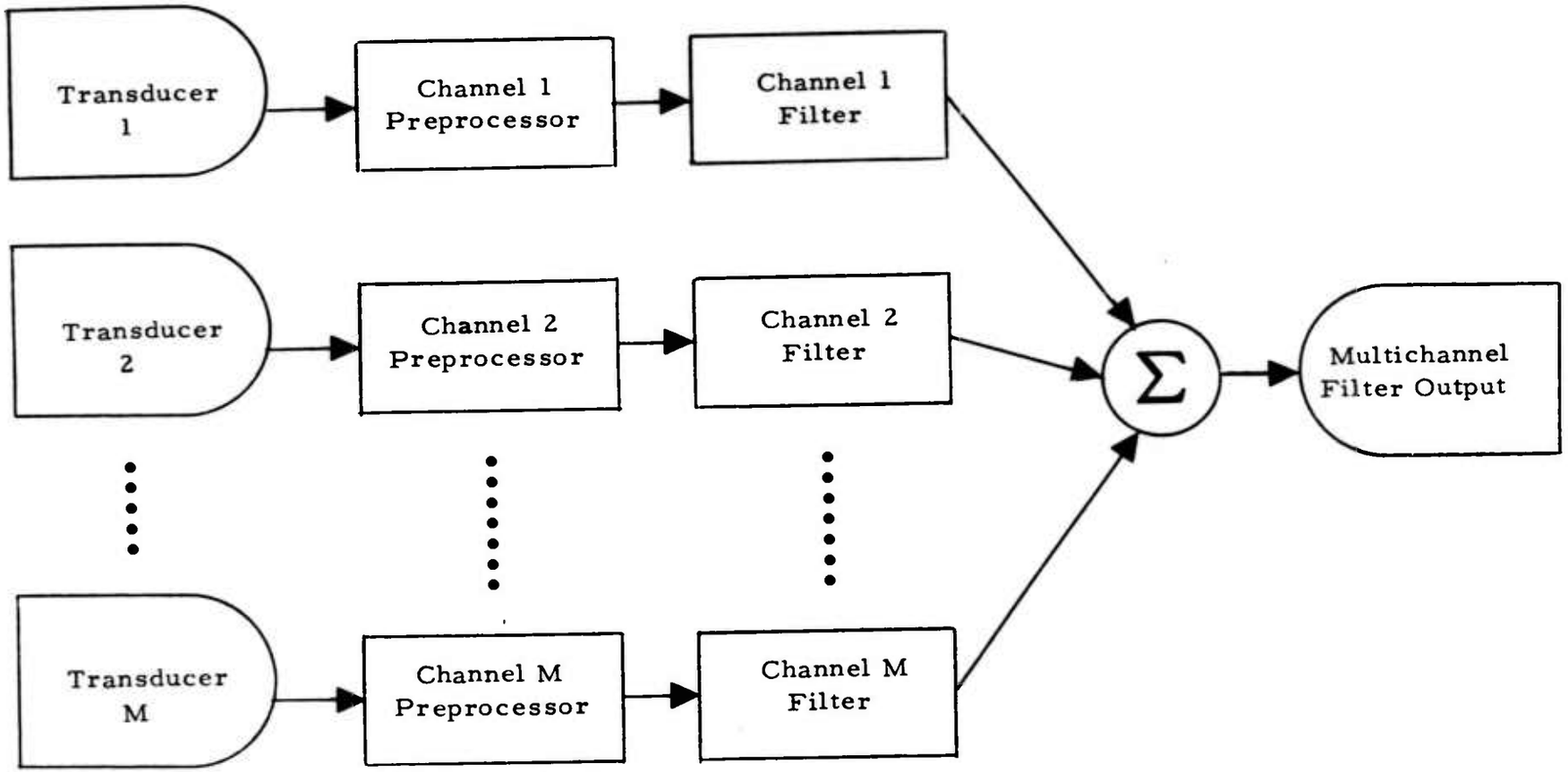

FIGURE I-2

SCHEMATIC DIAGRAM OF MULTICHANNEL FILTERING

processor, the process is called adaptive filtering. Adaptive-filtering algorithms with significant computational advantages over fixed multichannel filtering are available. When the inputs to the multichannel processor are time-stationary (in the wide sense), these algorithms yield filter sets which converge in the mean to the corresponding fixed multichannel filter sets. After adaptive filter sets reach the vicinity of the corresponding fixed filter sets, they fluctuate about the fixed-filter solution in the presence of time-stationary data: the adaptive filters converge in the mean in the sense that the average position of the fluctuating adaptive filters is identical to the fixed-filter solution. When the statistics of the data entering the multichannel processor slowly change with time, adaptive filtering can react to the changes in a semi-continuous manner. If fixed filtering is used in this situation, newly-designed filters change in a more abrupt fashion. When, as in this case, the statistics of the data shift with time, the adaptive-filter solution lags behind the fixed-filter solution corresponding to the instantaneous statistics. The extent of the lag can be controlled by changing the adaptation rate. The choice of an adaptation rate involves a tradeoff between misadjustment (higher-than-optimum error or power due to the adaptive-filter fluctuations) and the lag behind the optimum instantaneous fixed-filter solution. A different kind of lag occurs when fixed filter sets are periodically redesigned: statistics must be accumulated over a design interval so that, as a result, the fixed-filter solution cannot be implemented until the next design interval.

In the conventional technique of array processing, simple time delays or phase shifts are applied to the input channels before summing to generate the beam output. Optimum multichannel filtering introduces considerable new flexibility into the beamforming process. Since it is possible to weight the input channels differently, channels with higher signal-to-noise ratios can be emphasized at the expense of noisier channels. When well instrumented arrays are utilized, this capability is generally of minor importance. A far more

consequential feature of adaptive filtering is the ability to form array antenna patterns which optimally pass a signal while simultaneously rejecting propagating noise. Deep nulls can be aimed toward off-beam noise sources. When strong off-azimuth noise sources are present, the creation of such nulls is an automatic result of the optimality of the multichannel processor. The conventional time-shift-and-sum or phase-shift processor, in contrast, has a beam pattern determined solely by the steer direction and the array geometry.

In most cases, the potential improvement of optimum multichannel filtering relative to beamsteering is determined by the coherence of the noise field across an array: the greater the similarity of the noise field from channel to channel, the greater is the optimum-multichannel-filter improvement over beamsteering. When, on the other hand, noise is completely uncorrelated between sensors and identical signal and noise power levels are encountered at all array sites, there is no potential for improvement: in this case, the optimum filter set is a beamsteer processor. The decision to employ or not to employ an optimum-filter technique of processing depends critically on measurements of the noise field at any given array. Once these measurements are available, the additional cost of implementing an optimum-filter system can be quantitatively weighed against the advantages of greater noise suppression relative to the conventional beamsteer processing technique.

D. DESCRIPTION OF THE MAXIMUM LIKELIHOOD ADAPTIVE FILTER ALGORITHM

The adaptive-filter output $y(t)$ at time t is formed by applying a convolution filter to each channel and summing the outputs of all channels:

$$y(t) = \sum_{i=1}^{M} \sum_{j=-N}^{N} a_i(j)\, x_i(t-j)$$

where $a_i(t)$ is the filter weight for the i-th channel at a lag of j sample points, $x_i(t-j)$ is the value of the channel i at time t-j, M is the number of channels, and 2N+1 is the total length of the filter in points. Prior to forming the filter output, each channel is time-shifted to time-align energy arriving from the desired steer direction.

The adaptive filter weights are updated by the following algorithm:

$$\underset{\text{new}}{a_i(j)} = \underset{\text{old}}{a_i(j)} + \lambda(t)\, y(t) \left[\bar{x}(t-j) - x_i(t-j) \right]$$

where

$$\bar{x}(t-j) = \frac{1}{M} \sum_{i=1}^{M} x_i(t-j)$$

and $\lambda(t)$ controls the adaptation rate at time t. This update algorithm incorporates the maximum likelihood constraints.

E. GEOMETRICAL INTERPRETATION OF THE ABF ALGORITHM

In vector form, the adaptive-beamforming filter update equation may be written

$$A(t + \Delta t) - A(t) = \lambda(t)\, X^T A(\bar{X} - X),$$

where the superscript T denotes transposition, and where the filter weight vector A, the data vector X, and the beamsteer output vector $\bar{X}$ are, respectively,

$$A = \begin{bmatrix} \begin{bmatrix} a_1(-N) \\ \vdots \\ a_M(-N) \end{bmatrix} \\ \vdots \\ \begin{bmatrix} a_1(0) \\ \vdots \\ a_M(0) \end{bmatrix} \\ \vdots \\ \begin{bmatrix} a_1(N) \\ \vdots \\ a_M(N) \end{bmatrix} \end{bmatrix}, \quad X = \begin{bmatrix} \begin{bmatrix} x_1(t+N) \\ \vdots \\ x_M(t+N) \end{bmatrix} \\ \vdots \\ \begin{bmatrix} x_1(t) \\ \vdots \\ x_M(t) \end{bmatrix} \\ \vdots \\ \begin{bmatrix} x_1(t-N) \\ \vdots \\ x_M(t-N) \end{bmatrix} \end{bmatrix} \text{ and } \bar{X} = \begin{bmatrix} \begin{bmatrix} \bar{x}(t+N) \\ \vdots \\ \bar{x}(t+N) \end{bmatrix} \\ \vdots \\ \begin{bmatrix} \bar{x}(t) \\ \vdots \\ \bar{x}(t) \end{bmatrix} \\ \vdots \\ \begin{bmatrix} \bar{x}(t-N) \\ \vdots \\ \bar{x}(t-N) \end{bmatrix} \end{bmatrix}.$$

The objective of maximum likelihood adaptive beamforming is to reduce the average squared filter output

$$\overline{y^2(t)} = \overline{(A^T X)(X^T A)} = A^T \overline{XX^T} A$$

subject to a set of signal-preservation constraints on the filter vector A. After preshifting the input channels to time-align energy from the look direction, these constraints can be written

$$\sum_{i=1}^{M} a_i(j) = d(j) \qquad (j = -N, \ldots, -1, 0, 1, \ldots, N),$$

where the constants $d(j)$ specify a convolution filter having the desired frequency response on a signal from the steer direction. When such a signal $s(t)$ appears in identical form on all channels, the signal output from the beamformer is

$$\sum_{j=-N}^{N} \left[\sum_{i=1}^{M} a_i(j) \right] s(t-j) = \sum_{j=-N}^{N} d(j)\, s(t-j) \ .$$

For the adaptive beamforming employed in this study, a white frequency response is specified by setting

$$d(j) = \delta_{jo} \qquad (j = -N, \ldots, -1, 0, 1, \ldots, N) \ ,$$

where δ_{jo} is the Kronecker delta operator

$$\delta_{jo} = \begin{cases} 1 & \text{if } j = 0 \\ 0 & \text{if } j \neq 0 \ . \end{cases}$$

To reduce the average squared filter output $\overline{y^2(t)}$, the method of steepest descent (with two modifications) is used. In the unmodified form of the method of steepest descent, the filter vector A moves in the direction opposite to the gradient of the average squared filter output $\overline{y^2(t)}$:

$$A(t + \Delta t) - A(t) = -c \nabla (A^T \overline{XX^T} A) = -2c\, \overline{XX^T} A \ .$$

The first modification is to replace the crosscorrelation matrix $\overline{XX^T}$ with the rank-one matrix XX^T formed from the instantaneous vector X at time t:

$$A(t + \Delta t) - A(t) = -2c\, X(X^T A) = -2c\, X\, y(t) \ .$$

This modification of Widrow (Widrow, 1966) approximates, in effect, the crosscorrelation-matrix time averaging through successive applications of the filter update algorithm. The approximation becomes increasingly accurate as the rate of change of the filter vector A is slowed by reducing the scalar convergence parameter c. The filter vector A converges in the mean under

suitably prescribed conditions (Daniell, 1968) to the vector obtained by using the crosscorrelation matrix $\overline{XX^T}$ in the update equation. Ultimately the filter vector A oscillates about its mean. The size of the oscillations can be controlled by varying the parameter c. The reason for the Widrow modification is a reduction in the computational operations required for the filter update from a number of proportional to the square of the dimension of the vectors X and A to a number linearly proportional to their dimension.

The second modification of the steepest-descent method is to alter the direction of the vector $-c\nabla\left[y^2(t)\right]$ so that the ensuing update vector $A(t + \Delta t) - A(t)$ is the vector nearest to $-c\nabla\left[y^2(t)\right]$ which satisfies the constraints on the filter update vector. Since the sum across channels

$$\sum_{i=1}^{M} a_i(j)$$

of the filter vector A is a fixed value d(j) at any lag value j, the filter update vector $A(t + \Delta t) - A(t)$ must sum to zero at each lag:

$$\sum_{i=1}^{M} \left[\begin{matrix} \text{new} \\ a_i(j) \end{matrix} - \begin{matrix} \text{old} \\ a_i(j) \end{matrix} \right] = 0 \quad (j = -N, \ldots, -1, 0, 1, \ldots, N) .$$

The filter update vector must be perpendicular to each of the (2N+1) unit vectors U_k specified by their components

$$\left[u_i(j)\right]_k = \delta_{jk}/\sqrt{M} \quad ,$$

where δ_{jk} is the Kronecker delta operator. Each of the vectors U_k is zero except in the k-th lag position, where all components are equal to $1/\sqrt{M}$. In vector form, the filter update vector must satisfy the (2N+1) constraints

$$U_k^T \left[A(t + \Delta t) - A(t)\right] = 0 \quad (j = -N, \ldots, -1, 0, 1, \ldots, N) .$$

The vector $\bar{X}$, since it has identical components at any lag value j, is a linear combination of the vectors U_k and is perpendicular to all possible update vectors satisfying the constraint conditions. The vector $(X-\bar{X})$, on the other hand, satisfies the constraint conditions:

$$\sqrt{M}\, U_k^T (X-\bar{X}) = \sum_{i=1}^{M} \sum_{j=-N}^{N} \delta_{jk} \left[x_i(j) - \bar{x}(j) \right]$$

$$= \sum_{i=1}^{M} \left[x_i(k) - \bar{x}(k) \right] = \left[\sum_{i=1}^{M} x_i(k) \right] - M\bar{x}(k)$$

$$= M\bar{x}(k) - M\bar{x}(k) = 0 .$$

Thus the vector X can be resolved into two mutually orthogonal components $\bar{X}$ (perpendicular to the constraint space for the filter update vector) and $X-\bar{X}$ (lying within the constraint space). The negative $-c\nabla\left[y^2(t)\right]$ of the scaled gradient of $y^2(t)$ is a scalar multiple $-\left[2cy(t)\right]X$ of the vector X. The nearest point to $-c\nabla\left[y^2(t)\right]$ on the constraint space is the vector $\left[2cy(t)\right](\bar{X}-X)$ formed by subtracting the component $-\left[2cy(t)\right]\bar{X}$ perpendicular to the contraint space from the scaled negative gradient vector $-\left[2cy(t)\right]X$. The final form of the filter update equation is, therefore,

$$A(t+\Delta t) - A(t) = \left[2\,c\,y(t)\right](\bar{X}-X) .$$

This situation is illustrated in Figure I-3. The resultant filter update vector is the projection of $-c\nabla\left[y^2(t)\right]$ onto the constraint space.

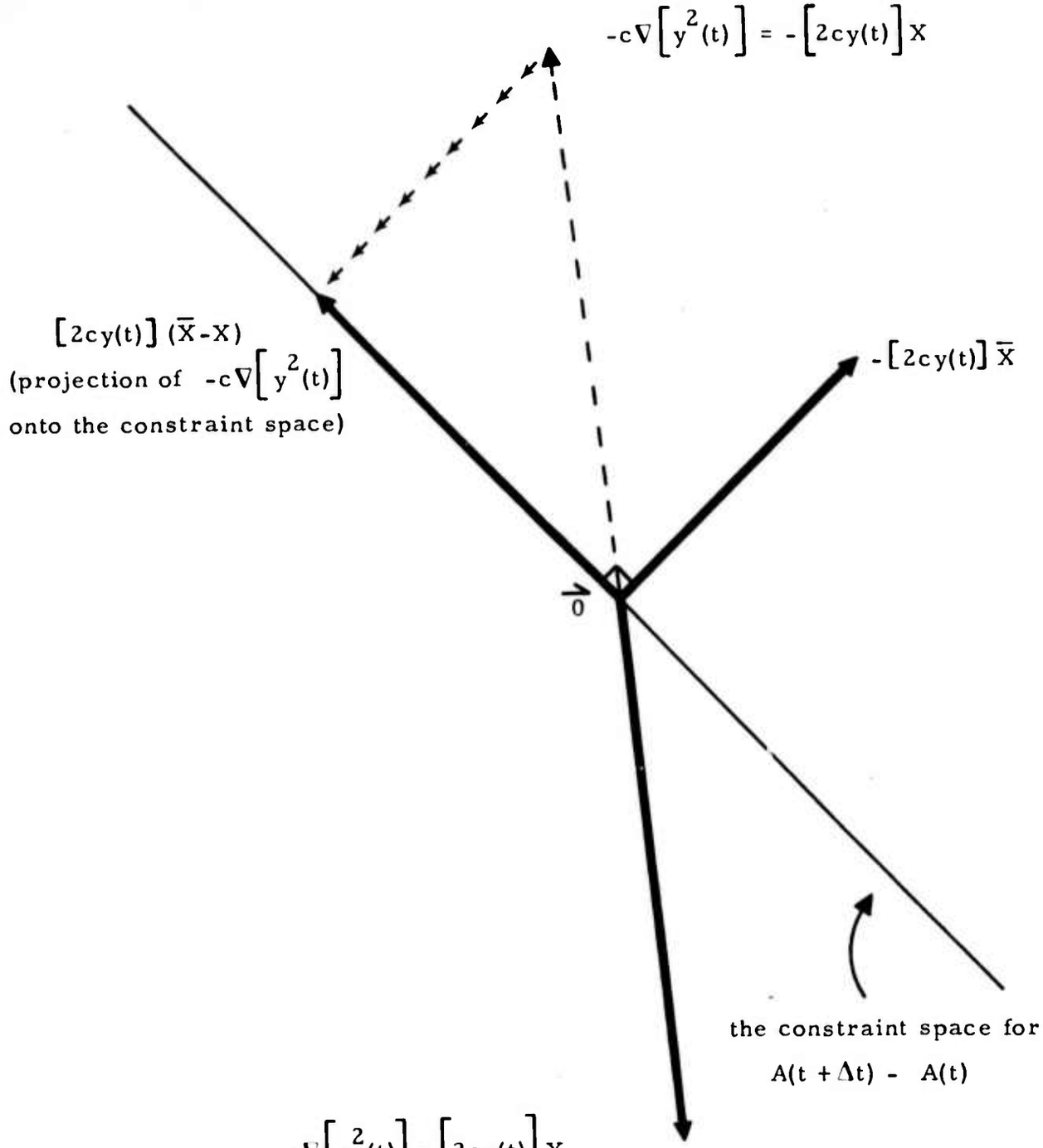

FIGURE I-3

A GEOMETRICAL INTERPRETATION OF TIME-DOMAIN MAXIMUM LIKELIHOOD ADAPTIVE FILTERING

F. A SIMPLE ILLUSTRATIVE EXAMPLE

Suppose that three channels are input to an adaptive beamformer with one lag per channel. Signals are defined to be simultaneous spikes on all three channels. Noise, on the other hand, appears in the form of unit-amplitude spikes on the second channel. When signal and noise occur, they are characterized by the respective vectors

$$S = \begin{bmatrix} x_1(t) = s \\ x_2(t) = s \\ x_3(t) = s \end{bmatrix} \quad \text{and} \quad N = \begin{bmatrix} x_1(t) = 0 \\ x_2(t) = 1 \\ x_3(t) = 0 \end{bmatrix}.$$

Figure I-4 depicts time series inputs for this simple example. The adaptive filter set is initialized with beamsteer weights:

$$A = \begin{bmatrix} a_1(0) = 1/3 \\ a_2(0) = 1/3 \\ a_3(0) = 1/3 \end{bmatrix}.$$

An optimum filter set is

$$A = \begin{bmatrix} a_1(0) = 1/2 \\ a_2(0) = 0 \\ a_3(0) = 1/2 \end{bmatrix}.$$

Whenever a noise spike first appears on channel 2, the filter vector A is updated according to the equation

$$A(t + \Delta t) = A(t) + 2cy(t)\,(\bar{N}-N)$$

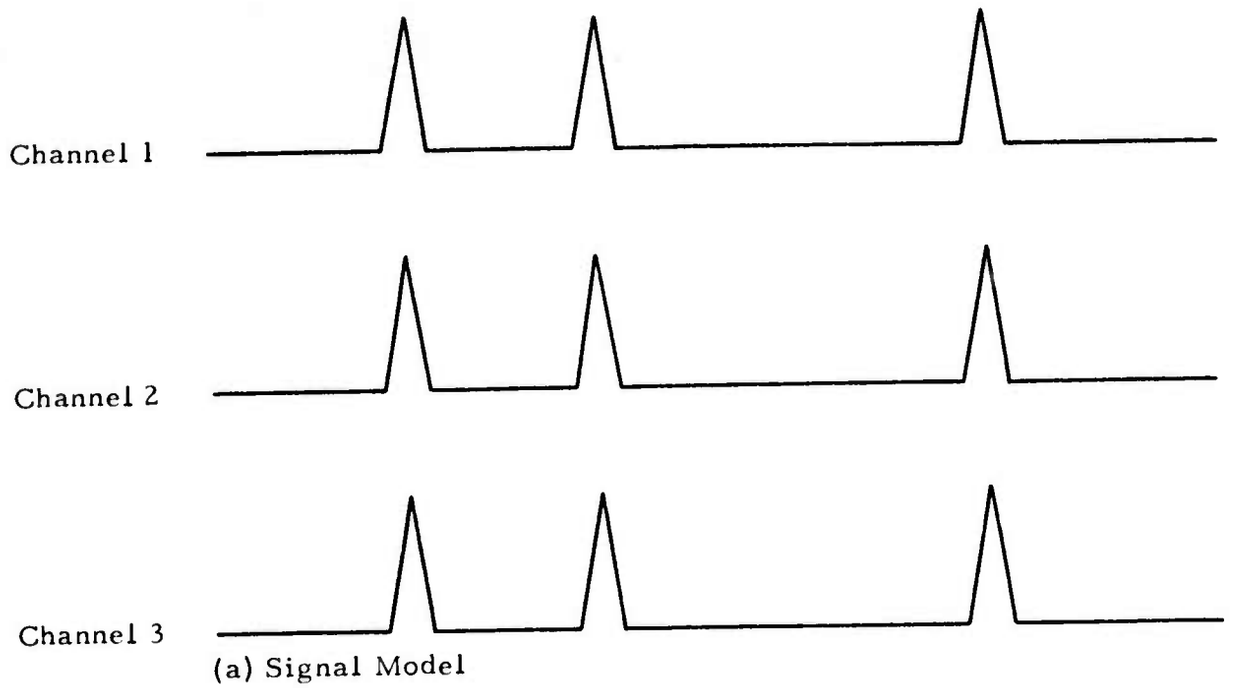

(a) Signal Model

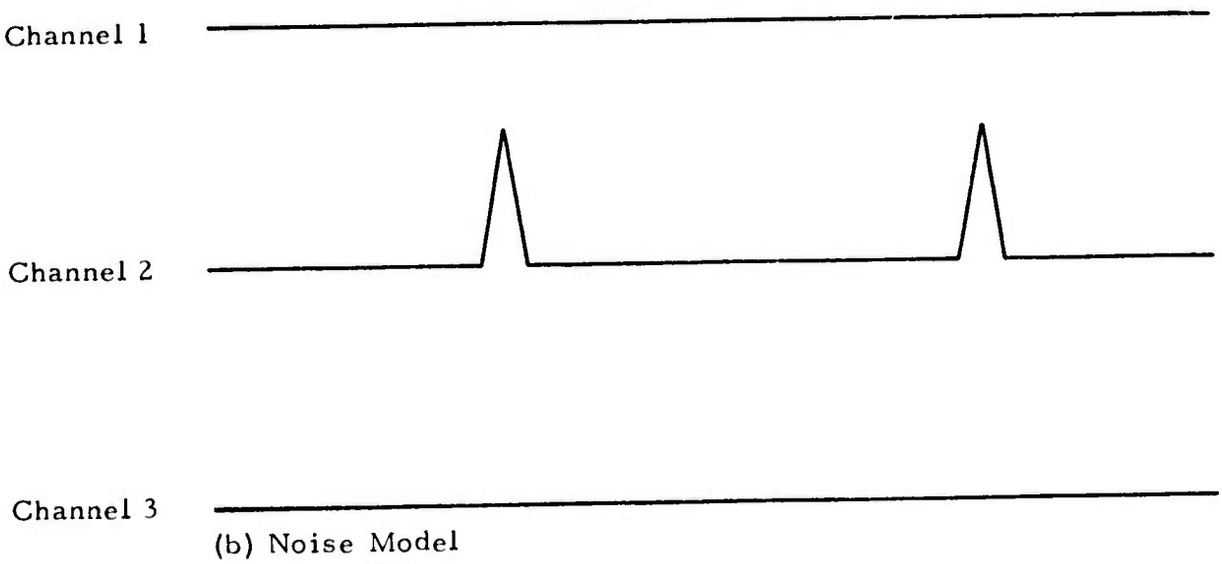

(b) Noise Model

FIGURE I-4

A SIMULATED DISPLAY OF THE TIME SERIES INPUT
CORRESPONDING TO THE ILLUSTRATIVE EXAMPLE

or

$$A(t + \Delta t) = \begin{bmatrix} \frac{1}{3} \\ \frac{1}{3} \\ \frac{1}{3} \end{bmatrix} + 2c \begin{bmatrix} 0 & 1 & 0 \end{bmatrix} \begin{bmatrix} \frac{1}{3} \\ \frac{1}{3} \\ \frac{1}{3} \end{bmatrix} \begin{bmatrix} \frac{1}{3} - 0 \\ \frac{1}{3} - 1 \\ \frac{1}{3} - 0 \end{bmatrix}$$

$$= \begin{bmatrix} \frac{1}{3} \\ \frac{1}{3} \\ \frac{1}{3} \end{bmatrix} + \frac{2}{3}c \begin{bmatrix} \frac{1}{3} \\ -\frac{2}{3} \\ \frac{1}{3} \end{bmatrix}$$

$$= \begin{bmatrix} \frac{1}{3} + \frac{2}{9}c \\ \frac{1}{3} - \frac{4}{9}c \\ \frac{1}{3} + \frac{2}{9}c \end{bmatrix}.$$

The adaptive update equation shifts its weighting from channel 2 to channels 1 and 3. The second time the noise spike appears on channel 2, the filter output is

$$y(t) = \begin{bmatrix} 0 & 1 & 0 \end{bmatrix} \begin{bmatrix} \frac{1}{3} + \frac{2}{9}c \\ \frac{1}{3} - \frac{4}{9}c \\ \frac{1}{3} + \frac{2}{9}c \end{bmatrix} = \frac{1}{3} - \frac{4}{9}c \ .$$

The amplitude of the noise output is diminished whenever $0 < c < 3/2$. After k updates, the adaptive filter vector is

$$\begin{bmatrix} \frac{1}{2} - \frac{1}{6}\left(1 - \frac{4}{3}c\right)^k \\ \frac{1}{3}\left(1 - \frac{4}{3}c\right)^k \\ \frac{1}{2} - \frac{1}{6}\left(1 - \frac{4}{3}c\right)^k \end{bmatrix}$$

When the (k+1)-st noise spike appears on channel 2, the output of the adaptive beamformer is

$$y(t) = \frac{1}{3}\left(1 - \frac{4}{3}c\right)^k .$$

Each time a new noise spike appears on channel 2, the adaptive filter output is $(1 - 4c/3)$ times its previous value. After each new noise spike, the difference between the optimum filter vector and the old filter vector is reduced by the same factor $(1 - 4c/3)$. In this simple example where the noise crosscorrelation matrix $\overline{NN^T}$ has a single non-zero eigenvalue, the average squared filtered noise output $\overline{y^2(t)}$ is minimized when $c = 3/4$. In this case, noise is completely eliminated starting with the second noise spike on channel 2. When $0 < c < 3/4$, the noise output always has the same sign as the spike on channel 2. When $c > 3/4$, however, the noise output alternately differs and agrees in sign with the input spike on channel 2. The magnitude of the output spike always diminishes as long as $0 < c < 3/2$. When $c > 3/2$, on the other hand, the adaptive filter vector diverges and the ABF output increases in magnitude with the arrival of each new noise spike.

In this idealized example, the signal does not affect the filter update since

$$\bar{S} - S = \begin{bmatrix} s \\ s \\ s \end{bmatrix} - \begin{bmatrix} s \\ s \\ s \end{bmatrix} = \begin{bmatrix} 0 \\ 0 \\ 0 \end{bmatrix}.$$

In the event that a signal spike appears simultaneously on all channels, the output from the beamformer is s since the filter weights sum to one.

G. ORGANIZATION OF REPORT

Section II studies the effect of some changes made since the previous adaptive processing study in the procedures used to implement time-domain maximum likelihood adaptive multichannel filtering. The criterion for evaluating these changes is the adaptive-beamforming signal-to-noise gain relative to beamsteering for unmixed long-period seismic events in the presence of background noise. The first topic examined is the effect of replacing the previously-employed adaptive update algorithm, which speeds up in the presence of a signal, with a new adaptive update algorithm which slows down in the same situation. Next, using the new adaptive algorithm, adaptive beamforming improvement over beamsteering for the full ALPA array is compared with that obtained with closely-spaced six-channel partial ALPA arrays. Finally, the effectiveness of a new prefilter for the individual vertical-component channels input to the beamformers is assessed in terms of its detection capability. This assessment of the new prefilter utilizes adaptive filter lengths of both 31 and 15 points per channel in order to determine whether any meaningful processing loss occurs with the shorter filter length, which halves the computational load. This section is intended to aid in evaluating the potential usefulness of adaptive filtering systems for processing long-period arrays similar to ALPA.

Section III examines the possibility that adaptive beamforming can detect signals buried in off-azimuth interfering events when the conventional

time-shift-and-sum processor is unable to do so. To simulate mixed events, two separately-recorded data samples are scaled and summed to create a composite sample used in the adaptive-filter update procedure. Beam outputs are computed for both data samples individually to ascertain the effect of the adaptive beamforming process on each sample in the composite data sample. Then the beam outputs for both samples in the composite sample are summed in order to observe the result of combining the two samples. The detection capability of adaptive processing is determined from a visual examination of the composite beam-output trace. This investigation of the ability of adaptive multichannel filtering to detect signals masked by off-azimuth interfering events employs both long-period ALPA data and Korean short-period data. The preliminary results presented in this section should assist those people interested in improved separation of mixed events.

Section IV presents the conclusions of this study. For those with insufficient time to analyze in detail the results in Sections II and III of this report, this section gives the highlights of this investigation.

SECTION II

COMPARISON OF PROCESSING PROCEDURES

A. INTRODUCTION

This section presents a comparison of various techniques for implementing adaptive beamforming. The previous adaptive processing study (Barnard, 1973) employed the adaptive filter update algorithm

$$A(t + \Delta t) = A + \frac{2\mu X^T A (\bar{X}-X)}{(\bar{X}-X)^T(\bar{X}-X)},$$

which speeds up in the presence of an on-azimuth signal. The first topic of investigation is the effect on signal-to-noise ratio improvement relative to beamsteering when the old adaptive algorithm is replaced by a new adaptive filter update algorithm

$$A(t + \Delta t) = A + \frac{2\mu X^T A (\bar{X}-X)}{X^T X},$$

which slows down in the presence of an on-azimuth signal. The next subject of examination is the performance of the new adaptive algorithm compared with beamsteering when all available sensors at ALPA are input to the time-shift-and-sum and adaptive beamformers. Of particular interest are the differences between the full-array results and the results obtained with closely-spaced six-channel arrays such as the ones used to compare the new adaptive algorithm with the old adaptive algorithm. Finally, the effect of a new specially designed signal-enhancement prefilter on detection performance and adaptive processing signal-to-noise gain over beamsteering is compared with that of the old prefilter applied during the previous contract to the site

vertical-component data entering the beamformers. The new prefilter is evaluated using adaptive filter lengths of 31 and 15 points per channel in order to determine whether the shorter filter length produces any meaningful processing loss.

All results in this section apply to individual unmixed seismic events in the presence of background noise. To maintain compatibility with the processing results obtained previously for the old adaptive algorithm, adaptive filter sets are designed individually for the data sample containing background noise and for the data sample used in signal-degradation measurements. The criterion of performance in evaluating the various techniques for implementing adaptive beamforming is the estimated signal-to-noise ratio improvement relative to beamsteering. The method of approach used to estimate signal-to-noise ratio improvement is to measure the difference between noise reduction and signal degradation. Both noise reduction and signal degradation are computed in terms of the drop in power for the adaptive filter output relative to the beamsteer output. Since it is impossible in the case of real data to distinguish between signal power and noise power when a signal is present, the data samples for signal measurements are different from those used for noise measurements. Noise reduction is computed over data samples approximately four hours long. Signal degradation, on the other hand, is computed over gates approximately five minutes long. In the case of signal degradation measurements, the effect of adaptive filtering on contaminating noise is lumped together with the effect on the signal proper. As long as the adaptive filter set reduces the contaminating noise power at least as much as the signal power, the signal degradation is not underestimated and the signal-to-noise ratio improvement is not overestimated. Noise reduction and signal degradation are calculated for the same pair of data samples over a range of convergence rates. From these values, the signal-to-noise gain is estimated as a function of convergence rate.

Subsection B is a mathematical discussion of the reasons why the new adaptive algorithm should outperform the old adaptive algorithm. Subsection C is an empirical comparison of the two adaptive algorithms. In Subsection D, full-array processing results and six-channel processing results are compared for the new adaptive algorithm when the site vertical components, before input to the beamformers, are passed through the old prefilter used during the previous study. A heuristic development of the techniques used in designing a new signal-enhancement prefilter for detection purposes appears in Subsection E. The effect of applying the new prefilter to the vertical-component data is examined in Subsection F for adaptive filter lengths of 31 and 15 points per channel. Finally, Subsection G summarizes the results obtained with the adaptive beamforming techniques studied in this section.

B. CHARACTERISTICS OF SELECTED MAXIMUM LIKELIHOOD ADAPTIVE ALGORITHMS

The basic maximum likelihood adaptive algorithm

$$A(t + \Delta t) = A + 2\mu X^T A(\bar{X}-X)$$

attempts to minimize the mean square adaptive filter output $A^T E[XX^T]A$ subject to the signal-preservation constraint conditions $\sum_{i=1}^{M} a_i(j) = \delta_{oj}$ ($j = -N, \ldots, -1, 0, 1, \ldots, N$). When a constant, data-independent convergence parameter μ is used to process seismic data, this basic algorithm has two noteworthy disadvantages.

First, because of seismic-event amplitudes often spanning several orders of magnitude, the convergence parameter must be selected on the basis of the specific situations encountered in a particular data sample. The convergence-parameter range within which no divergence occurs is a function of those sections of data where the power is greatest. Likewise, the

convergence-parameter range where signal-to-noise gain is maximized ordinarily differs from data sample to data sample. Even after the development of suitable convergence-rate normalization and power-measurement procedures, the adaptive filter vector A in many cases moves exceedingly slowly in the presence of the only stable feature of the noise field-background noise.

The second important drawback of the basic algorithm is the undue emphasis it places on transient bursts of energy from seismic events. Frequently, in the case of long-period data, events are the dominant power source. After an event dies out, a new event from the same general direction cannot, in general, be expected for some time. Immediately after an event, therefore, the data is no longer quasi-stationary: the exponentially-smoothed time average for the matrix XX^T does not approximate the probabilistic matrix expectation $E[XX^T]$ at the instant of filter application. As a result, adaptive beamforming cannot achieve near-optimum noise suppression until exponential damping reduces the discrepancy between the time average and the probabilistic expectation to an acceptable level. After large events, this exponential-decay process may be lengthy. In seismic processing, the basic algorithm can be improved by emphasizing the stable background noise field at the expense of seismic events.

In the previous adaptive processing study (Barnard, 1973), the modified adaptive algorithm

$$A(t+\Delta t) = A + \frac{2\mu X^T A\,(\bar{X}-X)}{(\bar{X}-X)^T(\bar{X}-X)}$$

was employed. This algorithm attempts to minimize the quantity

$$A^T E\left[\frac{X^T X}{(\bar{X}-X)^T(\bar{X}-X)}\right] A$$

subject to the maximum likelihood constraints $\sum_{i=1}^{M} a_i(j) = \delta_{oj}$. A disadvantage of this algorithm is that each update reduces the power output for the old data vector by a factor $(1 - 2\mu)^2$ regardless of the fact that the data vector X may be consistent with a signal:

$$X^T A(t + \Delta t) = X^T A \left[1 + \frac{2\mu X^T (\bar{X} - X)}{(\bar{X} - X)^T (\bar{X} - X)} \right]$$

$$= X^T A \left[1 - \frac{2\mu (\bar{X} - X)^T (\bar{X} - X)}{(\bar{X} - X)^T (\bar{X} - X)} \right]$$

$$= X^T A (1 - 2\mu),$$

so that

$$A^T(t + \Delta t) XX^T A(t + \Delta t) = A^T XX^T A(1 - 2\mu)^2.$$

Furthermore, to prevent the squared magnitude

$$|A(t + \Delta t) - A|^2 = \frac{4\mu^2 y^2(t)}{(\bar{X} - X)^T (\bar{X} - X)}$$

of the filter update vector for this algorithm from becoming enormous when a strong signal traverses the array, the adaptive filter set must be frozen whenever a signal is detected. A filter-freeze procedure using the Fisher detector algorithm

$$F = \frac{(M-1)\bar{X}^T \bar{X}}{(\bar{X} - X)^T (\bar{X} - X)}$$

was used in the previous study to curb excessive movement of the filter vector A.

In the current study, the adaptive algorithm

$$A(t+\Delta t) = A + \frac{2\mu X^T A(\bar{X}-X)}{X^T X}$$

is utilized in an attempt to minimize the quantity

$$A^T E\left[\frac{XX^T}{X^T X}\right] A$$

subject to the same maximum likelihood constraints. With this algorithm, the squared magnitude

$$|A(t+\Delta t) - A|^2 = \frac{4\mu^2 y^2(t)\,(\bar{X}-X)^T(\bar{X}-X)}{(X^T X)^2}$$

of the filter update vector decreases when a strong signal propagates across the array. If the updated filter vector were applied to the old data vector, moreover, the adaptive filter output would be

$$X^T A(t+\Delta t) = X^T A\left[1 + \frac{2\mu X^T(\bar{X}-X)}{X^T X}\right]$$

$$= X^T A\left[1 - \frac{2\mu(\bar{X}-X)^T(\bar{X}-X)}{X^T X}\right],$$

so that the squared filter output would be reduced by a factor of $[1 - 2\mu(\bar{X}-X)^T(\bar{X}-X)/X^T X]^2$ instead of $(1 - 2\mu)^2$. In conformity with the design goals of the maximum likelihood multichannel filter, there would be no attenuation at all in the case of an ideal signal. With weak signals having signal-to-noise ratios too low to trigger a filter freeze, this algorithm appears to have a definite advantage over the algorithm previously employed: the convergence parameter μ for the new algorithm would probably be significantly greater than for the old algorithm if signal degradation were the

same for both algorithms, so that greater noise reduction and hence greater signal-to-noise gain might be achieved by the new algorithm. The new algorithm, like the old one, would also be less sensitive to power bursts from seismic events, so that non-repeating seismic events would be forgotten more rapidly than with the basic maximum likelihood algorithm

$$A(t + \Delta t) = A + 2\mu X^T A(\bar{X}-X).$$

Normalization of the data vector X by its absolute value $|X|$ in the new algorithm instead of the absolute value $|\bar{X}-X|$, furthermore, is sensibly motivated: the adaptive filter responds to the phase characteristics of the data vector X and not to its magnitude. It is difficult to describe precisely the effect of the normalizing factor $|\bar{X}-X|$ for the old algorithm.

C. COMPARISON OF THE NEW ADAPTIVE ALGORITHM WITH THE OLD

This subsection contains an empirical comparison of the adaptive algorithm

$$A(t + \Delta t) = A + \frac{2\mu X^T A(\bar{X}-X)}{X^T X}$$

used in this study with the algorithm

$$A(t + \Delta t) = A + \frac{2\mu X^T A(\bar{X}-X)}{(\bar{X}-X)^T(\bar{X}-X)}$$

employed during the previous contract. In order to make a meaningful comparison of the two adaptive algorithms, the same two data samples which provided the critical results of the previous investigation serve as input to the new adaptive algorithm. The principal criterion for evaluating algorithm

performance is the signal-to-noise ratio improvement of the adaptive beamformer relative to beamsteering. The approach used to estimate signal-to-noise ratio improvement is to measure the difference between noise reduction and signal degradation. Both noise reduction and signal degradation are computed in terms of the drop in power for the adaptive filter output relative to the beamsteer output. For consistency, adaptive filter sets are designed individually (as before) for the data sample containing background noise and for the data sample used in signal-degradation measurements. The results presented give signal-to-noise ratio improvement as a function of convergence rate. Results for the old algorithm come from the previous study, while results for the new algorithm originate from work performed during the current contract.

To obtain noise reduction measurements for the old algorithm, a noise sample spanning the period 0800 to 1145 on day 238 of 1970 is utilized. The steer direction corresponds to an azimuth of 270° and an apparent velocity of 3.5 km/sec. Noise reduction is computed as a function of the convergence parameter μ over the entire frequency band 0 to 0.5 Hz. The vertical components of sites 1, 2, 3, 6, 8, and 9 from ALPA are passed through a prefilter with the frequency response shown in Figure II-1 before input to the adaptive beamformer. (All beamforming results in this subsection and the next employ data passing through the prefilter.) The PDE bulletin lists no events between 0639 and 1502 on August 26 of 1970. A small signal reached ALPA at 1021, however, from an azimuth just under 60°. The energy from this signal is only a small fraction of the total energy within the entire sample and should have only a minor effect on the reported noise reduction values. Table II-1 and Figure II-2 present the noise reduction in dB for the old algorithm as a function of the convergence parameter μ.

To obtain signal degradation measurements for the old algorithm, three signals were selected out of a data sample from 2000 to 2345 on day

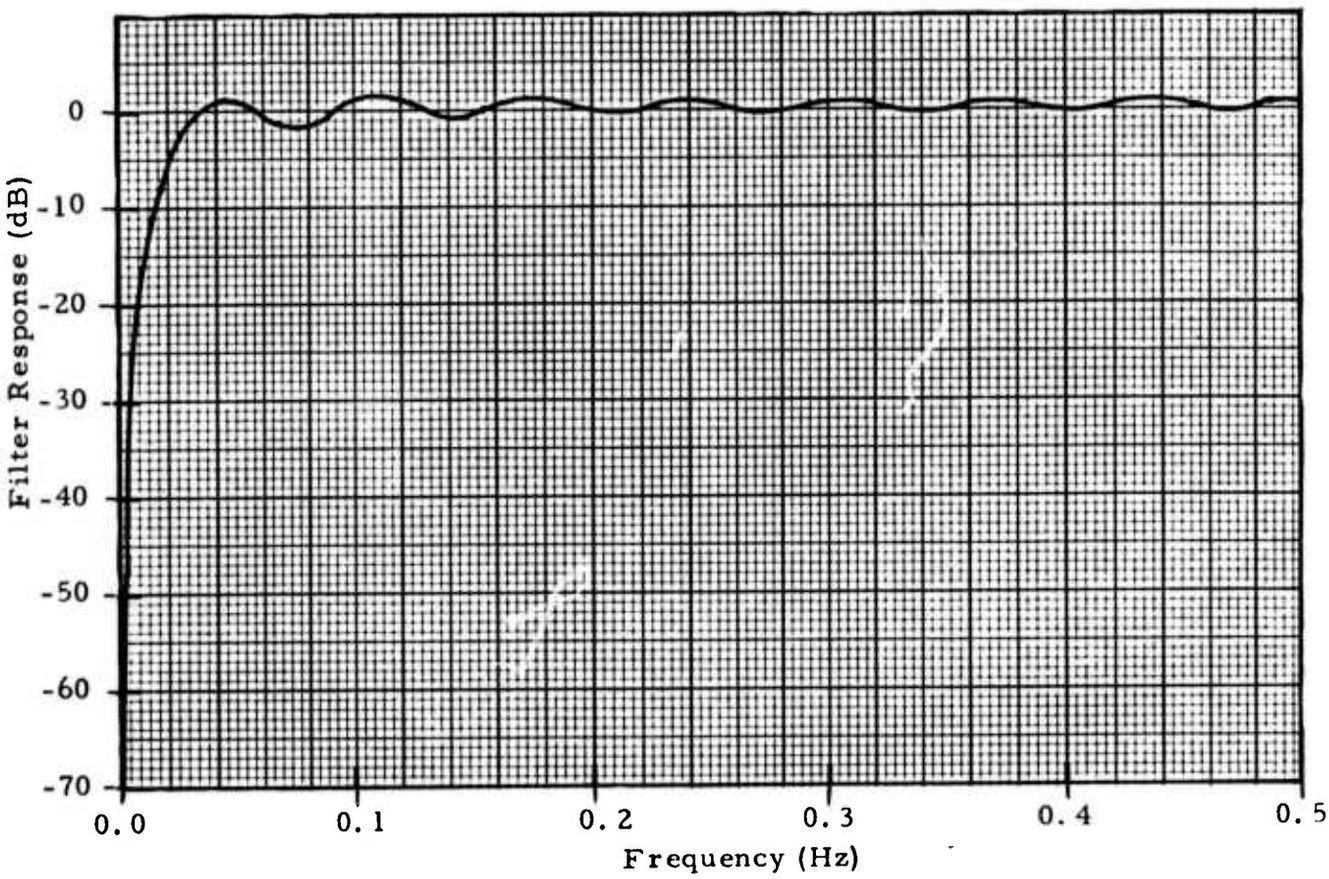

FIGURE II-1

OLD PREFILTER RESPONSE

TABLE II-1

ADAPTIVE FILTERING NOISE REDUCTION VERSUS CONVERGENCE RATE FOR OLD ALGORITHM (ALPA, 6 SITES, 1970 DAY 238 0800-1145)

Convergence Rate (μ)	Noise Reduction (dB)
0.002	1.099
0.003	1.359
0.004	1.521
0.005	1.639
0.007	1.813
0.010	1.983
0.015	2.186
0.020	2.346
0.030	2.635
0.050	3.135
0.070	3.562
0.100	4.056
0.150	4.547
0.200	4.786
0.250	4.892
0.300	4.940
0.350	4.945
0.400	4.939
0.500	4.896

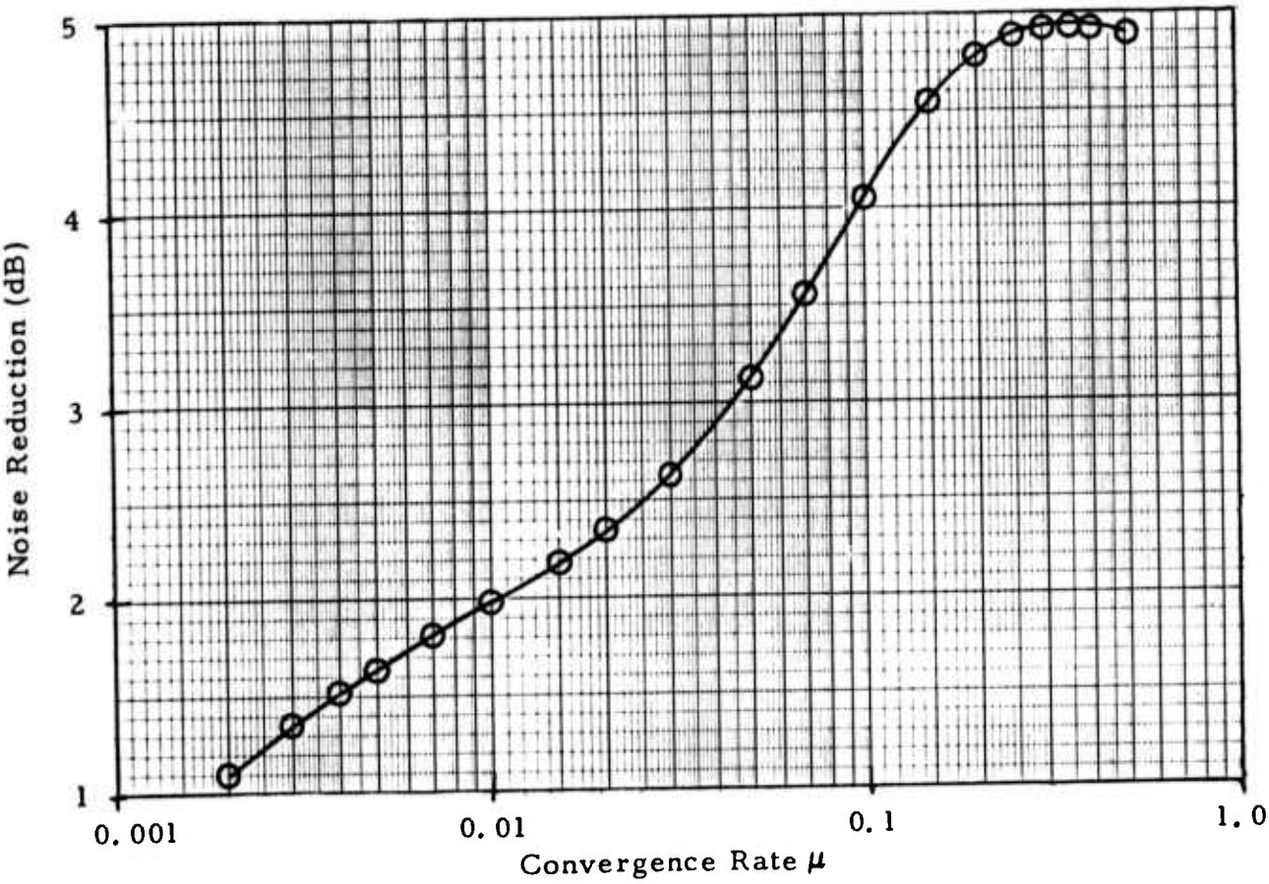

FIGURE II-2

NOISE REDUCTION AS A FUNCTION OF CONVERGENCE RATE FOR OLD ALGORITHM (ALPA, 6 SITES, 1970 DAY 238 0800-1145)

276 of 1971 (October 3). Several events from the PDE bulletin and LASA bulletin had arrival times within this period. Table II-2 gives the PDE events which arrived during the sample interval. In addition to these events, two events located within three degrees of the Panama event were included in the LASA bulletin for this time interval. The first of these had a measured LASA bodywave magnitude of 3.6 and arrived at LASA 47 minutes and 34 seconds before the PDE event from Panama. The second had a measured LASA bodywave magnitude of 3.9 and arrived at LASA 6 minutes and 38 seconds before the PDE event from Panama. In processing the three signals selected, sites 8, 9, 12, 15, 16, and 17 are input to the time-shift-and-sum and adaptive filter beams.

A weak signal arrived at ALPA at approximately 2138. The signal-to-noise ratio on the beamsteer output is about 6 dB. No event corresponding to this signal can be found on either the PDE bulletin or LASA bulletin. Frequency-wavenumber spectra, Fisher-detector scans, and beamsteer-output power comparisons indicate an arrival azimuth between 300° and 305°. The beamsteer and adaptive-filter beams are aimed toward 302.5°. Table II-3 and Figure II-3 depict signal degradation for the old algorithm as a function of convergence rate over the frequency band 0 to 0.5 Hz. The negative degradation at $\mu = 0.002$ means that the adaptive filter trace contains more energy than the beamsteer output trace over the 512-point computation gate. Combining these signal degradation measurements with the noise reduction measurements from day 238 of 1970 yields an estimate of the signal-to-noise gain which would have occurred on day 238 of 1970 if the weak signal had arrived at ALPA during the period 0800-1145. Table II-4 and Figure II-4 contain the resulting signal-to-noise gain estimate as a function of convergence rate. Best signal-to-noise ratio improvement is obtained at $\mu = 0.004$.

The remaining two signals used in signal-degradation measurements are large signals from near the east coast of Kamchatka. The first of these

TABLE II-2

PDE EVENTS ARRIVING AT ALPA
BETWEEN 2000 AND 2345 ON OCTOBER 3, 1971

Origin Time (Hr-Min-Sec)	Lat (Deg)	Long (Deg)	Region	m_b	Azimuth (Deg)
20:42:46.7	3.5N	82.9W	South of Panama	4.7	113
20:54:48.5	55.7N	162.1E	Near East Coast of Kamchatka	4.5	273
21:54:12.9	55.8N	162.2E	Near East Coast of Kamchatka	4.9	273
22:34:54.8	4.2S	152.7E	New Britain Region	4.8	240
23:17:26.4	51.8N	173.3W	Andreanof Islands, Aleutian Is.	4.3	237

TABLE II-3

ADAPTIVE FILTERING SIGNAL DEGRADATION VERSUS CONVERGENCE RATE WITH OLD ALGORITHM FOR A WEAK SIGNAL FROM 300°-305°
(ALPA, 6 SITES, 1971 DAY 276 21.37.01-21.45.32)

Convergence Rate (μ)	Signal Degradation (dB)
0.002	-0.024
0.003	0.104
0.004	0.255
0.005	0.408
0.007	0.650
0.010	0.945
0.015	1.301
0.020	1.569
0.030	1.970
0.050	2.562
0.070	3.049
0.100	3.713
0.150	4.505
0.200	4.973
0.250	5.176

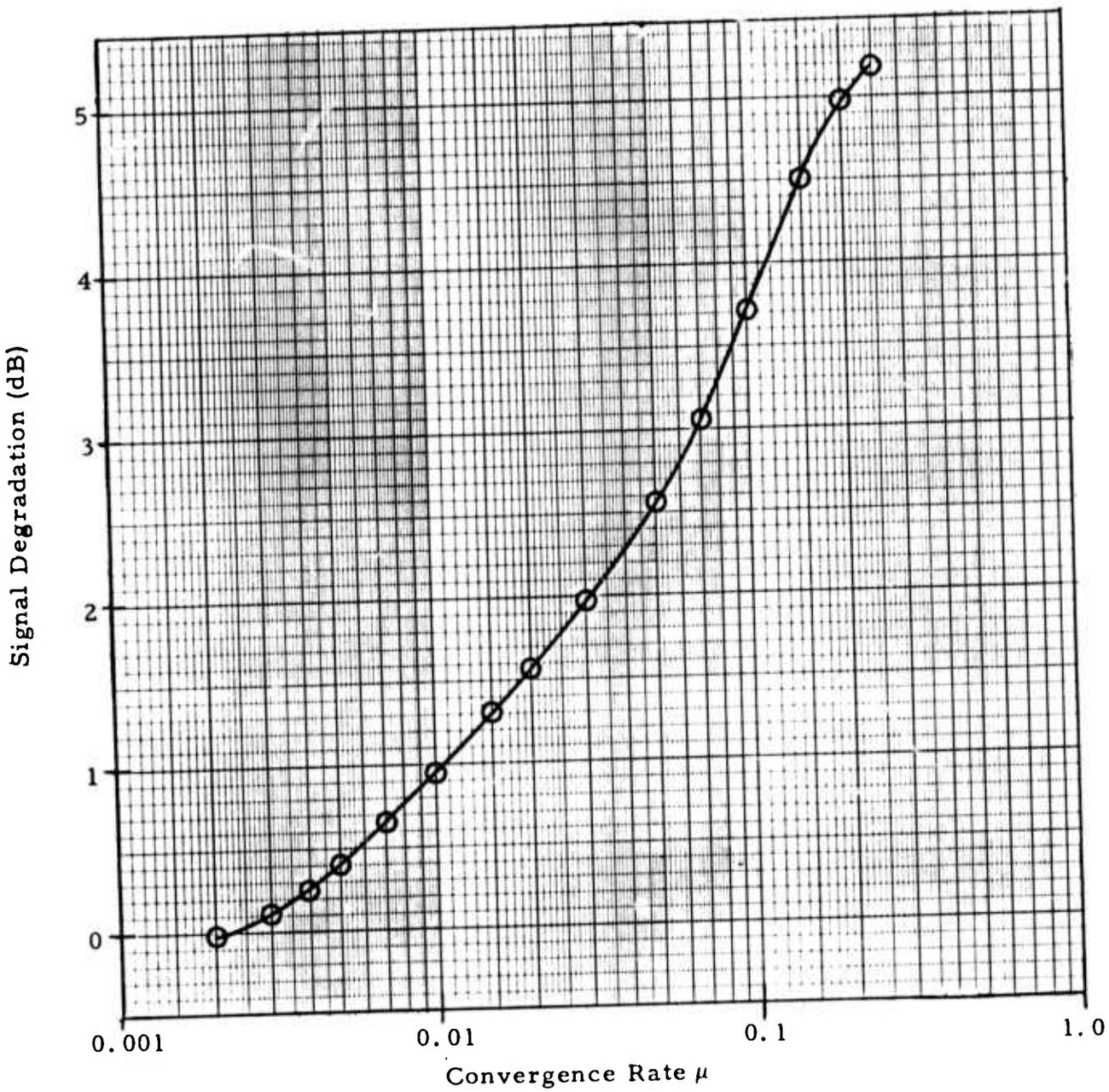

FIGURE II-3

SIGNAL DEGRADATION AS A FUNCTION OF CONVERGENCE RATE WITH OLD ALGORITHM FOR A WEAK SIGNAL FROM 300^{o} - 305^{o} (ALPA, 6 SITES, 1971 DAY 276 21.37.01-21.45.32)

TABLE II-4

ADAPTIVE FILTERING SIGNAL-TO-NOISE GAIN VERSUS CONVERGENCE RATE WITH OLD ALGORITHM FOR A WEAK SIGNAL FROM 300°-305° (ALPA, 6 SITES, 1971 DAY 276 21.37.01 - 21.45.32, USING NOISE FROM 1970 DAY 238 0800-1145)

Convergence Rate (μ)	Signal-to-Noise Gain (dB)
0.002	1.123
0.003	1.255
0.004	1.266
0.005	1.231
0.007	1.163
0.010	1.038
0.015	0.885
0.020	0.777
0.030	0.665
0.050	0.573
0.070	0.513
0.100	0.343
0.150	0.042
0.200	-0.187
0.250	-0.284

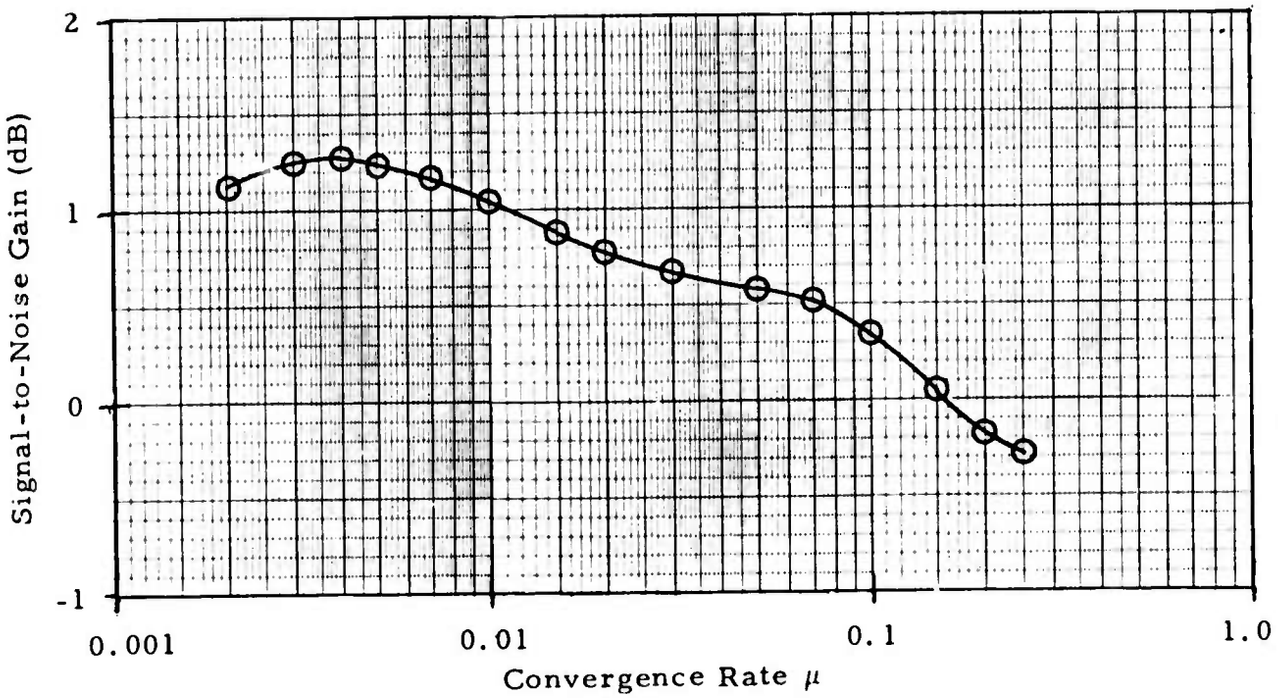

FIGURE II-4

SIGNAL-TO-NOISE GAIN AS A FUNCTION OF CONVERGENCE RATE WITH OLD ALGORITHM FOR A WEAK SIGNAL FROM 300^{o}-305^{o} (ALPA, 6 SITES, 1971 DAY 276 21.37.01-21.45.32, USING NOISE FROM 1970 DAY 238 0800-1145)

has a bodywave magnitude of 4.5, an origin time of 20:54:48.5, a latitude of 55.7 N, and a longitude of 162.1 E. The azimuth with respect to ALPA is 273°. Accordingly, the beams are trained in this direction. Eighteen dB is the estimated signal-to-noise ratio on the beamsteer output. Table II-5 and Figure II-5 show the signal degradation for this signal using the old algorithm. The computation gate for this signal is 256 seconds instead of 512 seconds (as in the case of the weak signal from 300°-305°). The resulting estimated signal-to-noise ratio improvement using noise reduction measurements from day 238 of 1970 appears in Table II-6 and Figure II-6. Best ABF performance again occurs at $\mu = 0.004$.

The last signal used to measure signal degradation is a magnitude 4.9 event from almost exactly the same location. The PDE bulletin gives the origin time as 21:54:12.9, the latitude as 55.8 N, and the longitude as 162.2 E. Again the beams are directed toward a 273° azimuth. For this event, the signal-to-noise ratio on the beamsteer output is close to 24 dB. Signal degradation over a 256-point interval for the old algorithm is portrayed in Table II-7 and Figure II-7. It is considerably greater than for the event with an 18-dB signal-to-noise ratio. Using the day 238 noise sample for noise reduction measurements, the resulting signal-to-noise gain for the old algorithm is represented in Table II-8 and Figure II-8. Maximum improvement is obtained at the slowest convergence rate.

The principal result in processing the three signals with the old algorithm is that the signal degradation increases as the signal-to-noise ratio increases. With the old algorithm, at least, the maximum likelihood constraints do not guarantee preservation of the signal. When no noise is present, the constraint conditions and differences in successive realizations of the data vector X ultimately limit the signal-degradation levels which are possible. As the influence of noise becomes significant, the resultant retardation of the effective adaptation rate reduces the measured signal-degradation values.

TABLE II-5

ADAPTIVE FILTERING SIGNAL DEGRADATION VERSUS CONVERGENCE RATE WITH OLD ALGORITHM FOR A STRONG SIGNAL FROM KAMCHATKA (ALPA, 6 SITES, 1971 DAY 276 21.07.18-21.11.33)

Convergence Rate (μ)	Signal Degradation (dB)
0.002	0.269
0.003	0.416
0.004	0.556
0.005	0.693
0.007	0.944
0.010	1.279
0.015	1.743
0.020	2.137
0.030	2.718
0.050	3.423
0.070	3.775
0.100	3.989
0.150	4.119
0.200	4.203
0.250	4.243

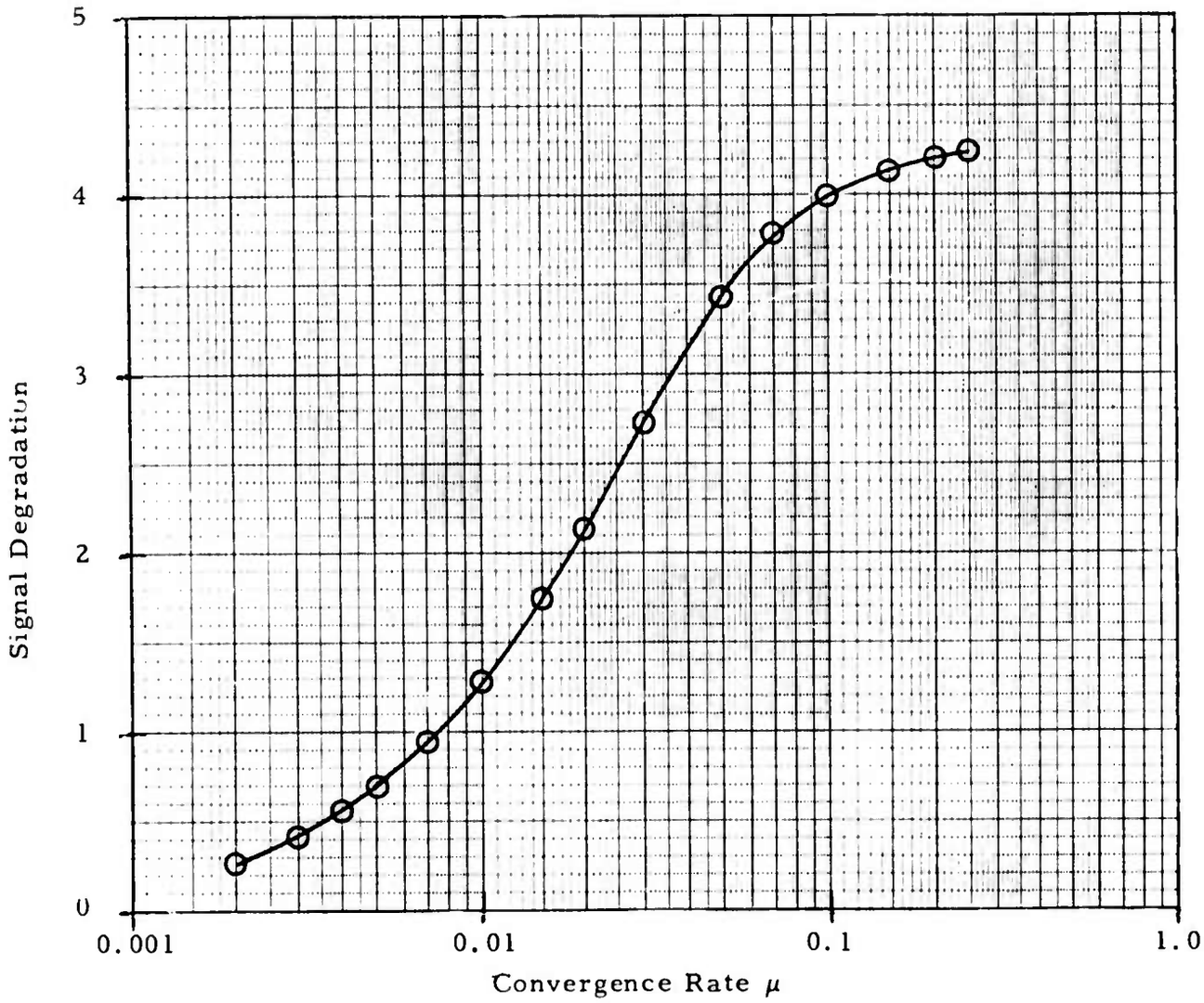

FIGURE II-5

SIGNAL DEGRADATION AS A FUNCTION OF CONVERGENCE RATE WITH OLD ALGORITHM FOR A STRONG SIGNAL FROM KAMCHATKA (ALPA, 6 SITES, 1971 DAY 276 21.07.18-21.11.33)

TABLE II-6

ADAPTIVE FILTERING SIGNAL-TO-NOISE GAIN VERSUS CONVERGENCE RATE WITH OLD ALGORITHM FOR A STRONG SIGNAL FROM KAMCHATKA (ALPA, 6 SITES, 1971 DAY 276 21.07.18-21.11.33, USING NOISE FROM 1970 DAY 238 0800-1145)

Convergence Rate (μ)	Signal-to-Noise Gain (dB)
0.002	0.830
0.003	0.943
0.004	0.965
0.005	0.946
0.007	0.869
0.010	0.704
0.015	0.443
0.020	0.209
0.030	-0.083
0.050	-0.288
0.070	-0.213
0.100	0.067
0.150	0.428
0.200	0.589
0.250	0.649

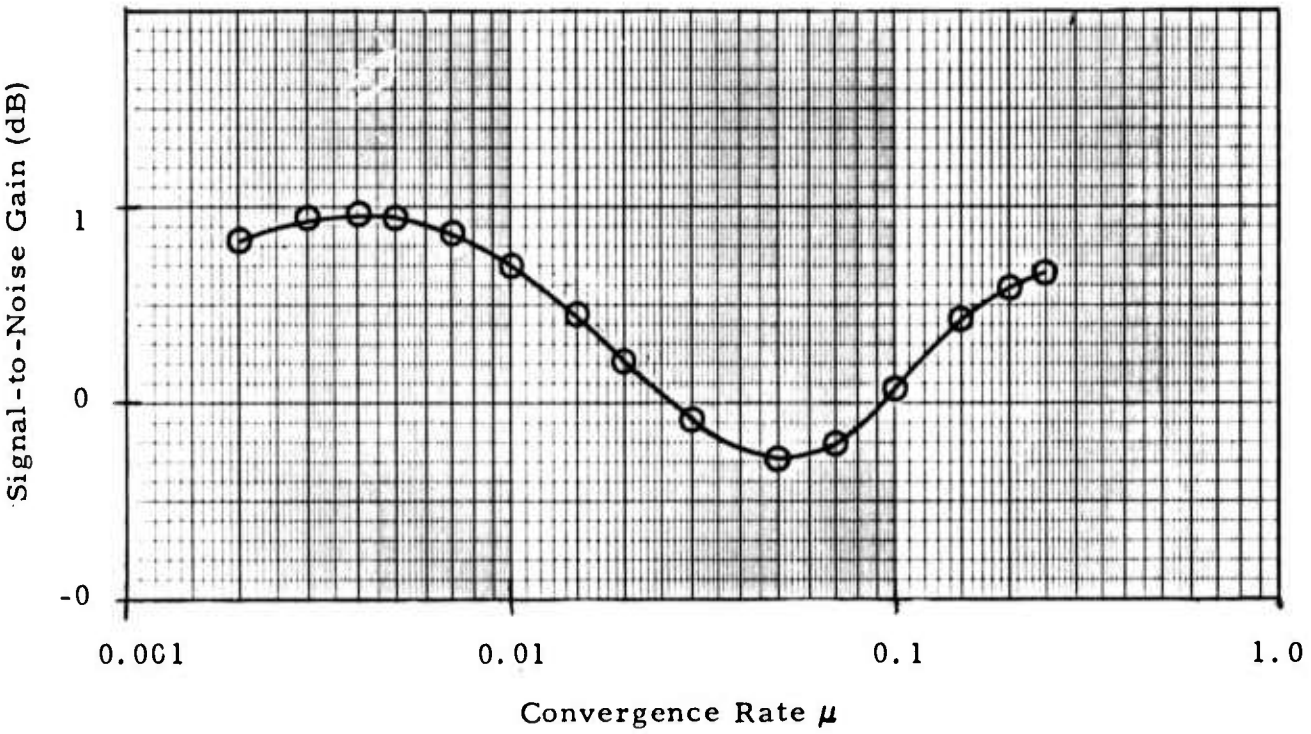

FIGURE II-6

SIGNAL-TO-NOISE GAIN AS A FUNCTION OF CONVERGENCE RATE WITH OLD ALGORITHM FOR A STRONG SIGNAL FROM KAMCHATKA (ALPA, 6 SITES, 1971 DAY 276 21.07.18-21.11.33, USING NOISE FROM 1970 DAY 238 0800-1145)

TABLE II-7

ADAPTIVE FILTERING SIGNAL DEGRADATION VERSUS CONVERGENCE RATE WITH OLD ALGORITHM FOR A VERY STRONG SIGNAL FROM KAMCHATKA (ALPA, 6 SITES, 1971 DAY 276 22.07.02-22.11.17)

Convergence Rate (μ)	Signal Degradation (dB)
0.002	0.963
0.003	1.324
0.004	1.655
0.005	1.977
0.007	2.571
0.010	3.360
0.015	4.450
0.020	5.294
0.030	6.367
0.050	7.179
0.070	7.418
0.100	7.461
0.150	7.465
0.200	7.495
0.250	7.497

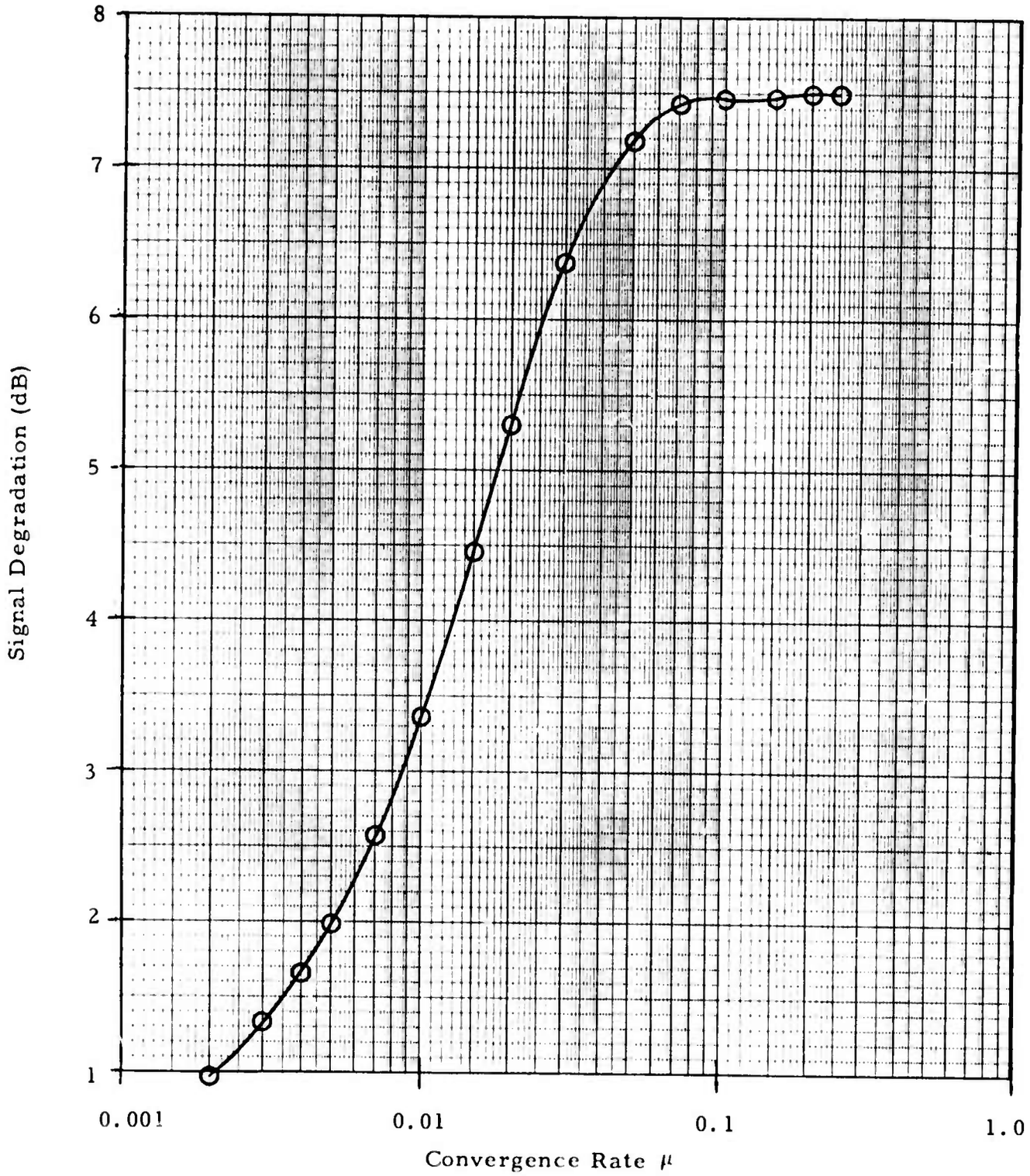

FIGURE II-7

SIGNAL DEGRADATION AS A FUNCTION OF CONVERGENCE RATE WITH OLD ALGORITHM FOR A VERY STRONG SIGNAL FROM KAMCHATKA (ALPA, 6 SITES, 1971 DAY 276 22.07.02-22.11.17)

TABLE II-8

ADAPTIVE FILTERING SIGNAL-TO-NOISE GAIN VERSUS CONVERGENCE RATE WITH OLD ALGORITHM FOR A VERY STRONG SIGNAL FROM KAMCHATKA (ALPA, 6 SITES, 1971 DAY 276 22.07.02-22.11.17, USING NOISE FROM 1970 DAY 238 0800-1145)

Convergence Rate (μ)	Signal-to-Noise Gain (dB)
0.002	0.136
0.003	0.035
0.004	-0.134
0.005	-0.338
0.007	-0.758
0.010	-1.377
0.015	-2.264
0.020	-2.948
0.030	-3.732
0.050	-4.044
0.070	-3.856
0.100	-3.405
0.150	-2.918
0.200	-2.709
0.250	-2.605

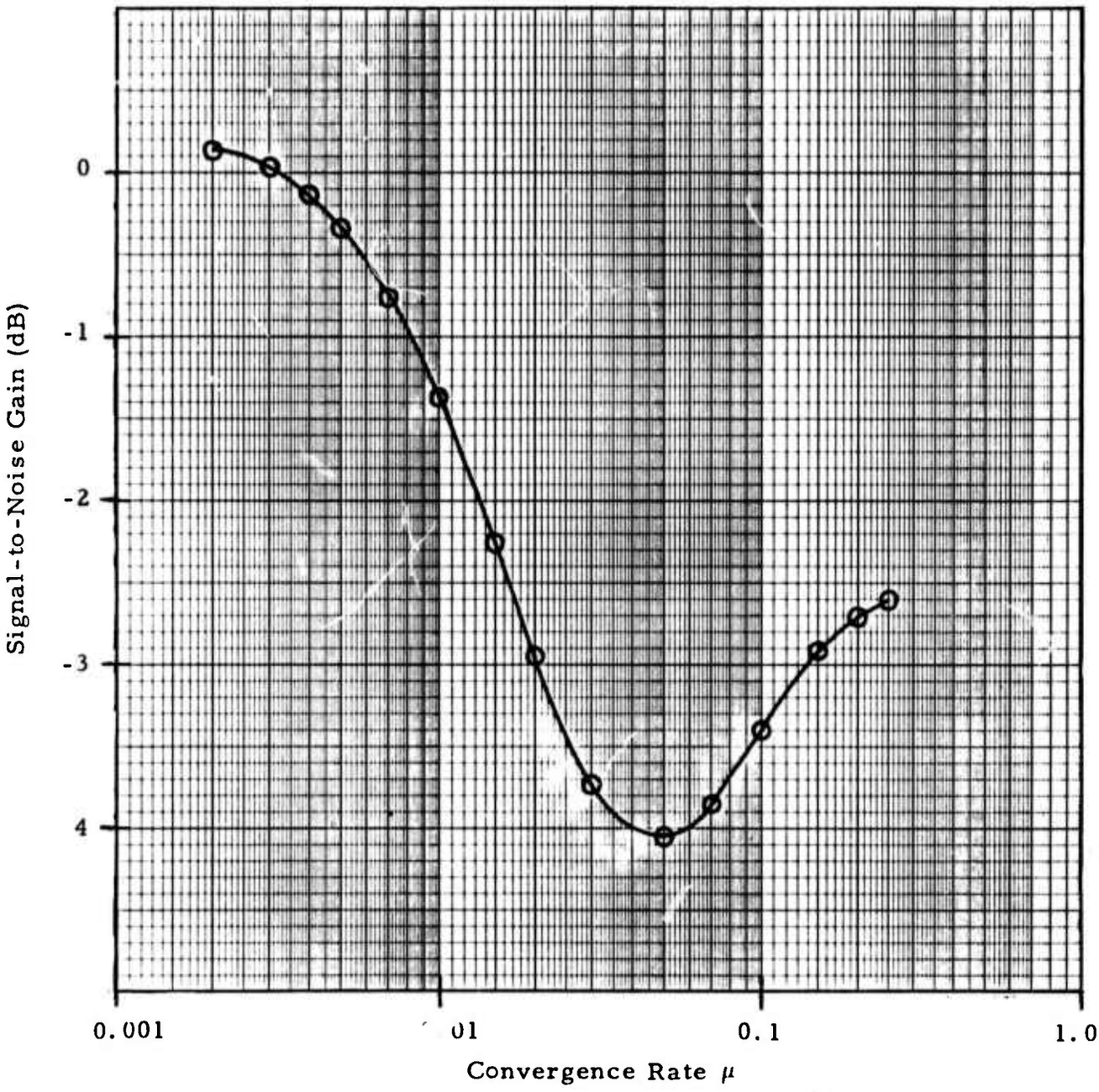

FIGURE II-8

SIGNAL-TO-NOISE GAIN AS A FUNCTION OF CONVERGENCE RATE WITH OLD ALGORITHM FOR A VERY STRONG SIGNAL FROM KAMCHATKA (ALPA, 6 SITES, 1971 DAY 276 22.07.02-22.11.17, USING NOISE FROM 1970 DAY 238 0800-1145)

Sections IV and V of the previous report (Barnard, 1973) contain a more comprehensive discussion of the results for the old algorithm and present several Calcomp plots of the beamsteer and adaptive filter output traces from the data samples processed so far in this subsection. To conserve space, they do not appear in this report.

In the computer program implementing the old algorithm, the components of the adaptive filter vector A are expressed in 16-bit integer form. In addition, the denominator term $(\bar{X}-X)^T(\bar{X}-X)$ is approximated by the quantity $(2N+1)\sum_{i=1}^{M} P_i(t)$, where $P_i(t)$ is an exponentially-smoothed power average for the i-th channel. $P_i(t)$ is computed by the formula

$$P_i(t) = (1-\epsilon)P_i(t-\Delta t) + \epsilon\left[\bar{x}(t) - x_i(t)\right]^2 ,$$

where ϵ is an input parameter. Initially, $P_i(t)$ is zero, and several values of $P_i(t)$ are computed before the filter vector A is allowed to update. By way of contrast, in the computer program for the current study, computations utilize standard IBM 360 32-bit floating-point arithmetic, and the denominator term X^TX is the true dot product of the instantaneous data vector X with itself. The inability of the old algorithm at high convergence rates to achieve noise reduction values as great as those for the new algorithm may be due to the computational differences described here.

Noise reduction measurements for the new algorithm come from the same data sample used in noise reduction measurements for the old algorithm. The sample extends from 0800 to 1145 on day 238 of 1970. The only difference in processing is that an apparent velocity of 3.6 km/sec is specified instead of the 3.5 km/sec velocity employed with the old algorithm. The 3.6 km/sec velocity is probably a slightly more realistic value and is the default value in the current computer program. The 3.5 km/sec velocity was used in the old computer program to obtain the results for the old adaptive algorithm. The

slight difference in velocity should have only a minor effect on the processing results. Table II-9 and Figure II-9 give the noise reduction measurements for the new algorithm as a function of the convergence parameter μ. The adaptation rate is always slower with the new algorithm than with the old algorithm at any particular value of the convergence parameter μ. The reason is that the denominator term

$$(\bar{X}-X)^T(\bar{X}-X) = X^TX - \bar{X}^T\bar{X}$$

of the old algorithm is always smaller than the corresponding term X^TX of the new algorithm. For spatially uncorrelated noise of equal strength on all sensors, the beamsteer output power is $1/M$ times the average power across the sensors (where M is the number of sensors). Consequently, the effective adaptation rate of the new algorithm is $(M-1)/M$ times the rate of the old algorithm in that case. For propagating plane wave energy reasonably far from the steer direction, the same is true in an average sense. In any specific case, however, the result depends on the array geometry, the frequency content of the incoming energy, the steer direction, and the direction of the incoming energy. For an ideal signal (where $\bar{X} = X$), the filter vector A stops completely with the new algorithm, whereas the step size $|A(t+\Delta t) - A(t)|$ becomes infinite with the old algorithm. To compare noise reduction measurements between algorithms, the convergence parameter values μ for the old algorithm need to be multiplied by $M/(M-1)$, or 1.2, to obtain the most reasonable equivalent values for the new algorithm. That is to say, the value $\mu = 0.05$ for the old algorithm corresponds to the value $\mu = 0.06$ for the new algorithm. At $\mu = 0.5$, the noise reduction for the new algorithm is 6.5 dB and is still increasing. At no convergence rate did the noise reduction for the old algorithm exceed 5 dB. Roundoff error and estimation of the denominator term $(\bar{X}-X)^T(\bar{X}-X)$ with an exponentially-smoothed power average may account for the lower noise reduction values with the old

TABLE II-9

ADAPTIVE FILTERING NOISE REDUCTION VERSUS CONVERGENCE RATE FOR NEW ALGORITHM (ALPA, 6 SITES, 1970 DAY 238 0800-1145)

Convergence Rate (μ)	Noise Reduction (dB)
0.0010	0.641
0.0015	0.825
0.0020	0.969
0.0030	1.183
0.0040	1.334
0.0050	1.447
0.0070	1.609
0.0100	1.772
0.0150	1.960
0.0200	2.106
0.0300	2.352
0.0400	2.571
0.0500	2.775
0.0700	3.146
0.1000	3.628
0.1500	4.292
0.2000	4.829
0.3000	5.644
0.4000	6.193
0.5000	6.527

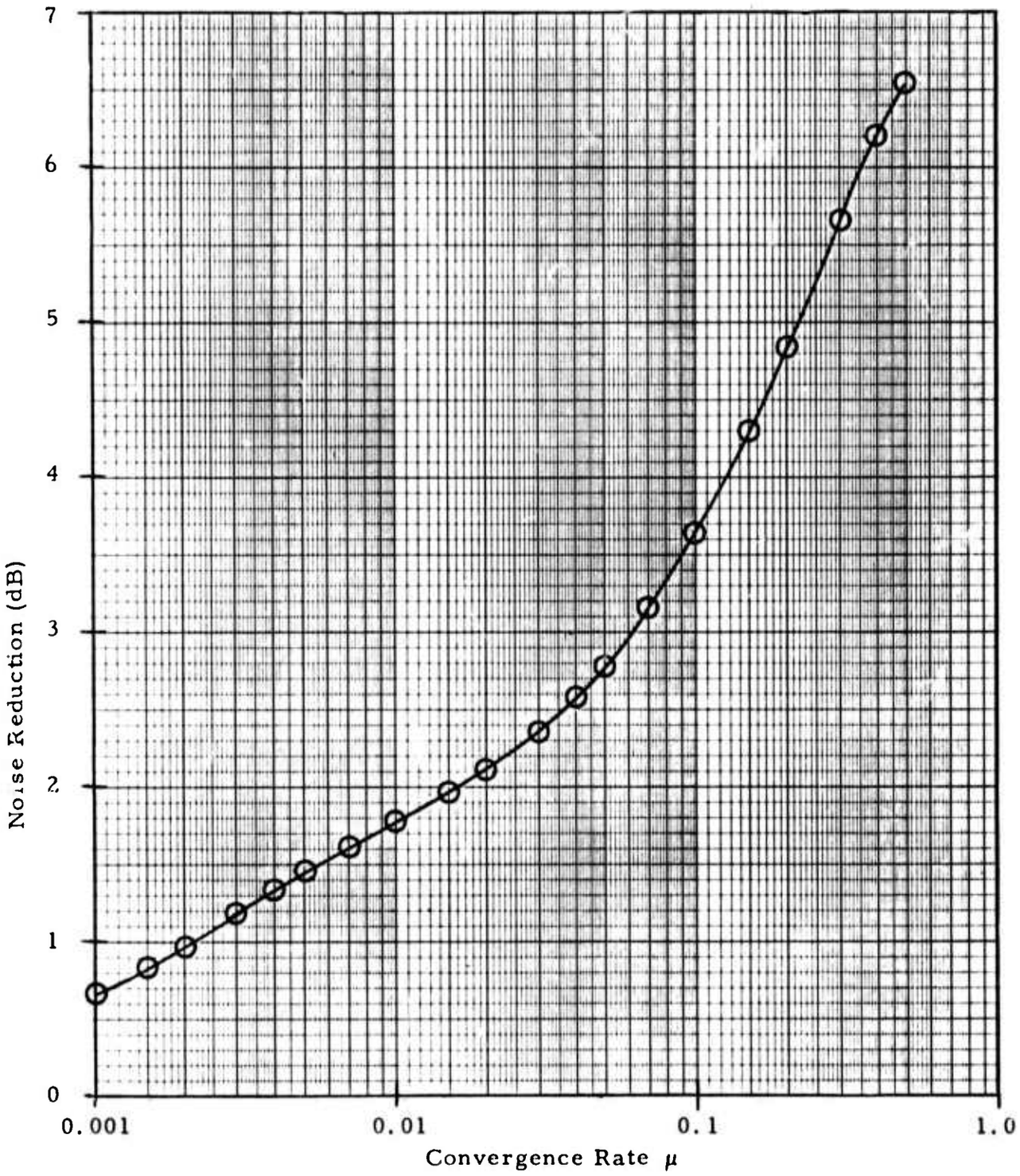

FIGURE II-9

NOISE REDUCTION AS A FUNCTION OF CONVERGENCE RATE FOR NEW ALGORITHM (ALPA, 6 SITES, 1970 DAY 238 0800-1145)

algorithm. At high convergence rates, the major roundoff-error problem seems to be in the adaptive filter output $y(t) = X^T A$. Error in the data vector X may change the sign of $y(t)$. In addition, rounding the adaptive filter output $y(t)$ to the nearest integer may result in a zero value and prevent any update of the filter vector A. A more detailed discussion of this situation appears in Subsection III-D of the previous report (Barnard, 1973). Other factors contributing to the difference in performance for the two algorithms may be the clipping of the filter weights at an absolute value of one half (with the old algorithm) and, of course, the algorithms themselves.

In the noise sample from day 238 of 1970, a weak signal reached ALPA at 1021 from an azimuth of approximately 60°. Figure II-10 shows the beamsteer output and adaptive-filter output with the new algorithm at $\mu = 0.005$ and $\mu = 0.5$ for this event. Tick marks at the zero levels of all three beams are spaced 5 minutes apart and correspond to the time immediately above the middle trace. The beamsteer output appears in the top trace, the adaptive-filter output for $\mu = 0.005$ in the middle trace, and the adaptive-filter output at $\mu = 0.5$ in the bottom trace. At the lower convergence rate, the adaptive-filter output is slightly attenuated relative to the beamsteer output. In contrast, the adaptive-filter output at $\mu = 0.5$ in the bottom trace is negligible in comparison with the beamsteer output. At slow convergence rates, the effect of the beamsteer and adaptive beamformers is reflected in the array wavenumber response

$$A(f, \vec{k}) = \sum_{j=1}^{M} A_j(f) \; e^{i2\pi(f\tau_j - \vec{k}\cdot\vec{x}_j)}$$

for the time-shift-and-sum processor and the adaptive processor. The response $A(f, \vec{k})$ is the complex amplification factor for a hypothetical plane wave of frequency f and wavenumber

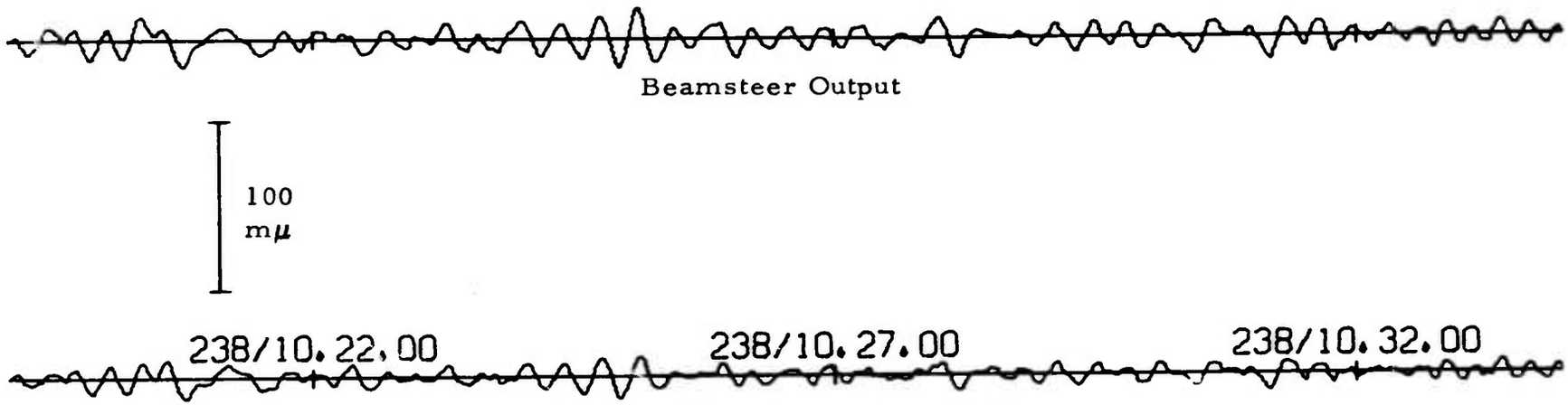

Adaptive Filter Output ($\mu = 0.5$)

FIGURE II-10

EVENT FROM 60°
(DAY 238 1970, STEER DIRECTION 270°)

$$\vec{k} = \left(-\frac{f}{V} \sin\theta, -\frac{f}{V} \cos\theta \right),$$

where V is the apparent velocity across the array and θ is the azimuth from which the plane wave arrives. In the formula for $A(f, \vec{k})$, the vector $\vec{x}_j = (x_j, y_j)$ is the position of the j-th sensor relative to the array reference location, τ_j is the time delay (rounded to the nearest sample interval) required to time-align a signal from the look direction (as seen by the j-th sensor) with the signal as seen at the array reference location, and $A_j(f)$ is the Fourier transform of the convolution filter applied to the j-th sensor. For the beamsteer processor, the Fourier transform $A_j(f)$ is the constant value $1/M$, where M is the number of sensors used to form the beam. For a fixed look velocity and look azimuth, the array response $A(f, \vec{k})$ can be computed as a function of azimuth for waves propagating at the look velocity. Figure II-11 is the beamsteer response $10 \log_{10} |A(f, \vec{k})|^2$ computed in this way for the six-sensor noise sample from day 238 of 1970 when the steer azimuth is 270°. For energy arriving from the west (the look direction), the beamsteer pattern achieves its maximum response of approximately zero dB. Unlike the beamsteer array response, the ABF response changes with time. Figures II-12 through II-15 display the adaptive processor response at 1020, 1025, 1030, and 1035. By 1035, a null has formed at the 60° azimuth of the signal presented in Figure II-10. The creation of the null is an automatic consequence of the adaptive algorithm, which attempts to minimize the filter output power subject to signal-preservation constraints. The constraints are reflected at an azimuth of 270°, where the ABF response is approximately zero dB. (Slight variations from unity response at the look azimuth are possible because the sensor time delays are rounded to the nearest integer sample interval.)

Signal degradation measurements for the new algorithm again use the same three signals contained in the previously processed data sample from

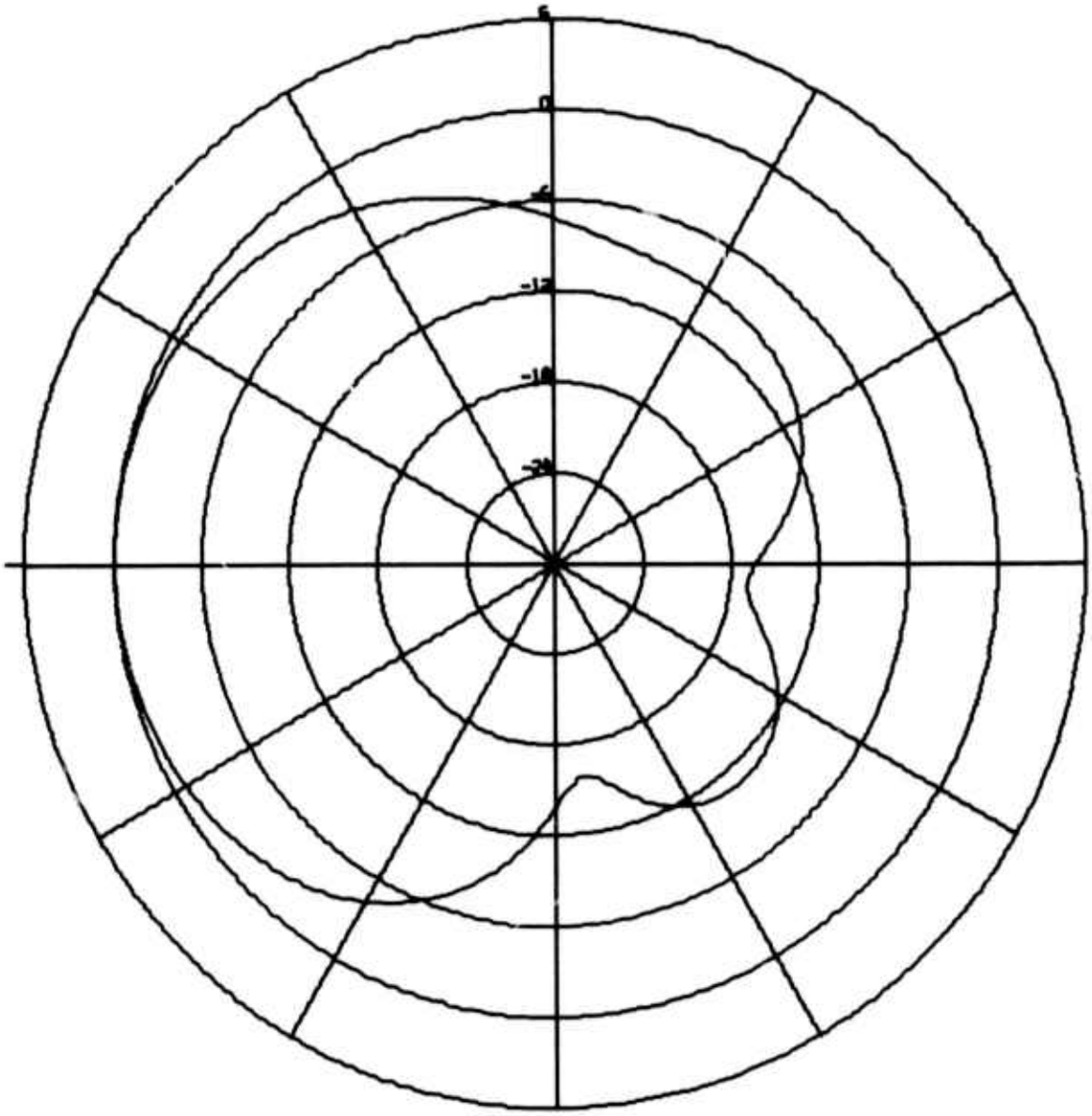

ALPA
TIME-SHIFT-AND-SUM BEAM PATTERN
BEAM LOOK VELOCITY IS 3.6, LOOK AZIMUTH 270.0
FREQUENCY IS 0.04000 HZ, PERIOD 25.0 SECONDS

FIGURE II-11

BEAMSTEER RESPONSE FOR SIX-CHANNEL NOISE SAMPLE
FROM DAY 238 OF 1970

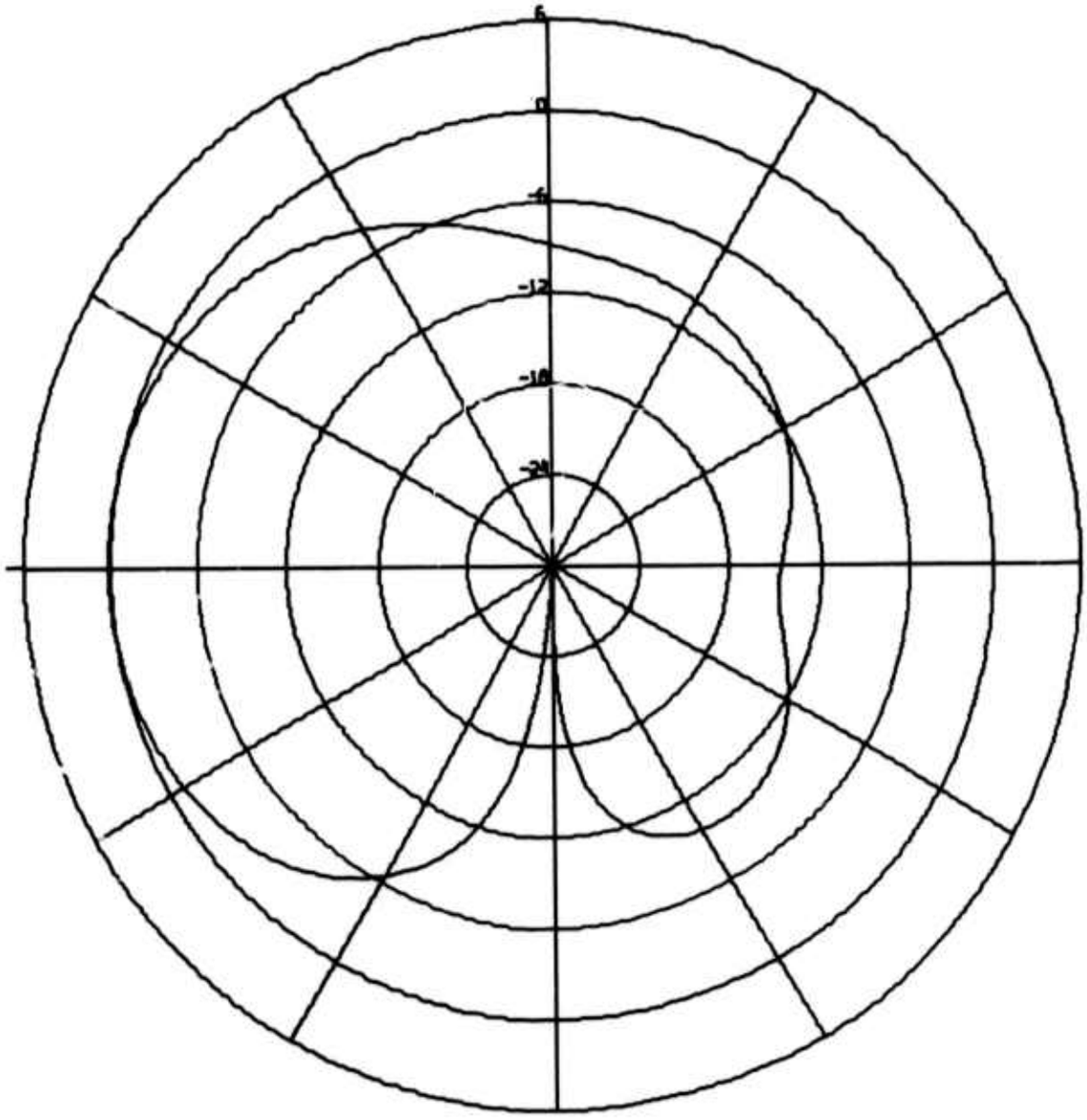

ALPA
ABF BEAM PATTERN AT 238/10.20.00
CONVERGENCE RATE IS 0.0050
BEAM LOOK VELOCITY IS 3.6, LOOK AZIMUTH 270.0
FREQUENCY IS 0.04000 HZ, PERIOD 25.0 SECONDS

FIGURE II-12

ABF RESPONSE FOR SIX-CHANNEL NOISE SAMPLE
AT 1020 ON DAY 238 OF 1970

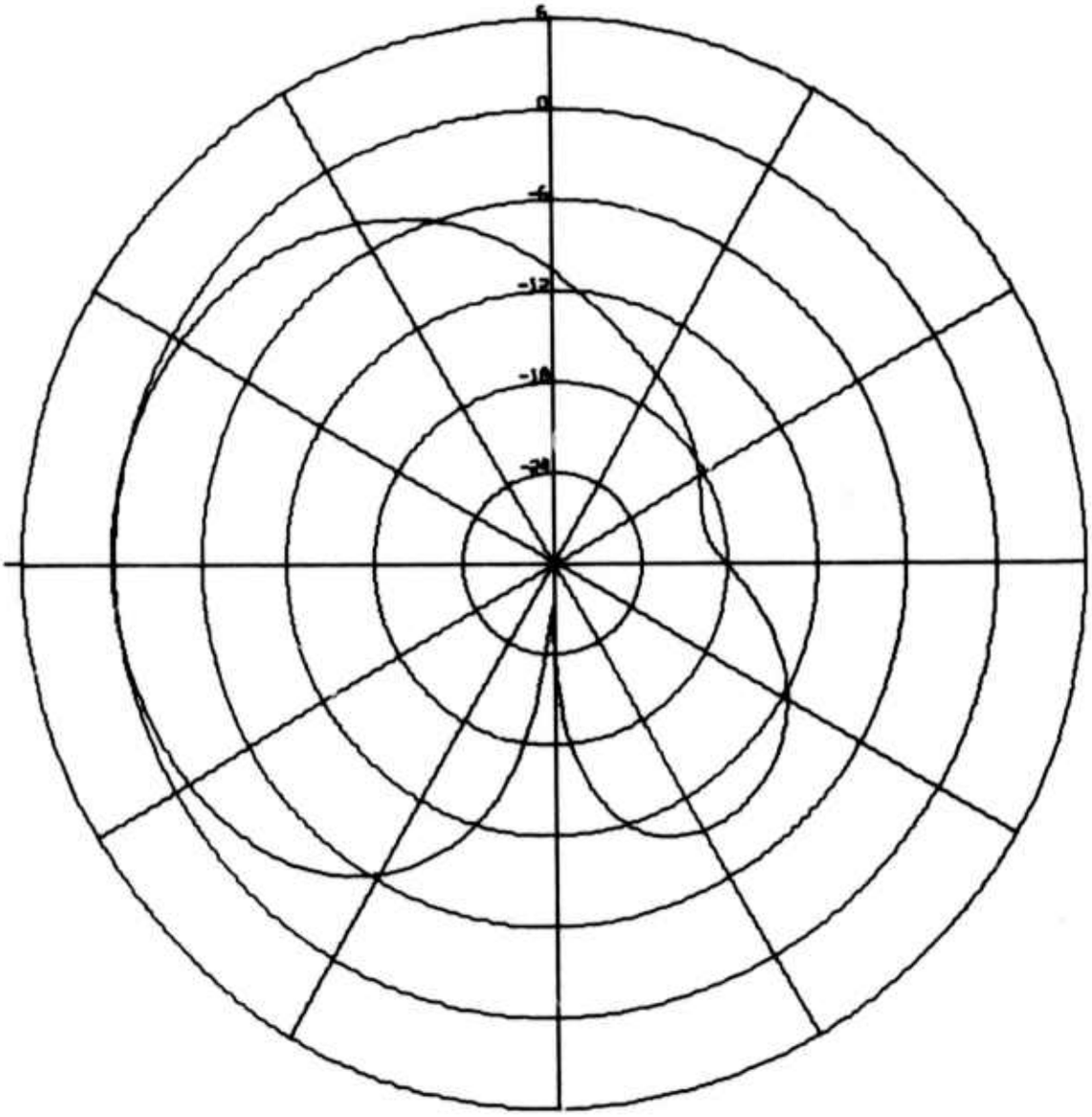

ALPA
ABF BEAM PATTERN AT 238/10.25.00
CONVERGENCE RATE IS 0.0050
BEAM LOOK VELOCITY IS 3.6, LOOK AZIMUTH 270.0
FREQUENCY IS 0.04000 HZ, PERIOD 25.0 SECONDS

FIGURE II-13

ABF RESPONSE FOR SIX-CHANNEL NOISE SAMPLE
AT 1025 ON DAY 238 OF 1970

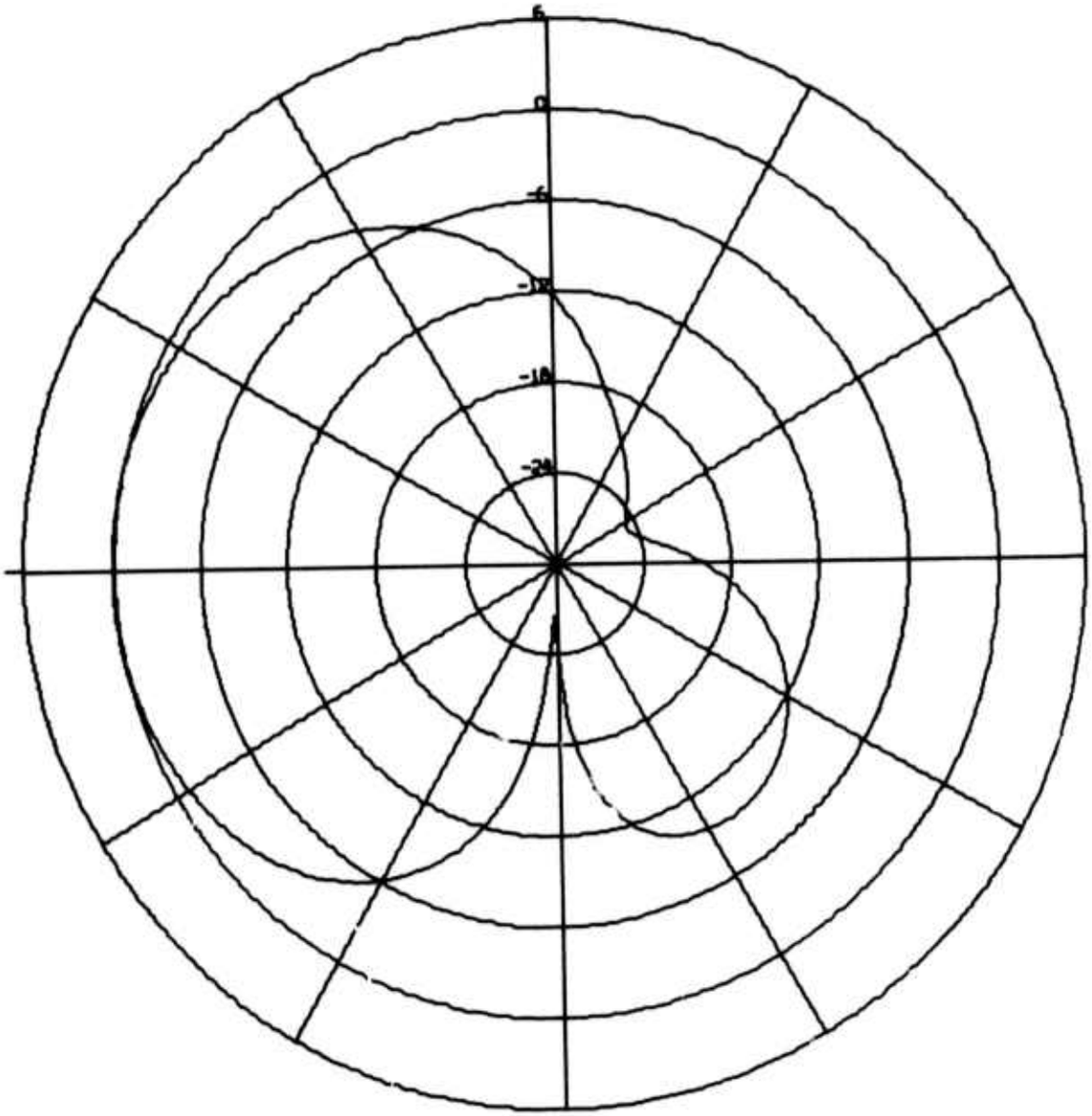

FIGURE II-14

ABF RESPONSE FOR SIX-CHANNEL NOISE SAMPLE
AT 1030 ON DAY 238 OF 1970

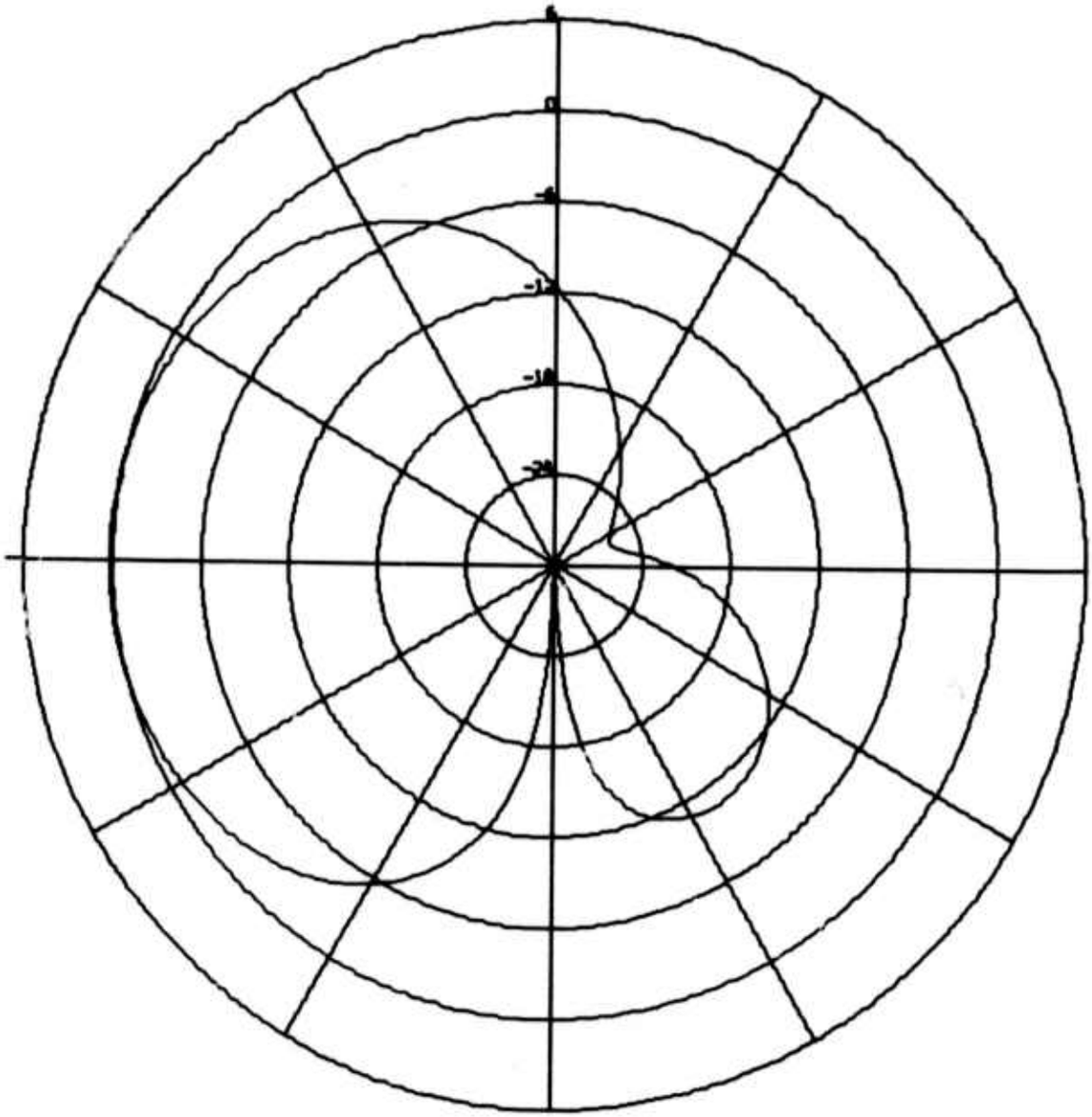

FIGURE II-15

ABF RESPONSE FOR SIX-CHANNEL NOISE SAMPLE
AT 1035 ON DAY 238 OF 1970

2000 to 2345 on day 276 of 1971. As in the case of noise reduction measurements for the new algorithm, the only difference in processing is the substitution of 3.6 km/sec for the 3.5 km/sec apparent velocity employed with the old algorithm. The first signal examined is the weak signal arriving at approximately 2138 from an azimuth between 300^{o} and 305^{o}. The steer direction for this event is 302.5^{o}. Table II-10 and Figure II-16 portray signal degradation as a function of convergence rate for this event with the new addaptive algorithm. As in the case of the old algorithm, negative signal degradation is obtained at the low convergence rates. The amplification of the signal relative to the beamsteer output may be due to rounding the steer delays to the nearest sample interval. This rounding procedure permits slight deviations from the unity-response constraint condition for the look direction. Figure II-17, which is a plot of the ABF beam pattern at $\mu = 0.005$ shortly after signal onset, confirms the measured signal degradation of -0.022 dB may correspond to an array response greater than 0 dB in the look direction. No such phenomenon appears in the time-shift-and-sum beam pattern for this array configuration and look direction (Figure II-18). A comparison of the ABF pattern in Figure II-17 with the beamsteer pattern in Figure II-18 illustrates the capability of adaptive processing to create a superdirective array response. Using the noise reduction measurements from day 238 of 1970 for the new algorithm, the resulting signal-to-noise ratio improvement estimates as a function of convergence rate appear in Table II-11 and Figure II-19. The maximum signal-to-noise gain of 1.47 dB occurs at $\mu = 0.005$. This gain is about 0.2 dB higher than the maximum gain of 1.27 dB for this weak signal with the old algorithm. At the higher convergence rates, the new algorithm outperforms the old by more than 0.5 dB. A visual examination of the site vertical-component traces shows poor signal similarity across the array for this particular weak event. This fact probably explains the high signal degradation values at the more rapid convergence rates. Later in this section, when utilization of the full array and a signal-enhancement prefilter permits

TABLE II-10

ADAPTIVE FILTERING SIGNAL DEGRADATION VERSUS CONVERGENCE RATE WITH NEW ALGORITHM FOR A WEAK SIGNAL FROM 300°-305°
(ALPA, 6 SITES, 1971 DAY 276 21.37.01-21.45.32)

Convergence Rate (μ)	Noise Reduction (dB)
0.0010	- 0.233
0.0015	- 0.263
0.0020	- 0.261
0.0030	- 0.203
0.0040	- 0.116
0.0050	- 0.022
0.0070	0.161
0.0100	0.408
0.0150	0.755
0.0200	1.042
0.0300	1.490
0.0400	1.829
0.0500	2.101
0.0700	2.531
0.1000	3.023
0.1500	3.639
0.2000	4.115
0.3000	4.857
0.4000	5.457
0.5000	5.976

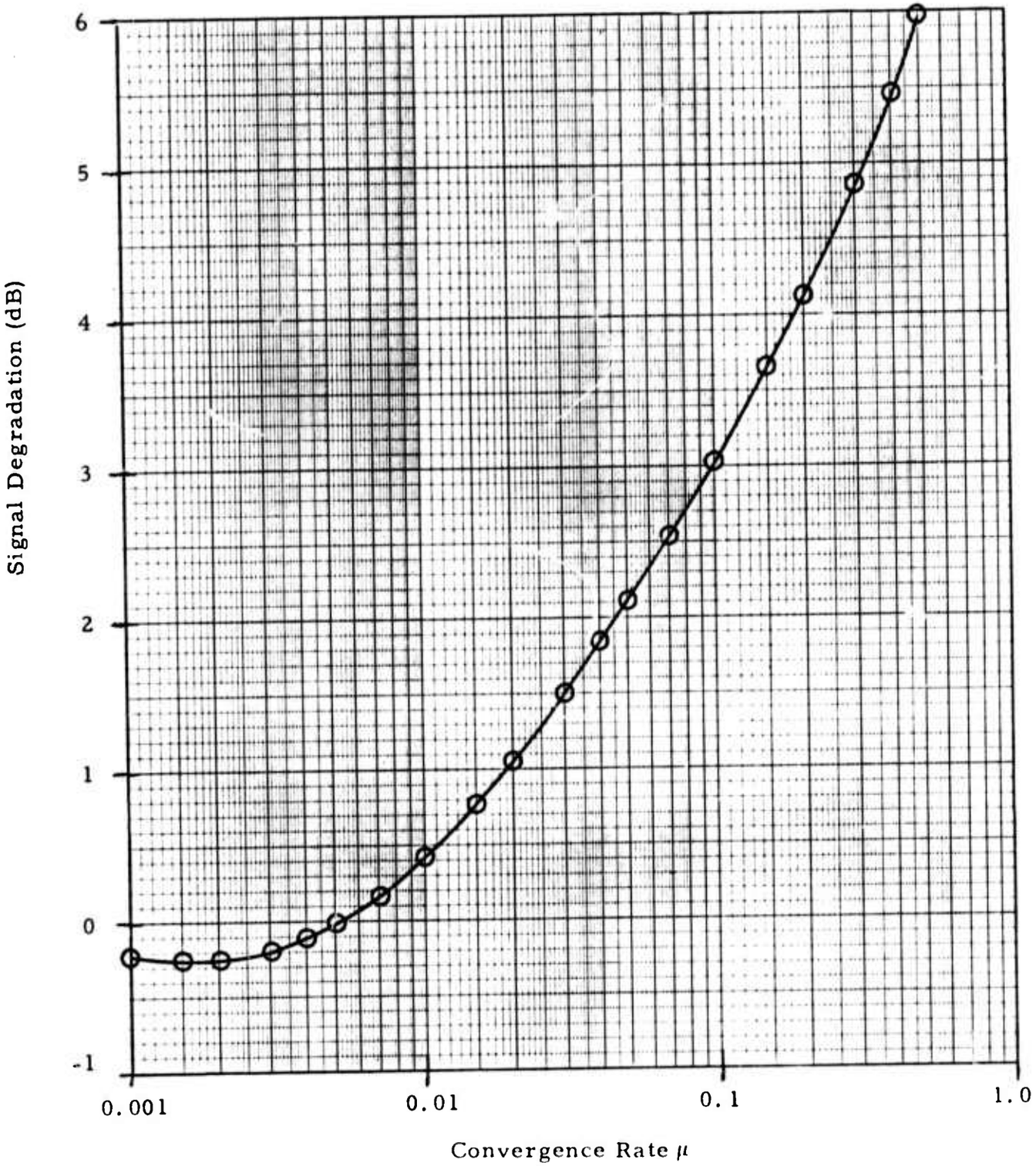

FIGURE II-16

SIGNAL DEGRADATION AS A FUNCTION OF CONVERGENCE RATE WITH NEW ALGORITHM FOR A WEAK SIGNAL FROM 300°-305° (ALPA, 6 SITES, 1971 DAY 276 21.37.01-21.45.32)

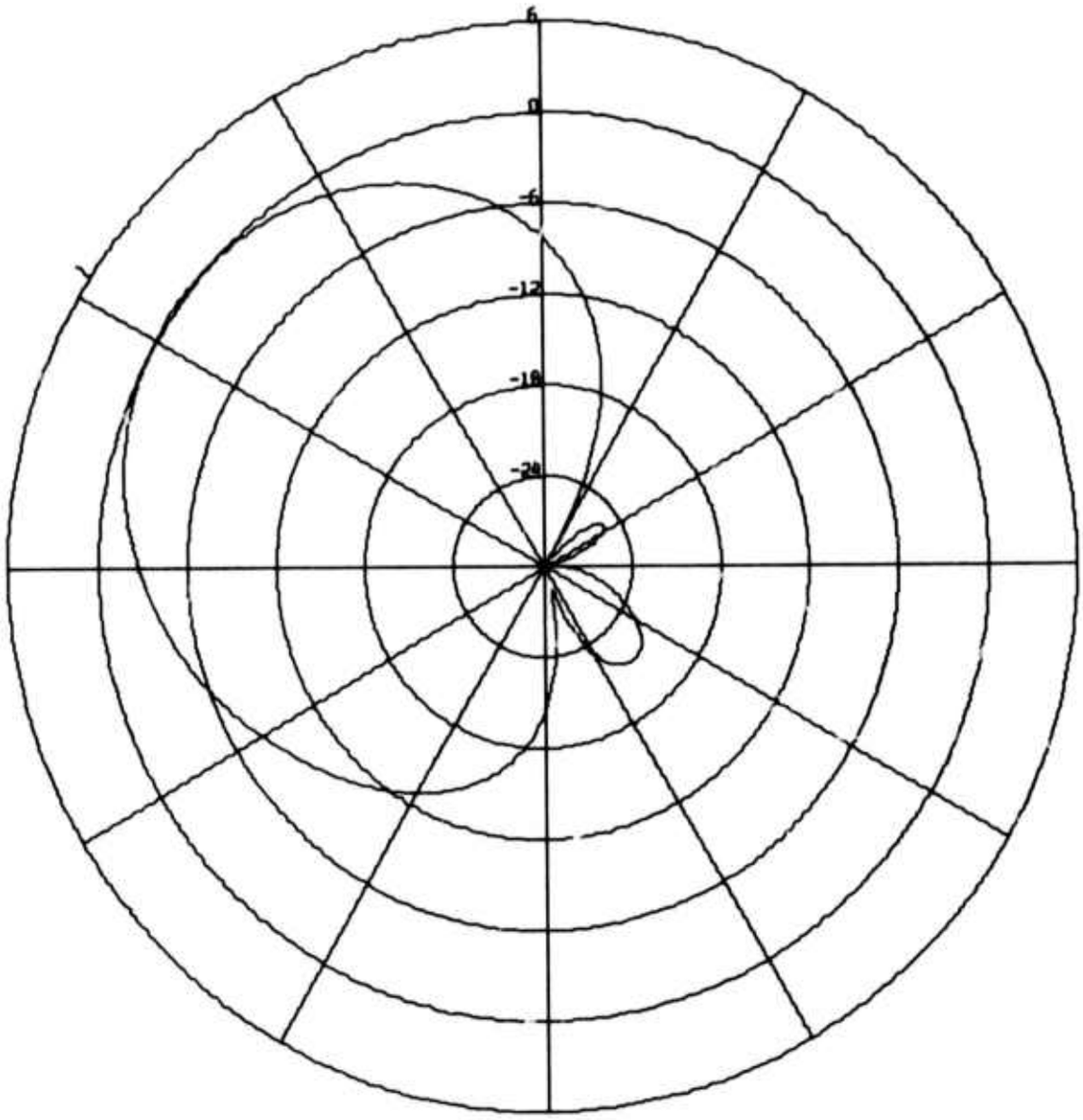

ALPA
ABF BEAM PATTERN AT 276/21.39.00
CONVERGENCE RATE IS 0.0050
BEAM LOOK VELOCITY IS 3.6, LOOK AZIMUTH 302.5
FREQUENCY IS 0.04000 HZ, PERIOD 25.0 SECONDS

FIGURE II-17

SIX-CHANNEL ABF RESPONSE FOR WEAK EVENT FROM 300°-305°
AT 2139 ON DAY 276 OF 1971

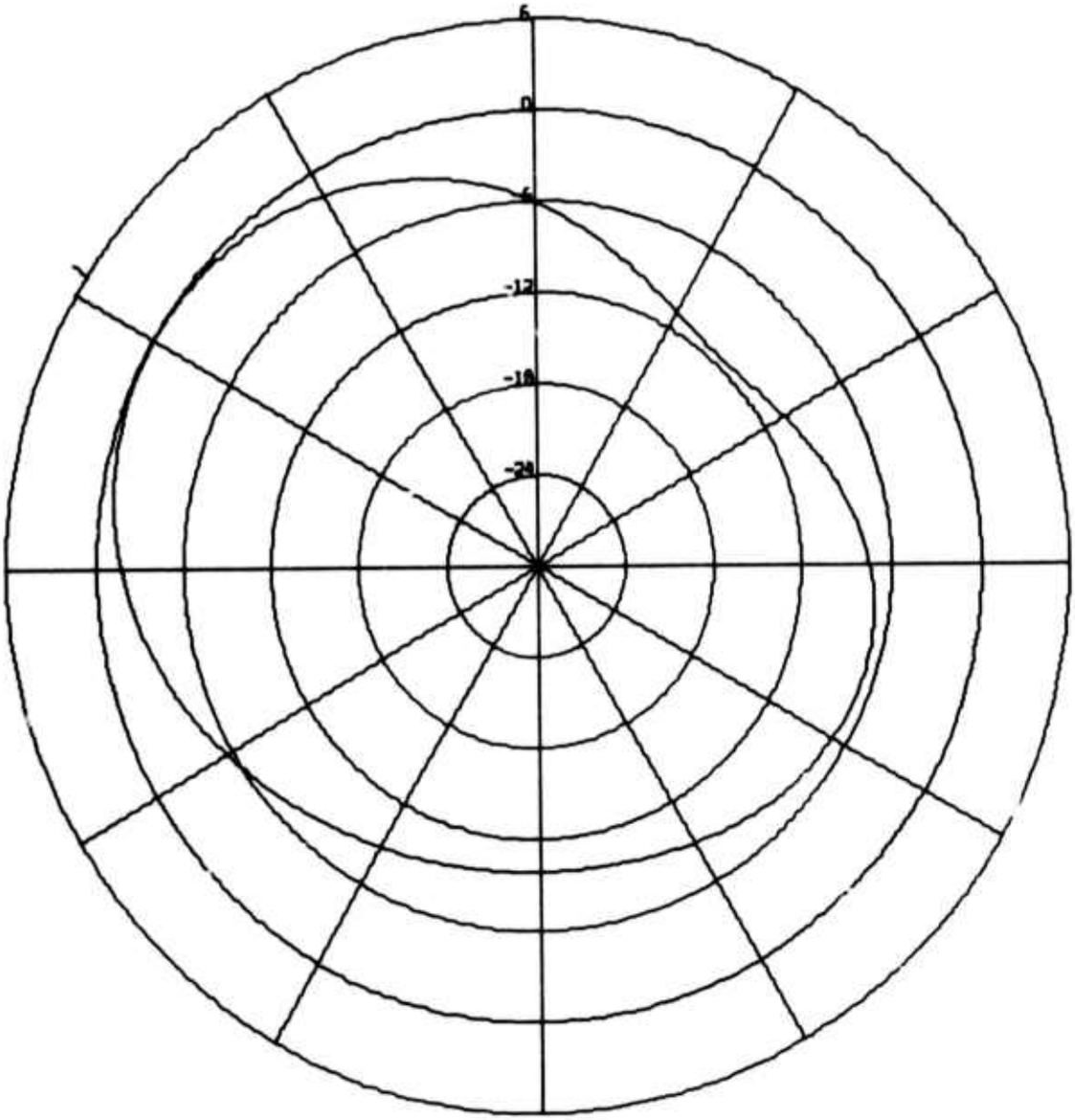

ALPA
TIME-SHIFT-AND-SUM BEAM PATTERN
BEAM LOOK VELOCITY IS 3.6, LOOK AZIMUTH 302.5
FREQUENCY IS 0.04000 HZ, PERIOD 25.0 SECONDS

FIGURE II-18

BEAMSTEER RESPONSE FOR SIX-CHANNEL
SAMPLE FROM DAY 276 OF 1971

TABLE II-11

ADAPTIVE FILTERING SIGNAL-TO-NOISE GAIN VERSUS CONVERGENCE RATE WITH NEW ALGORITHM FOR A WEAK SIGNAL FROM 300° - 305° (ALPA, 6 SITES, 1971 DAY 276 21.37.01-21.45.32, USING NOISE FROM 1970 DAY 238 0800-1145)

Convergence Rate (μ)	Signal-to-Noise Gain (dB)
0.0010	0.874
0.0015	1.088
0.0020	1.230
0.0030	1.386
0.0040	1.450
0.0050	1.469
0.0070	1.448
0.0100	1.364
0.0150	1.205
0.0200	1.064
0.0300	0.862
0.0400	0.742
0.0500	0.674
0.0700	0.615
0.1000	0.605
0.1500	0.653
0.2000	0.714
0.3000	0.787
0.4000	0.736
0.5000	0.551

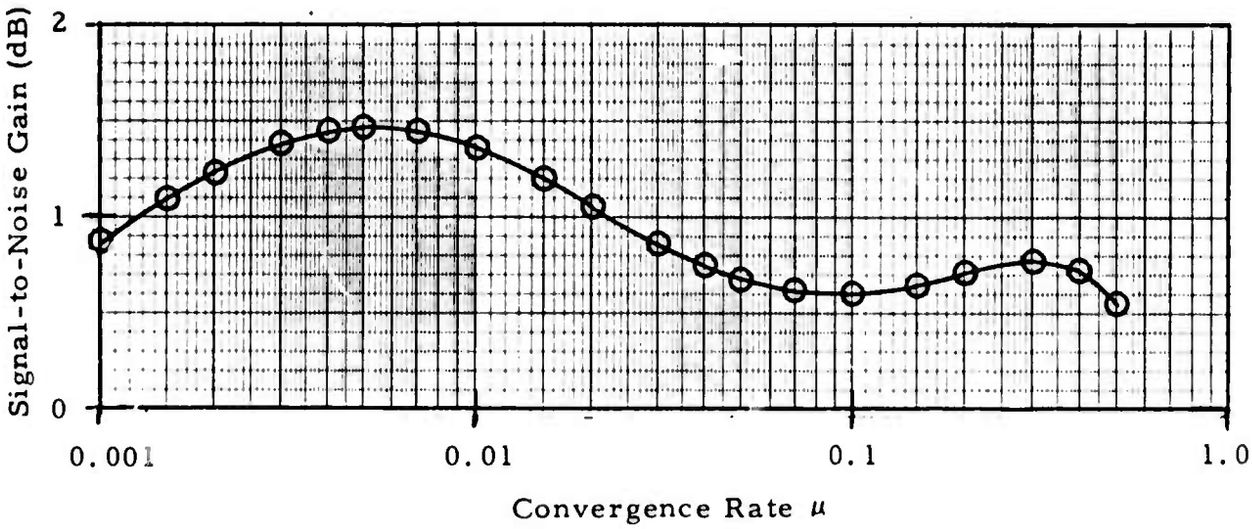

FIGURE II-19

SIGNAL-TO-NOISE GAIN AS A FUNCTION OF CONVERGENCE RATE WITH NEW ALGORITHM FOR A WEAK SIGNAL FROM 300°-305° (ALPA, 6 SITES, 1971 DAY 276 21.37.01-21.45.32, USING NOISE FROM 1970 DAY 238 0800-1145)

detection of the New Britain event, the processing results will shed further light on this possibility. Figure II-20 is a display of the weak event from 300°-305° for the beamsteer output and adaptive filter output at $\mu = 0.005$ and $\mu = 0.5$. On the middle trace (where $\mu = 0.005$), the signal is approximately as strong as on the beamsteer output. In contrast, all but the closing section of the event is greatly attenuated at $\mu = 0.5$ (the bottom trace). Even on the bottom trace, however, the signal remnants are conspicuous enough to suggest the presence of the weak event. In fact, since the noise surrounding the event is considerably weaker on the bottom trace, the signal detectability for the two ABF traces is closer than it seems at first glance. This fact is important when considering high convergence rates for detection processing.

Several events in the data sample from day 276 of 1971 come from azimuths different from the 302.5° steer azimuth of the time-shift-and-sum and adaptive beams which provided the signal degradation measurements for the weak event from 300°-305°. The ability to suppress such off-azimuth events is an important measure of ABF performance, particularly in detection processing. If the ABF traces are significantly weaker than the corresponding beamsteer traces for off-azimuth events, adaptive processing can reduce the number of false alarms from off-azimuth events and provide better event arrival-direction estimates. A further potential advantage is the possibility of separating interfering events. To demonstrate interfering-event separation capability, however, it must be shown that adaptive beamforming will not manipulate interfering events in such a way that they cancel each other. Table II-12 presents the power reduction relative to beamsteering at $\mu = 0.005$ and $\mu = 0.5$ over the time gates indicated for five events with azimuths away from the 302.5° steer direction. In the case of the Panama and Kamchatka events, the latter event of each pair is the stronger. If signal degradation with the new algorithm can be kept within reasonable bounds, the

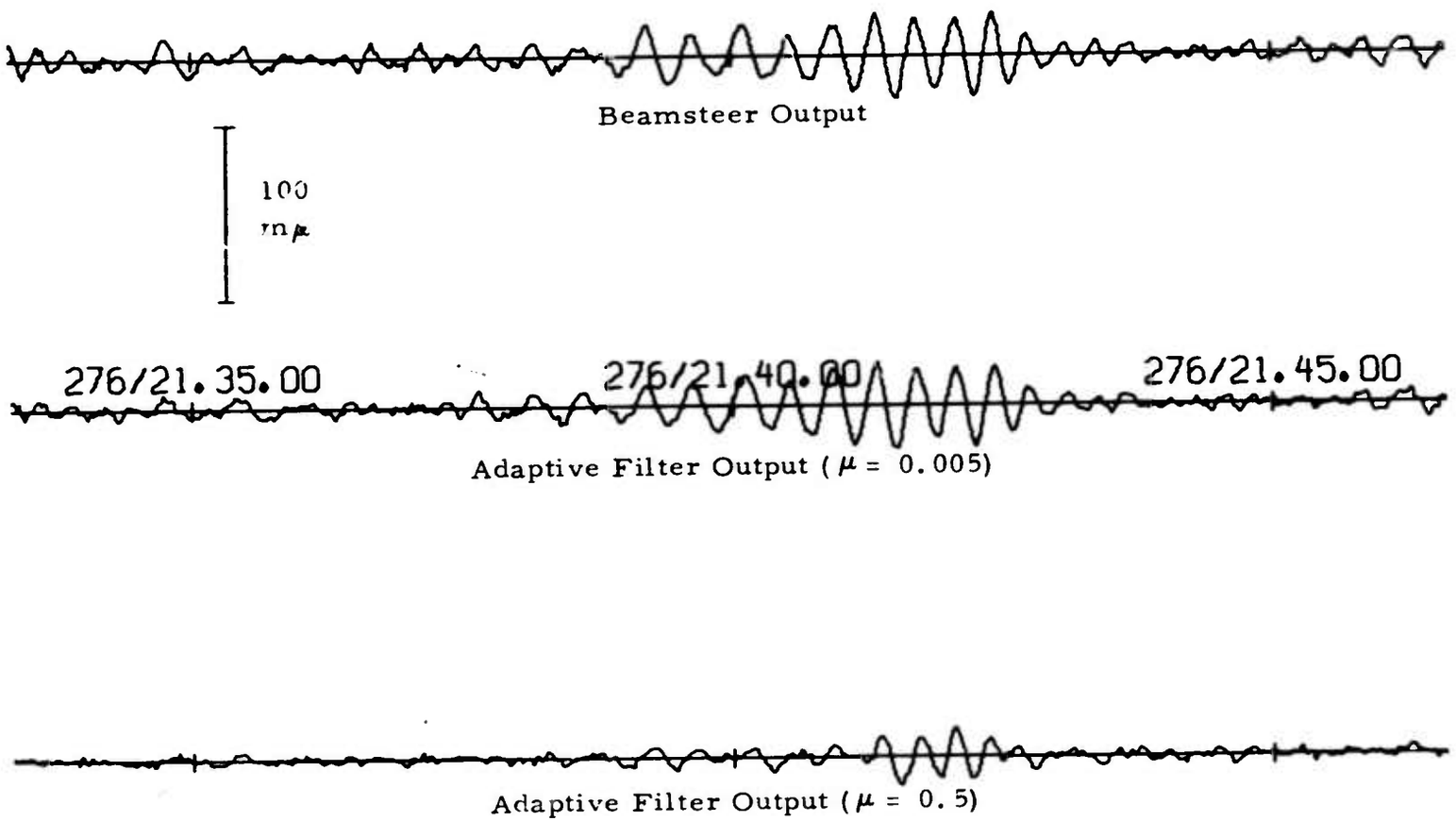

FIGURE II-20

SIX-CHANNEL BEAMS FOR WEAK EVENT FROM
300°-305° (DAY 276 1971, STEER DIRECTION 302.5°)

TABLE II-12

SIX-CHANNEL OFF-AZIMUTH EVENT
SUPPRESSION FOR 302.5° STEER DIRECTION

Event	Azimuth	Computation Gate		Power Reduction (dB)	
		Start Time	Stop Time	$\mu = 0.005$	$\mu = 0.5$
Panama	113°	20:33:00	20:40:00	6.606	17.142
Kamchatka	273°	21:07:30	21:15:00	2.531	15.815
Panama	113°	21:20:00	21:28:00	13.875	20.890
Kamchatka	273°	22:07:00	22:14:00	5.404	19.164
Andreanof Islands	237°	23:25:00	23:35:00	7.068	14.632

dramatic event-suppression values at $\mu = 0.5$ suggest that operation at high convergence rates may result in greatly improved detection capability. Figures II-21 through II-23 illustrate the ABF performance for events close to the 302.5° steer direction. The source direction is 273° for the two Kamchatka events and 237° for the Andreanof Islands event. At the convergence parameter value $\mu = 0.5$, all three events are virtually obliterated. At the slower convergence rate in the middle traces, however, the attenuation for the two Kamchatka events (30° from the steer direction) is less than for the Andreanof Islands event (65° from the steer direction). To illustrate the way in which adaptive beamforming attenuates events close to the steer direction, Figures II-24 through II-26 present ABF beam patterns at $\mu = 0.005$ for the Andreanof Islands event at 2325, 2330, and 2335. The adaptive algorithm bends the main lobe of the beam pattern array from the off-azimuth event: the maximum response (which is greater than unity) occurs at an azimuth of approximately 315° instead of 302.5°. The corresponding beamsteer response for the 302.5° steer direction was presented earlier in Figure II-18.

The last two signals used for signal degradation measurements with the new algorithm arrive from Kamchatka at an azimuth of 273°. The first of these two Kamchatka events reached ALPA at approximately 2108. Table II-13 and Figure II-27 depict signal degradation as a function of convergence rate for this event with the new adaptive algorithm. The measured degradation values with the new algorithm are much lower than with the old algorithm (Table II-5 and Figure II-5). When the signal similarity across the array is good (as in this case), the differences between the old algorithm and the new algorithm emerge: the strength and similarity of the signal result in a much slower adaptation rate for the new algorithm; the fact that this event has greater signal similarity across the array than the weak event from 300°-305°, moreover, makes it more resistant to attenuation by the adaptive algorithm. Figure II-28 is a Calcomp plot of the beamsteer output and adaptive filter

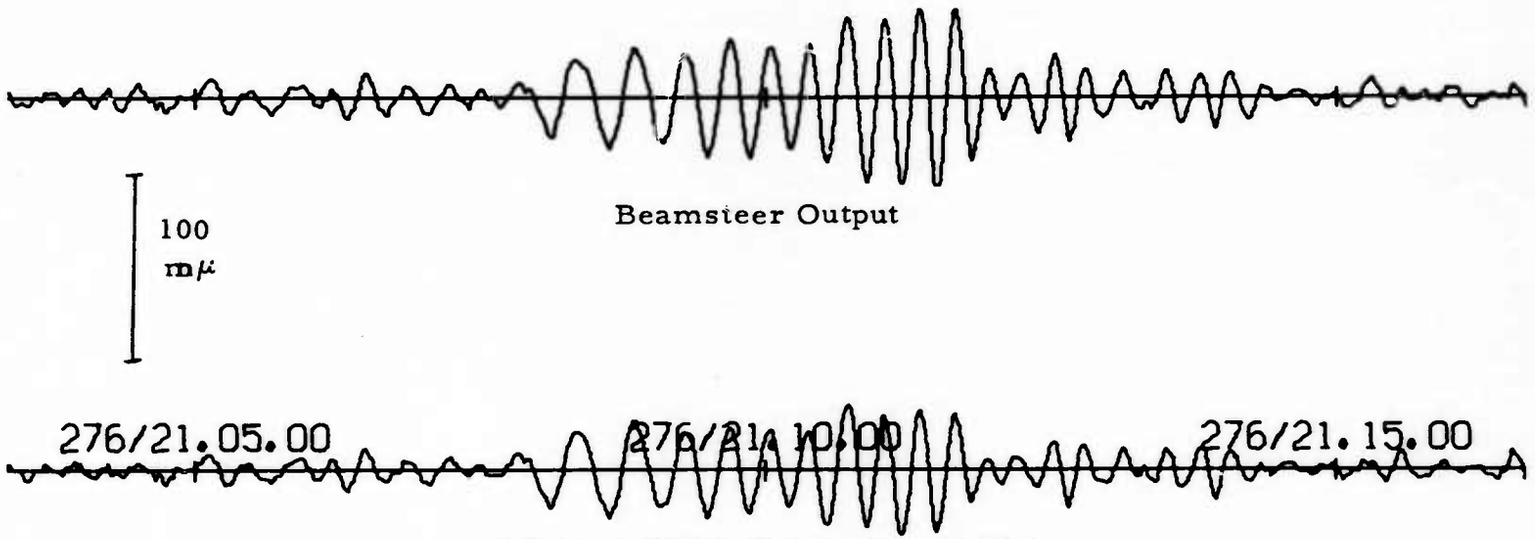

FIGURE II-21

SIX-CHANNEL BEAMS FOR MAGNITUDE 4.5 KAMCHATKA EVENT
(DAY 276 1971, STEER DIRECTION 302.5°)

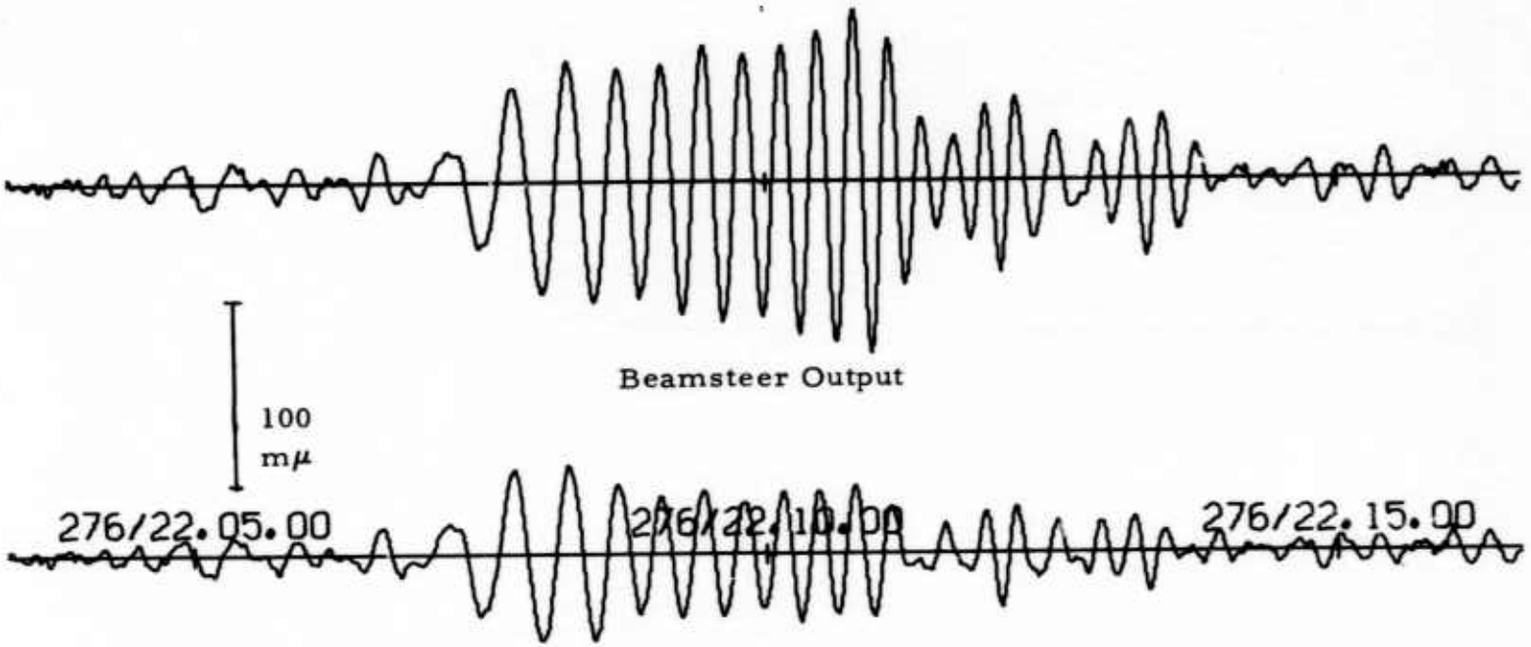

Adaptive Filter Output (μ = 0.005)

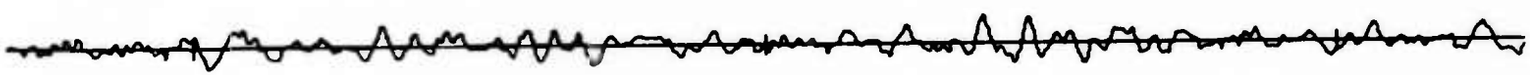

Adaptive Filter Output (μ = 0.5)

FIGURE II-22

SIX-CHANNEL BEAMS FOR MAGNITUDE 4.9
KAMCHATKA EVENT (DAY 276 1971,
STEER DIRECTION 302.5°)

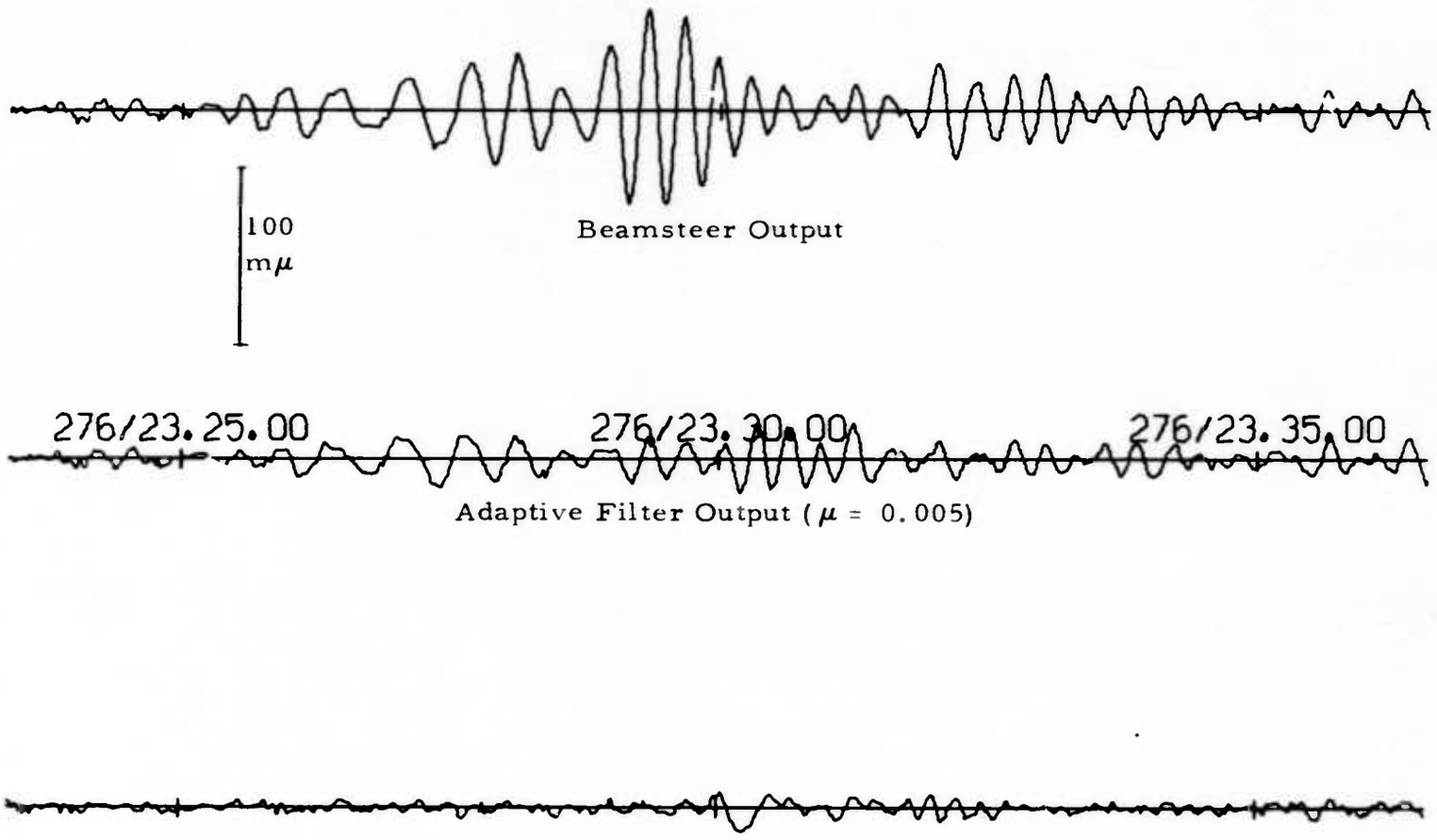

FIGURE II-23

SIX-CHANNEL BEAMS FOR MAGNITUDE 4.3
ANDREANOF ISLANDS EVENT (DAY 276 1971,
STEER DIRECTION 302.5°)

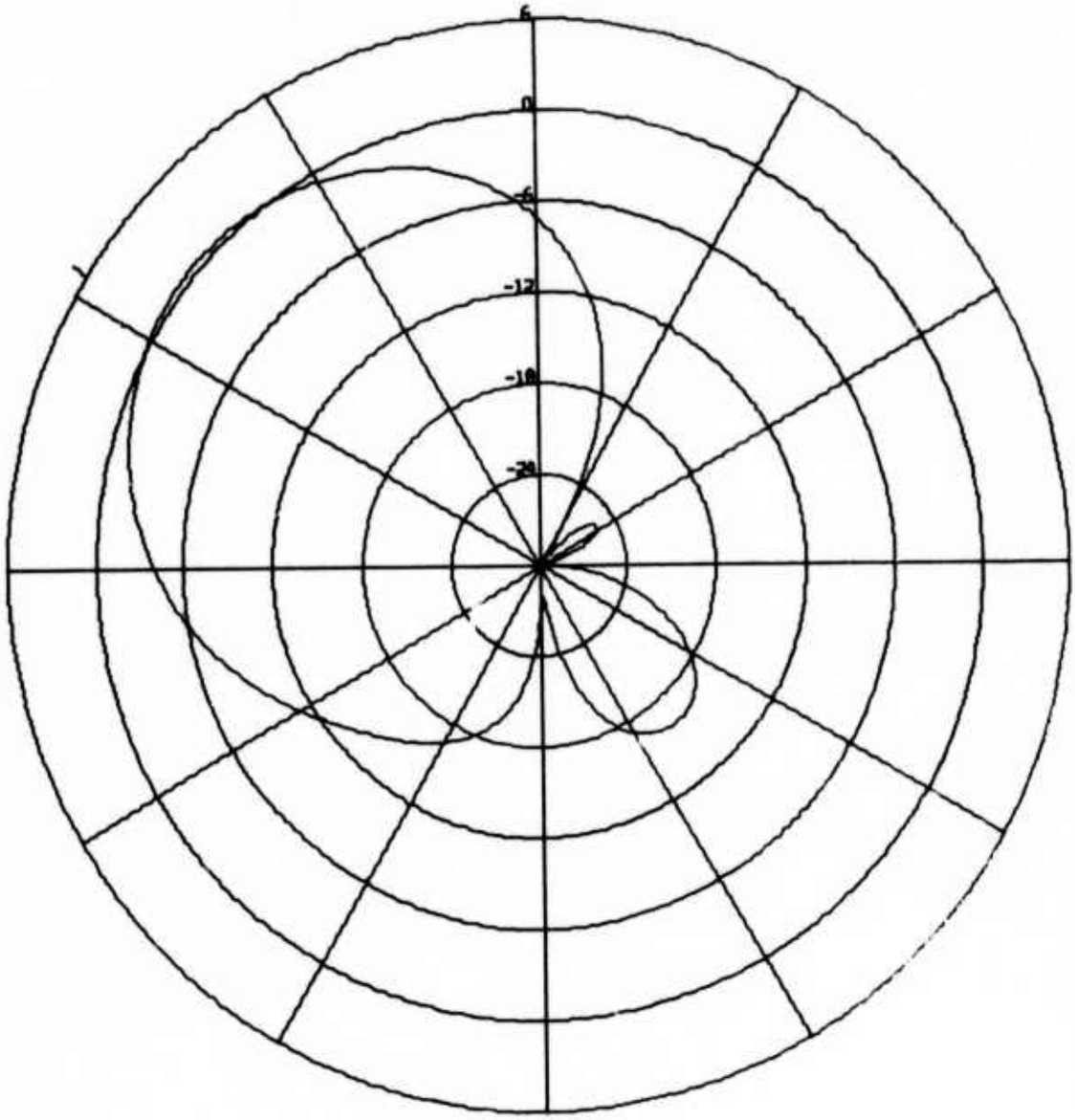

ALPA
ABF BEAM PATTERN AT 276/23.25.00
CONVERGENCE RATE IS 0.0050
BEAM LOOK VELOCITY IS 3.6, LOOK AZIMUTH 302.5
FREQUENCY IS 0.04000 HZ, PERIOD 25.0 SECONDS

FIGURE II-24

SIX-CHANNEL ABF RESPONSE FOR ANDREANOF ISLANDS EVENT AT 2325 ON DAY 276 OF 1971

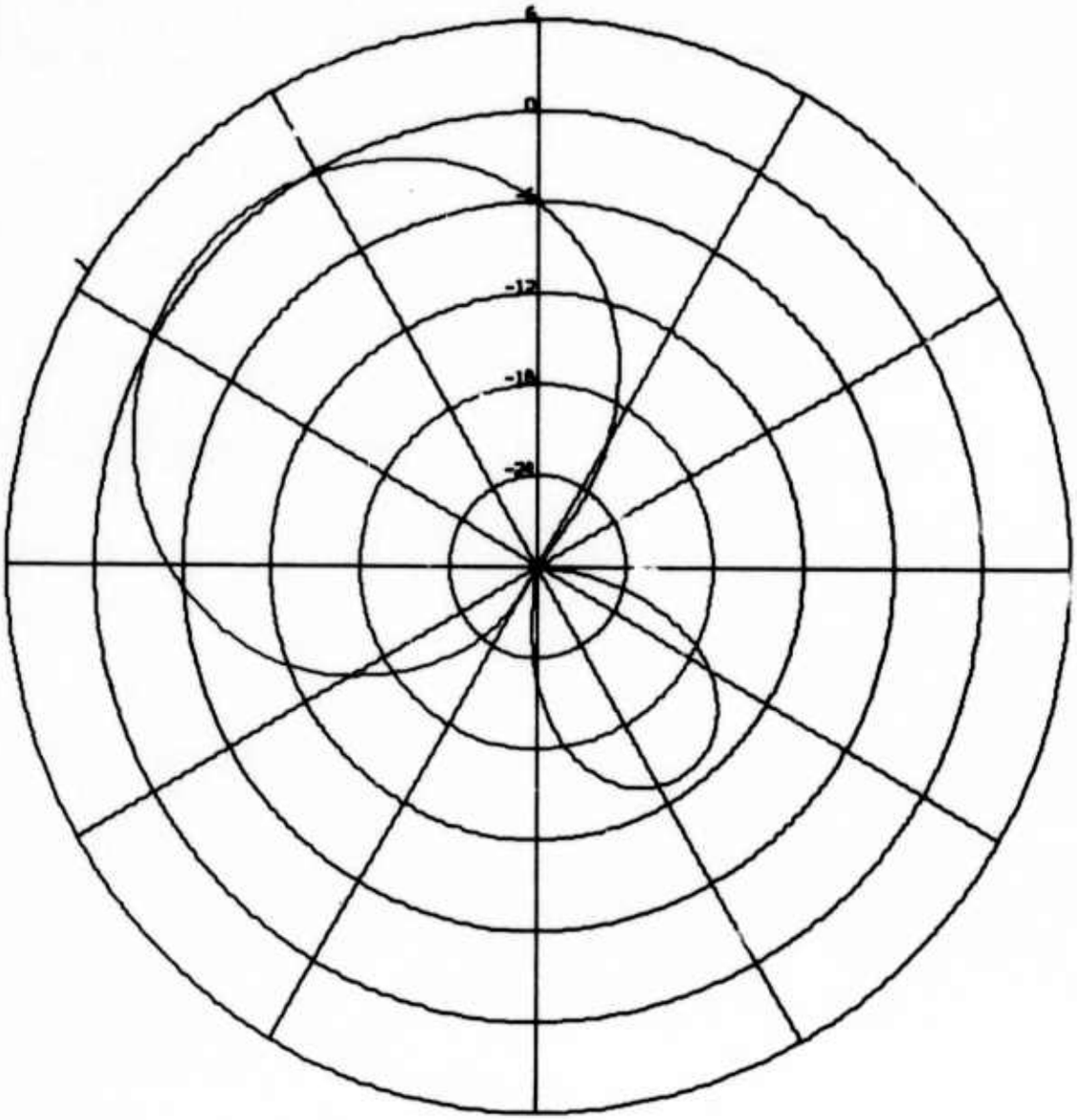

ALPA
ABF BEAM PATTERN AT 276/23.30.00
CONVERGENCE RATE IS 0.0050
BEAM LOOK VELOCITY IS 3.6, LOOK AZIMUTH 302.5
FREQUENCY IS 0.04000 HZ, PERIOD 25.0 SECONDS

FIGURE II-25

SIX-CHANNEL ABF RESPONSE FOR ANDREANOF ISLANDS
EVENT AT 2330 ON DAY 276 OF 1971

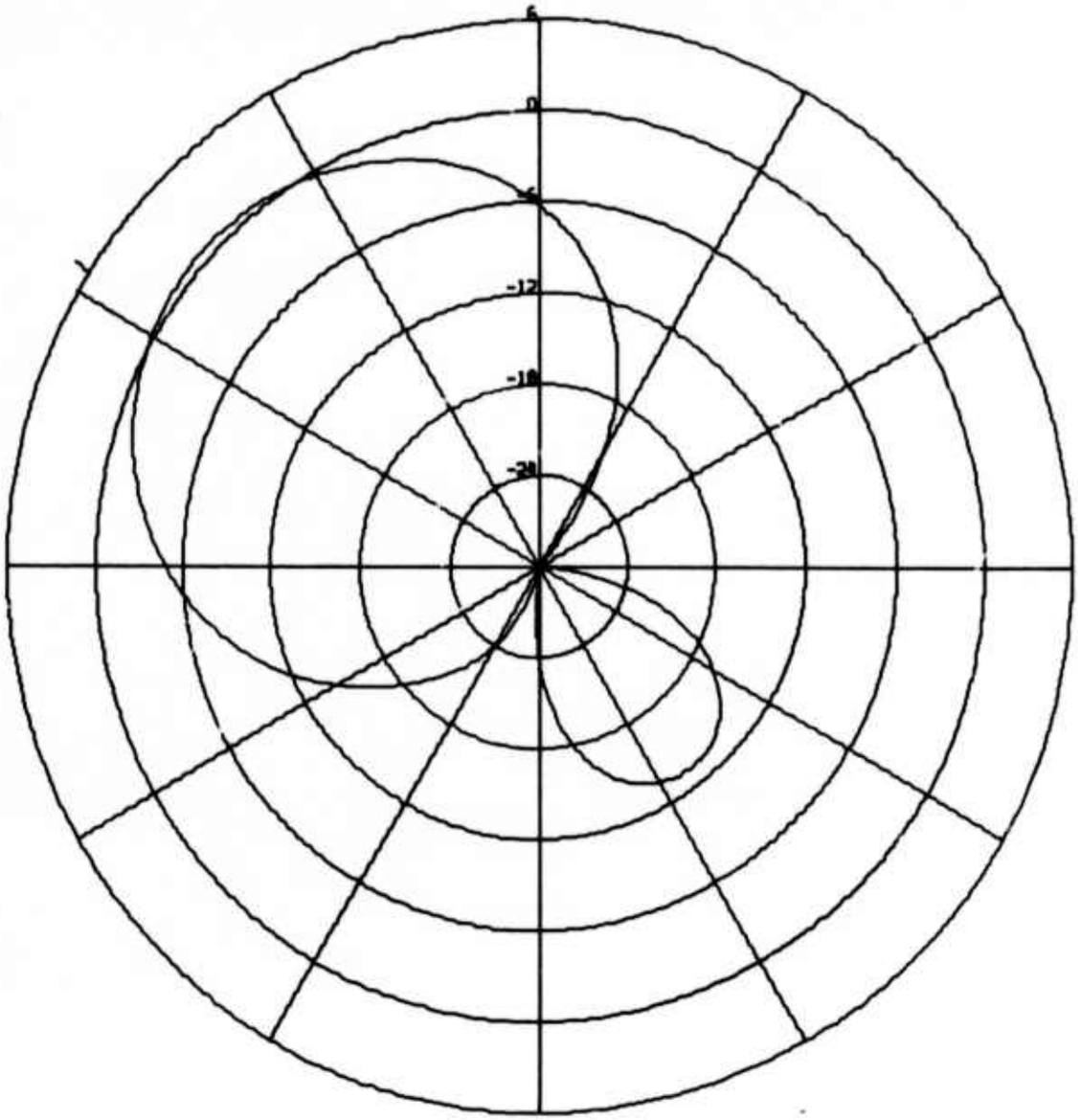

ALPA
ABF BEAM PATTERN AT 276/23.35.00
CONVERGENCE RATE IS 0.0050
BEAM LOOK VELOCITY IS 3.6, LOOK AZIMUTH 302.5
FREQUENCY IS 0.04000 HZ, PERIOD 25.0 SECONDS

FIGURE II-26

SIX-CHANNEL ABF RESPONSE FOR ANDREANOF ISLANDS
EVENT AT 2335 ON DAY 276 OF 1971

TABLE II-13

ADAPTIVE FILTERING SIGNAL DEGRADATION VERSUS CONVERGENCE RATE WITH NEW ALGORITHM FOR A STRONG SIGNAL FROM KAMCHATKA (ALPA, 6 SITES, 1971 DAY 276 21.07.18-21.11.33)

Convergence Rate (μ)	Signal Degradation (dB)
0.0010	0.031
0.0015	0.047
0.0020	0.062
0.0030	0.092
0.0040	0.118
0.0050	0.141
0.0070	0.177
0.0100	0.214
0.0150	0.246
0.0200	0.262
0.0300	0.281
0.0400	0.304
0.0500	0.336
0.0700	0.418
0.1000	0.551
0.1500	0.722
0.2000	0.814
0.3000	0.853
0.4000	0.819
0.5000	0.777

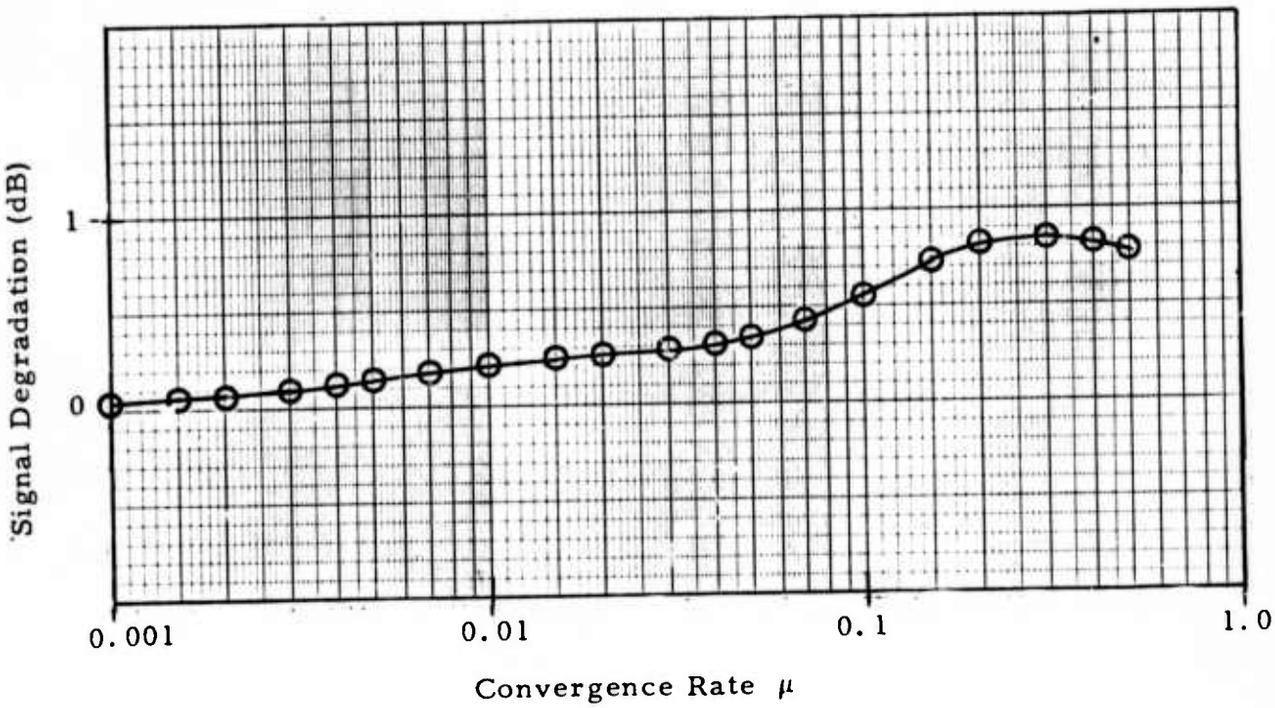

FIGURE II-27

SIGNAL DEGRADATION AS A FUNCTION OF CONVERGENCE RATE WITH NEW ALGORITHM FOR A STRONG SIGNAL FROM KAMCHATKA (ALPA, 6 SITES, 1971 DAY 276 21.07.18-21.11.33)

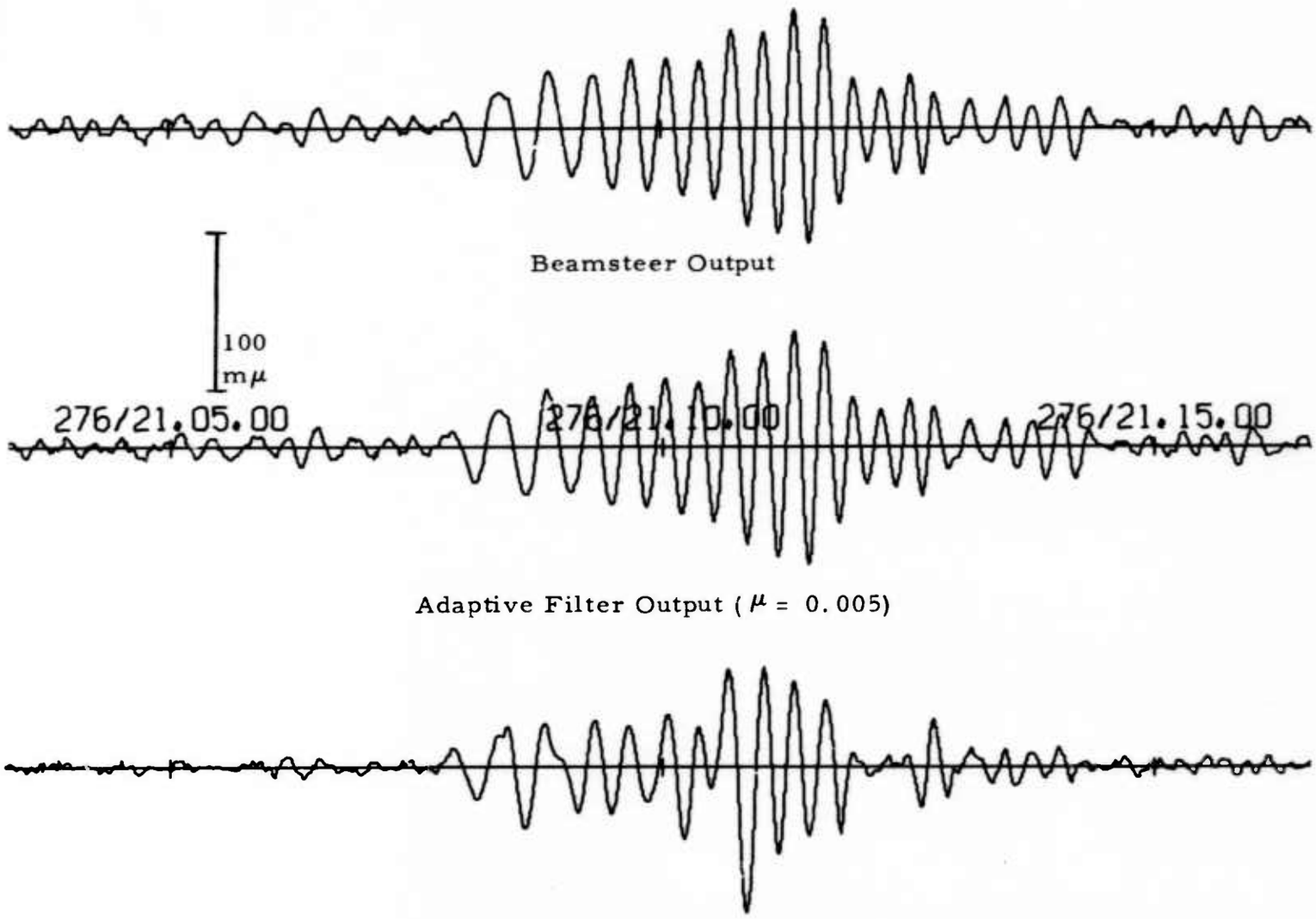

FIGURE II-28

SIX-CHANNEL BEAMS FOR MAGNITUDE 4.5 KAMCHATKA EVENT
(DAY 276 1971, STEER DIRECTION 273°)

outputs at $\mu = 0.005$ and $\mu = 0.5$ for this event with the new adaptive algorithm. The differences between the beamsteer output and the ABF output at the slower convergence rate are slight. Even at the more rapid rate, the ABF output is only slightly attenuated, although signal distortion is clearly evident. Table II-14 and Figure II-29 present the estimated signal-to-noise ratio improvement as a function of convergence rate for this event using noise reduction measurements from day 238 of 1970. The greatest gain relative to beamsteering occurs at $\mu = 0.5$, where the estimated improvement is 5.75 dB. Despite the signal distortion in the bottom trace of Figure II-28, the 5.75 dB gain estimate is definitely relevant for detection processing.

The second Kamchatka event reached ALPA at approximately 2207. Signal degradation as a function of convergence rate for this event with the new adaptive algorithm appears in Table II-15 and Figure II-30. Not only is the degradation slight for this event, but, indeed, even negative at the highest convergence rates. The amplification of the second Kamchatka event at $\mu = 0.5$ is illustrated by the bottom trace in Figure II-31. In contrast, the adaptive-filter output at $\mu = 0.005$ (the middle trace) is almost a carbon copy of the beamsteer output in the top trace. Table II-16 and Figure II-32 give the estimated signal-to-noise ratio improvement as a function of convergence rate for this event with the new adaptive algorithm (using noise reduction measurements from day 238 of 1970). Maximum estimated gain of 7.5 dB is realized at the highest convergence rate. The gain estimates for the new algorithm are distinctly higher than for the old algorithm (see Table II-8 and Figure II-8). The sharply improved performance is due to the greatly reduced effective adaptation rate of the new algorithm and the good signal similarity of the second Kamchatka event between sites.

Four of the events in the data sample from day 276 of 1971 arrive at azimuths different from the 273° steer azimuth used for the two Kamchatka events. Table II-17 gives the power reduction relative to beamsteering at

TABLE II-14

ADAPTIVE FILTERING SIGNAL-TO-NOISE GAIN VERSUS CONVERGENCE RATE WITH NEW ALGORITHM FOR A STRONG SIGNAL FROM KAMCHATKA (ALPA, 6 SITES, 1971 DAY 276 21.07.18-21.11.33, USING NOISE FROM 1970 DAY 238 0800-1145)

Convergence Rate (μ)	Signal-to-Noise Gain (dB)
0.0010	0.610
0.0015	0.778
0.0020	0.907
0.0030	1.091
0.0040	1.216
0.0050	1.306
0.0070	1.432
0.0100	1.558
0.0150	1.714
0.0200	1.844
0.0300	2.071
0.0400	2.267
0.0500	2.439
0.0700	2.728
0.1000	3.077
0.1500	3.570
0.2000	4.015
0.3000	4.791
0.4000	5.374
0.5000	5.750

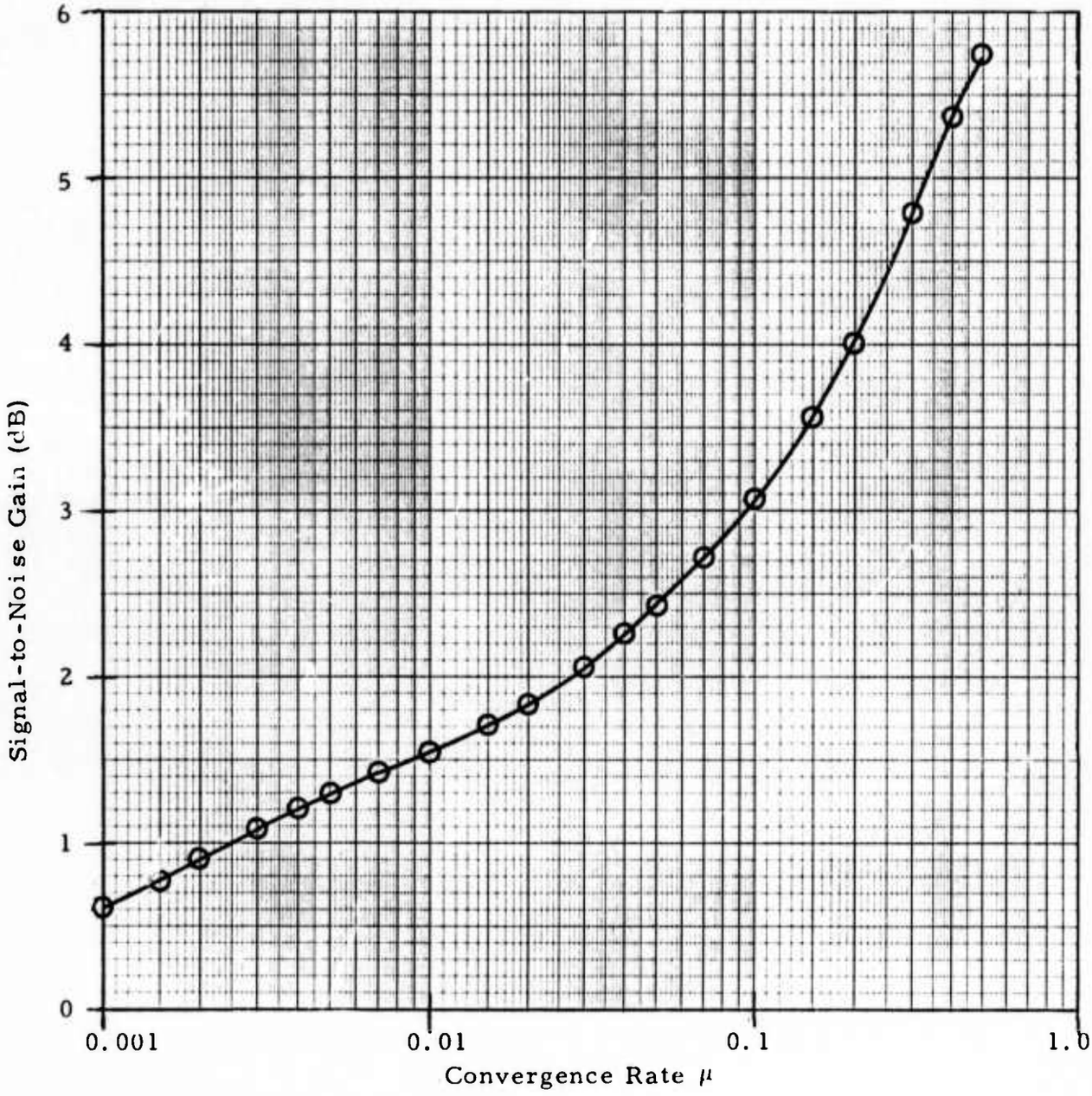

FIGURE II-29

SIGNAL-TO-NOISE GAIN AS A FUNCTION OF CONVERGENCE RATE WITH NEW ALGORITHM FOR A STRONG SIGNAL FROM KAMCHATKA (ALPA, 6 SITES, 1971 DAY 276 21.07.18-21.11.33, USING NOISE FROM 1970 DAY 238 0800-1145)

TABLE II-15

ADAPTIVE FILTERING SIGNAL DEGRADATION VERSUS CONVERGENCE RATE WITH NEW ALGORITHM FOR A VERY STRONG SIGNAL FROM KAMCHATKA (ALPA, 6 SITES, 1971 DAY 276 22.07.02-22.11.17)

Convergence Rate (μ)	Signal Degradation (dB)
0.0010	0.066
0.0015	0.093
0.0020	0.115
0.0030	0.145
0.0040	0.164
0.0050	0.177
0.0070	0.197
0.0100	0.223
0.0150	0.255
0.0200	0.276
0.0300	0.289
0.0400	0.279
0.0500	0.255
0.0700	0.185
0.1000	0.055
0.1500	-0.173
0.2000	-0.379
0.3000	-0.688
0.4000	-0.885
0.5000	-1.018

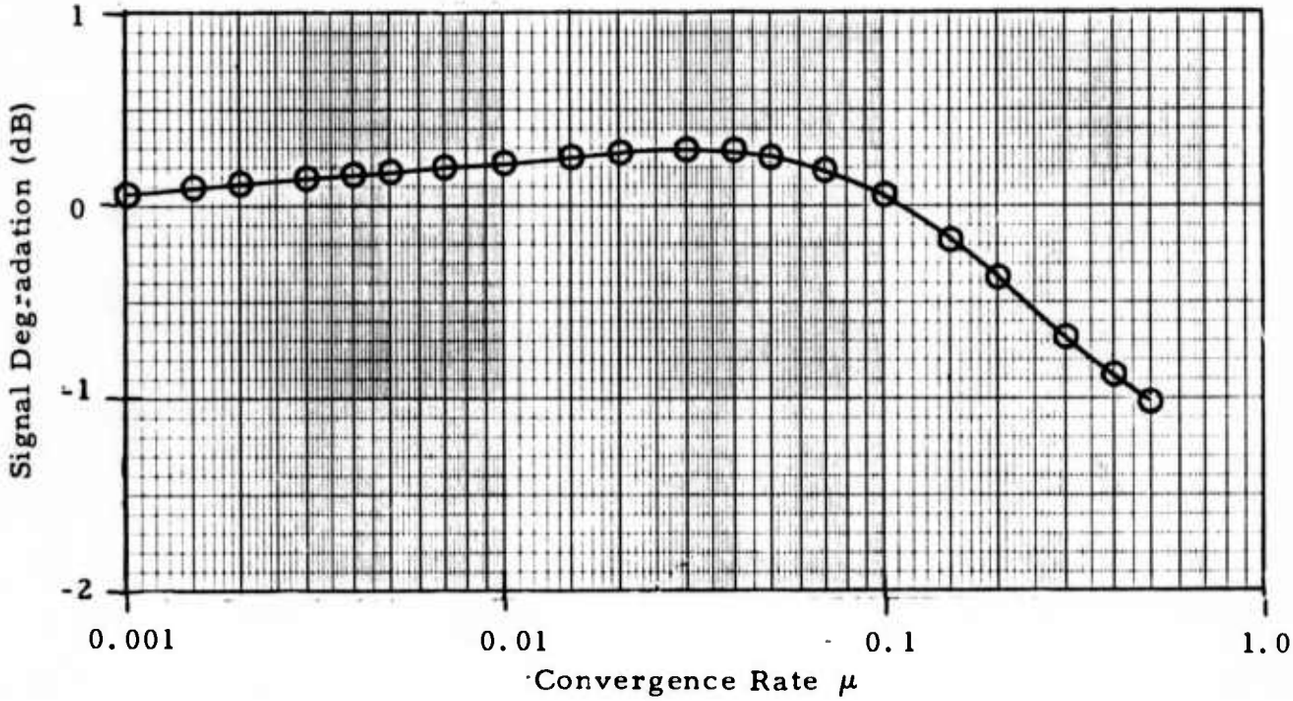

FIGURE II-30

SIGNAL DEGRADATION AS A FUNCTION OF CONVERGENCE RATE WITH NEW ALGORITHM FOR A VERY STRONG SIGNAL FROM KAMCHATKA (ALPA, 6 SITES, 1971 DAY 276 22.07.02-22.11.17)

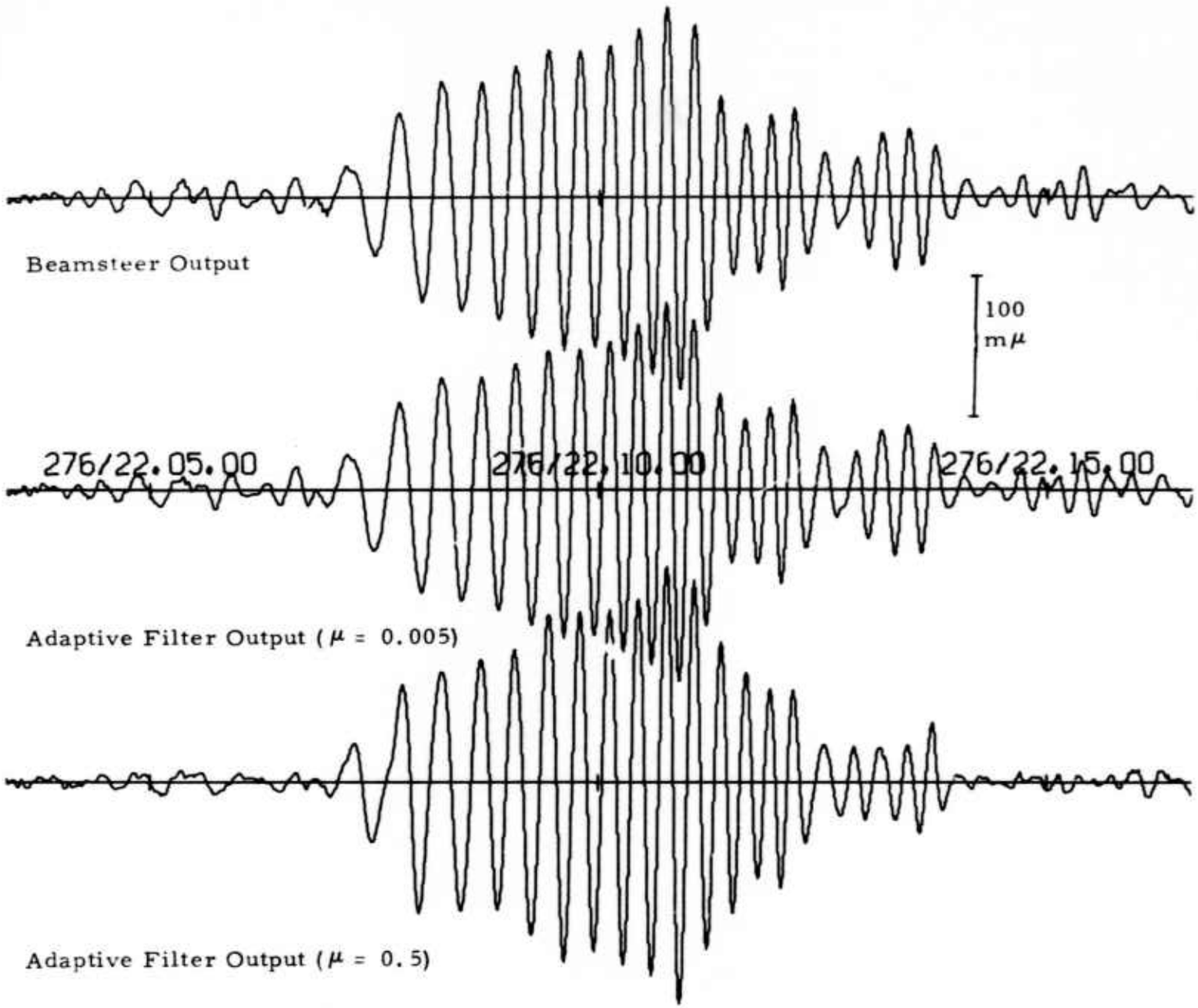

FIGURE II-31

SIX-CHANNEL BEAMS FOR A MAGNITUDE 4.9 KAMCHATKA EVENT
(DAY 276 1971, STEER DIRECTION 273°)

TABLE II-16

ADAPTIVE FILTERING SIGNAL-TO-NOISE GAIN VERSUS CONVERGENCE RATE WITH NEW ALGORITHM FOR A VERY STRONG SIGNAL FROM KAMCHATKA (ALPA, 6 SITES, 1971 DAY 276 22.07.02-22.11.17, USING NOISE FROM 1970 DAY 238 0800-1145)

Convergence Rate (μ)	Signal-to-Noise Gain (dB)
0.0010	0.575
0.0015	0.732
0.0020	0.854
0.0030	1.038
0.0040	1.170
0.0050	1.270
0.0070	1.412
0.0100	1.549
0.0150	1.705
0.0200	1.830
0.0300	2.063
0.0400	2.292
0.0500	2.520
0.0700	2.961
0.1000	3.573
0.1500	4.465
0.2000	5.208
0.3000	6.332
0.4000	7.078
0.5000	7.545

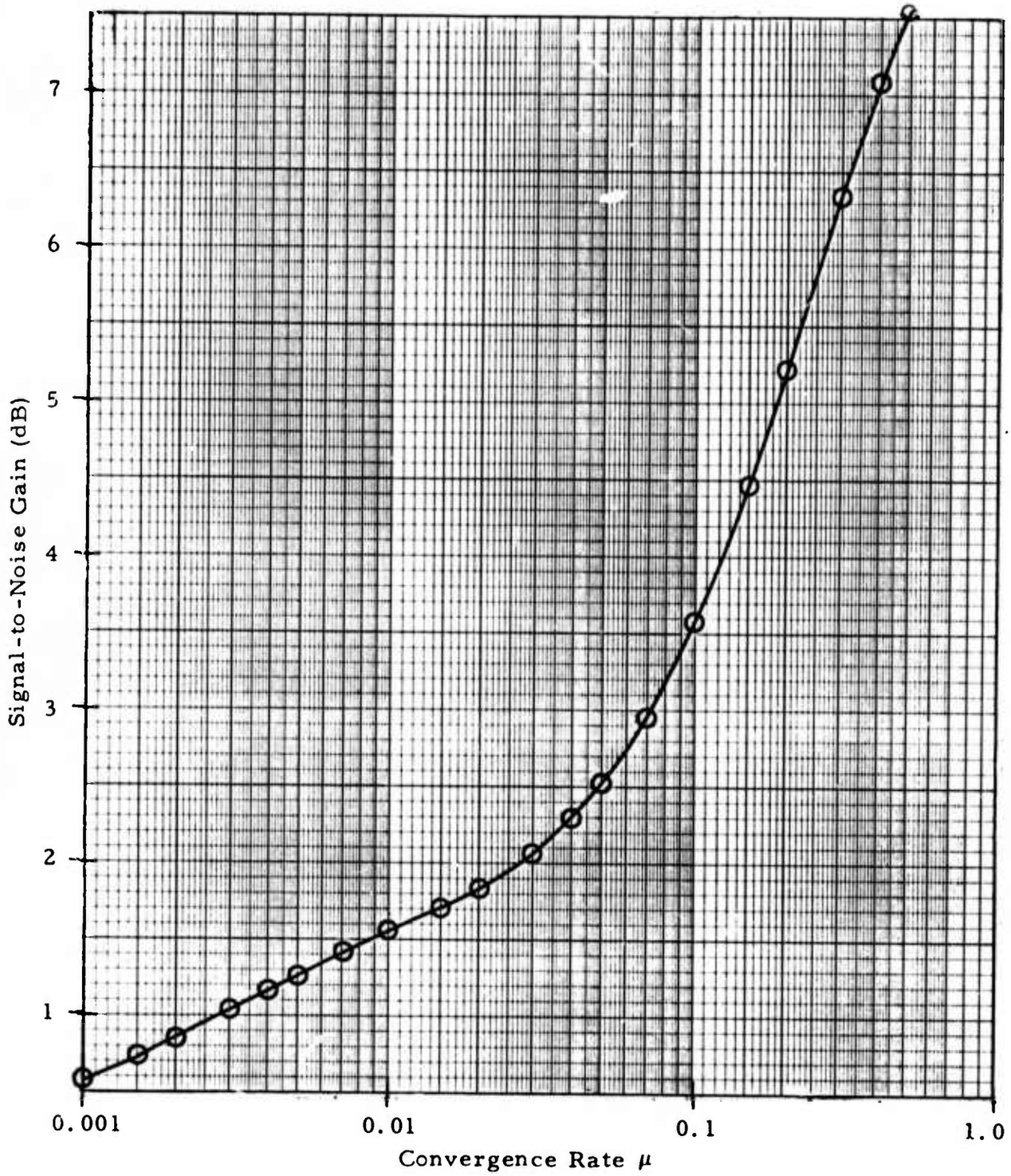

FIGURE II-32

SIGNAL-TO-NOISE GAIN AS A FUNCTION OF CONVERGENCE RATE WITH NEW ALGORITHM FOR A VERY STRONG SIGNAL FROM KAMCHATKA (ALPA, 6 SITES, 1971 DAY 276 22.07.02-22.11.17, USING NOISE FROM 1970 DAY 238 0800-1145)

TABLE II-17

SIX-CHANNEL OFF-AZIMUTH EVENT SUPPRESSION
FOR 273° STEER DIRECTION

Event	Azimuth	Computation Gate		Power Reduction (dB)	
		Start Time	Stop Time	$\mu = 0.005$	$\mu = 0.5$
Panama	113°	20:33:00	20:40:00	6.954	14.593
Panama	113°	21:20:[illegible]	21:28:00	13.973	18.869
Weak Event	302.5°	21:38:00	21:43:00	0.107	6.808
Andreanof Islands	237°	23:25:00	23:35:00	4.559	15.616

$\mu = 0.005$ and $\mu = 0.5$ for these four events. Except in the case of the weak event from 300°-305°, these events are attenuated by more than 12 dB at $\mu = 0.5$. Figure II-33 shows the beamsteer output and the adaptive filter output at $\mu = 0.005$ and $\mu = 0.5$ for the first Panama event. Figure II-34 is a plot of the corresponding beams for the other Panama event. The associated adaptive beam patterns in Figure II-35 through II-37 reflect the strong suppression of this event at $\mu = 0.005$. In the case of this event (160° away from the steer azimuth), the beam patterns at the times 2120, 2124, and 2128 illustrate the ability of adaptive processing to form deep nulls in the direction of off-azimuth energy sources. For purposes of comparison, the six-channel time-shift-and-sum pattern for a 273° steer azimuth appears in Figure II-38. The weak event from 300°-305° is portrayed in Figure II-39. At an azimuthal separation of 30° from the steer direction, the event is only slightly diminished relative to the beamsteer output in the adaptive filter output for $\mu = 0.005$ (the middle trace). Curiously enough, the ABF output for this event at $\mu = 0.5$ is stronger near the beginning than near the end. The converse was true for the corresponding adaptive beam at a steer azimuth of 302.5° (Figure II-20). Perhaps the arrival azimuth shifts significantly during this event. Another possioility is that two distinct earthquakes have arrived simultaneously at ALPA in the time period shown in Figure II-39. A situation such as this might explain the lack of signal similarity for this event. Figure II-40 shows the beam outputs for the Andreanof Islands event. Here, where the steer azimuth is only 36° from the event arrival azimuth, the signal is much stronger than in the beams for the 302.5° steer azimuth (Figure II-23), where the azimuthal separation is 65°. Even at $\mu = 0.5$, the signal is not completely eliminated.

The results presented so far in this section demonstrate the clear superiority of the new adaptive algorithm. This superiority manifests itself primarily in the form of reduced signal degradation. The differences are

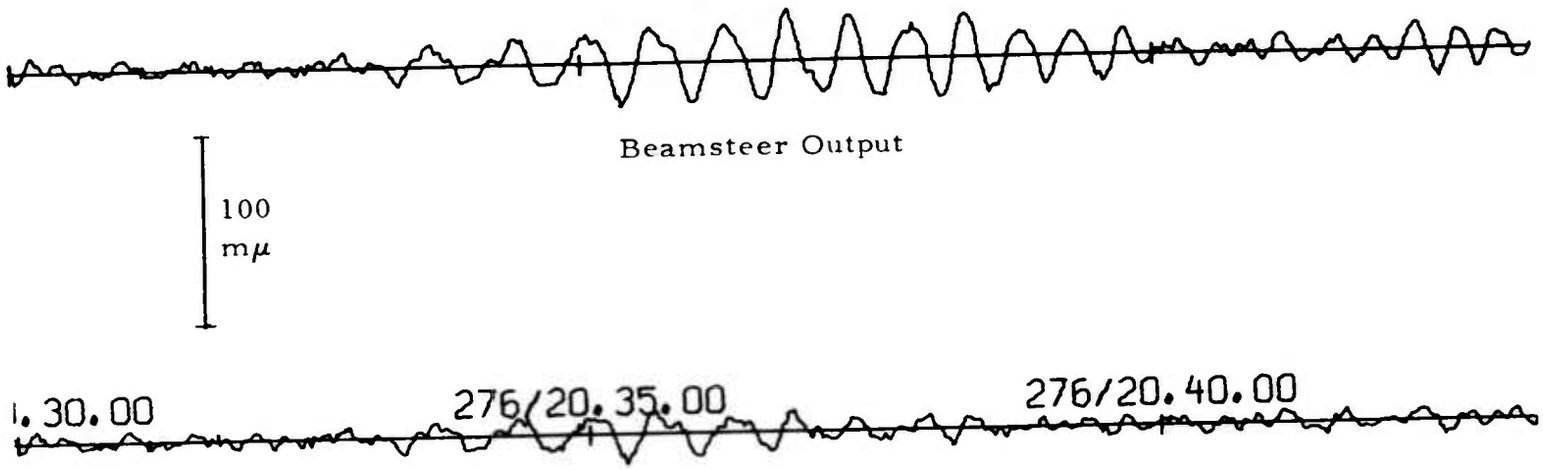

FIGURE II-33

SIX-CHANNEL BEAMS FOR MAGNITUDE 3.6 PANAMA EVENT
(DAY 276 1971, STEER DIRECTION 273°)

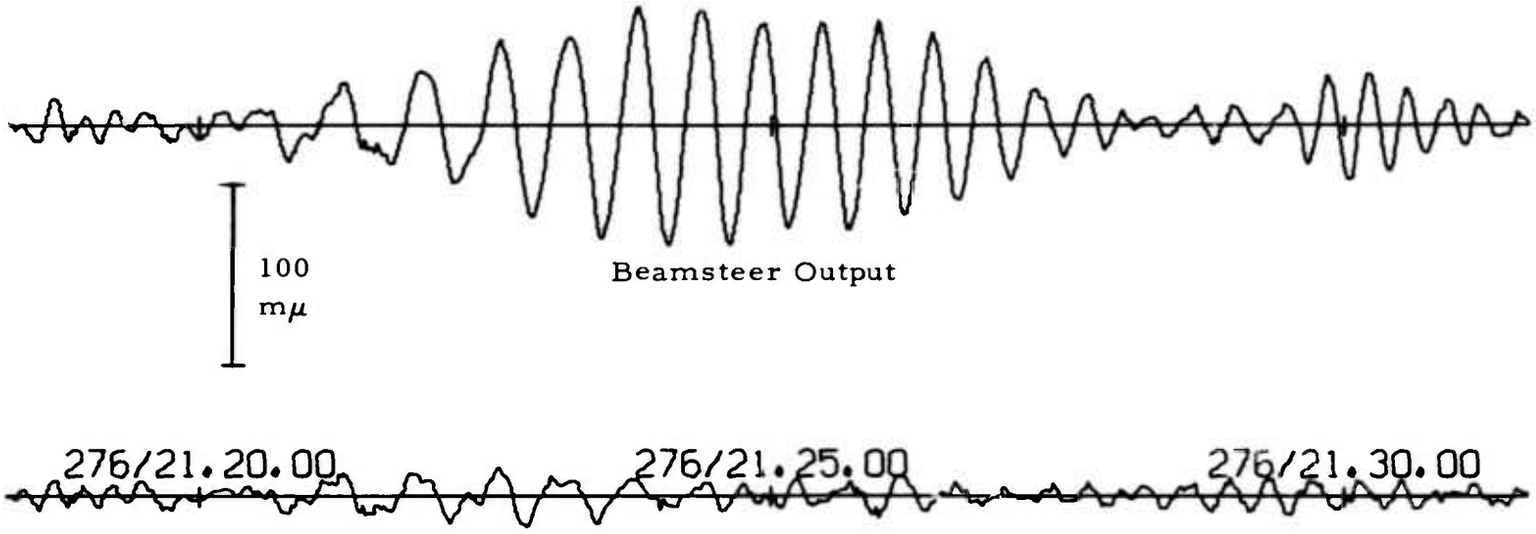

FIGURE II-34

SIX-CHANNEL BEAMS FOR MAGNITUDE 4.7 PANAMA EVENT
(DAY 276 1971, STEER DIRECTION 273°)

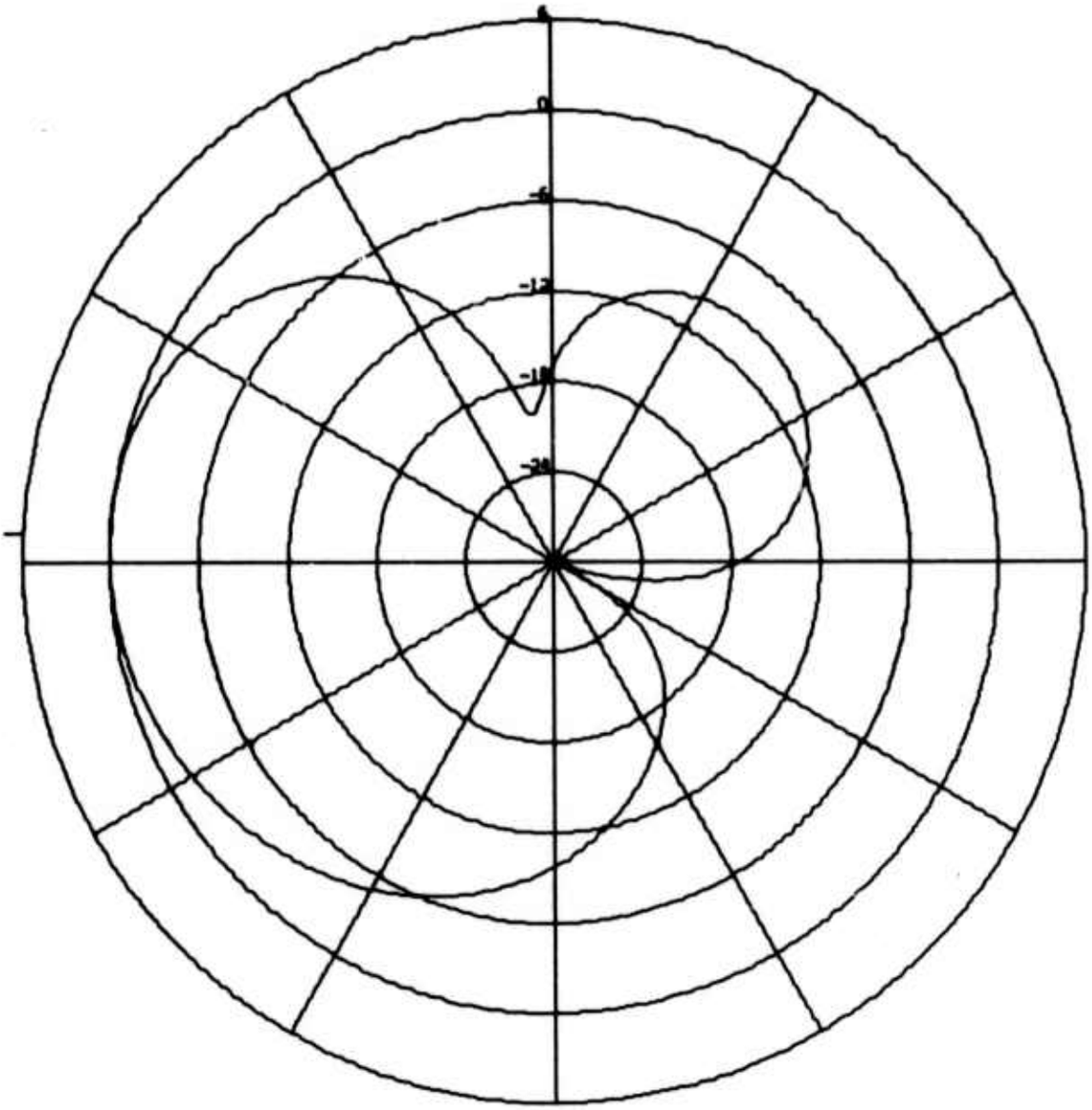

ALPA
ABF BEAM PATTERN AT 276/21.20.00
CONVERGENCE RATE IS 0.0050
BEAM LOOK VELOCITY IS 3.6, LOOK AZIMUTH 273.0
FREQUENCY IS 0.04000 HZ, PERIOD 25.0 SECONDS

FIGURE II-35

SIX-CHANNEL ABF RESPONSE FOR MAGNITUDE 4.7 PANAMA EVENT AT 2120 ON DAY 276 OF 1971

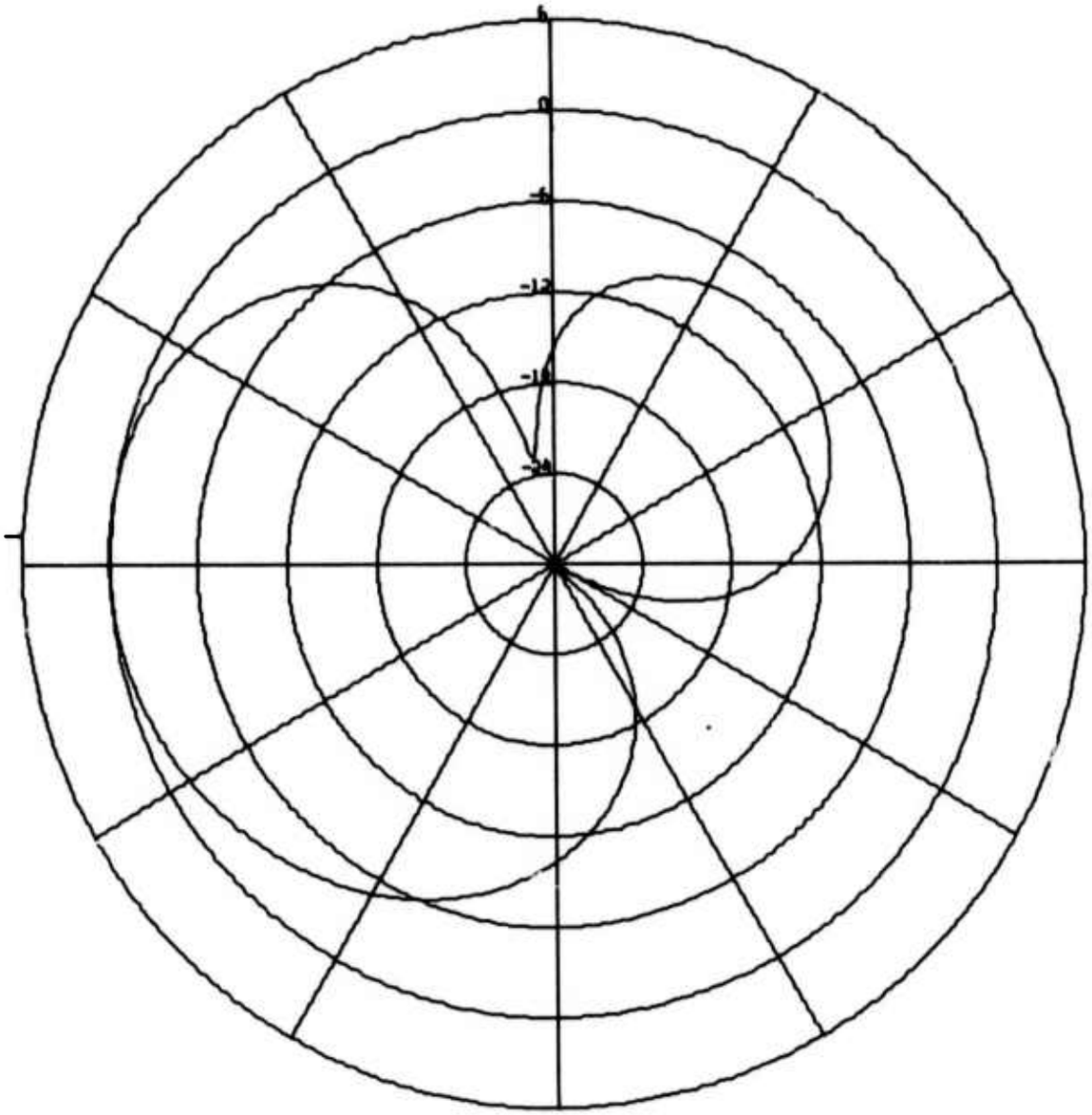

FIGURE II-36

SIX-CHANNEL ABF RESPONSE FOR MAGNITUDE 4.7 PANAMA EVENT AT 2124 ON DAY 276 OF 1971

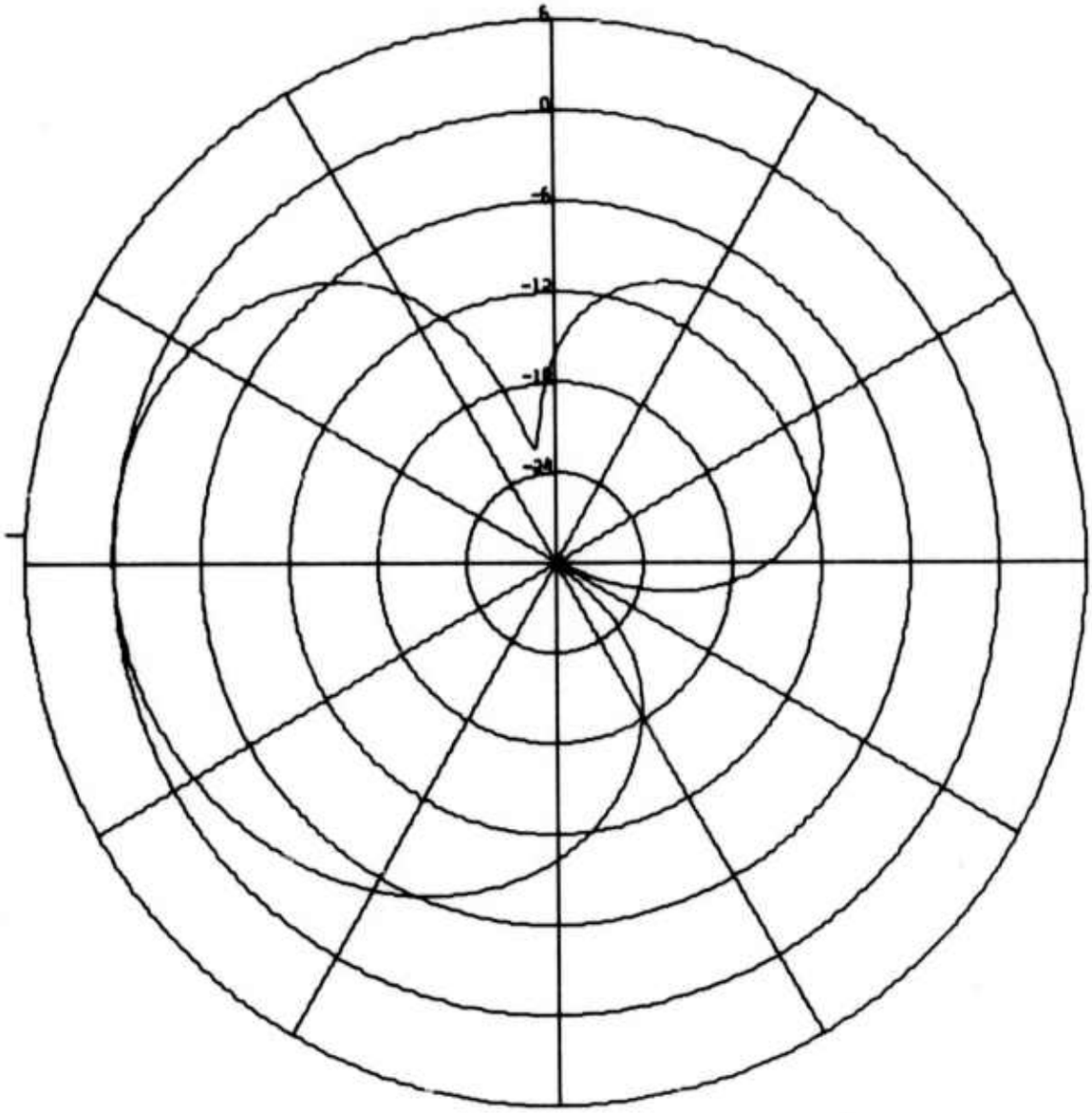

ALPA
ABF BEAM PATTERN AT 276/21.28.00
CONVERGENCE RATE IS 0.0050
BEAM LOOK VELOCITY IS 3.6, LOOK AZIMUTH 273.0
FREQUENCY IS 0.04000 HZ, PERIOD 25.0 SECONDS

FIGURE II-37

SIX-CHANNEL ABF RESPONSE FOR MAGNITUDE
4.7 PANAMA EVENT AT 2128 ON DAY 276 OF 1971

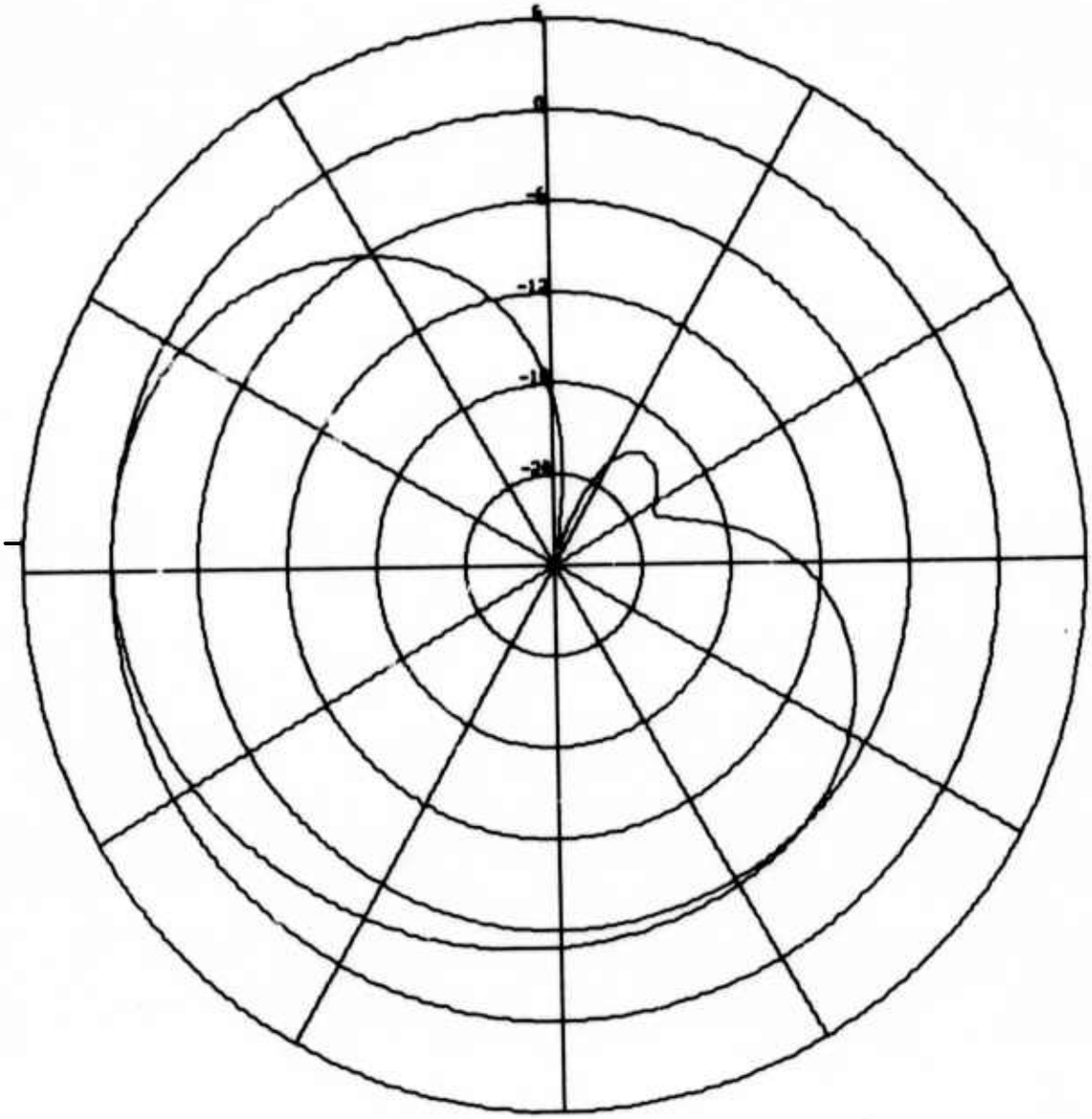

ALPA
TIME-SHIFT-AND-SUM BEAM PATTERN
BEAM LOOK VELOCITY IS 3.6, LOOK AZIMUTH 273.0
FREQUENCY IS 0.04000 HZ, PERIOD 25.0 SECONDS

FIGURE II-38

BEAMSTEER RESPONSE FOR SIX-CHANNEL SAMPLE
FROM DAY 276 OF 1971

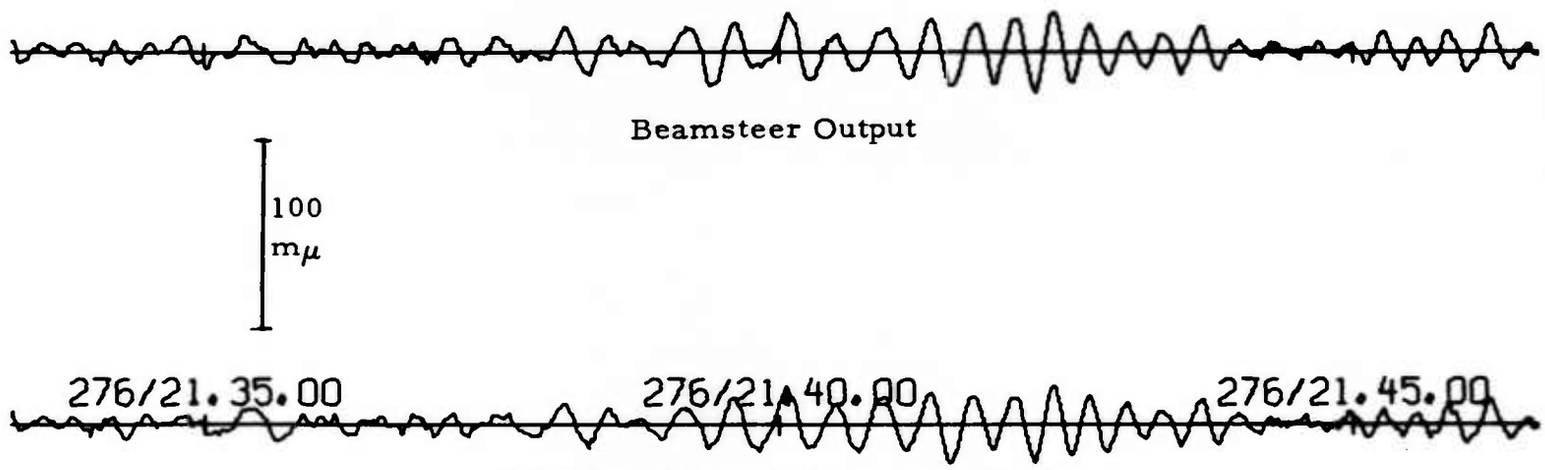

FIGURE II-39

SIX-CHANNEL BEAMS FOR WEAK EVENT FROM 300°-305°
(DAY 276 1971, STEER DIRECTION 273°)

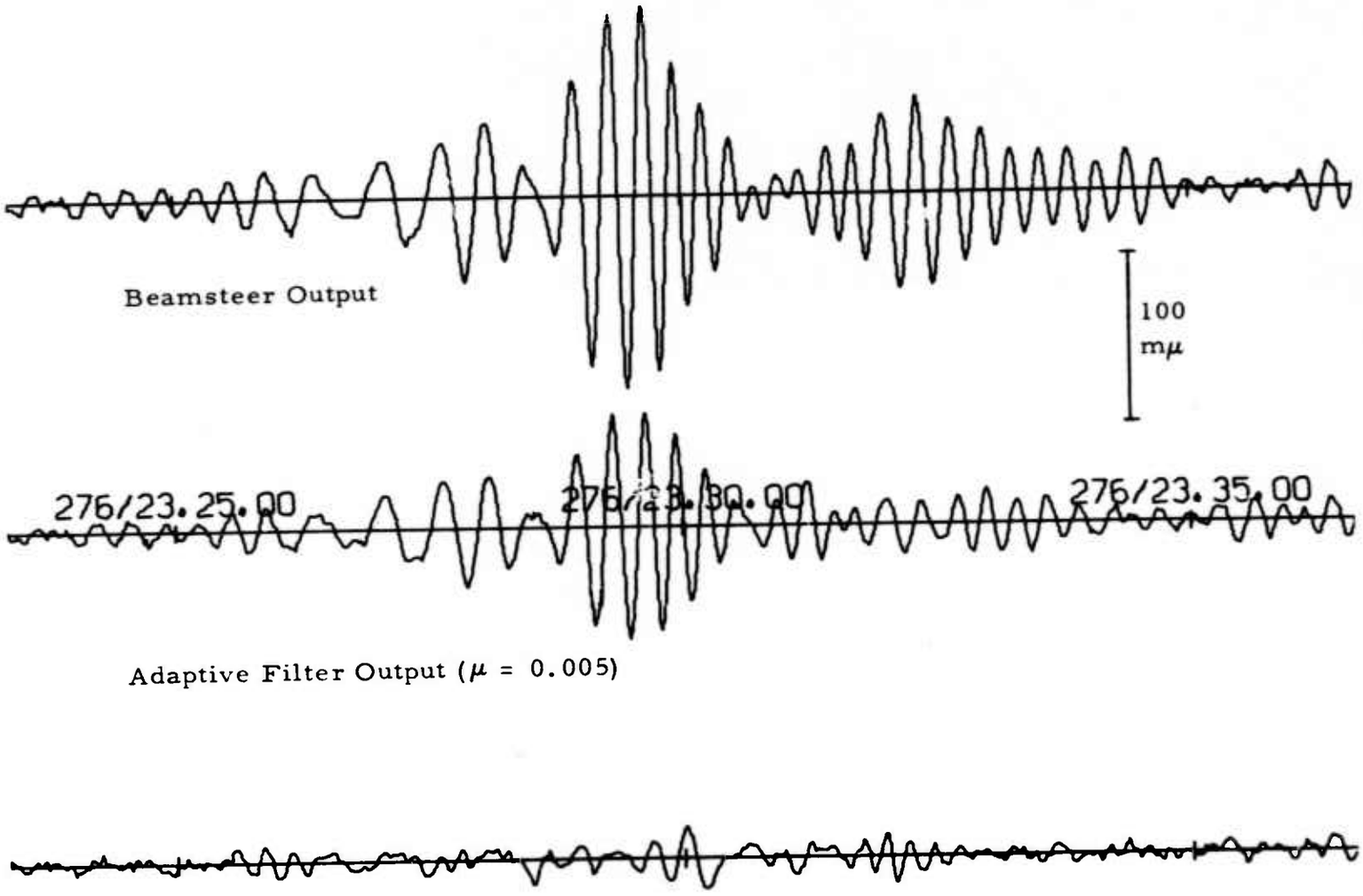

FIGURE II-40

SIX-CHANNEL BEAMS FOR ANDREANOF ISLANDS EVENT
(DAY 276 1971, STEER DIRECTION 273°)

particularly dramatic for the two Kamchatka events, which are strong events with good signal similarity. For the weak event from 300^{o}-305^{o}, the improvement in signal-to-noise gain with the new algorithm is only slight. The probable explanation is the poor signal similarity of this event. With the new adaptive algorithm, the best signal-to-noise gains occur at the most rapid convergence rate in the case of the two Kamchatka events. Even for the weak event from 300^{o}-305^{o}, the gain at $\mu = 0.5$ is only one dB less than the gain at $\mu = 0.005$. In detection processing, where signal distortion is a relatively minor consideration, these results suggest that significantly improved detection capability for events with good signal similarity is possible at high convergence rates. The probable price to be paid for this improved detection performance is a somewhat reduced capability with signals such as the weak event from 300^{o}-305^{o}, where the signal similarity is poor. Another effect of operating at rapid convergence rates is a narrowing of the adaptive processor beamwidth, as indicated by the greater suppression of off-azimuth events (see Tables II-12 and II-17). In one sense, the effect is beneficial since the direction of incoming events can be more accurately determined. In an operational surveillance mode, however, the improved resolution at high convergence rates raises the number of beams required to scan all azimuths without gaps in coverage. With reduced background noise levels at fast convergence rates, the probability of time-overlapped events is greater than the 0.05 - 0.10 figure normally given for ALPA. The off-azimuth event suppression results suggest, at least, that rapid adaptation can reduce the number of times that one event masks another.

D. ADAPTIVE PROCESSING WITH THE FULL ARRAY

The purpose of this subsection is to evaluate adaptive processing which uses all available sensors at ALPA as input to the time-shift-and-sum and adaptive beamformers. Of particular interest are any differences

between the full-array results and the results obtained with closely-spaced six-channel arrays such as the ones employed in Subsection C. Since the new adaptive algorithm outperforms the old adaptive algorithm, all adaptive beams in this subsection and the remainder of this report are formed with the new adaptive algorithm.

During 1970, a maximum of nine sensors were operational at ALPA. In order to compare full-array results with six-channel results, a noise sample from 0415 to 0815 on day 335 of 1972 was selected to replace the noise sample from day 238 of 1970. For the six-channel noise reduction measurements, the vertical components from sites 1, 2, 3, 6, 8, and 9 are input to the time-shift-and-sum and adaptive beams. The steer direction corresponds to an azimuth of 270° and an apparent velocity of 3.6 km/sec. The PDE, LASA, and NORSAR bulletins list no events arriving at ALPA between 0415 and 0815 on 30 November 1972. A Fisher detector scan indicates, however, that a small signal reached ALPA at 0458 from an azimuth of approximately 12°. The energy from this event should affect the measured noise reduction values only minimally. Table II-18 and Figure II-41 present the noise reduction for six channels as a function of the convergence parameter μ. The noise reduction values for this sample are lower than for the sample from day 238 of 1970, particularly at the higher convergence rates.

Signal degradation measurements from day 276 of 1972 are borrowed from Subsection C to obtain estimates of the signal-to-noise gains which would have occurred if a signal had arrived at ALPA between 0415 and 0815 on day 335 of 1972. Signal-to-noise ratio improvement relative to beamsteering is depicted as a function of convergence rate in Table II-19 and Figure II-42 for the weak event from 300°-305°, in Table II-20 and Figure II-43 for the strong signal from Kamchatka, and in Table II-21 and Figure II-44 for the very strong signal from Kamchatka. These gain estimates provide a basis for comparison with the full-array processing results which appear in the remainder of this subsection.

TABLE II-18

ADAPTIVE FILTERING NOISE REDUCTION
VERSUS CONVERGENCE RATE
(ALPA, 6 SITES, 1972 DAY 335 0415-0815)

Convergence Rate (μ)	Noise Reduction (dB)
0.0010	0.677
0.0015	0.852
0.0020	0.991
0.0030	1.208
0.0040	1.372
0.0050	1.502
0.0070	1.699
0.0100	1.901
0.0150	2.118
0.0200	2.264
0.0300	2.465
0.0400	2.611
0.0500	2.730
0.0700	2.928
0.1000	3.172
0.1500	3.507
0.2000	3.792
0.3000	4.265
0.4000	4.622
0.5000	4.856

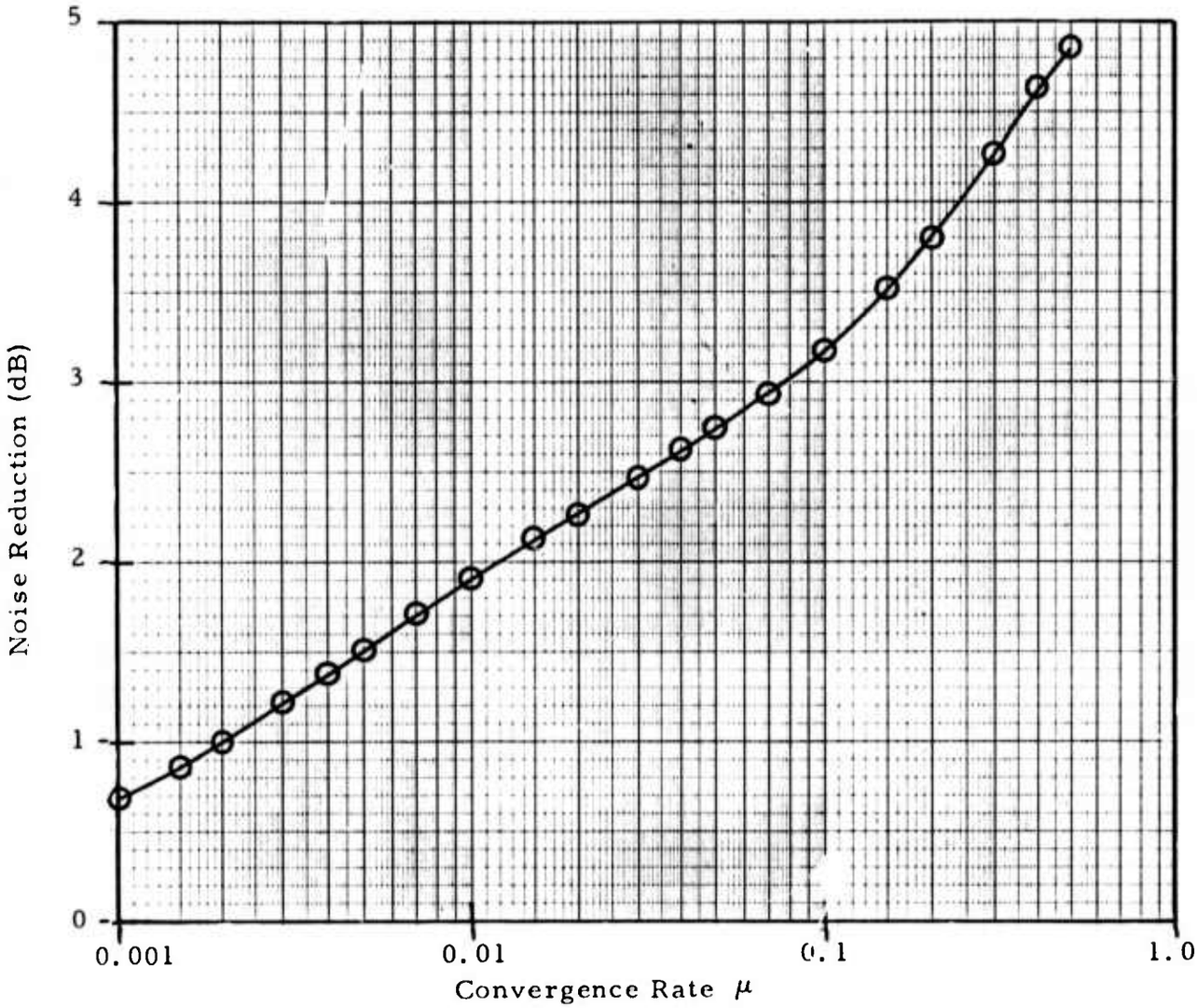

FIGURE II-41

NOISE REDUCTION AS A FUNCTION OF CONVERGENCE RATE (ALPA, 6 SITES, 1972 DAY 335 0415-0815)

TABLE II-19

ADAPTIVE FILTERING SIGNAL-TO-NOISE GAIN VERSUS CONVERGENCE RATE FOR A WEAK SIGNAL FROM 300°-305° (ALPA, 6 SITES, 1971 DAY 276 21.37.01- 21.45.32, USING NOISE FROM 1972 DAY 335 0415-0815)

Convergence Rate (μ)	Signal-to-Noise Gain (dB)
0.0010	0.910
0.0015	1.115
0.0020	1.252
0.0030	1.411
0.0040	1.488
0.0050	1.524
0.0070	1.538
0.0100	1.493
0.0150	1.363
0.0200	1.222
0.0300	0.975
0.0400	0.782
0.0500	0.629
0.0700	0.397
0.1000	0.149
0.1500	-0.132
0.2000	-0.323
0.3000	-0.588
0.4000	-0.835
0.5000	-1.120

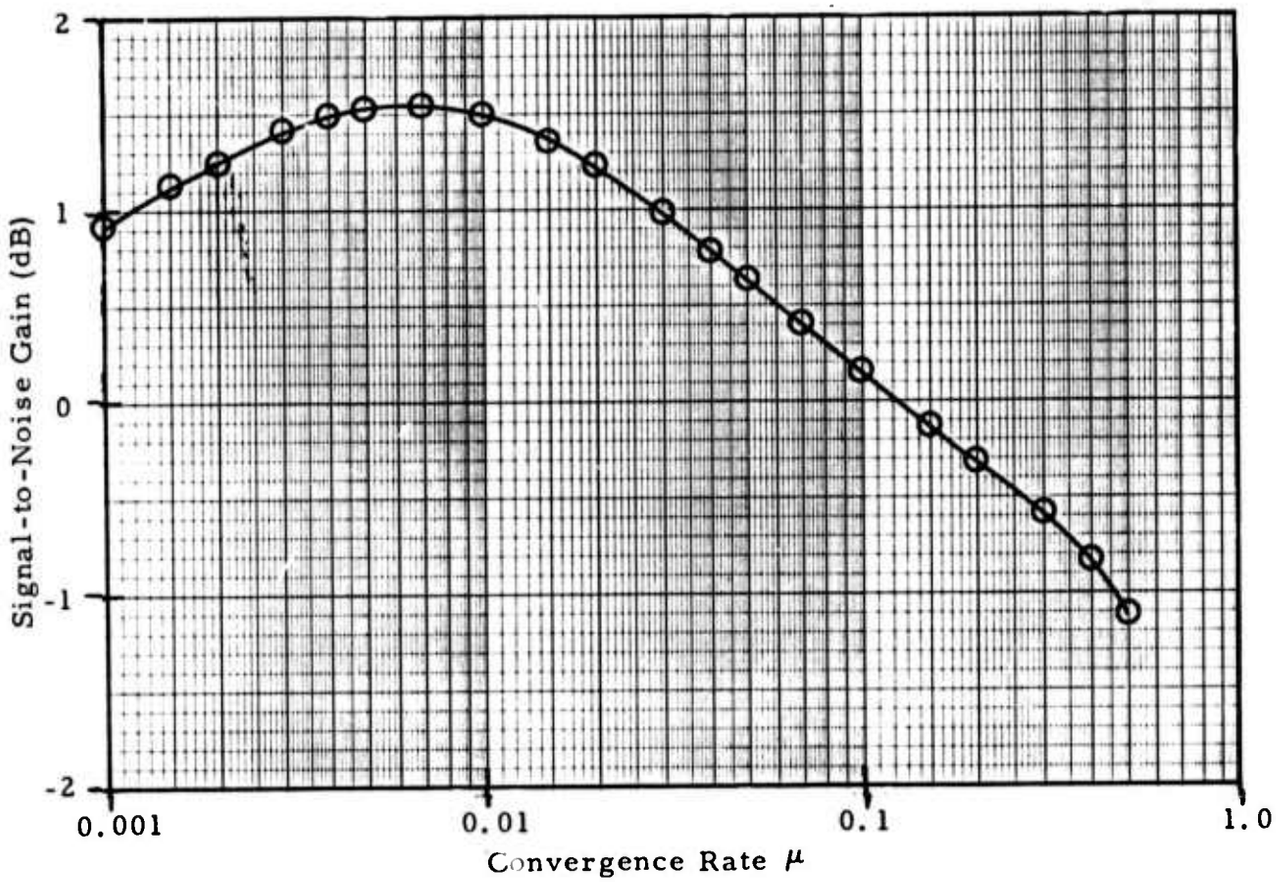

FIGURE II-42

SIGNAL-TO-NOISE GAIN AS A FUNCTION OF CONVERGENCE RATE FOR A WEAK SIGNAL FROM 300^{o}-305^{o} (ALPA, 6 SITES, 1971 DAY 276 21.37.01-21.45.32, USING NOISE FROM 1972 DAY 335 0415-0815)

TABLE II-20

ADAPTIVE FILTERING SIGNAL-TO-NOISE GAIN VERSUS CONVERGENCE RATE FOR A STRONG SIGNAL FROM KAMCHATKA (ALPA, 6 SITES, 1971 DAY 276 21.07.18-21.11.33, USING NOISE FROM 1972 DAY 335 0415-0815)

Convergence Rate (μ)	Signal-to-Noise Gain (dB)
0.0010	0.646
0.0015	0.805
0.0020	0.929
0.0030	1.116
0.0040	1.254
0.0050	1.361
0.0070	1.522
0.0100	1.687
0.0150	1.872
0.0200	2.002
0.0300	2.184
0.0400	2.307
0.0500	2.394
0.0700	2.510
0.1000	2.621
0.1500	2.785
0.2000	2.978
0.3000	3.412
0.4000	3.803
0.5000	4.079

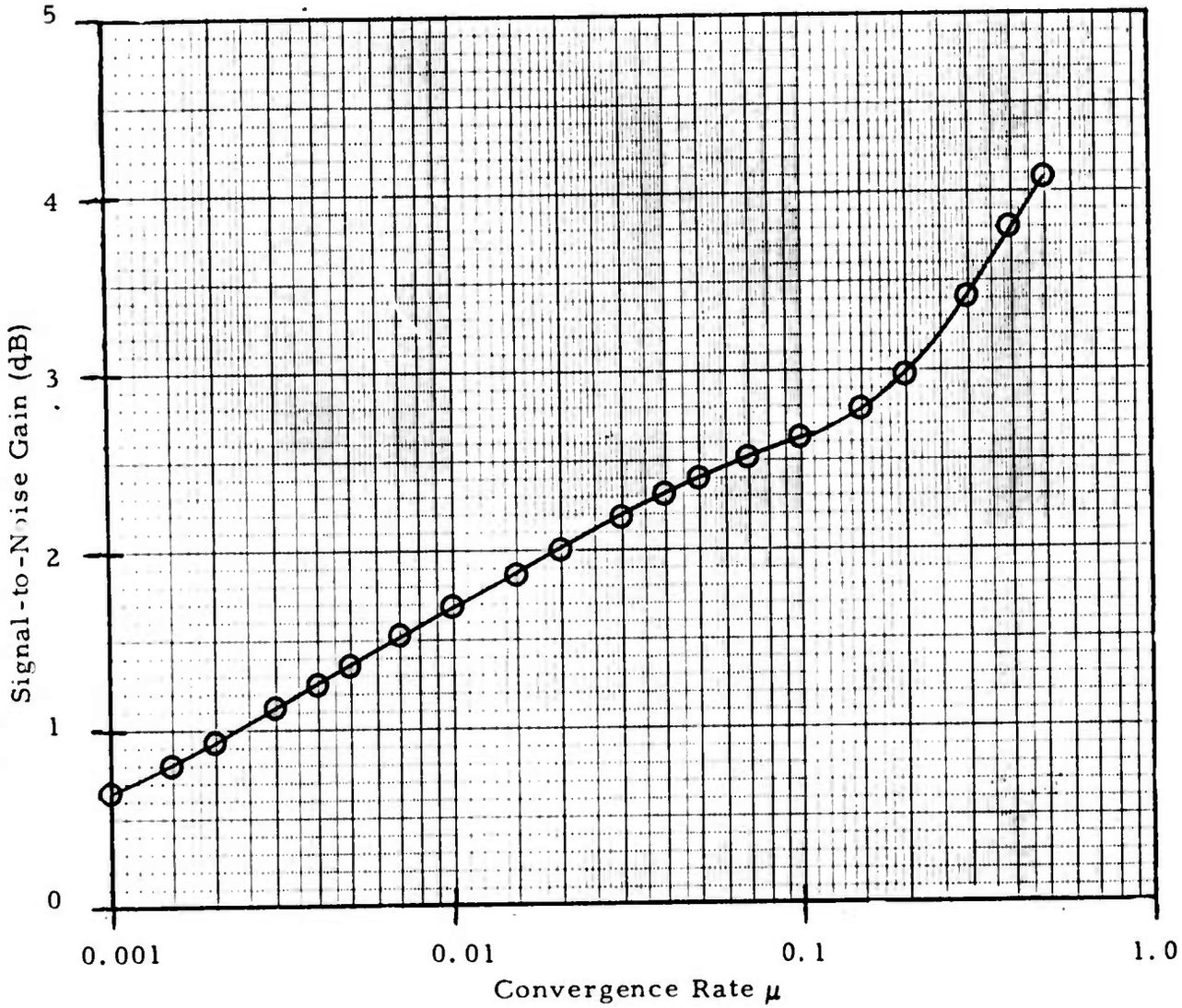

FIGURE II-43

SIGNAL-TO-NOISE GAIN AS A FUNCTION OF CONVERGENCE RATE FOR A STRONG SIGNAL FROM KAMCHATKA (ALPA, 6 SITES, 1971 DAY 276 21.07.18-21.11.33, USING NOISE FROM 1972 DAY 335 0415-0815)

TABLE II-21

ADAPTIVE FILTERING SIGNAL-TO-NOISE GAIN VERSUS CONVERGENCE RATE FOR A VERY STRONG SIGNAL FROM KAMCHATKA (ALPA, 6 SITES, 1971 DAY 276 22.07.02-22.11.17, USING NOISE FROM 1972 DAY 335 0415-0815)

Convergence Rate (μ)	Signal-to-Noise Gain (dB)
0.0010	0.611
0.0015	0.759
0.0020	0.876
0.0030	1.063
0.0040	1.208
0.0050	1.325
0.0070	1.502
0.0100	1.678
0.0150	1.863
0.0200	1.988
0.0300	2.176
0.0400	2.332
0.0500	2.475
0.0700	2.743
0.1000	3.117
0.1500	3.680
0.2000	4.171
0.3000	4.953
0.4000	5.507
0.5000	5.874

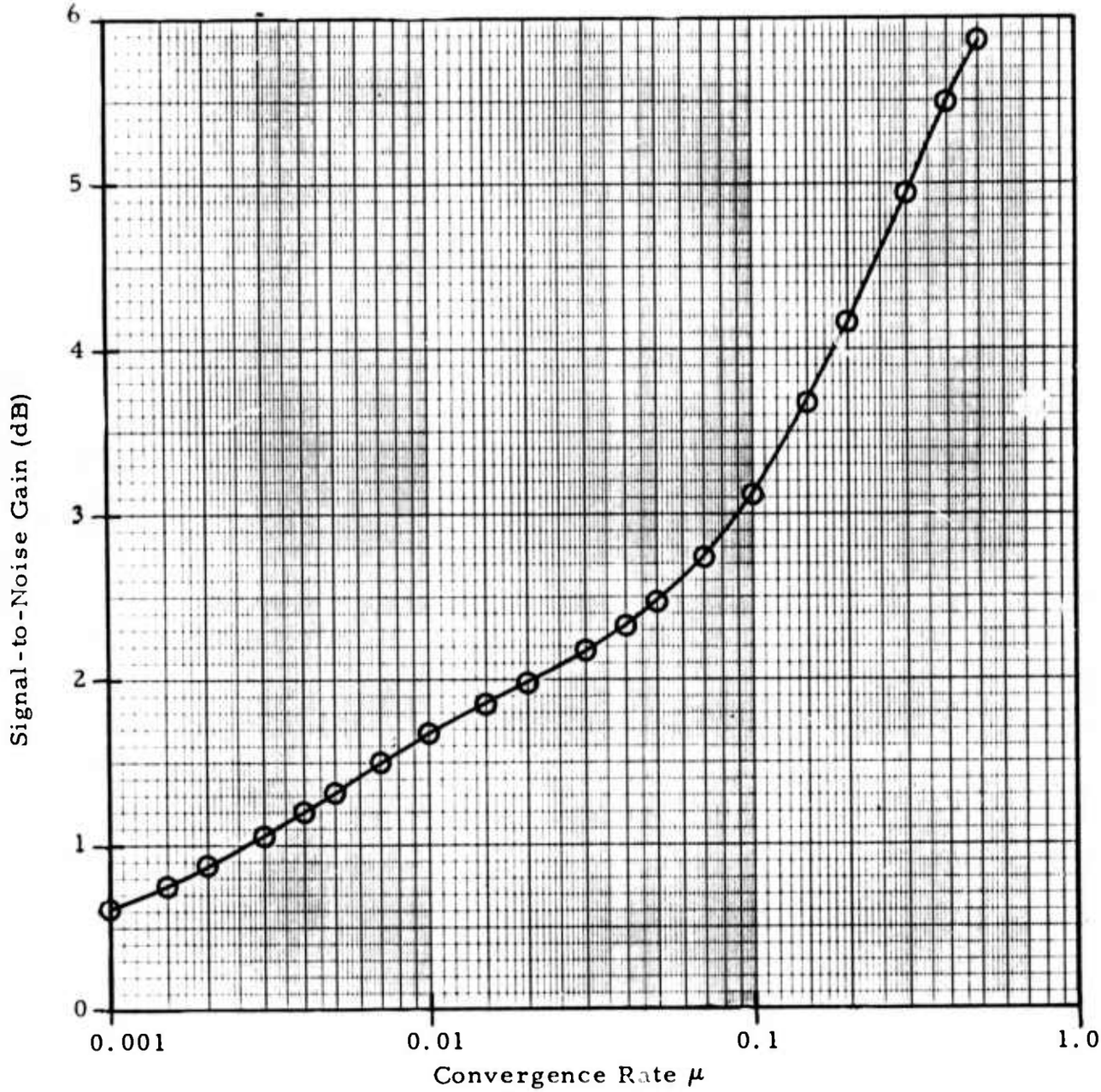

FIGURE II-44

SIGNAL-TO-NOISE GAIN AS A FUNCTION OF CONVERGENCE RATE FOR A VERY STRONG SIGNAL FROM KAMCHATKA (ALPA, 6 SITES, 1971 DAY 276 22.17.02-22.11.17, USING NOISE FROM 1972 DAY 335 0415-0815)

The full-array noise reduction measurements utilize the same noise sample from 0415 to 0815 on day 335 of 1972 as was used for the six-channel results. The only difference in processing is that fifteen sites (all but sites 7, 16, 18, and 19) form the channel inputs to the time-shift-and-sum and adaptive beamformers. Table II-22 and Figure II-45 portray the noise reduction for fifteen channels as a function of convergence rate.

Signal degradation measurements for the full array again employ the same three signals in the previously processed data sample from 2000 to 2345 on day 276 of 1971. All processing procedures for this sample are identical to those which yielded the signal degradation measurements in Subsection C for the new adaptive algorithm except that sixteen sites (all but sites 7, 11, and 18) constitute the input to the beamformers. The first signal considered is the weak signal from 300°-305°. The look azimuth for this event is 302.5°. Table II-23 and Figure II-46 depict signal degradation as a function of convergence rate for this event. The resulting signal-to-noise gain estimates corresponding to the noise sample from day 335 of 1972 appear in Table II-24 and Figure II-47. Maximum signal-to-noise ratio improvement is 1.15 dB at $\mu = 0.5$. There is also a local maximum at $\mu = 0.004$, where the estimated gain is 0.26 dB. The shape of the gain curve is distinctly different from the corresponding six-channel gain curve in Figure II-42, where maximum improvement relative to beamsteering is 1.5 dB at $\mu = 0.007$. Figure II-48 is a display of the weak event from 300°-305° for the beamsteer output and ABF output at $\mu = 0.005$ and $\mu = 0.5$. Note that the peak-to-peak amplitude at the end of the event in the bottom trace is comparable to the peak-to-peak amplitude of the event in the beamsteer output. The noise level before and after the event, in contrast, is greatly attenuated at $\mu = 0.5$. Thus, if signal detection were based on peak-to-peak amplitude measurements, the best detection results for this event would occur at the highest convergence rate.

TABLE II-22

ADAPTIVE FILTERING NOISE REDUCTION
VERSUS CONVERGENCE RATE
(ALPA, 15 SITES, 1972 DAY 335 0415-0815)

Convergence Rate (μ)	Noise Reduction (dB)
0.0010	0.357
0.0015	0.482
0.0020	0.587
0.0030	0.759
0.0040	0.895
0.0050	1.007
0.0070	1.187
0.0100	1.386
0.0150	1.622
0.0200	1.794
0.0300	2.046
0.0400	2.234
0.0500	2.385
0.0700	2.628
0.1000	2.914
0.1500	3.295
0.2000	3.617
0.3000	4.151
0.4000	4.557
0.5000	4.819

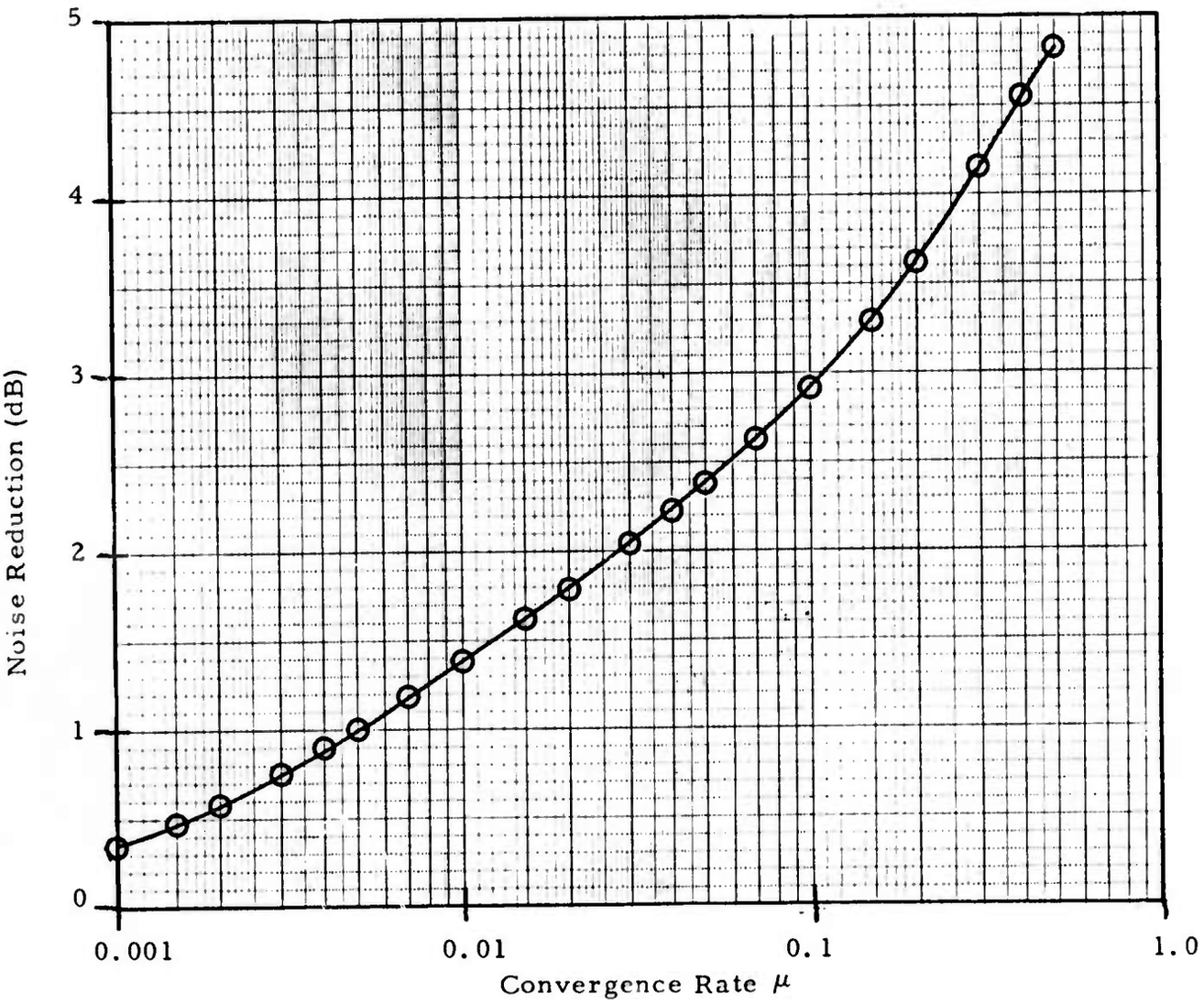

FIGURE II-45

NOISE REDUCTION AS A FUNCTION OF CONVERGENCE RATE (ALPA, 15 SITES, 1972 DAY 335 0415-0815)

TABLE II-23

ADAPTIVE FILTERING SIGNAL DEGRADATION
VERSUS CONVERGENCE RATE
FOR A WEAK SIGNAL FROM 300°-305°
(ALPA, 16 SITES, 1971 DAY 276 21.37.01-21.45.32)

Convergence Rate (μ)	Signal Degradation (dB)
0.0010	0.203
0.0015	0.288
0.0020	0.367
0.0030	0.507
0.0040	0.632
0.0050	0.744
0.0070	0.942
0.0100	1.191
0.0150	1.517
0.0200	1.766
0.0300	2.137
0.0400	2.423
0.0500	2.663
0.0700	3.057
0.1000	3.485
0.1500	3.895
0.2000	4.077
0.3000	4.104
0.4000	3.921
0.5000	3.670

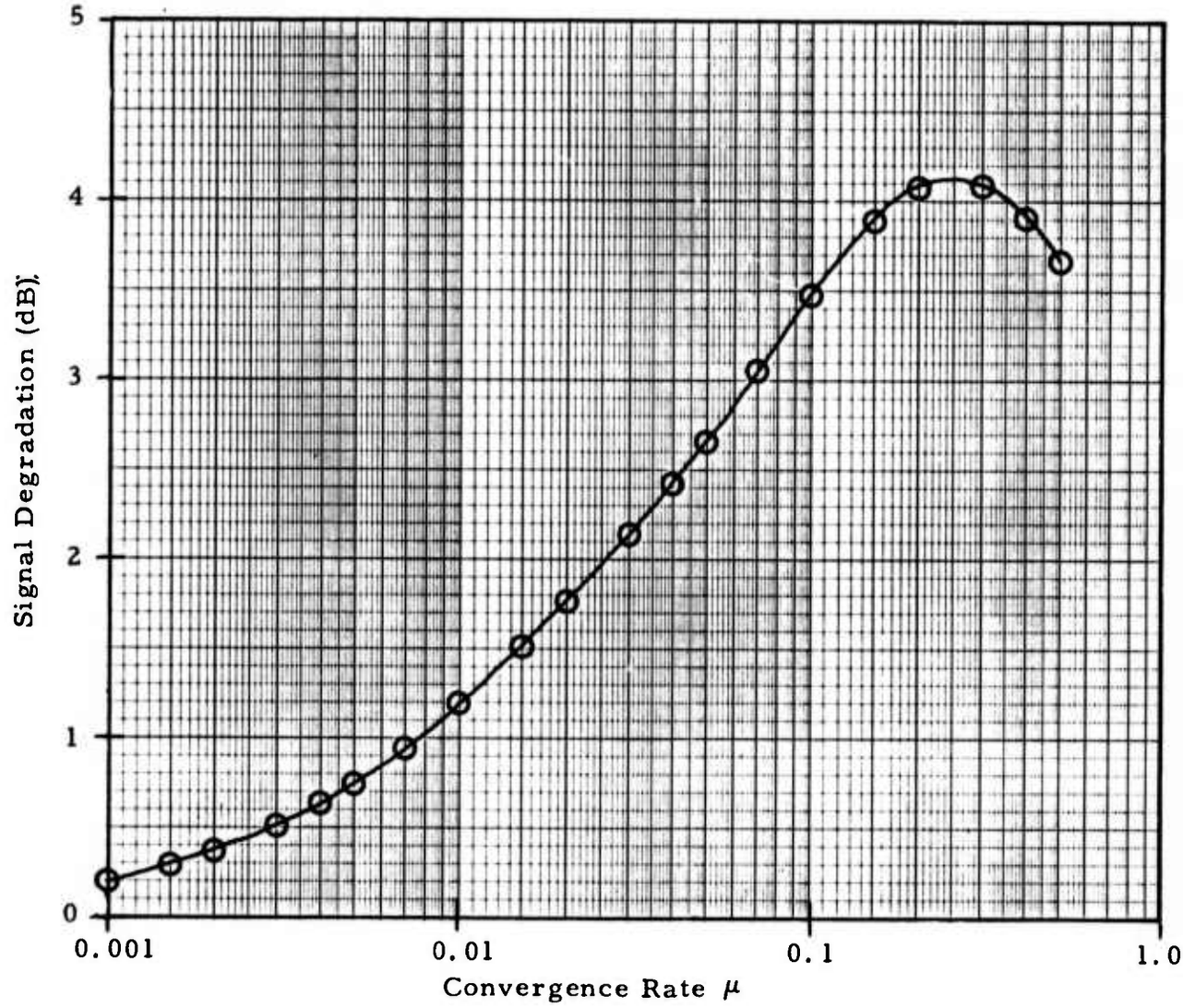

FIGURE II-46

SIGNAL DEGRADATION AS A FUNCTION OF CONVERGENCE RATE FOR A WEAK SIGNAL FROM 300° -305° (ALPA, 16 SITES, 1971 DAY 276 21.37.01-21.45.32)

TABLE II-24

ADAPTIVE FILTERING SIGNAL-TO-NOISE GAIN VERSUS CONVERGENCE RATE FOR A WEAK SIGNAL FROM 300°-305° (ALPA, FULL ARRAY, 1971 DAY 276 21.37.01-21.45.32, USING NOISE FROM 1972 DAY 335 0415-0815)

Convergence Rate (μ)	Signal-to-Noise Gain (dB)
0.0010	0.154
0.0015	0.194
0.0020	0.220
0.0030	0.252
0.0040	0.263
0.0050	0.257
0.0070	0.245
0.0100	0.195
0.0150	0.105
0.0200	0.028
0.0300	-0.091
0.0400	-0.189
0.0500	-0.278
0.0700	-0.429
0.1000	-0.571
0.1500	-0.600
0.2000	-0.460
0.3000	0.047
0.4000	0.636
0.5000	1.149

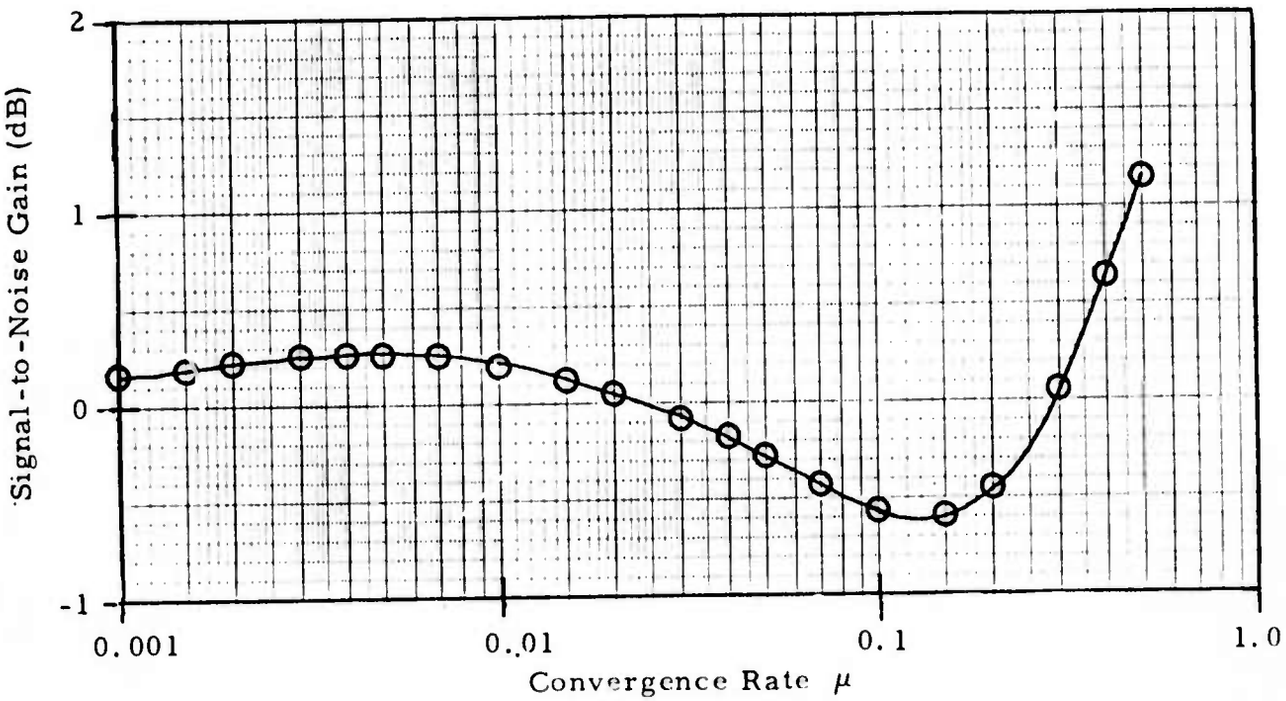

FIGURE II-47

SIGNAL-TO-NOISE GAIN AS A FUNCTION OF CONVERGENCE RATE FOR A WEAK SIGNAL FROM 300°-305° (ALPA, FULL ARRAY, 1971 DAY 276 21.37.01-21.45.32, USING NOISE FROM 1972 DAY 335 0415-0815)

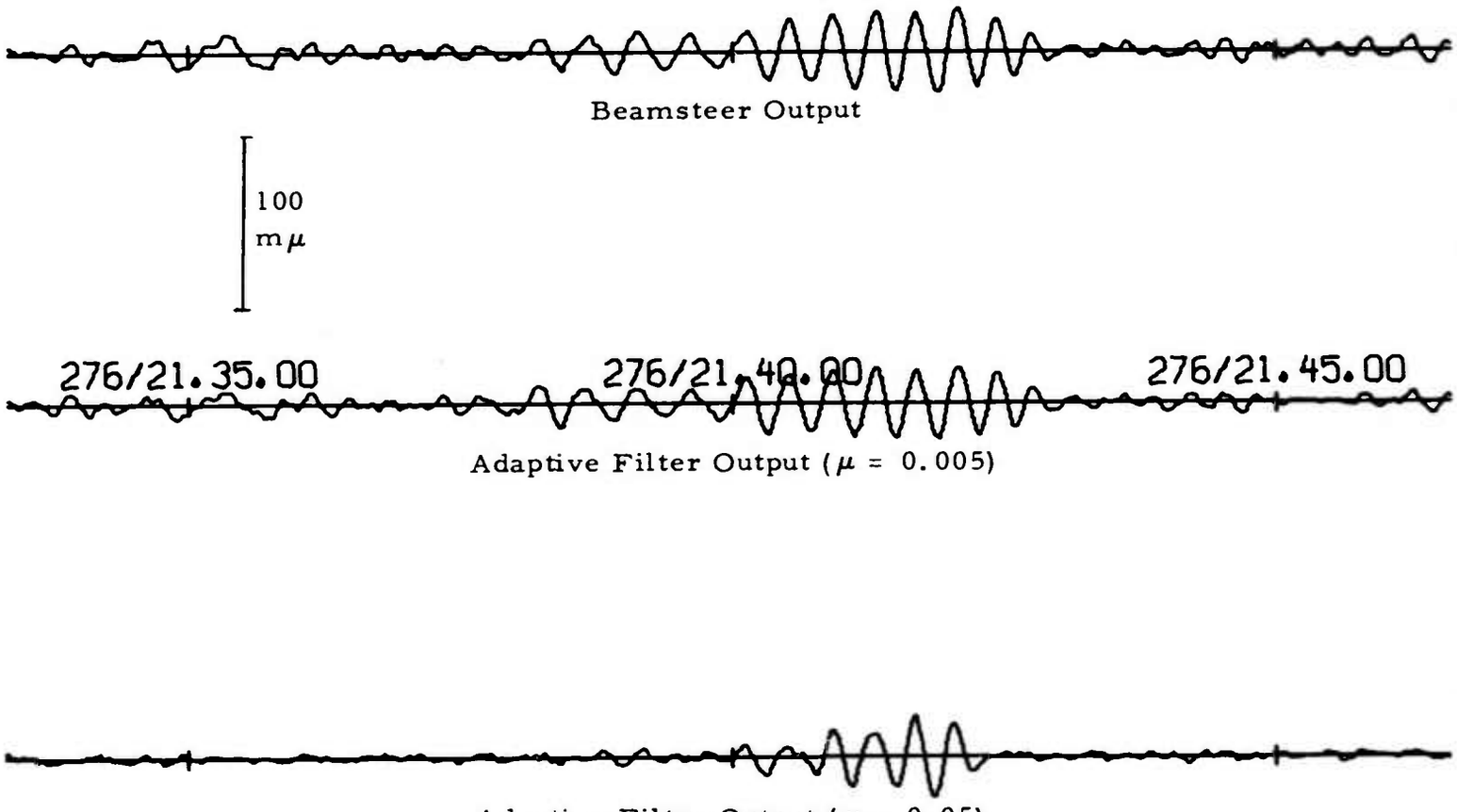

FIGURE II-48

FULL-ARRAY BEAMS FOR WEAK EVENT FROM 300^{o}-305^{o}
(DAY 276 1971, STEER DIRECTION 302.5^{o})

Table II-25 presents the power reduction relative to beamsteering at $\mu = 0.005$ and $\mu = 0.5$ over the specified time gates for five events with azimuths away from the 302.5° steer direction. As in the case of the corresponding six-channel results for the 302.5° steer direction (Table II-12), all off-azimuth events are reduced by more than 12 dB at $\mu = 0.5$. Figures II-49 through II-53 show the beamsteer output and ABF output at $\mu = 0.005$ and $\mu = 0.5$ for the five events in Table II-25. The amplitude of the beamsteer output in the top trace of each figure is smaller than the corresponding six-channel beamsteer-output amplitudes since the time-shift-and-sum amplification factors for the full array (Figure II-54) are lower than the corresponding factors for the six-channel array (Figure II-18) at all azimuths away from the 302.5° steer azimuth. Figures II-55 and II-56 present adaptive beam patterns for $\mu = 0.005$ at the beginning and middle of the latter Panama event. The 8 dB suppression of this event is reflected by the deepening null at the 113° azimuth. This null persists until the end of the event at 2128, when the beam pattern is essentially the same as at 2124. In contrast, the adaptive beamformer achieved the 6 dB suppression of the second Kamchatka event at $\mu = 0.005$ by deflecting the main lobe of the beam pattern away from the 273° arrival azimuth of the event. Figures II-57 through II-59, which show the adaptive beam pattern at the beginning, middle, and end of the event, demonstrate this deflection process.

The last two signals used for full-array signal degradation measurements are the two Kamchatka events from an azimuth of 273°. Again, all processing procedures for these two events are the same as those which produced the signal degradation measurements in Subsection C for the new adaptive algorithm except for the sites employed (all but 7, 11, and 18). The first of these events arrived at about 2108. Table II-26 and Figure II-60 present the full-array signal degradation for this event as a function of convergence rate. The corresponding signal-to-noise gain values based on the full-array

TABLE II-25

FULL-ARRAY OFF-AZIMUTH EVENT SUPPRESSION
FOR 302.5° STEER DIRECTION

Event	Azimuth	Computation Gate		Power Reduction (dB)	
		Start Time	Stop Time	$\mu = 0.005$	$\mu = 0.5$
Panama	113°	20:33:00	20:40:00	1.980	12.127
Kamchatka	273°	21:07:30	21:15:00	3.424	17.911
Panama	113°	21:20:00	21:28:00	8.191	17.725
Kamchatka	273°	22:07:00	22:14:00	6.779	20.643
Andreanof Islands	237°	23:25:00	23:35:00	3.447	14.189

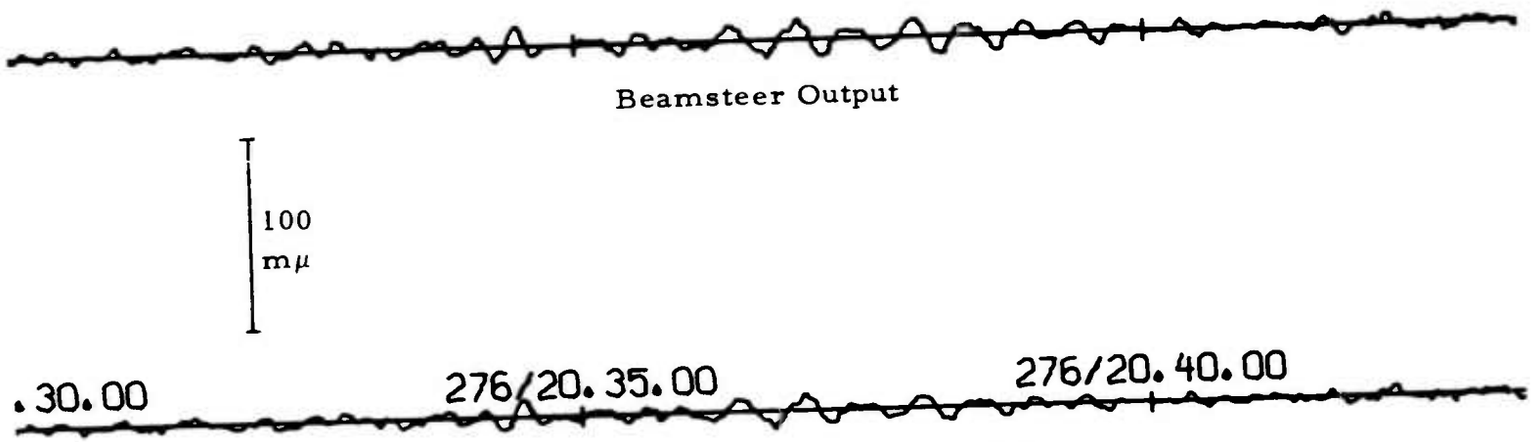

FIGURE II-49

FULL-ARRAY BEAMS FOR MAGNITUDE 3.6 PANAMA EVENT
(DAY 276 1971, STEER DIRECTION 302.5°)

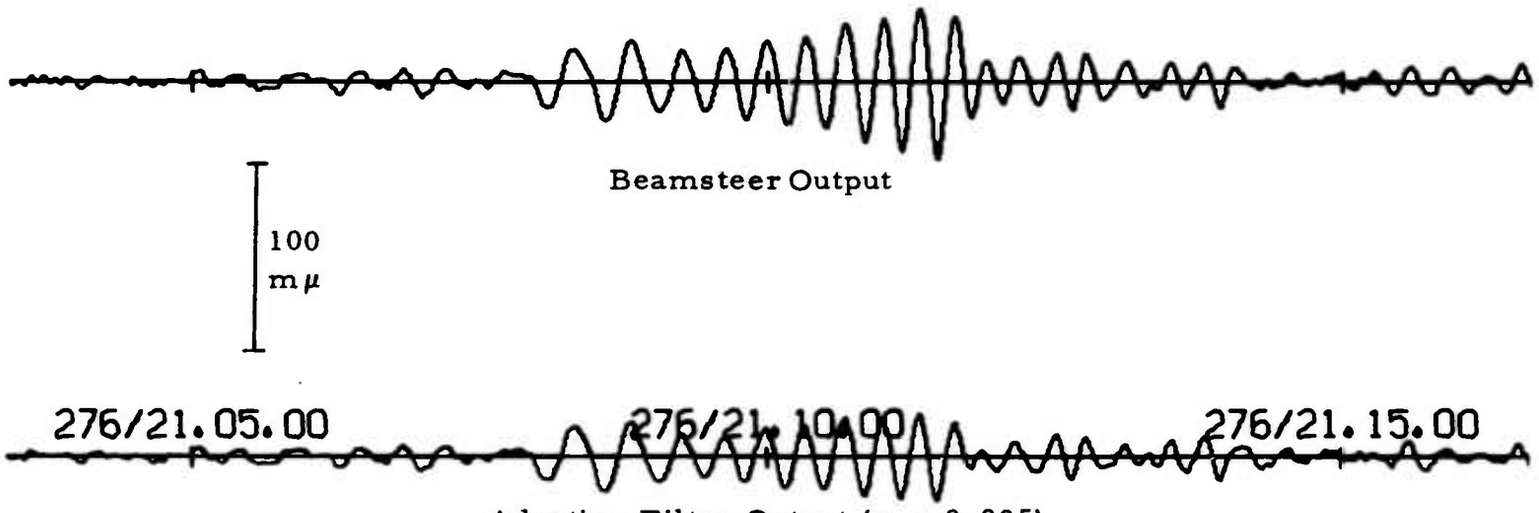

FIGURE II-50

FULL-ARRAY BEAMS FOR MAGNITUDE 4.5 KAMCHATKA EVENT
(DAY 276 1971, STEER DIRECTION 302.5°)

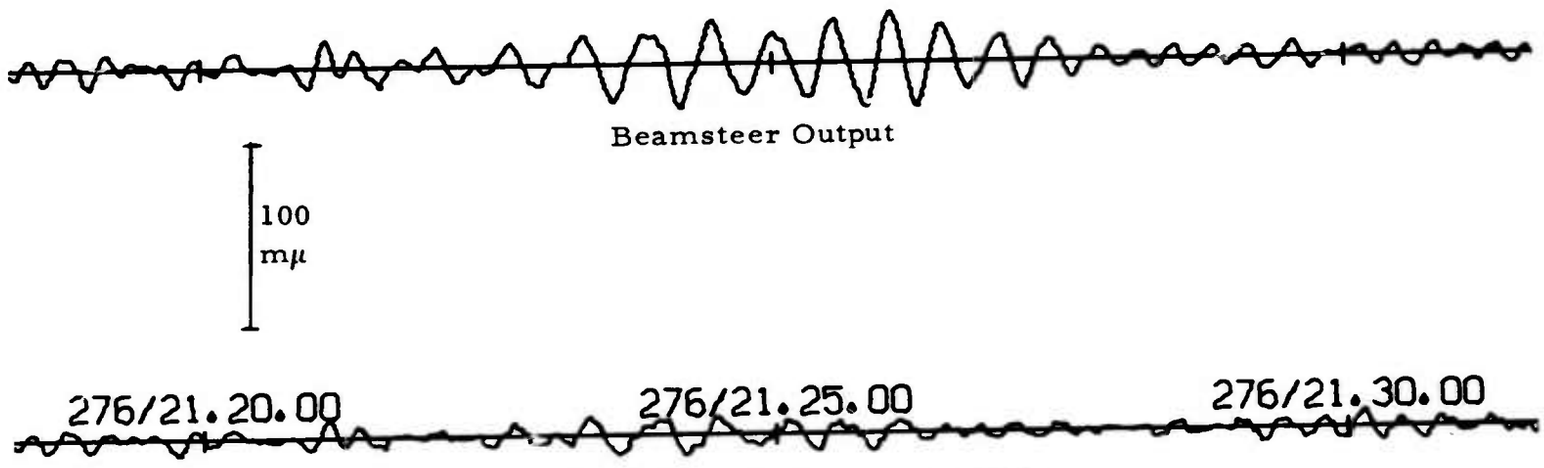

FIGURE II-51

FULL-ARRAY BEAMS FOR MAGNITUDE 4.7 PANAMA EVENT
(DAY 276 1971, STEER DIRECTION 302.5°)

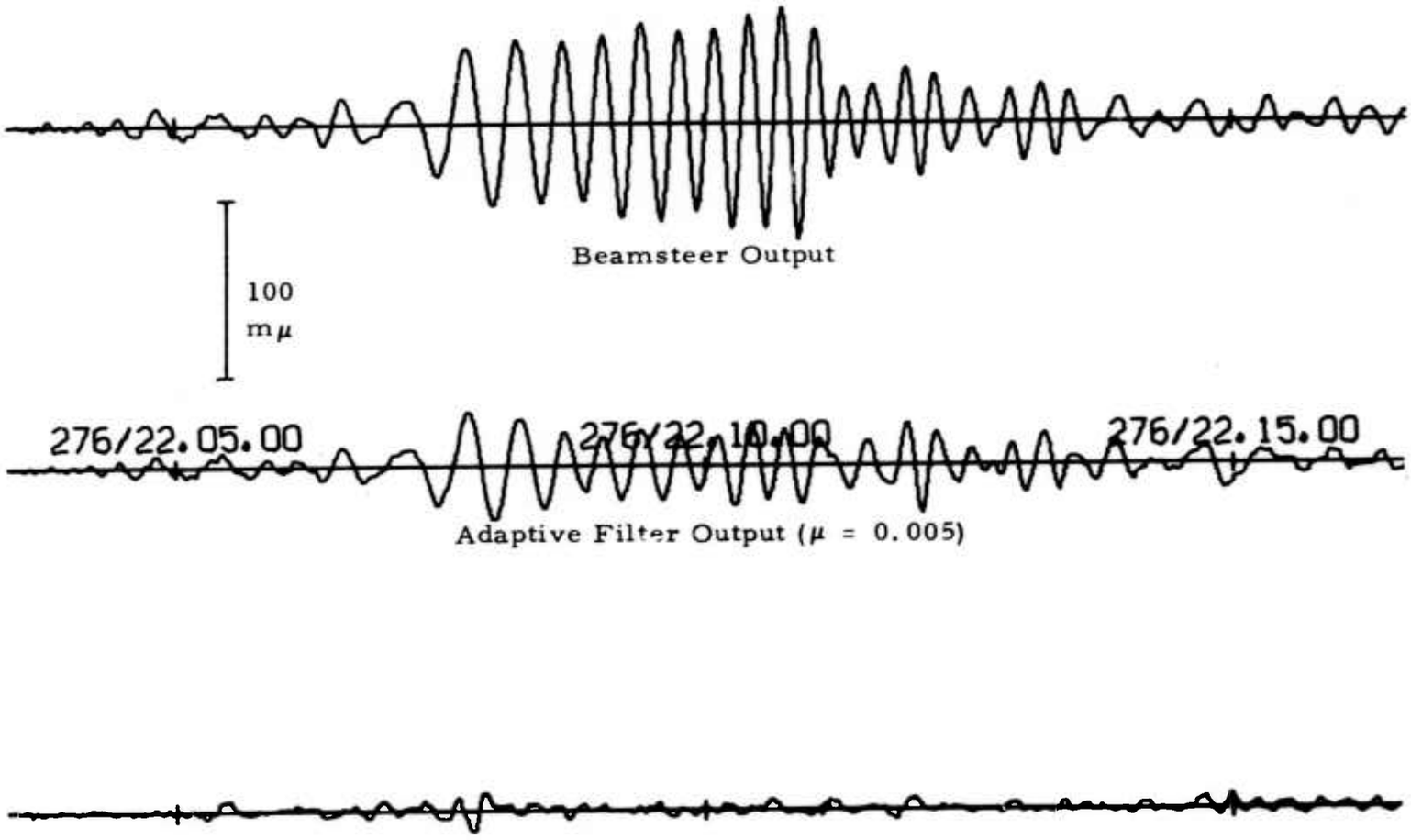

FIGURE II-52

FULL-ARRAY BEAMS FOR MAGNITUDE 4.9 KAMCHATKA EVENT
(DAY 276 1971, STEER DIRECTION 302.5°)

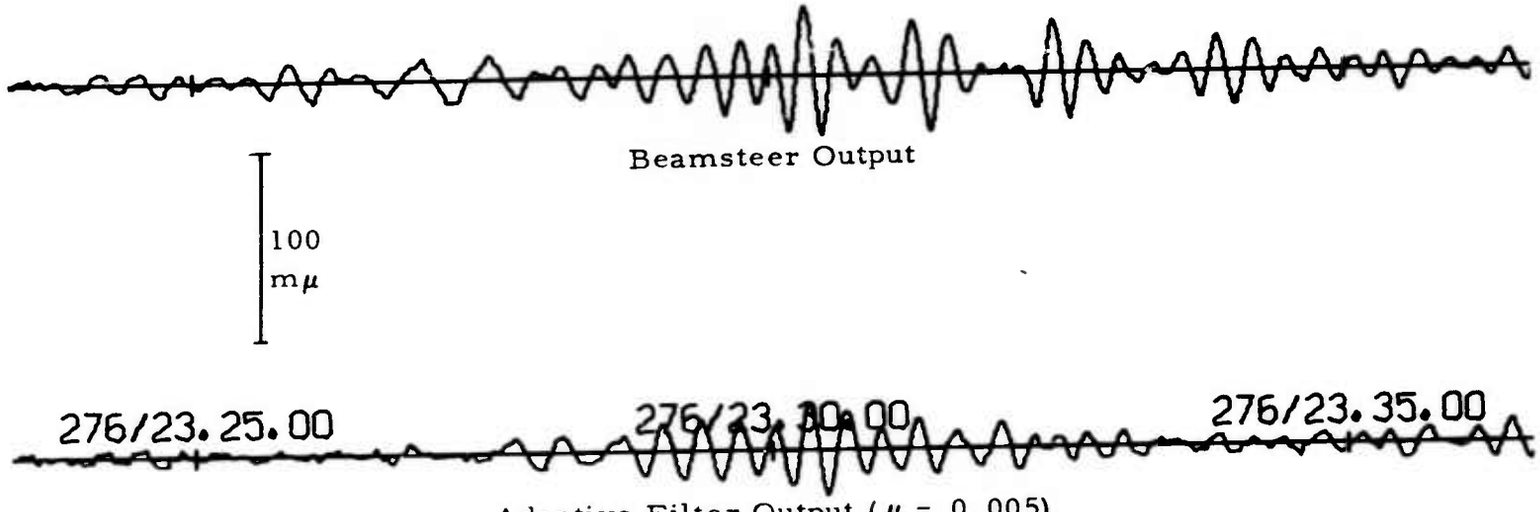

FIGURE II-53

FULL-ARRAY BEAMS FOR ANDREANOF ISLANDS EVENT
(DAY 276 1971, STEER DIRECTION 302.5°)

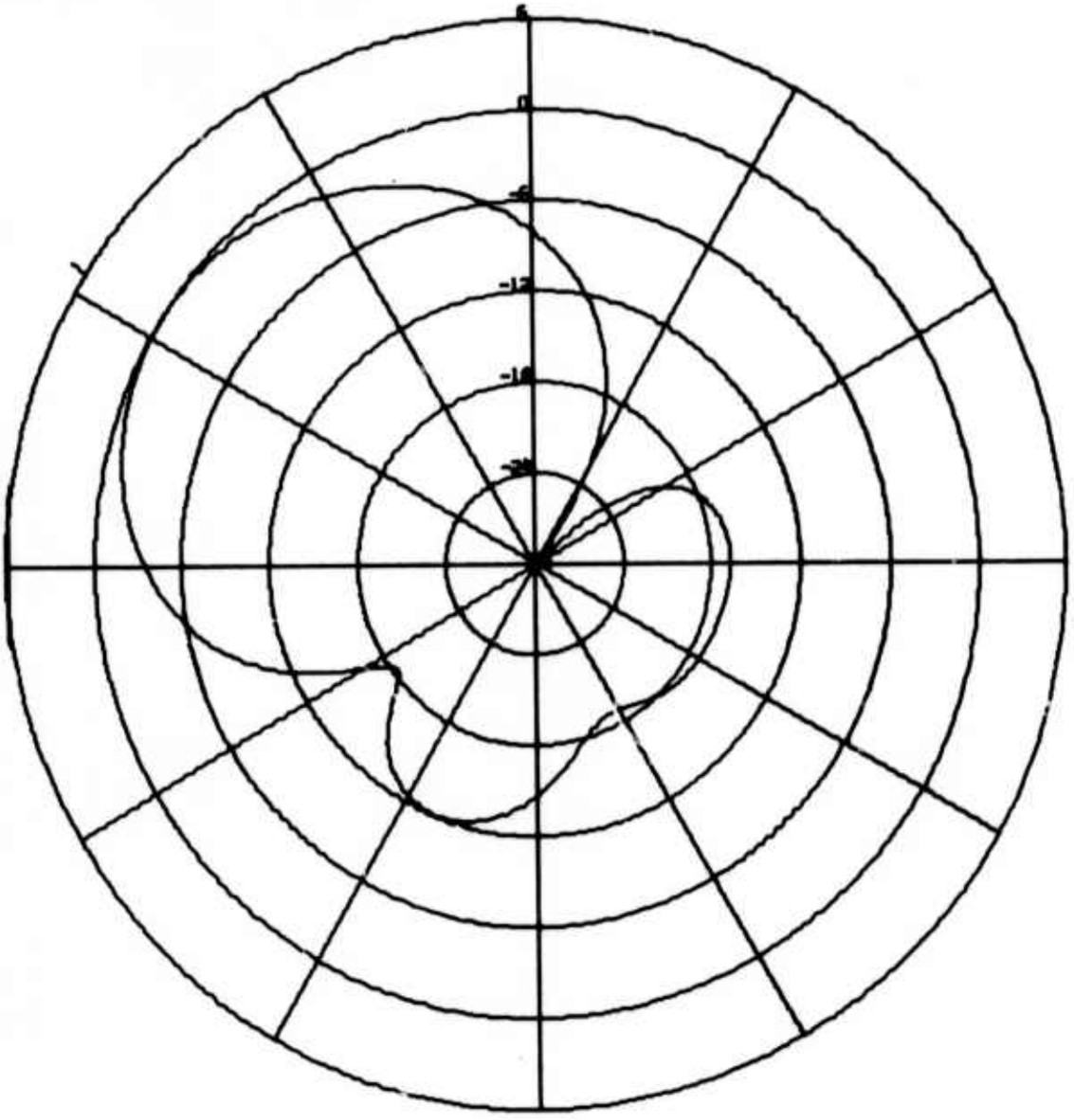

FIGURE II-54

BEAMSTEER RESPONSE FOR FULL-ARRAY SAMPLE
FROM DAY 276 OF 1971

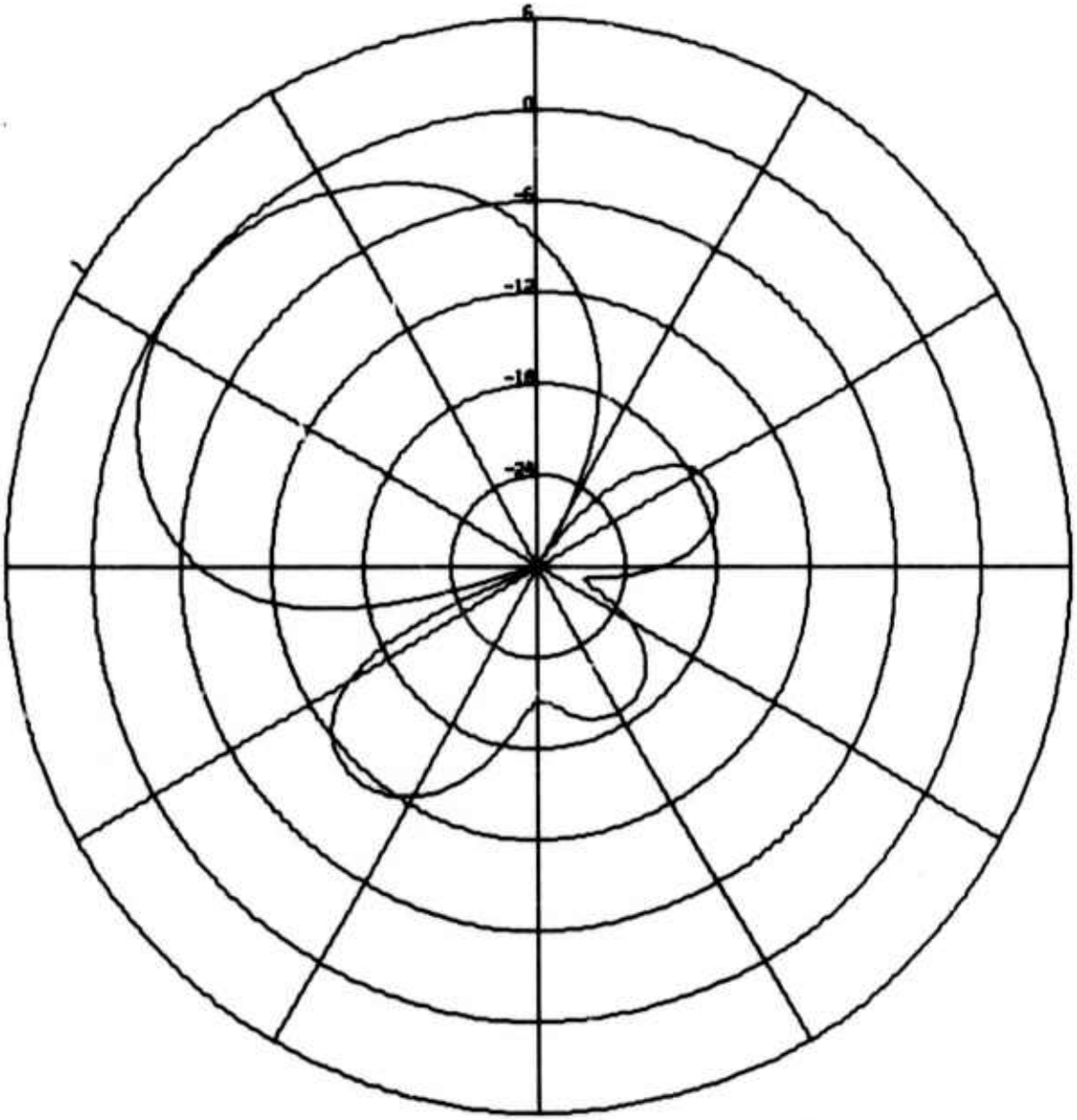

ALPA
ABF BEAM PATTERN AT 276/21.20.00
CONVERGENCE RATE IS 0.0050
BEAM LOOK VELOCITY IS 3.6, LOOK AZIMUTH 302.5
FREQUENCY IS 0.04000 HZ, PERIOD 25.0 SECONDS

FIGURE II-55

FULL-ARRAY ABF RESPONSE FOR MAGNITUDE
4.7 PANAMA EVENT AT 2120 ON DAY 276 OF 1971

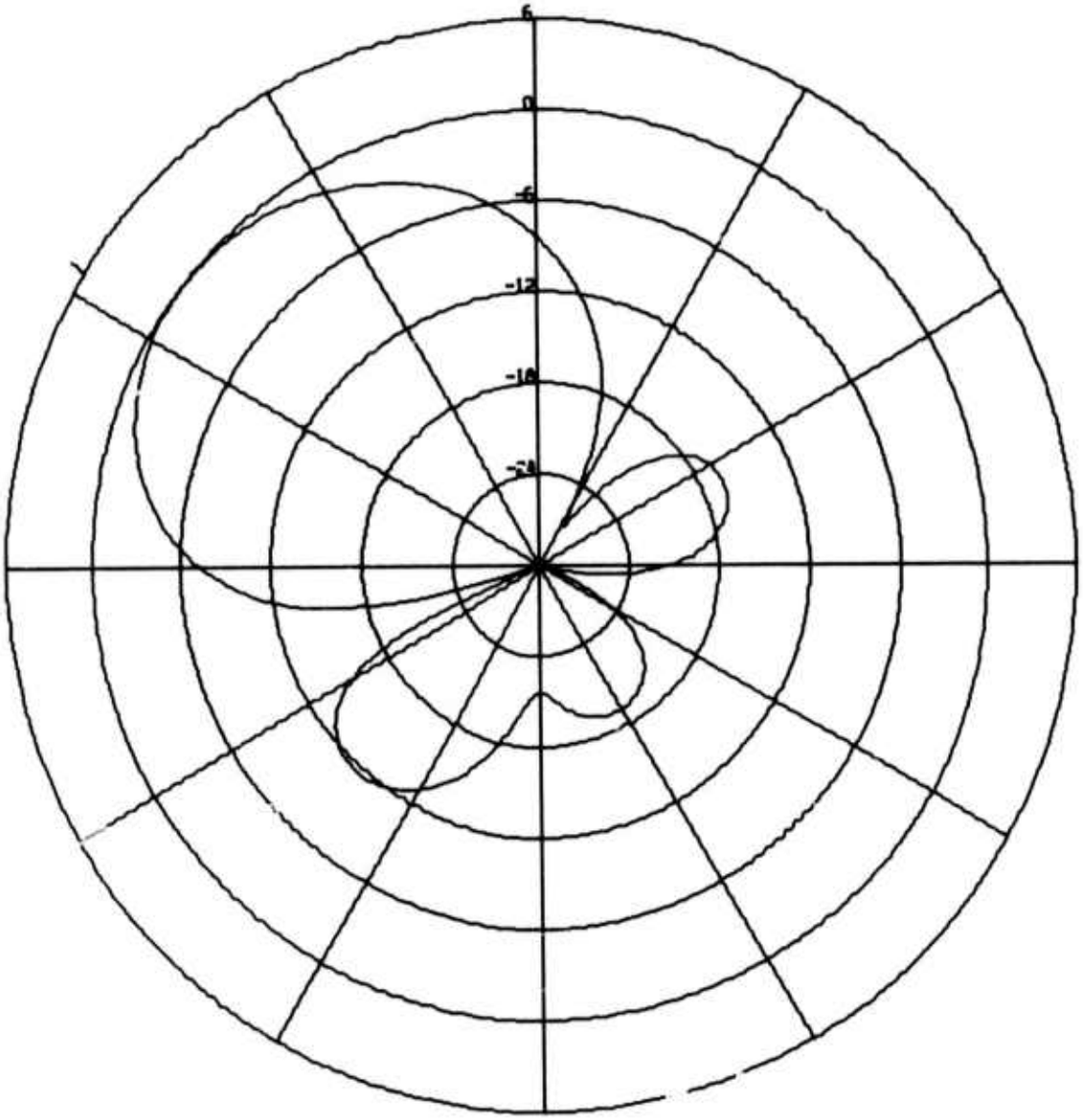

ALPA
ABF BEAM PATTERN AT 276/21.24.00
CONVERGENCE RATE IS 0.0050
BEAM LOOK VELOCITY IS 3.6, LOOK AZIMUTH 302.5
FREQUENCY IS 0.04000 HZ, PERIOD 25.0 SECONDS

FIGURE II-56

FULL-ARRAY ABF RESPONSE FOR MAGNITUDE
4.7 PANAMA EVENT AT 2124 ON DAY 276 OF 1971

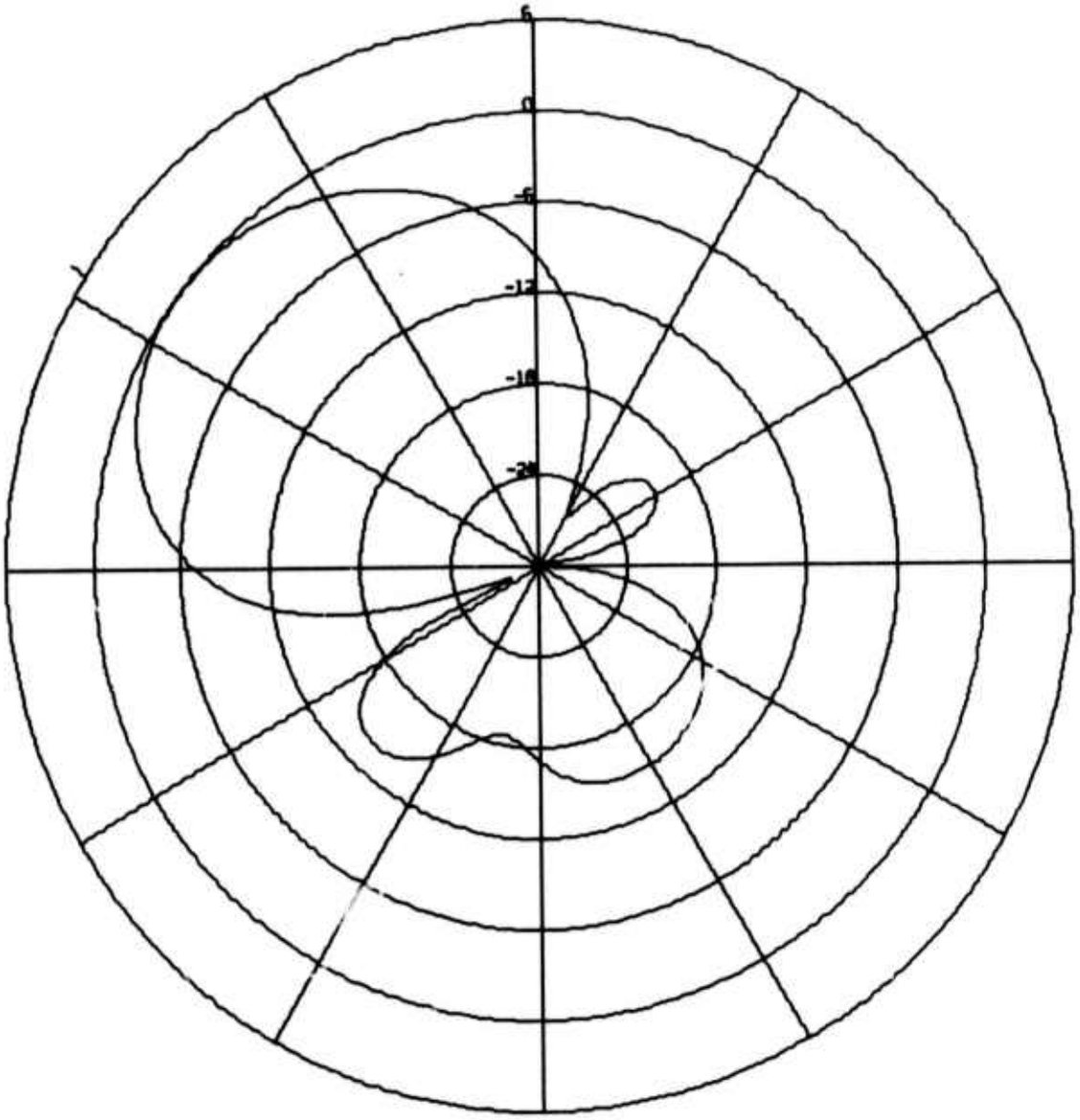

ALPA
ABF BEAM PATTERN AT 276/22.07.00
CONVERGENCE RATE IS 0.0050
BEAM LOOK VELOCITY IS 3.6, LOOK AZIMUTH 302.5
FREQUENCY IS 0.04000 HZ, PERIOD 25.0 SECONDS

FIGURE II-57

FULL-ARRAY ABF RESPONSE FOR MAGNITUDE
4.9 KAMCHATKA EVENT AT 2207 ON DAY 276 OF 1971

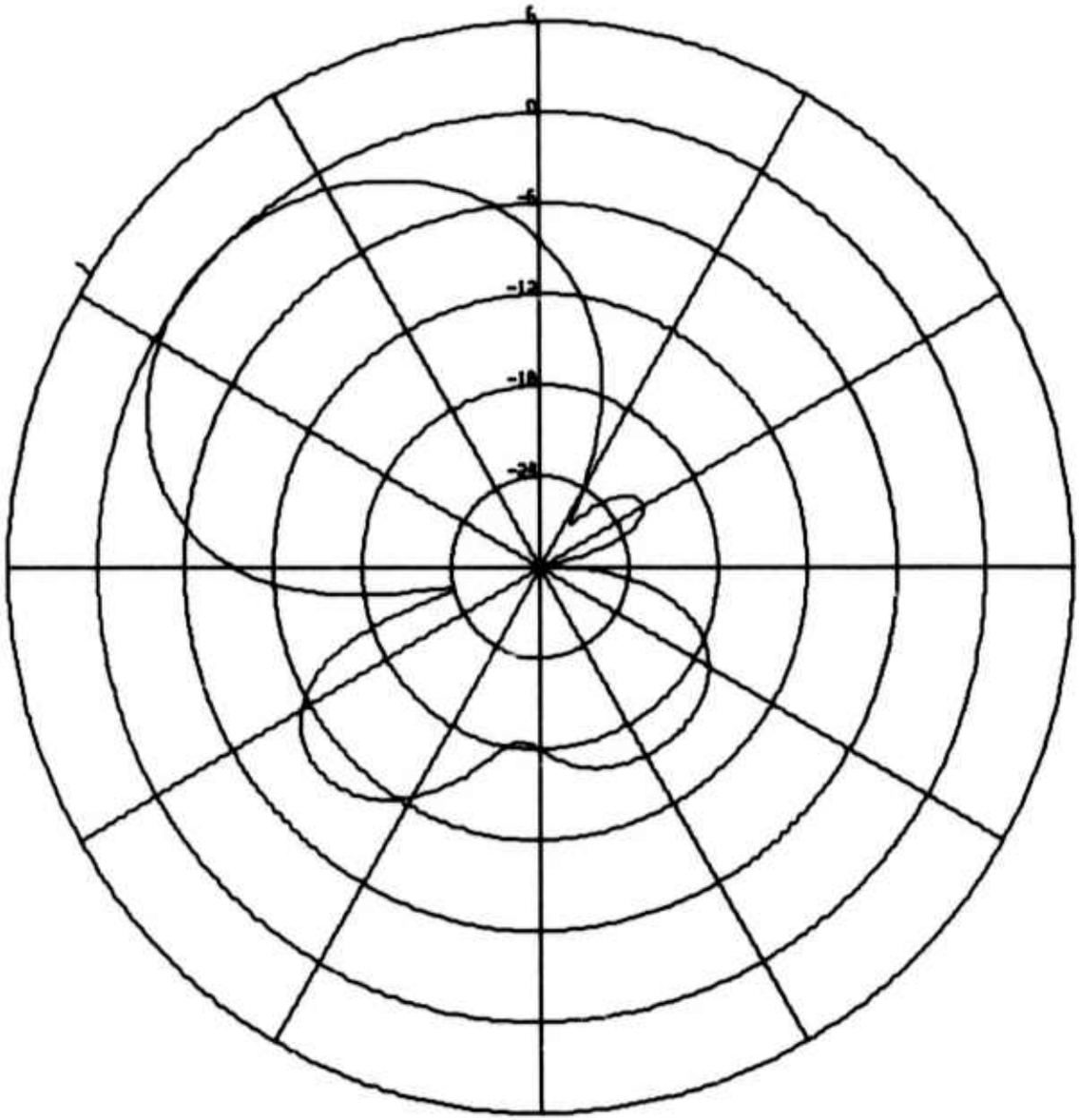

ALPA
ABF BEAM PATTERN AT 276/22.10.30
CONVERGENCE RATE IS 0.0050
BEAM LOOK VELOCITY IS 3.6, LOOK AZIMUTH 302.5
FREQUENCY IS 0.04000 HZ, PERIOD 25.0 SECONDS

FIGURE II-58

FULL-ARRAY ABF RESPONSE FOR MAGNITUDE
4.9 KAMCHATKA EVENT AT 2210 1/2 ON DAY 276 OF 1971

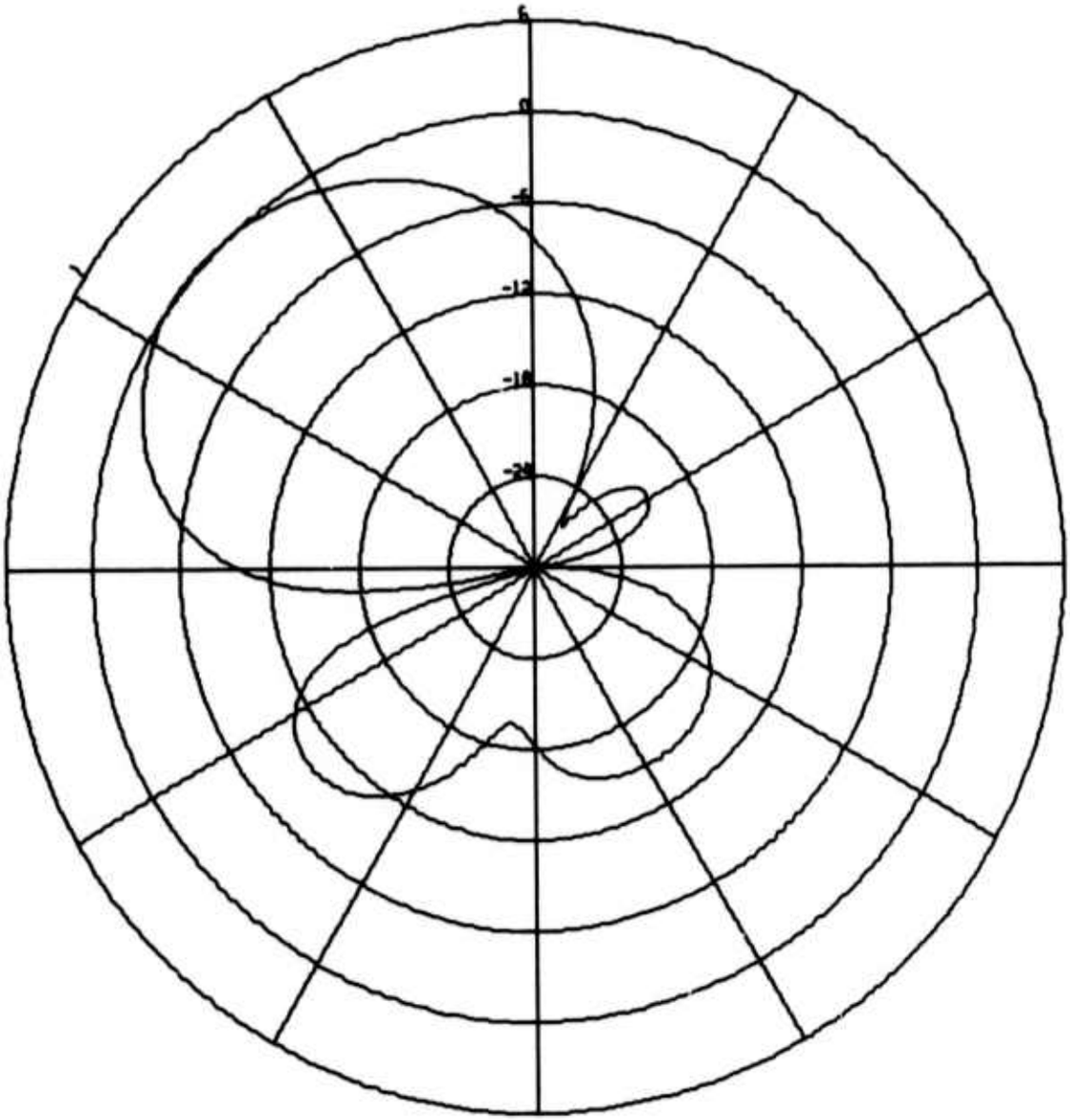

FIGURE II-59

FULL-ARRAY ABF RESPONSE FOR MAGNITUDE
4.9 KAMCHATKA EVENT AT 2214 ON DAY 276 OF 1971

TABLE II-26

ADAPTIVE FILTERING SIGNAL DEGRADATION VERSUS CONVERGENCE RATE FOR A STRONG SIGNAL FROM KAMCHATKA (ALPA, 16 SITES, 1971 DAY 276 21.07.18-21.11.33)

Convergence Rate (μ)	Signal Degradation (dB)
0.0010	0.018
0.0015	0.028
0.0020	0.040
0.0030	0.064
0.0040	0.091
0.0050	0.118
0.0070	0.174
0.0100	0.255
0.0150	0.372
0.0200	0.469
0.0300	0.613
0.0400	0.711
0.0500	0.778
0.0700	0.851
0.1000	0.874
0.1500	0.812
0.2000	0.706
0.3000	0.486
0.4000	0.305
0.5000	0.173

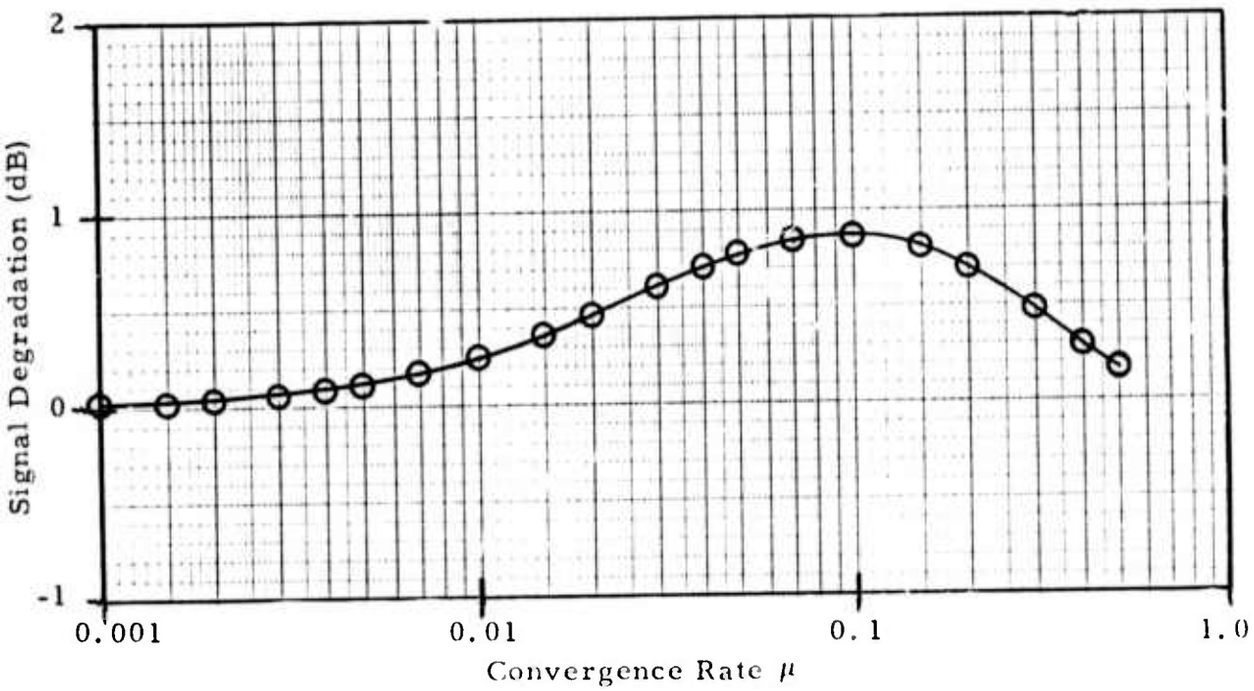

FIGURE II-60

SIGNAL DEGRADATION AS A FUNCTION OF CONVERGENCE RATE FOR A STRONG SIGNAL FROM KAMCHATKA (ALPA, 16 SITES, 1971 DAY 276 21.07.18-21.11.33)

noise reduction measurements for day 335 of 1972 appear in Table II-27 and Figure II-61. The beamsteer traces and adaptive filter traces at $\mu = 0.005$ and $\mu = 0.5$ are shown for this event in Figure II-62. Some signal distortion is evident in the bottom trace for the highest convergence rate. The second Kamchatka event reached ALPA at approximately 2207. The full-array signal degradation for this event is given in Table II-28 and Figure II-63 as a function of convergence rate. Using the full-array noise reduction measurements from day 335 of 1972, the resulting signal-to-noise ratio improvement values are depicted in Table II-29 and Figure II-64. The estimated full array signal-to-noise gains for this event are lower than the corresponding six-channel values at all convergence rates. The greatest difference of about 2 dB at $\mu = 0.5$ is due to the greater signal degradation with the full array. Figure II-65 displays the beam outputs for the second Kamchatka event. Slight attenuation occurs in both adaptive filter beams.

Table II-20 gives the full array power reduction relative to beamsteering at $\mu = 0.005$ and $\mu = 0.5$ for four events away from the 273° steer direction in the data sample used to obtain signal degradation measurements for the two Kamchatka events. Event suppression at $\mu = 0.5$ is greater than 12 dB for all events but the first Panama event. Figure II-66 is a Calcomp plot of the beamsteer output and ABF outputs at $\mu = 0.005$ and $\mu = 0.5$ for the weak event from 300°-305°. The corresponding plot for the Andreanof Islands event is displayed in Figure II-67 .

The signal-to-noise ratio improvement of adaptive beamforming relative to beamsteering is, in general, lower with the full array than with the six channels. Differences between the full array and the closely-spaced six-channel array in measured signal degradation are highly variable. This fact is particularly evident at the more rapid convergence rates, where 2 dB differences occur for the weak event from 300°-305° and the second Kamchatka

TABLE II-27

ADAPTIVE FILTERING SIGNAL-TO-NOISE GAIN VERSUS CONVERGENCE RATE FOR A STRONG SIGNAL FROM KAMCHATKA (ALPA, FULL ARRAY, 1971 DAY 276 21.07.18-21.11.33, USING NOISE FROM 1972 DAY 335 0415-0815)

Convergence Rate (μ)	Signal-to-Noise Gain (dB)
0.0010	0.339
0.0015	0.454
0.0020	0.547
0.0030	0.695
0.0040	0.804
0.0050	0.889
0.0070	1.013
0.0100	1.131
0.0150	1.250
0.0200	1.325
0.0300	1.433
0.0400	1.523
0.0500	1.607
0.0700	1.777
0.1000	2.040
0.1500	2.483
0.2000	2.911
0.3000	3.665
0.4000	4.252
0.5000	4.646

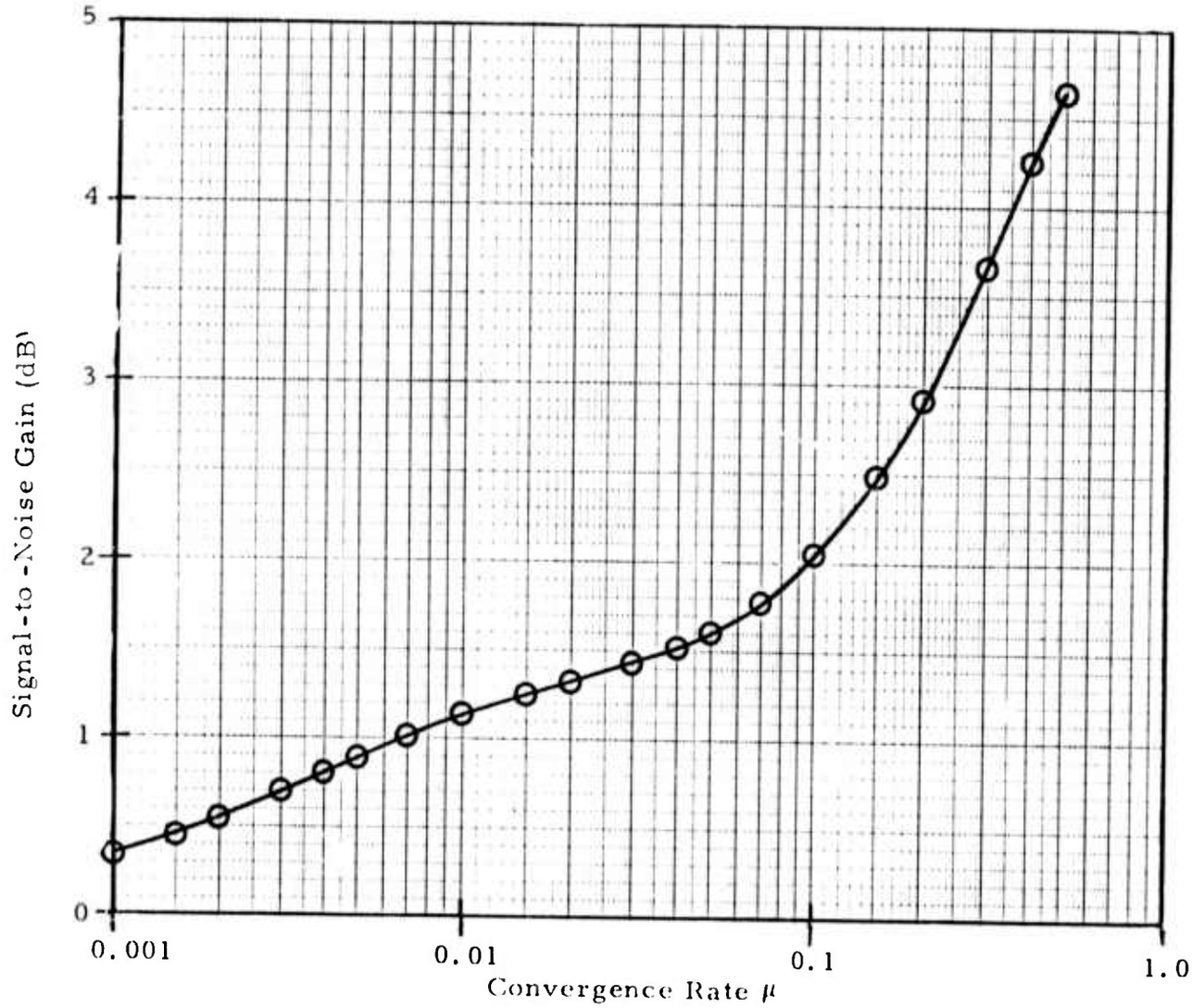

FIGURE II-61

SIGNAL-TO-NOISE GAIN AS A FUNCTION OF CONVERGENCE RATE FOR A STRONG SIGNAL FROM KAMCHATKA (ALPA, FULL ARRAY, 1971 DAY 276 21.07.18-21.11.33, USING NOISE FROM 1972 DAY 335 0415-0815)

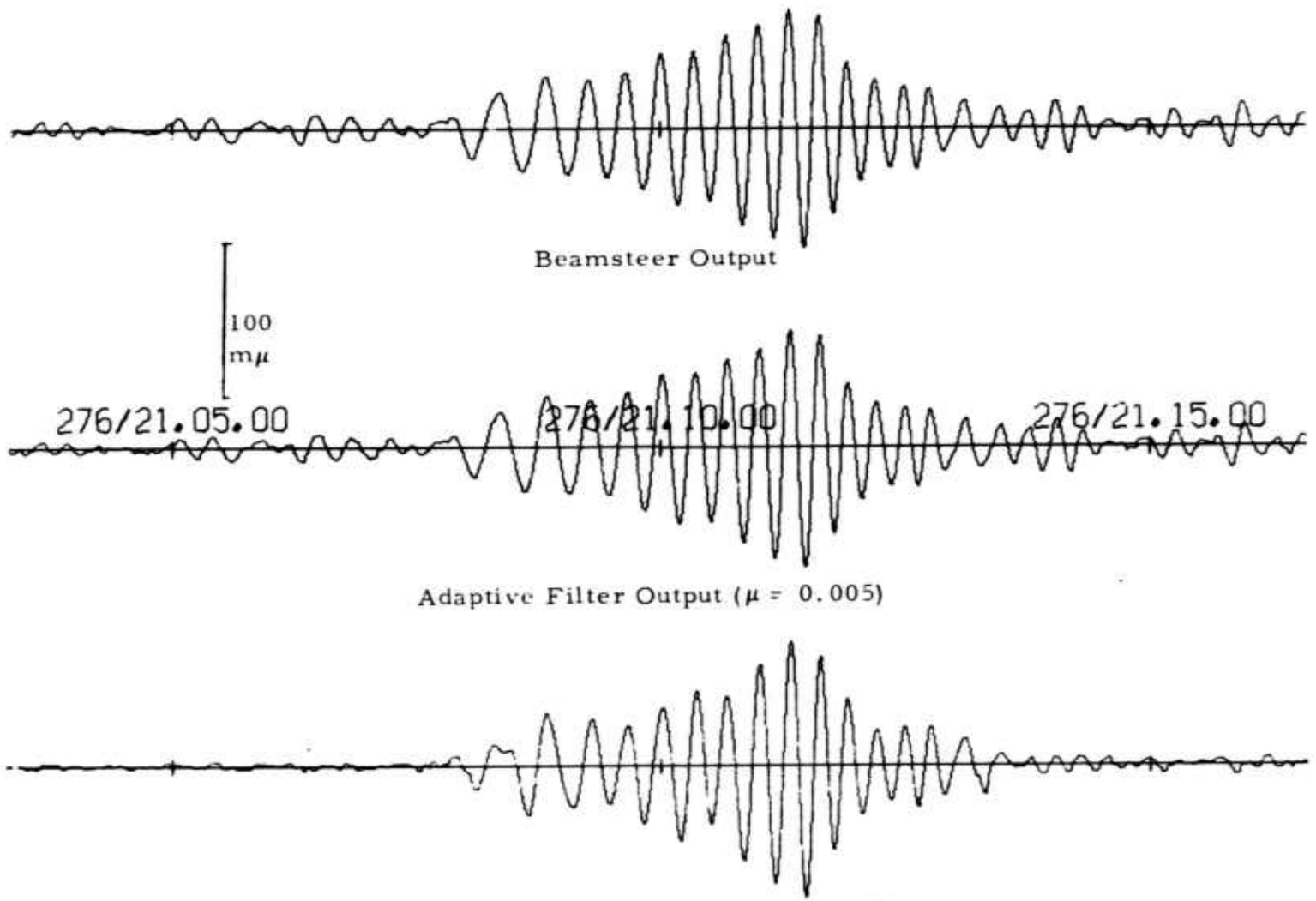

FIGURE II-62

FULL-ARRAY BEAMS FOR MAGNITUDE 4.5 KAMCHATKA EVENT
(DAY 276 1971, STEER DIRECTION 273°)

TABLE II-28

ADAPTIVE FILTERING SIGNAL DEGRADATION VERSUS CONVERGENCE RATE FOR A VERY STRONG SIGNAL FROM KAMCHATKA (ALPA, 16 SITES, 1971 DAY 276 22.07.02-22.11.17)

Convergence Rate (μ)	Signal Degradation (dB)
0.0010	0.088
0.0015	0.131
0.0020	0.173
0.0030	0.253
0.0040	0.325
0.0050	0.392
0.0070	0.506
0.0100	0.642
0.0150	0.804
0.0200	0.917
0.0300	1.056
0.0400	1.129
0.0500	1.167
0.0700	1.192
0.1000	1.185
0.1500	1.162
0.2000	1.150
0.3000	1.125
0.4000	1.068
0.5000	0.973

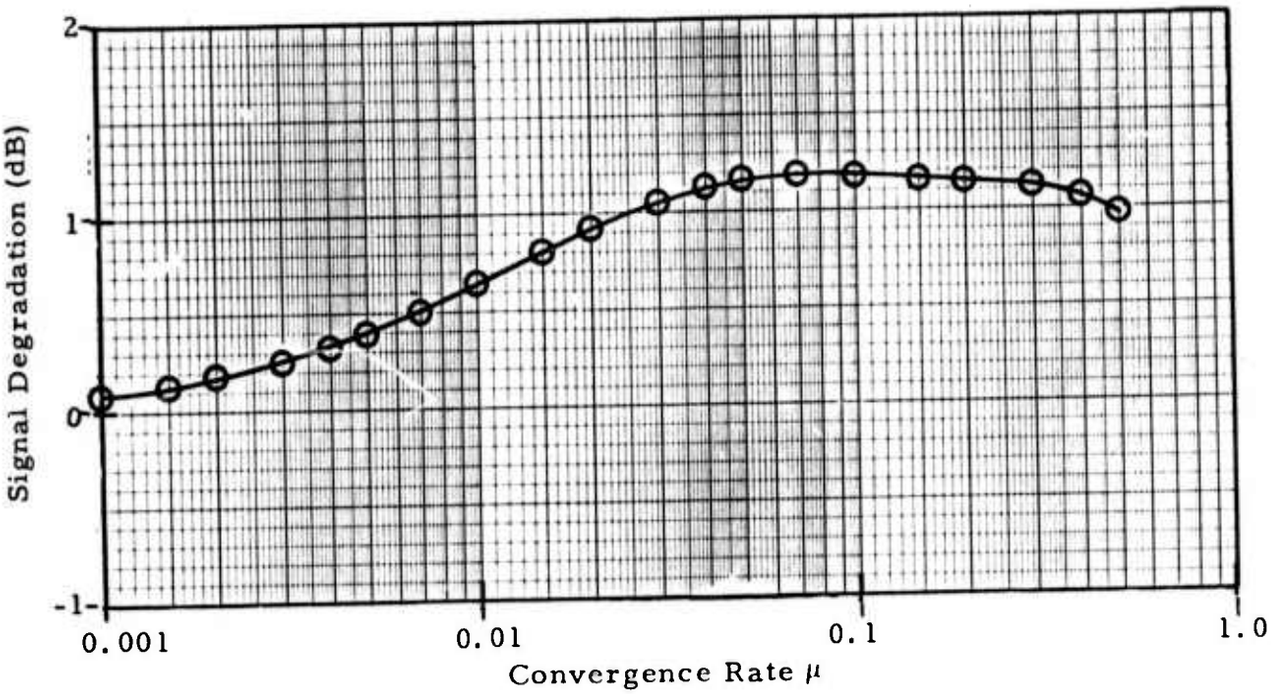

FIGURE II-63

SIGNAL DEGRADATION AS A FUNCTION OF CONVERGENCE RATE FOR A VERY STRONG SIGNAL FROM KAMCHATKA (ALPA, 16 SITES, 1971 DAY 276 22.07.02-22.11.17)

TABLE II-29

ADAPTIVE FILTERING SIGNAL-TO-NOISE GAIN VERSUS CONVERGENCE RATE FOR A VERY STRONG SIGNAL FROM KAMCHATKA (ALPA, FULL ARRAY, 1971 DAY 276 22.07.02-22.11.17, USING NOISE FROM 1972 DAY 335 0415-0815)

Convergence Rate (μ)	Signal-to-Noise Gain (dB)
0.0010	0.269
0.0015	0.351
0.0020	0.414
0.0030	0.506
0.0040	0.570
0.0050	0.615
0.0070	0.681
0.0100	0.744
0.0150	0.818
0.0200	0.877
0.0300	0.990
0.0400	1.105
0.0500	1.218
0.0700	1.436
0.1000	1.729
0.1500	2.133
0.2000	2.467
0.3000	3.026
0.4000	3.489
0.5000	3.846

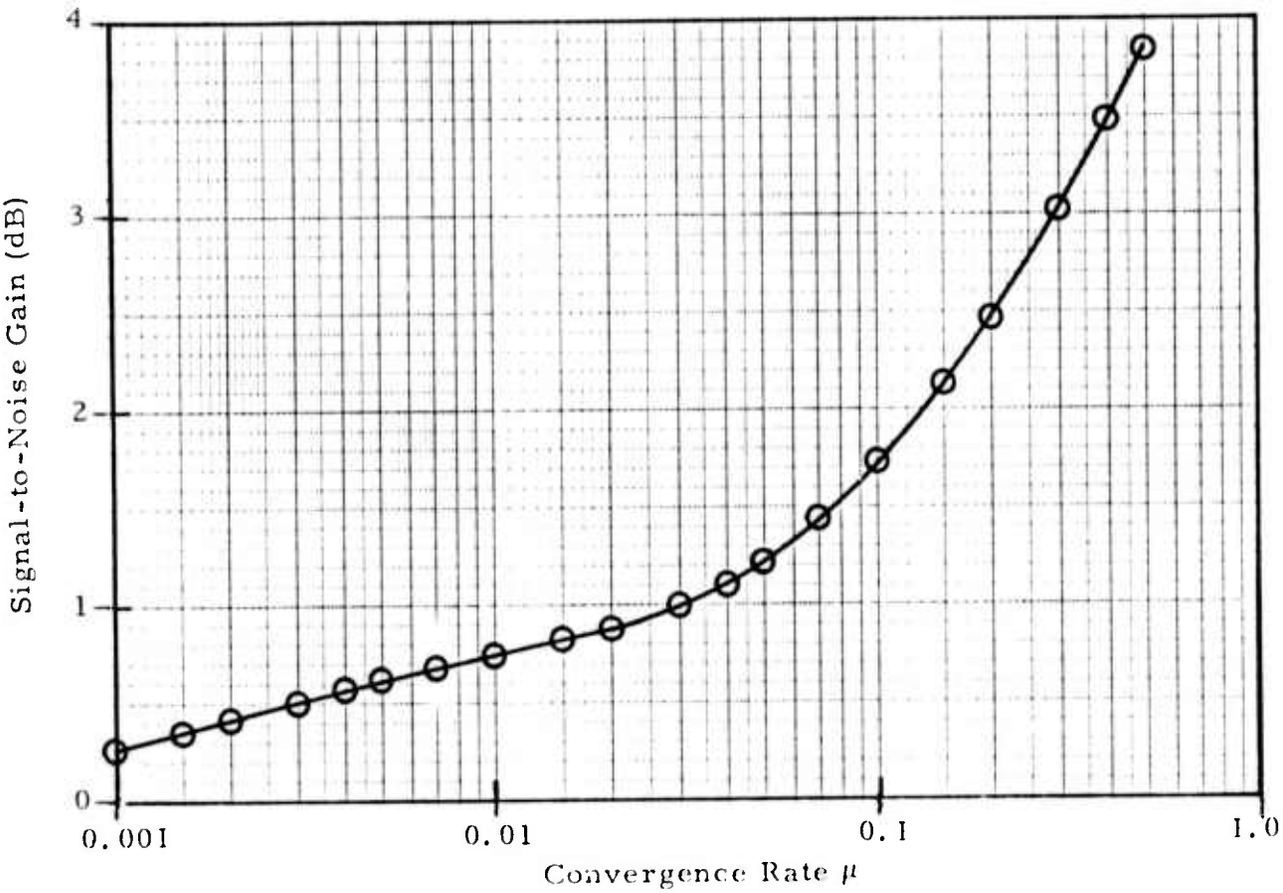

FIGURE II-64

SIGNAL-TO-NOISE GAIN AS A FUNCTION OF CONVERGENCE RATE FOR A VERY STRONG SIGNAL FROM KAMCHATKA (ALPA, FULL ARRAY, 1971 DAY 276 22.07.02-22.11.17, USING NOISE FROM 1972 DAY 335 0415-0815)

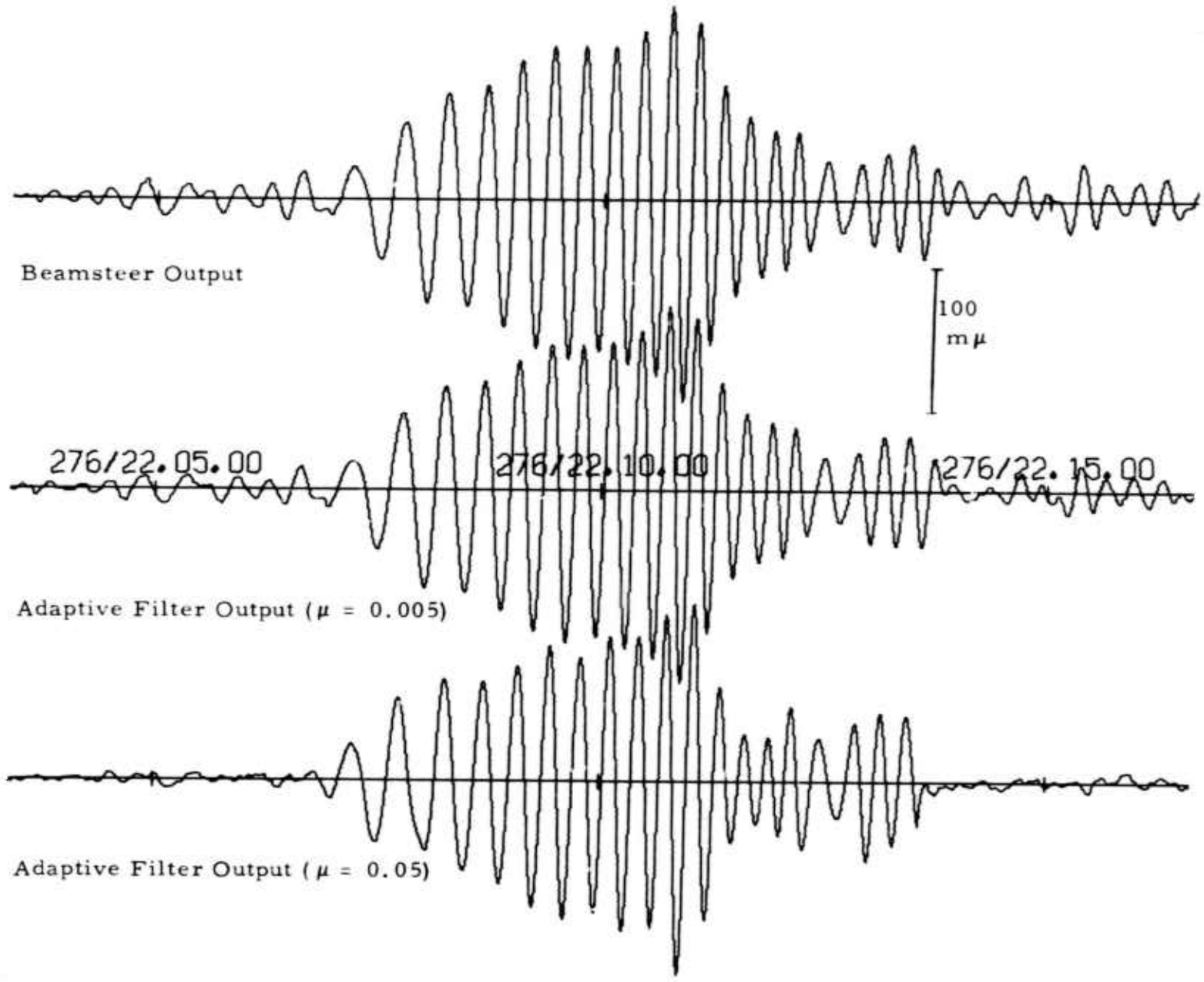

FIGURE II-65

FULL-ARRAY BEAMS FOR MAGNITUDE 4.9 KAMCHATKA EVENT
(DAY 276 1971, STEER DIRECTION 273°)

TABLE II-30

FULL-ARRAY OFF-AZIMUTH EVENT SUPPRESSION
FOR 273° STEER DIRECTION

Event	Azimuth	Computation Gate		Power Reduction (dB)	
		Start Time	Stop Time	$\mu = 0.005$	$\mu = 0.5$
Panama	113°	20:33:00	20:40:00	0.414	10.221
Panama	113°	21:20:00	21:28:00	3.806	14.868
Weak Event	302.5°	21:38:00	21:43:00	1.833	12.811
Andreanof Islands	237°	23:25:00	23:35:00	5.663	18.110

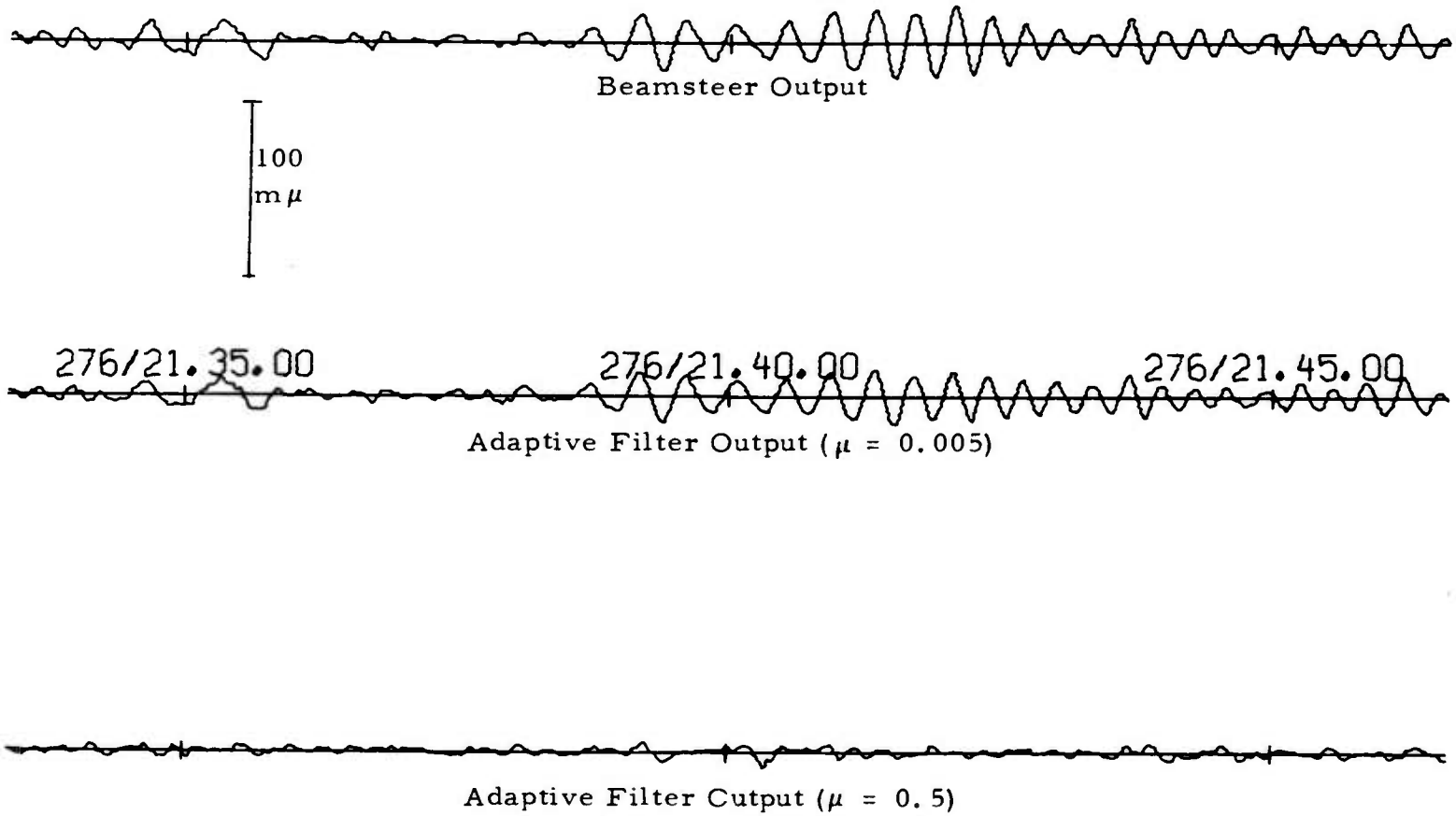

FIGURE II-66

FULL-ARRAY BEAMS FOR A WEAK EVENT FROM 300°-305°
(DAY 276 1971, STEER DIRECTION 273°)

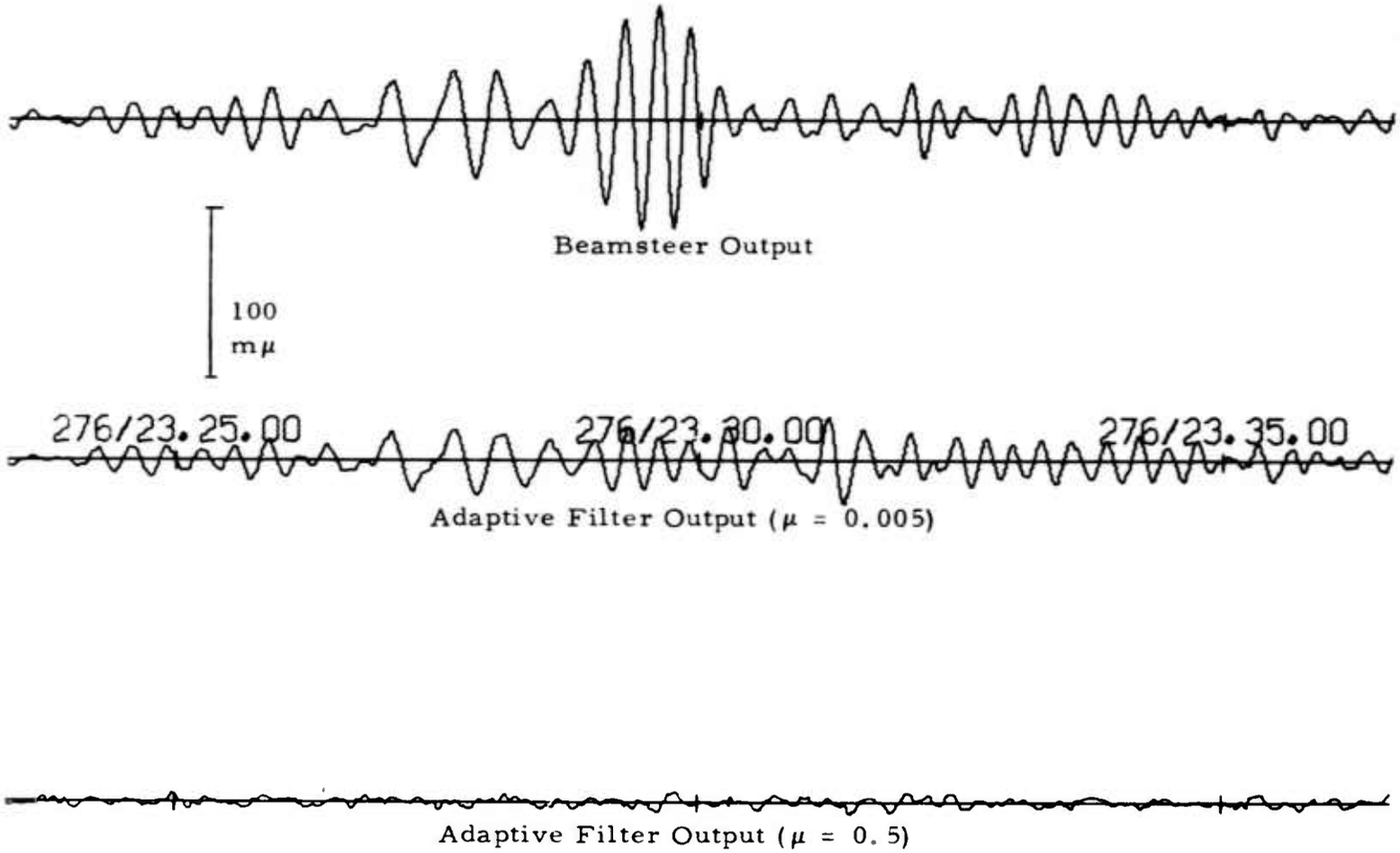

FIGURE II-67

FULL-ARRAY BEAMS FOR ANDREANOF ISLANDS EVENT
(DAY 276 1971, STEER DIRECTION 273°)

event. Differences in measured signal degradation are not the main reason for the reduced improvement relative to beamsteering with the full array. On the contrary, the principal factor contributing to this result is the measured noise reduction for the data sample from 0415 to 0815 on day 335 of 1972: at all convergence rates, the noise reduction is lower with the full array than with six channels. One of the reasons for the lower full-array noise reduction is that the more widely-spaced sensors of the full array have less coherence between sensor pairs than the closely-packed elements of the array used for the six-channel measurements. Another reason is that, for the arrays employed in the noise reduction measurements, the ratio of the directivity index

$$2\pi \Big/ \int_0^{2\pi} |A(f,\theta)|^2 \, d\theta$$

for the fifteen-channel array to that for the six-channel array is greater than 15/6 (≈ 4 dB). In the formula above, $A(f,\theta)$ is the array amplification factor for a plane wave of frequency f arriving from an azimuth of $(360/2\pi)\theta$ degrees. Figures II-68 and II-69, which picture the time-shift-and-sum beam patterns for the six-channel array and fifteen-channel array, respectively, at 0.04 Hz and 3.6 km/sec, demonstrate that the directivity-index ratio is greater than 4 dB. This fact implies that the ratio of coherent energy to spatially uncorrelated energy in the beamsteer output is less for the fifteen-channel array than for the six-channel array if coherent energy is equally likely at all azimuths. As a result, the potential signal-to-noise gain of adaptive beamforming relative to beamsteering is less for fifteen channels than for six channels.

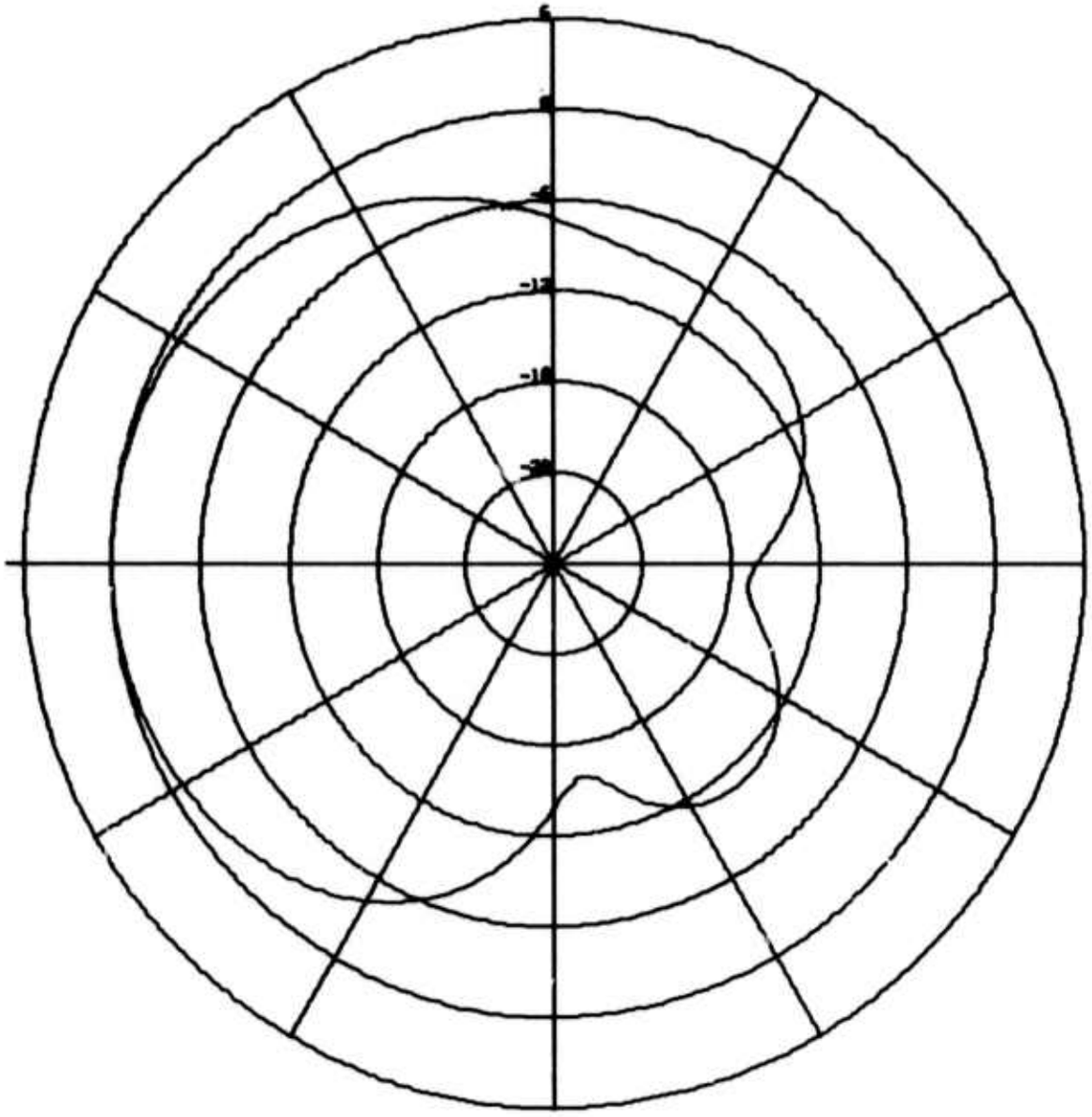

FIGURE II-68

BEAMSTEER RESPONSE FOR SIX-CHANNEL
NOISE SAMPLE FROM DAY 335 OF 1972

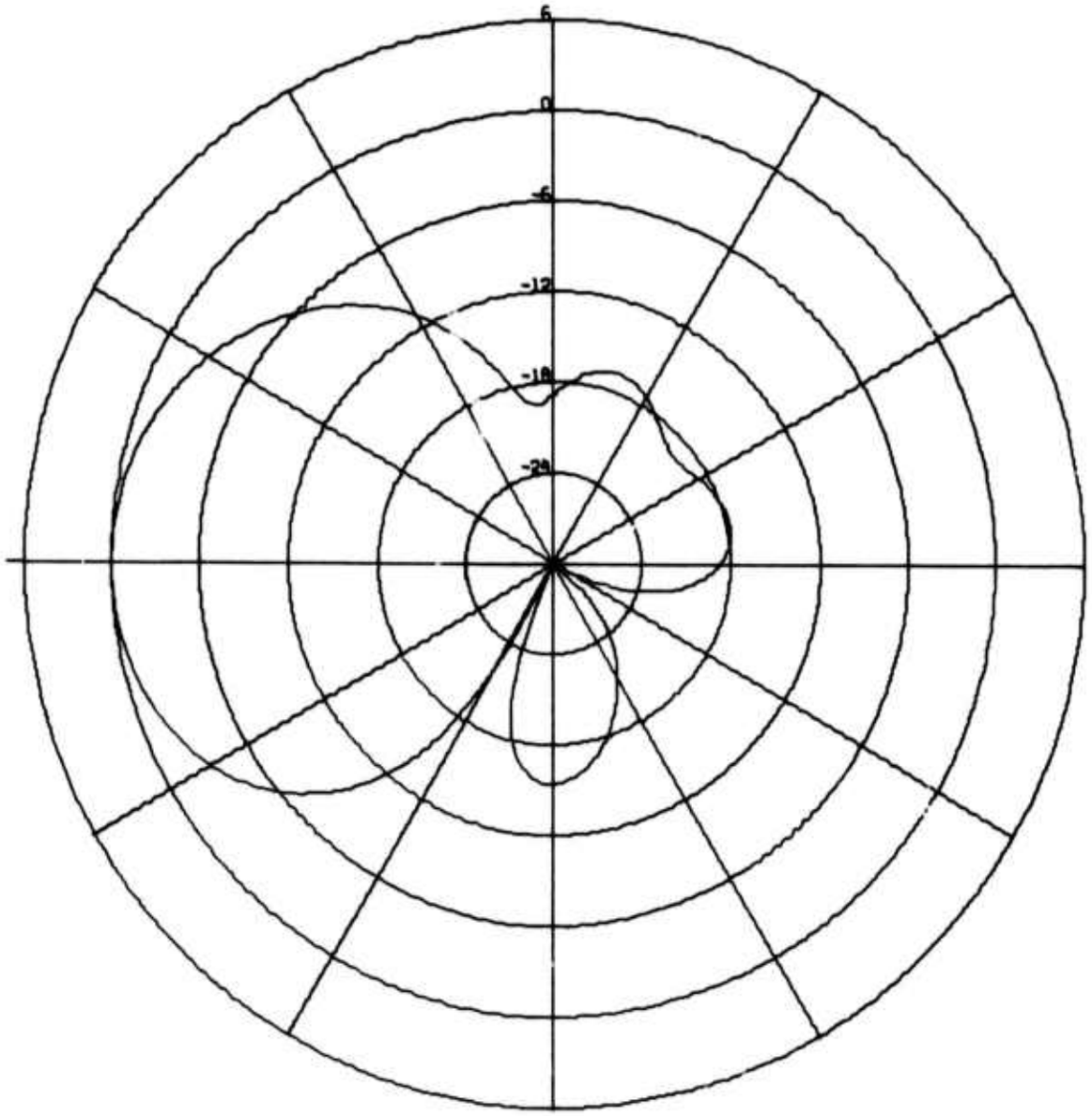

ALPA
TIME-SHIFT-AND-SUM BEAM PATTERN
BEAM LOOK VELOCITY IS 3.6, LOOK AZIMUTH 270.0
FREQUENCY IS 0.04000 HZ, PERIOD 25.0 SECONDS

FIGURE II-69

BEAMSTEER RESPONSE FOR FULL-ARRAY
NOISE SAMPLE FROM DAY 335 OF 1972

E. FREQUENCY FILTERING FOR IMPROVED DETECTION

So far, the focus of attention in this report has been the improved detection performance obtained from the directional-filtering capability of adaptive beamforming. Another important factor affecting detector performance is the relative weighting given to the various frequency components in the data. In short, what frequency filter should be applied to the data in order to achieve best detection results? An additional question is whether this frequency filter should be applied to the vertical-component data of the individual sites before adaptive beamforming or whether it should be applied to the beam outputs after adaptive filtering. In a time-domain adaptive filtering system such as the one employed in this study, the answer to this question is that the frequency filter should be applied before adaptive processing so that the adaptive beamformer can concentrate on achieving processing gain at the frequencies most useful for detection. If, instead, the frequency filter is applied to the beam outputs, the adaptive processing gains at frequencies relevant to detection are reduced by the mean-square-power performance criterion, which forces the adaptive-filtering system to react to conditions at frequencies of little use in detection processing. The precise nature of the prefilter to be applied to the site vertical component data before input to the multichannel-filtering system has yet to be discussed. The remainder of this subsection is devoted to the development of a technique for determining the frequency weightings for this prefilter.

One frequently employed detection system is a square-law (or power) detector, in which the average power of a beam over some specified time gate is the detector output. Since noise fluctuates in a random fashion, the noise output power over the specified gate length has a characteristic probability density function. If a specific signal (uncorrelated with the noise) is added to the noise, the resulting power probability density function shifts upward by an amount equal to the signal power over the detection gate. Figure II-70

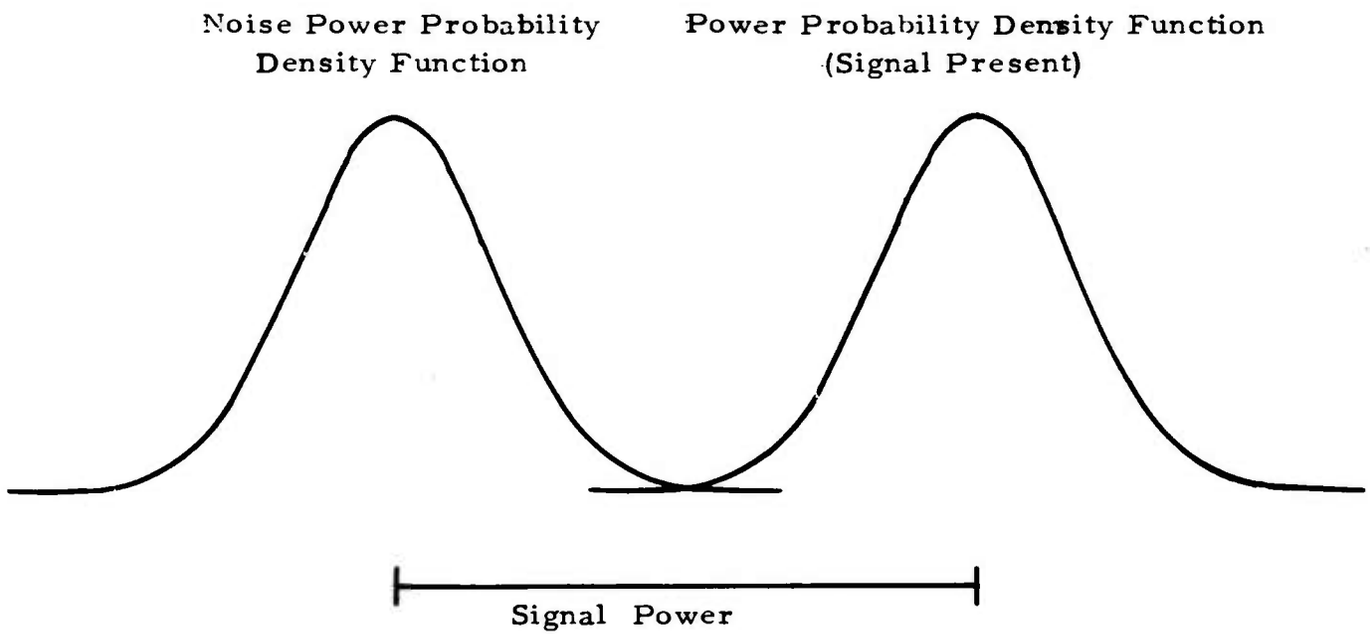

FIGURE II-70

HYPOTHETICAL POWER PROBABILITY DENSITY FUNCTIONS
FOR NOISE ALONE AND FOR SIGNAL PLUS NOISE

illustrates this situation. If the noise power has a Gaussian probability distribution, the best detection results occur when the ratio of the signal power to the noise-power standard deviation is a maximum. The best frequency filter for detection is the filter which maximizes this ratio. Suppose that a discrete Fourier transform is taken over the detection gate. Let $\Phi_{ss}(f_k)$ and $\Phi_{nn}(f_k)$ denote the squared amplitude of the signal and noise, respectively, at the discrete-Fourier-transform frequency f_k. Let $W(f_k)$ denote the power weight given to the frequency f_k. Then the signal power over the detection gate is $W^T S$, and the noise power variance is $W^T \overline{ZZ^T} W$, where the K-component vectors W, S, and Z are, respectively,

$$W = \begin{bmatrix} W(f_1) \\ W(f_2) \\ \vdots \\ W(f_K) \end{bmatrix}, \quad S = \begin{bmatrix} \Phi_{ss}(f_1) \\ \Phi_{ss}(f_2) \\ \vdots \\ \Phi_{ss}(f_K) \end{bmatrix}, \quad \text{and } Z = \begin{bmatrix} \Phi_{nn}(f_1) - \overline{\Phi_{nn}(f_1)} \\ \Phi_{nn}(f_2) - \overline{\Phi_{nn}(f_2)} \\ \vdots \\ \Phi_{nn}(f_K) - \overline{\Phi_{nn}(f_K)} \end{bmatrix}.$$

Here $\overline{\Phi_{nn}(f_k)}$ denotes the expectation of the squared noise amplitude $\Phi_{nn}(f_k)$ at the frequency f_k. That is to say, $\overline{\Phi_{nn}(f_k)}$ is the noise power density spectrum at f_k. The matrix expectation $\overline{ZZ^T}$ is the covariance matrix for the noise power density. The ratio $W^T S \Big/ \sqrt{W^T \overline{ZZ^T} W}$ or, equivalently, $W^T S S^T W \Big/ W^T \overline{ZZ^T} W$ is maximized when the weight vector W is proportional to $(\overline{ZZ^T})^{-1} S$. Hopefully all components of W are positive. This condition is met when the quantities $\Phi_{nn}(f_k) - \overline{\Phi_{nn}(f_k)}$ are independent from frequency to frequency, so that $\overline{ZZ^T}$ is a diagonal matrix. To design a filter in this way, fourth-order moments must be measured. No software is currently available for these measurements, so that matrices $\overline{ZZ^T}$ are not available.

If the noise is colored and Gaussian, simplifying assumptions are possible. As an artifice, let the data be passed through a noise-whitening filter, so that the elements $\Phi_{nn}(f_k)$ of S are replaced by $\Phi_{ss}(f_k) \Big/ \overline{\Phi_{nn}(f_k)}$ and the elements $\Phi_{nn}(f_k) - \overline{\Phi_{nn}(f_k)}$ of Z by $\left[\Phi_{nn}(f) \Big/ \overline{\Phi_{nn}(f)}\right] - 1$. Since the noise is now white and Gaussian, the variables $\Phi_{nn}(f_k) \Big/ \overline{\Phi_{nn}(f_k)}$ are independent and each have a χ^2 distribution, so that their variance is proportional to their expectation, which is one. Then the quantity $W^T S S W^T \Big/ W^T \overline{Z Z^T} W$ to be maximized is proportional to $W^T S S^T W \Big/ W^T W$, or

$$\left[\frac{\vec{W}}{|\vec{W}|} \cdot \vec{S}\right]^2 .$$

Maximization is achieved when the vector W points toward the same direction as the vector S. Thus the components of the weight vector W are proportional to $\Phi_{ss}(f_k) \Big/ \overline{\Phi_{nn}(f_k)}$, and the combined power response of the noise-whitening filter and the frequency weighting $W(f_k)$ is proportional to $\Phi_{ss}(f_k) \Big/ \left[\overline{\Phi_{nn}(f_k)}\right]^2$. The associated amplitude weighting is proportional to the signal amplitude divided by the noise power. As the equivalent number of degrees of freedom in the filtered noise power spectrum increases, the noise power probability distribution approaches a Gaussian distribution, so that the amplitude weighting $\sqrt{\Phi_{ss}(f)} \Big/ \overline{\Phi_{nn}(f)}$ is near-optimum for detection. The equivalent number of degrees of freedom in the filtered noise power spectrum can be increased by lengthening the specified detection gate length.

Using the power spectrum of the weak event from 300^o-305^o in the data sample from day 276 of 1971 and some noise spectra from late autumn of 1971, a detection filter was specified with amplitude response $\sqrt{\Phi_{ss}(f)} \Big/ \overline{\Phi_{nn}(f)}$. A zero-phase time-domain convolution filter was designed to approximate this

amplitude response. Figure II-71 pictures the response of the time-domain filter as a function of frequency. Note the slight depression at periods between 16 and 18 seconds. In the 6 to 8-second band, the desired zero response was weighted especially heavily to produce the lower sidelobes there. The prefilter whose response is shown in Figure II-71 is used in all long-period processing for the remainder of this report unless specifically noted otherwise.

I ADAPTIVE PROCESSING WITH THE NEW PREFILTER

The purpose of this subsection is to determine the effect of the prefilter in Figure II-71 on adaptive beamforming signal-to-noise ratio improvement relative to beamsteering. Since this prefilter is applied to data sampled once every two seconds, an adaptive-filter length of fifteen points per channel is sufficient to span all possible propagation delays across ALPA at the 3.6 km/sec apparent velocity of Rayleigh waves. In the beginning of this subsection, the adaptive-filter length remains at the 31-point-per-channel value used previously in this section. The final part of this subsection examines the effect of cutting the adaptive-filter length to fifteen points per channel.

Noise reduction measurements with the 31-point-long adaptive filter employ the data sample from 0415 to 0815 on day 335 of 1972. Processing is exactly the same as in Subsection D except for a two-second sample interval and the application of the new prefilter in Figure II-71. Table II-31 and Figure II-72 present the noise reduction as a function of the convergence parameter μ. A comparison of Table II-31 with Table II-22 in Subsection D reveals that the noise reduction is significantly greater with data passed through the new prefilter. The probable explanation for the increased noise reduction is the additional emphasis given to the more coherent energy at low frequencies.

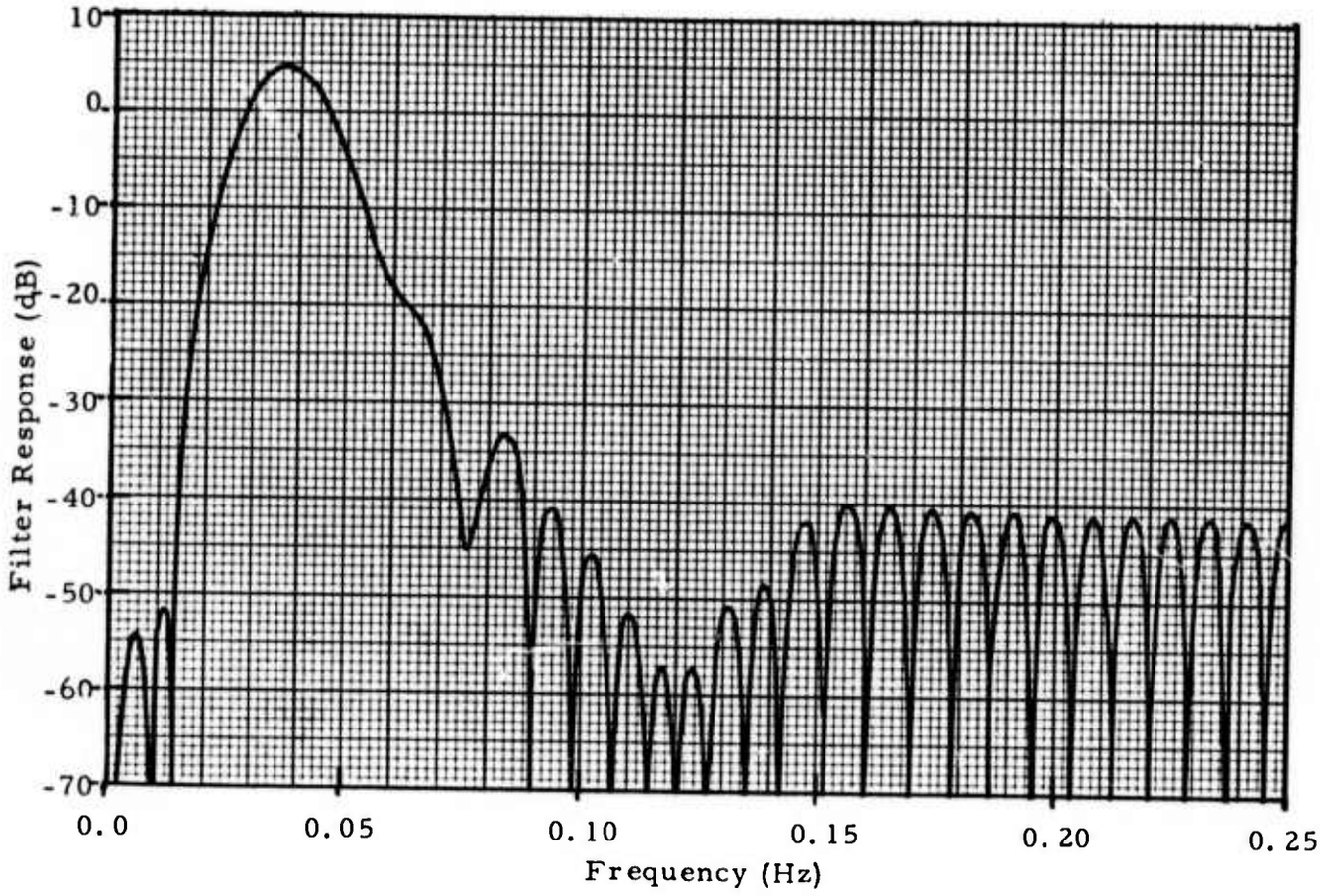

FIGURE II-71

NEW PREFILTER RESPONSE

TABLE II-31

NOISE REDUCTION VERSUS CONVERGENCE RATE
WITH 31-POINT-LONG ADAPTIVE FILTER
(ALPA, 15 SITES, 1972 DAY 335 0415-0815)

Convergence Rate (μ)	Signal-to-Noise Gain (dB)
0.0010	0.499
0.0015	0.679
0.0020	0.830
0.0030	1.075
0.0040	1.268
0.0050	1.427
0.0070	1.678
0.0100	1.958
0.0150	2.297
0.0200	2.555
0.0300	2.959
0.0400	3.283
0.0500	3.563
0.0700	4.043
0.1000	4.640
0.1500	5.445
0.2000	6.094
0.3000	7.074
0.4000	7.749
0.5000	8.204

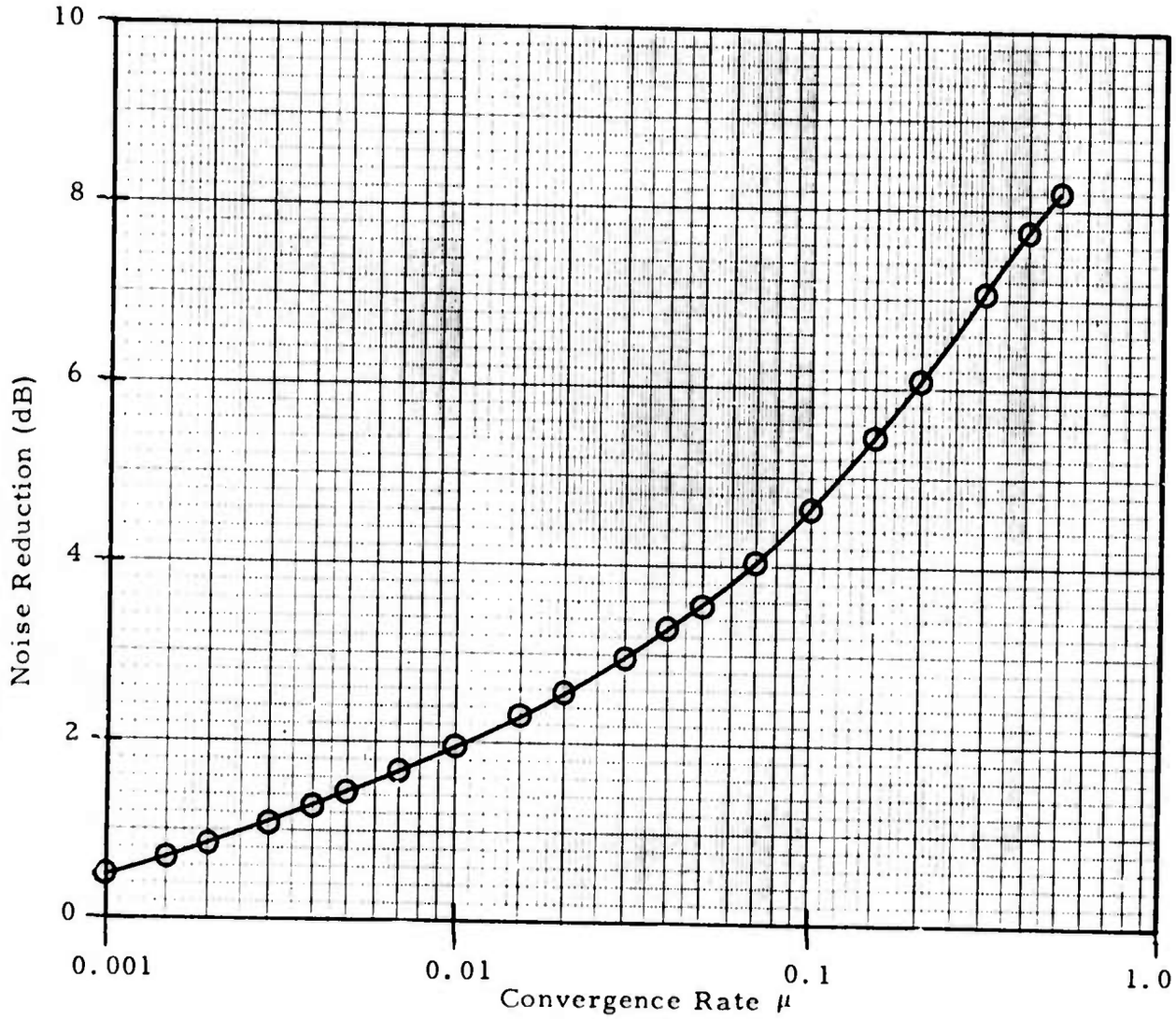

FIGURE II-72

NOISE REDUCTION AS A FUNCTION OF CONVERGENCE RATE WITH 31-POINT-LONG ADAPTIVE FILTER (ALPA, 15 SITES, 1972 DAY 335 0415-0815)

The same three events in the data sample from 2000 to 2345 on day 276 of 1971 provide signal degradation measurements for the 31-point-long adaptive filter. The first of these is the weak event from 300°-305°. Table II-32 and Figure II-73 portray signal degradation with the new prefilter as a function of convergence rate over a 512-second gate. For this event, signal-to-noise gain estimates based on the noise sample from day 335 of 1972 appear in Table II-33 and Figure II-74. The improvement relative to beamsteering is slightly higher than with the old prefilter (Table II-24) at all convergence rates.

At the 302.5° steer direction used for the weak event from 300°-305°, there are five off-azimuth events in the data sample from day 276 of 1971. Table II-34 gives the power reduction relative to beamsteering at $\mu = 0.007$ and $\mu = 0.5$ for these events. For the two Panama events and the Andreanof Islands event, the suppression of these events is comparable to the suppression obtained with the old prefilter (Table II-25). For the two Kamchatka events 30° away from the steer direction, however, the attenuation is significantly lower with the new prefilter. The emphasis given to low-frequency energy by the new prefilter not only increases the effective beamwidth of the adaptive beamformer but also concentrates more energy near the beginning of the events, so that the adaptive filter set cannot react as effectively to the presence of these events.

These two Kamchatka events arriving from a 273° azimuth also furnish the remaining signal degradation measurements for the 31-point-long adaptive filter. The first arrived at about 2108. For this event, Table II-35 and Figure II-75 depict signal degradation with the new prefilter as a function of the convergence parameter μ. The resulting signal-to-noise gain estimates corresponding to the noise sample from day 335 of 1972 appear in Table II-36 and Figure II-76. Maximum signal-to-noise gain of 6.36 dB relative to beamsteering at $\mu = 0.5$ is significantly higher than the corresponding 4.65 dB

TABLE II-32

SIGNAL DEGRADATION VERSUS CONVERGENCE RATE WITH 31-POINT-LONG ADAPTIVE FILTER FOR A WEAK SIGNAL FROM 300^{o}-305^{o} (ALPA, 16 SITES, 1971 DAY 276 21.37.01-21.45.32)

Convergence Rate (μ)	Signal-to-Noise Gain (dB)
0.0010	0.102
0.0015	0.157
0.0020	0.213
0.0030	0.328
0.0040	0.443
0.0050	0.557
0.0070	0.775
0.0100	1.080
0.0150	1.533
0.0200	1.929
0.0300	2.592
0.0400	3.129
0.0500	3.579
0.0700	4.303
0.1000	5.104
0.1500	5.975
0.2000	6.479
0.3000	6.869
0.4000	6.859
0.5000	6.692

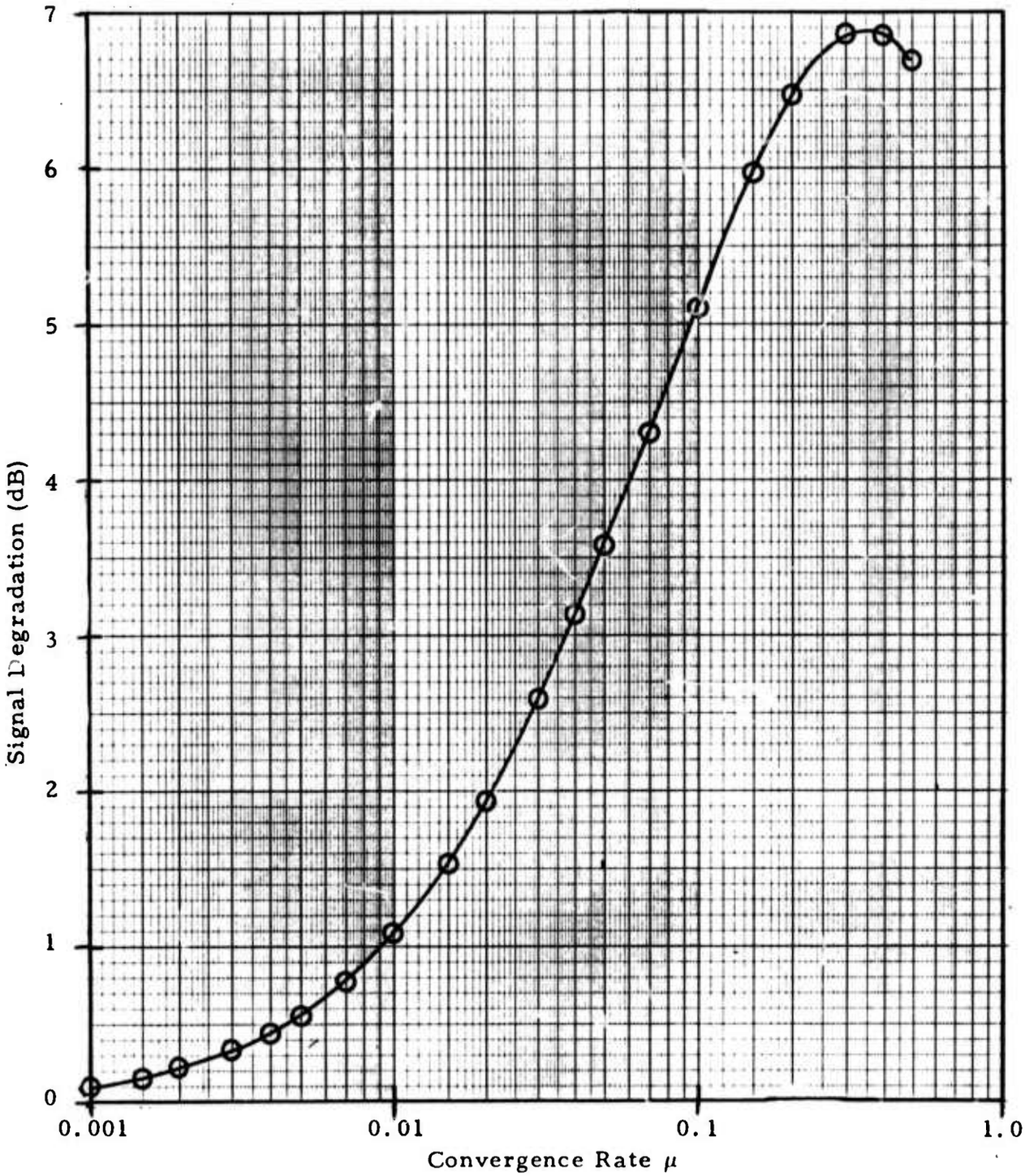

FIGURE II-73

SIGNAL DEGRADATION AS A FUNCTION OF CONVERGENCE RATE WITH 31-POINT-LONG ADAPTIVE FILTER FOR A WEAK SIGNAL FROM 300°-305° (ALPA, 16 SITES, 1971 DAY 276 21.37.01-21.45.32)

TABLE II-33

SIGNAL-TO-NOISE GAIN VERSUS CONVERGENCE RATE WITH 31-POINT-LONG ADAPTIVE FILTER FOR A WEAK SIGNAL FROM 300^{o}-305^{o} (ALPA, FULL ARRAY, 1971 DAY 276 21.37.01-21.45.32, USING NOISE FROM 1972 DAY 335 0415-0815)

Convergence Rate (μ)	Signal-to-Noise Gain (dB)
0.0010	0.397
0.0015	0.522
0.0020	0.617
0.0030	0.747
0.0040	0.825
0.0050	0.870
0.0070	0.903
0.0100	0.878
0.0150	0.764
0.0200	0.626
0.0300	0.367
0.0400	0.154
0.0500	-0.016
0.0700	-0.260
0.1000	-0.464
0.1500	-0.530
0.2000	-0.385
0.3000	0.205
0.4000	0.890
0.5000	1.512

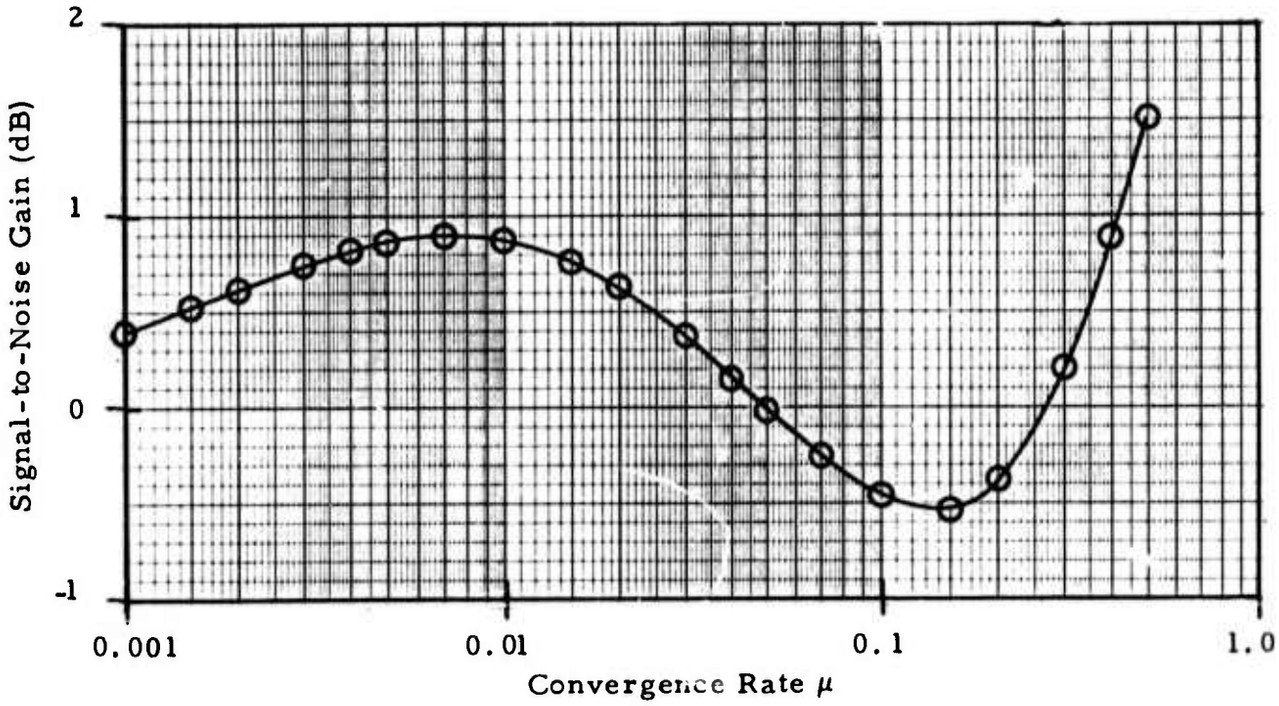

FIGURE II-74

SIGNAL-TO-NOISE GAIN AS A FUNCTION OF CONVERGENCE RATE WITH 31-POINT-LONG ADAPTIVE FILTER FOR A WEAK SIGNAL FROM 300°-305° (ALPA, FULL ARRAY, 1971 DAY 276 21.32.01-21.45.32, USING NOISE FROM 1972 DAY 335 0415-0815)

TABLE II-34

OFF-AZIMUTH EVENT SUPPRESSION
FOR 302.5° STEER DIRECTION
WITH 31-POINT-LONG ADAPTIVE FILTER

Event	Azimuth	Computation Gate		Power Reduction (dB)	
		Start Time	Stop Time	$\mu = 0.007$	$\mu = 0.5$
Panama	113°	20:33:00	20:40:00	1.238	15.183
Kamchatka	273°	21:07:00	21:15:00	0.885	9.103
Panama	113°	21:20:00	21:28:00	8.848	20.751
Kamchatka	273°	22:07:00	22:14:00	2.880	18.881
Andreanof Islands	237°	23:25:00	23:35:00	5.084	10.591

TABLE II-35

SIGNAL DEGRADATION VERSUS CONVERGENCE RATE WITH 31-POINT-LONG ADAPTIVE FILTER FOR A STRONG SIGNAL FROM KAMCHATKA (ALPA, 16 SITES, 1971 DAY 276 21.07.18-21.11.33)

Convergence Rate (μ)	Signal Degradation (dB)
0.0010	0.038
0.0015	0.055
0.0020	0.071
0.0030	0.102
0.0040	0.131
0.0050	0.160
0.0070	0.214
0.0100	0.292
0.0150	0.411
0.0200	0.516
0.0300	0.689
0.0400	0.824
0.0500	0.931
0.0700	1.091
0.1000	1.243
0.1500	1.386
0.2000	1.475
0.3000	1.614
0.4000	1.737
0.5000	1.846

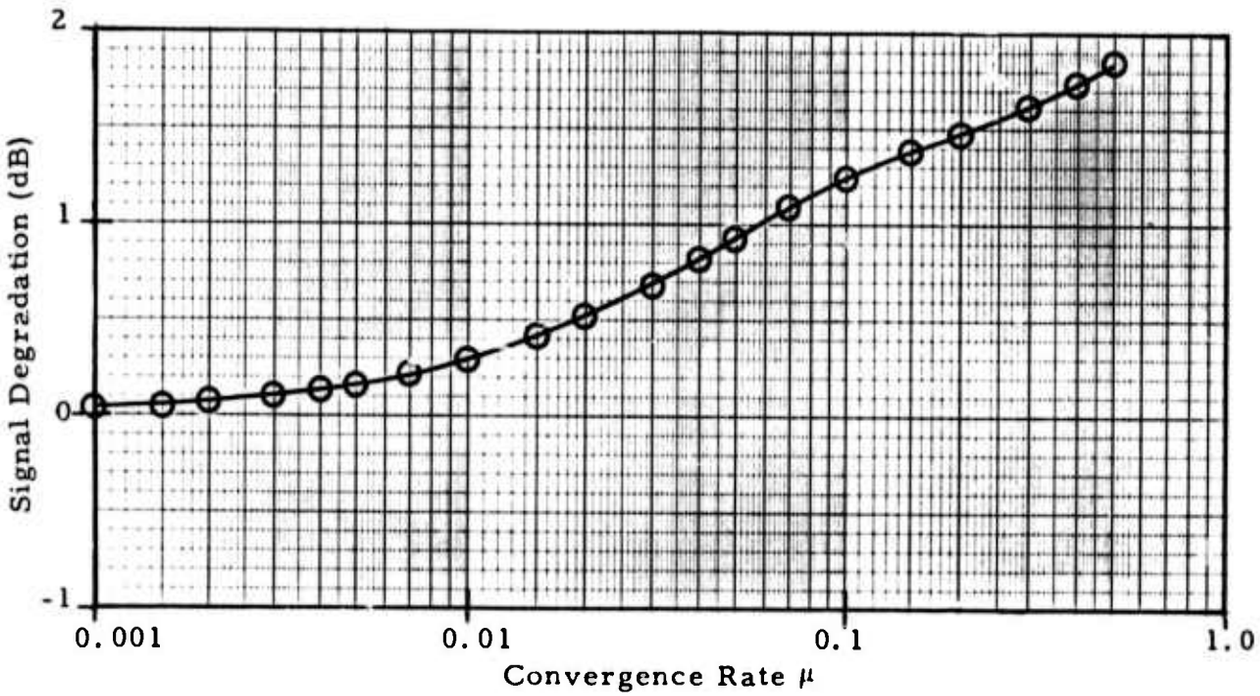

FIGURE II-75

SIGNAL DEGRADATION AS A FUNCTION OF CONVERGENCE RATE WITH 31-POINT-LONG ADAPTIVE FILTER FOR A STRONG SIGNAL FROM KAMCHATKA (ALPA, 16 SITES, 1971 DAY 276 21.07.18-21.11.33)

TABLE II-36

SIGNAL-TO-NOISE GAIN VERSUS CONVERGENCE RATE WITH 31-POINT-LONG ADAPTIVE FILTER FOR A STRONG SIGNAL FROM KAMCHATKA (ALPA, FULL ARRAY, 1971 DAY 276 21.07.18-21.11.33, USING NOISE FROM 1972 DAY 335 0415-0815)

Convergence Rate (μ)	Signal-to-Noise Gain (dB)
0.0010	0.461
0.0015	0.624
0.0020	0.759
0.0030	0.973
0.0040	1.137
0.0050	1.267
0.0070	1.464
0.0100	1.666
0.0150	1.886
0.0200	2.039
0.0300	2.270
0.0400	2.459
0.0500	2.632
0.0700	2.952
0.1000	3.397
0.1500	4.059
0.2000	4.619
0.3000	5.460
0.4000	6.012
0.5000	6.358

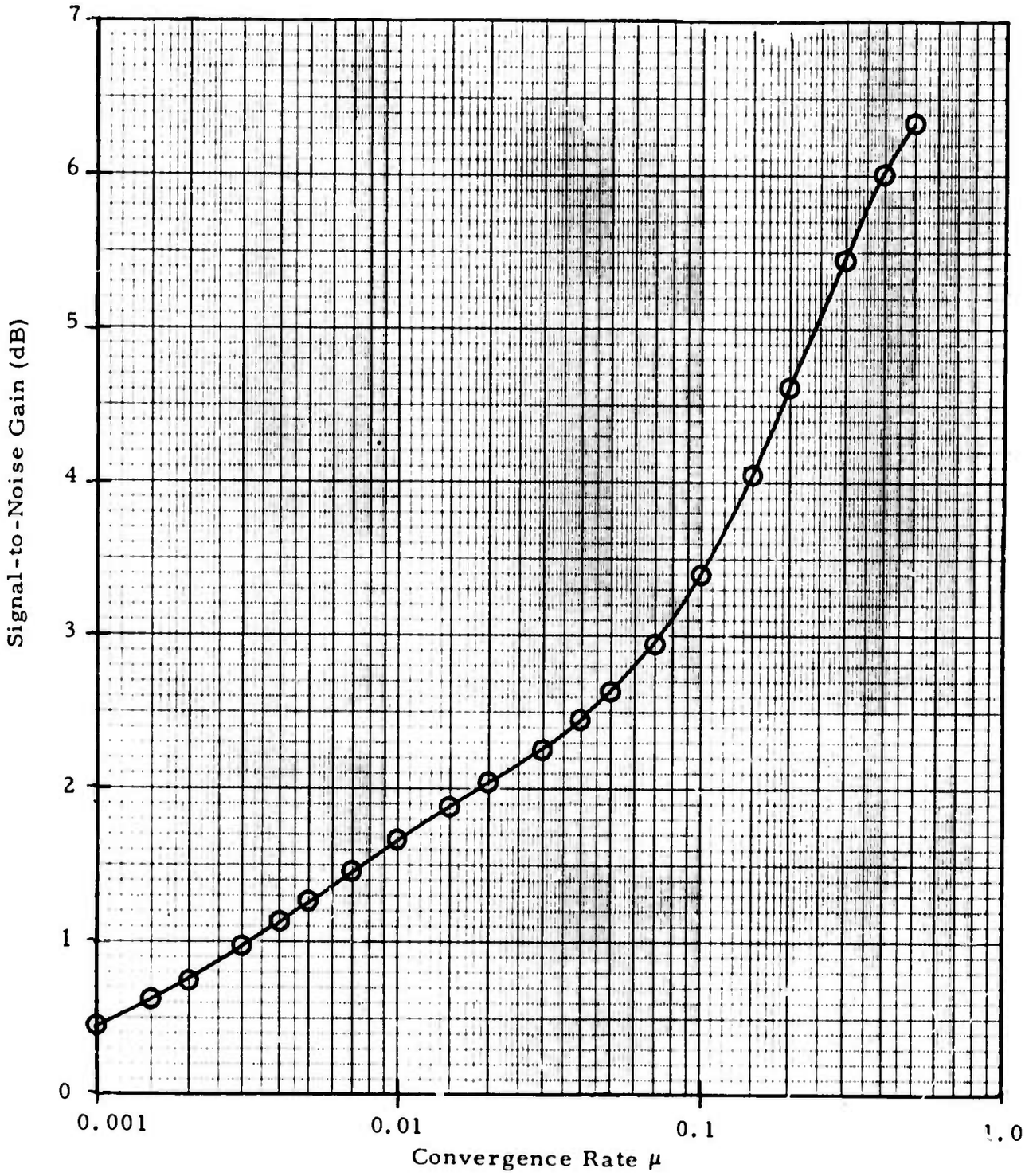

FIGURE II-76

SIGNAL-TO-NOISE GAIN AS A FUNCTION OF CONVERGENCE RATE WITH 31-POINT-LONG ADAPTIVE FILTER FOR A STRONG SIGNAL FROM KAMCHATKA (ALPA, FULL ARRAY, 1971 DAY 276 21.07.18-21.11.33, USING NOISE FROM 1972 DAY 335 0415-0815)

gain with the old prefilter. The increased adaptive filtering gain due to the new prefilter is an added benefit over and above any detection improvement obtained through frequency filtering. The second of the two Kamchatka events reached ALPA at approximately 2207. Table II-37 and Figure II-77 present signal degradation as a function of convergence rate with the new prefilter for this event. The signal-to-noise gain estimates obtained by combining the signal degradation measurements for the second Kamchatka event with noise reduction measurements for day 335 of 1972 are given in Table II-38 and Figure II-78. In this case, the signal-to-noise ratio improvement relative to beamsteering at $\mu = 0.5$ is more than four dB greater than with the old prefilter (Table II-29).

Table II-39 gives the power reduction relative to beamsteering at $\mu = 0.007$ and $\mu = 0.5$ for four events away from the 273° azimuth of the two Kamchatka events in the data sample from day 276 of 1971. Event suppression for the Andreanof Islands event 36° from the look direction is less for the new prefilter than for the old prefilter. Otherwise the event-suppression results are comparable for both prefilters. The fact that the ABF output at $\mu = 0.007$ is slightly stronger than the beamsteer output for the first Panama event is due to an initial ABF response greater than the beamsteer response toward the 113° azimuth of that event: the new prefilter's enhancement of the low-frequency energy near the beginning of the event does not allow sufficient time to attenuate the event on the adaptive beam output.

Past experience with multichannel filtering systems has shown that a filter length greater than the travel time across an array seldom produces any significant additional processing gain. In the case of adaptive beamforming, moreover, signal degradation might conceivably increase substantially with a greater filter length than necessary. Likewise, another reason for examining the effect of adaptive filter length is the resulting computational load, which is proportional to the number of components in the adaptive filter vector.

TABLE II-37

SIGNAL DEGRADATION VERSUS CONVERGENCE RATE WITH 31-POINT-LONG ADAPTIVE FILTER FOR A VERY STRONG SIGNAL FROM KAMCHATKA (ALPA, 16 SITES, 1971 DAY 276 22.07.02-22.11.17)

Convergence Rate (μ)	Signal Degradation (dB)
0.0010	0.059
0.0015	0.087
0.0020	0.113
0.0030	0.163
0.0040	0.209
0.0050	0.252
0.0070	0.328
0.0100	0.423
0.0150	0.543
0.0200	0.630
0.0300	0.747
0.0400	0.814
0.0500	0.851
0.0700	0.879
0.1000	0.868
0.1500	0.800
0.2000	0.707
0.3000	0.506
0.4000	0.314
0.5000	0.137

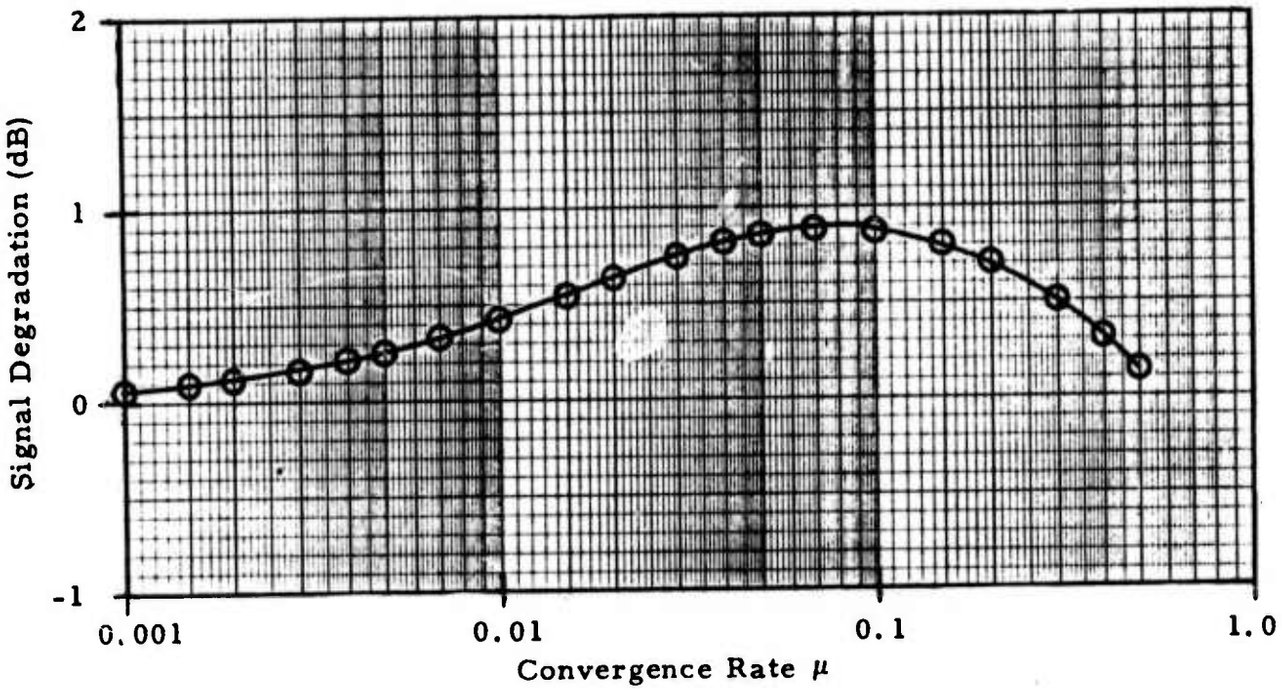

FIGURE II-77

SIGNAL DEGRADATION AS A FUNCTION OF CONVERGENCE RATE WITH 31-POINT-LONG ADAPTIVE FILTER FOR A VERY STRONG SIGNAL FROM KAMCHATKA (ALPA, 16 SITES, 1971 DAY 276 22.07.02-22.11.17)

TABLE II-38

SIGNAL-TO-NOISE GAIN VERSUS CONVERGENCE RATE WITH 31-POINT-LONG ADAPTIVE FILTER FOR A VERY STRONG SIGNAL FROM KAMCHATKA (ALPA, FULL ARRAY, 1971 DAY 276 22.07.02-22.11.17, USING NOISE FROM 1972 DAY 335 0415-0815)

Convergence Rate (μ)	Signal-to-Noise Gain (dB)
0.0010	0.440
0.0015	0.592
0.0020	0.717
0.0030	0.912
0.0040	1.059
0.0050	1.175
0.0070	1.350
0.0100	1.535
0.0150	1.754
0.0200	1.925
0.0300	2.212
0.0400	2.469
0.0500	2.712
0.0700	3.164
0.1000	3.772
0.1500	4.645
0.2000	5.387
0.3000	6.568
0.4000	7.435
0.5000	8.067

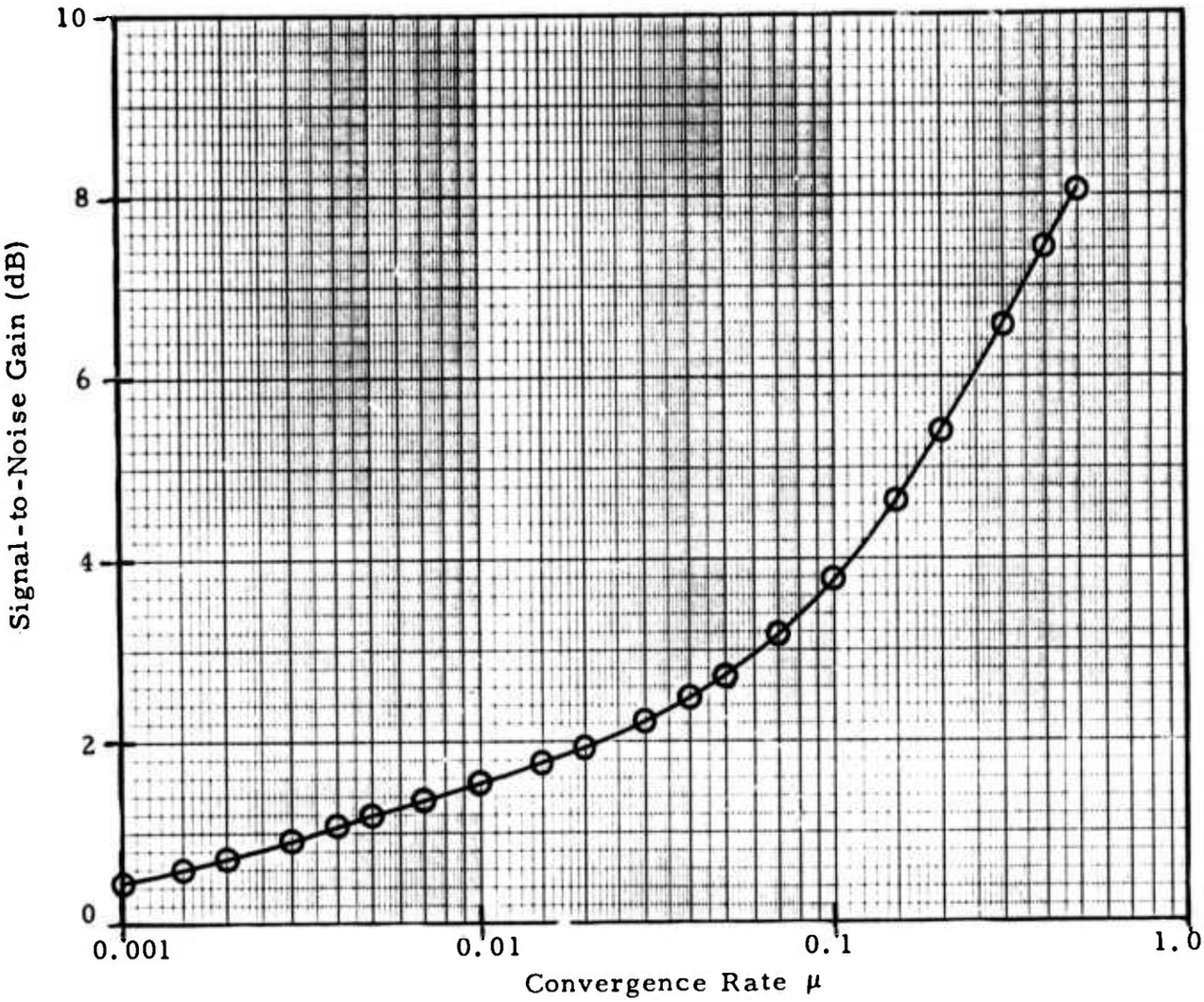

FIGURE II-78

SIGNAL-TO-NOISE GAIN AS A FUNCTION OF CONVERGENCE RATE WITH 31-POINT-LONG ADAPTIVE FILTER FOR A VERY STRONG SIGNAL FROM KAMCHATKA (ALPA, FULL ARRAY, 1971 DAY 276 22.07.02-22.11.17, USING NOISE FROM 1972 DAY 335 0415-0815)

TABLE II-39

OFF-AZIMUTH EVENT SUPPRESSION
FOR 273° STEER DIRECTION
WITH 31-POINT-LONG ADAPTIVE FILTER

Event	Azimuth	Computation Gate		Power Reduction (dB)	
		Start Time	Stop Time	$\mu = 0.007$	$\mu = 0.5$
Panama	113°	20:33:00	20:40:00	-0.763	12.956
Panama	113°	21:20:00	21:28:00	8.123	14.855
Weak Event	302.5°	21:38:00	21:43:00	1.766	11.766
Andreanof Islands	237°	23:25:00	23:35:00	3.557	13.786

If there are no meaningful processing losses at a reduced filter length, then operational considerations favor a shorter filter. For these reasons just discussed, the remainder of this subsection presents results obtained with an adaptive filter length of fifteen points per channel.

The data sample from 0415 to 0815 on day 335 of 1972 provides noise reduction measurements at the shorter filter length. The steer azimuth is again 270°. Table II-40 and Figure II-79 give the noise reduction as a function of convergence rate. At $\mu = 0.04$ and below, the noise is actually lower with the fifteen-point filter than with the 31-point filter (Table II-31). At $\mu = 0.5$, the longer filter produces only about 0.3 dB more noise reduction.

The weak event from 300°-305°, the two Kamchatka events from 273°, and the New Britain event from 240° in the data sample from 2000 to 2345 on day 276 of 1971 furnish signal degradation measurements for the 15-point-long adaptive filter. Table II-41 and Figure II-80 depict signal degradation for the weak event from 300°-305° at the shorter filter length. For this event, Table II-42 and Figure II-81 reveal that the estimated signal-to-noise gain using the noise sample from day 335 of 1972 is higher at all convergence rates with a 15-point filter than with a 31-point filter (Table II-33). In fact, the difference is more than 1.8 dB at $\mu = 0.5$. For this event, where signal similarity across the array is relatively poor, the shortened adaptive-filter length seems to obstruct the signal-degradation process. Figure II-82 pictures the beamsteer output and adaptive beams at $\mu = 0.007$ and $\mu = 0.5$ for the weak event from 300°-305°. This figure provides the first opportunity to examine the time traces for beams formed from vertical-component data passed through the new prefilter. Compared with the corresponding traces for the old prefilter in Figure II-48, the beam outputs have a much smoother appearance due to the elimination of high-frequency energy by the new prefilter. The lower signal degradation with the new prefilter at the maximum convergence rate is reflected in the bottom trace, where more cycles of the event are preserved

TABLE II-40

NOISE REDUCTION VERSUS CONVERGENCE RATE WITH 15-POINT-LONG ADAPTIVE FILTER (ALPA, 15 SITES, 1972 DAY 335 0415-0815)

Convergence Rate (μ)	Noise Reduction (dB)
0.0010	0.595
0.0015	0.789
0.0020	0.946
0.0030	1.193
0.0040	1.383
0.0050	1.539
0.0070	1.787
0.0100	2.064
0.0150	2.394
0.0200	2.638
0.0300	3.007
0.0400	3.297
0.0500	3.547
0.0700	3.974
0.1000	4.511
0.1500	5.248
0.2000	5.853
0.3000	6.780
0.4000	7.430
0.5000	7.876

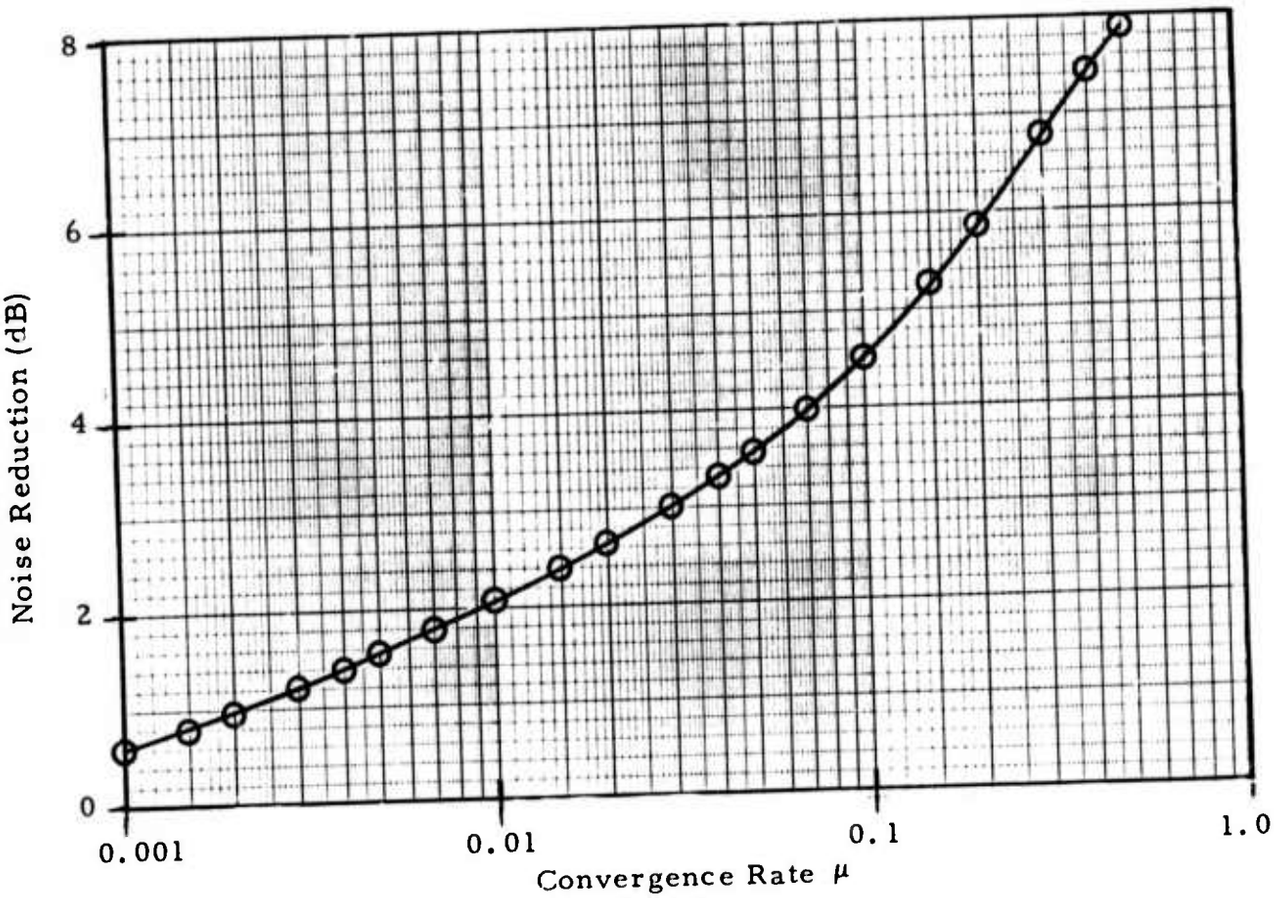

FIGURE II-79

NOISE REDUCTION AS A FUNCTION OF CONVERGENCE RATE WITH 15-POINT-LONG ADAPTIVE FILTER (ALPA, 15 SITES, 1972 DAY 335 0415-0815)

TABLE II-41

SIGNAL DEGRADATION VERSUS CONVERGENCE RATE WITH 15-POINT-LONG ADAPTIVE FILTER FOR A WEAK SIGNAL FROM 300°-305° (ALPA, 16 SITES, 1971 DAY 276 21.37.01-21.45.32)

Convergence Rate (μ)	Signal Degradation (dB)
0.0010	0.078
0.0015	0.127
0.0020	0.180
0.0030	0.293
0.0040	0.411
0.0050	0.530
0.0070	0.761
0.0100	1.081
0.0150	1.535
0.0200	1.902
0.0300	2.448
0.0400	2.844
0.0500	3.161
0.0700	3.667
0.1000	4.248
0.1500	4.922
0.2000	5.325
0.3000	5.519
0.4000	5.166
0.5000	4.538

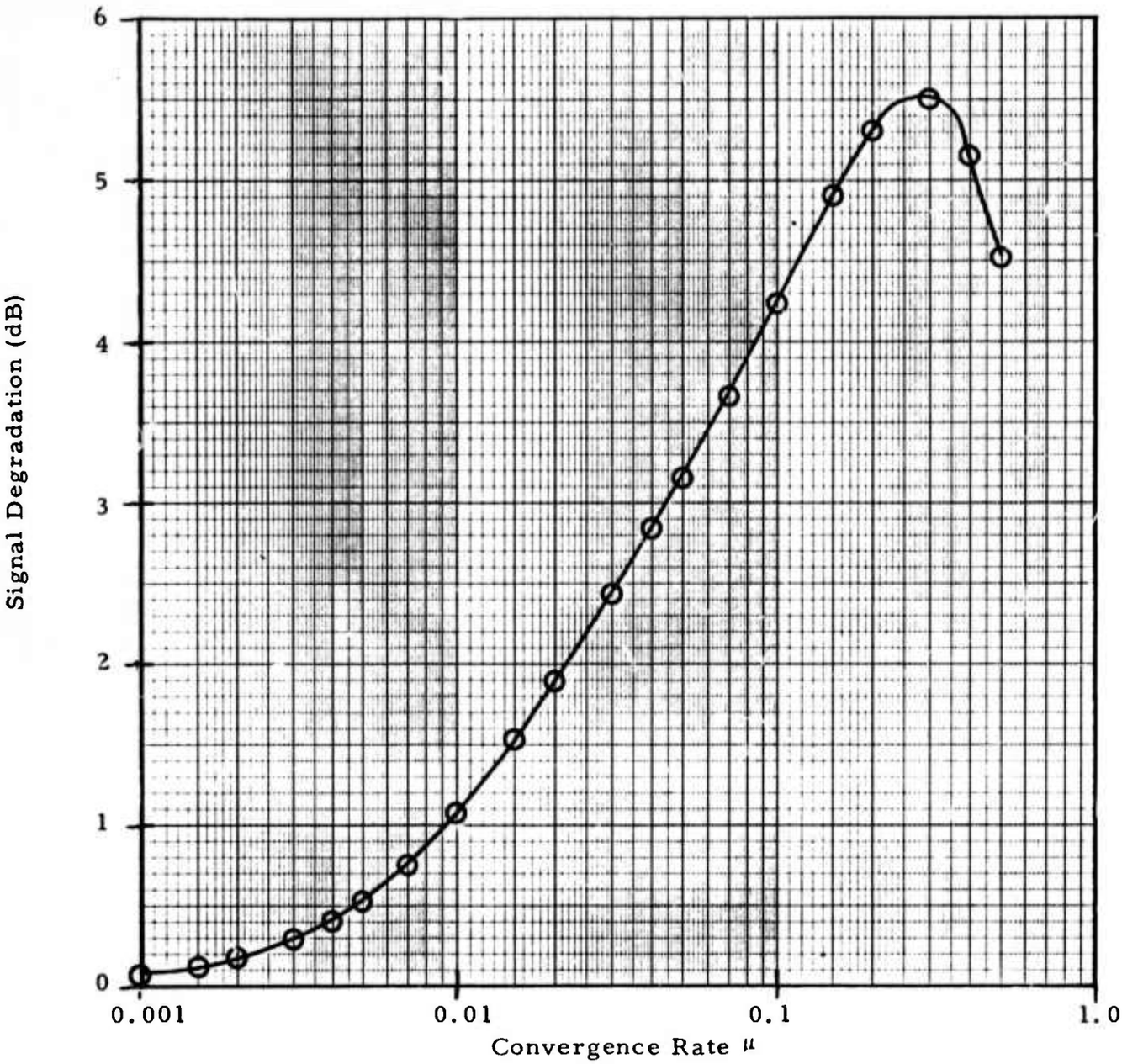

FIGURE II-80

SIGNAL DEGRADATION AS A FUNCTION OF CONVERGENCE RATE WITH 15-POINT-LONG ADAPTIVE FILTER FOR A WEAK SIGNAL FROM 300°-305° (ALPA, 16 SITES, 1971 DAY 276 21.37.01-21.45.32)

TABLE II-42

SIGNAL-TO-NOISE GAIN VERSUS CONVERGENCE RATE WITH 15-POINT-LONG ADAPTIVE FILTER FOR A WEAK SIGNAL FROM 300^{o}-305^{o} (ALPA, FULL ARRAY, 1971 DAY 276 21.37.01-21.45.32, USING NOISE FROM 1972 DAY 335 0415-0815)

Convergence Rate (μ)	Signal-to-Noise Gain (dB)
0.0010	0.517
0.0015	0.662
0.0020	0.766
0.0030	0.900
0.0040	0.972
0.0050	1.009
0.0070	1.026
0.0100	0.983
0.0150	0.859
0.0200	0.736
0.0300	0.559
0.0400	0.453
0.0500	0.386
0.0700	0.307
0.1000	0.263
0.1500	0.326
0.2000	0.528
0.3000	1.261
0.4000	2.264
0.5000	3.338

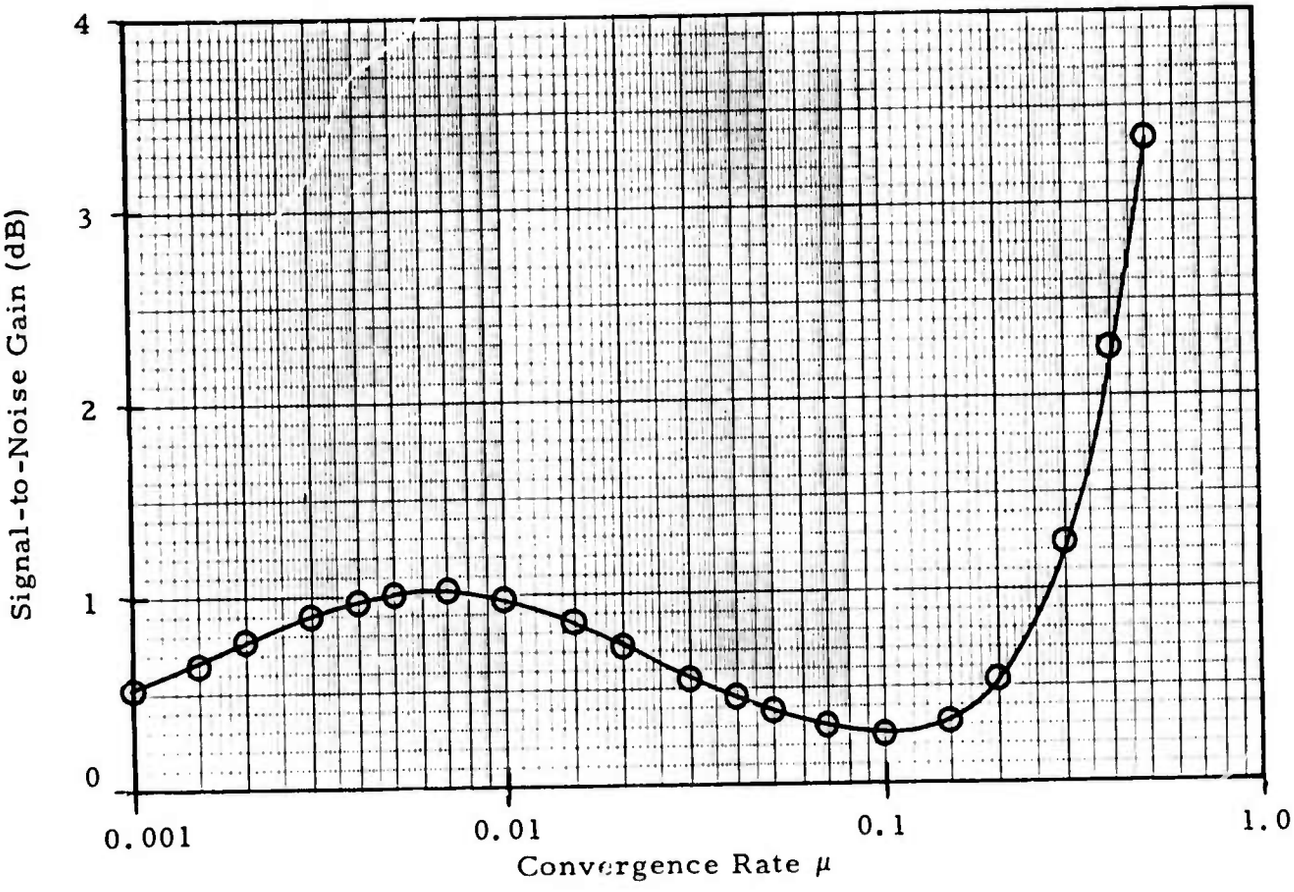

FIGURE II-81

SIGNAL-TO-NOISE GAIN AS A FUNCTION OF CONVERGENCE RATE WITH 15-POINT-LONG ADAPTIVE FILTER FOR A WEAK SIGNAL FROM 300°-305° (ALPA, FULL ARRAY, 1971 DAY 276 21.37.01-21.45.32, USING NOISE FROM 1972 DAY 335 0415-0815)

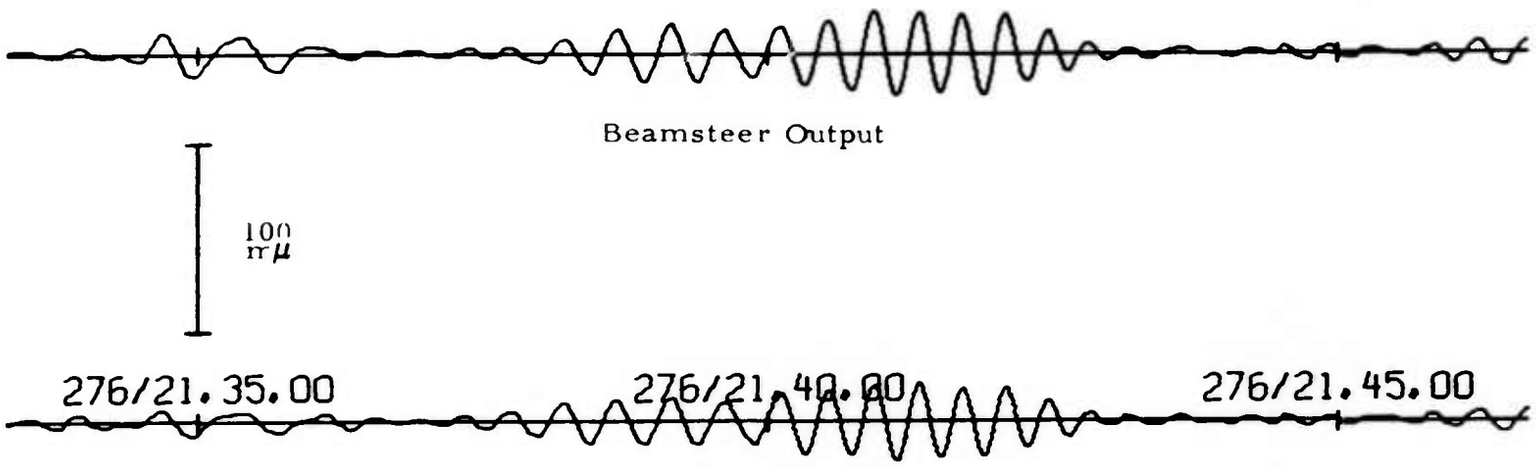

Adaptive Filter Output (μ = 0.5)

FIGURE II-82

BEAMS FOR WEAK EVENT FROM 300°-305° WITH 15-POINT-LONG ADAPTIVE FILTER (DAY 276 1971, STEER DIRECTION 302.5°)

than in the corresponding trace of Figure II-48. The ripples at 2135 in the upper two traces correspond to a data glitch at site 2 and are eliminated in the adaptive beam output for $\mu = 0.5$.

Table II-43 presents the power reduction relative to beamsteering at $\mu = 0.007$ and $\mu = 0.5$ with the 15-point-long adaptive filter for the five events away from the 302.5° steer direction used for the weak event from 300°-305°. The off-azimuth event suppression is close to that obtained with the 31-point-long adaptive filter (Table II-34). At $\mu = 0.007$, all but the first Panama event are attenuated more with the 15-point-long adaptive filter. At $\mu = 0.5$, three events are reduced more with the longer adaptive filter, two events less. Thus off-azimuth event suppression is hurt little, if any, by the shorter filter length. Figures II-83 through II-87 are Calcomp plots of the 302.5° beams obtained from data passed through the new prefilter for the five events in Table II-43. Compared with the corresponding beams for the old prefilter in Figure II-49 through II-53 of Subsection D, the trace outputs contain less high-frequency noise and tend to concentrate energy near the beginning of the events. In the case of the two Kamchatka events 30° from the look azimuth, a cycle or so at the beginning of the events escapes suppression on the adaptive beam outputs for $\mu = 0.5$.

The two Kamchatka events in the data sample from day 276 of 1971 supply signal degradation measurements for the 15-point-long adaptive filter at a steer azimuth of 273°. Signal degradation for the first of these events (arriving at about 2108) appears in Table II-44 and Figure II-88. The resulting signal-to-noise gain corresponding to the noise sample from day 335 is given in Table II-45 and Figure II-89. At the maximum convergence rate, the estimated signal-to-noise ratio improvement is 0.3 to 0.4 dB lower with the 15-point filter length than with the 31-point filter length (Table II-36). Figure II-90 displays the beamsteer output and adaptive-filter outputs at $\mu = 0.007$ and $\mu = 0.5$ for this event. Signal distortion and some signal degradation are

TABLE II-43

OFF-AZIMUTH EVENT SUPPRESSION
FOR 302.5° STEER DIRECTION
WITH 15-POINT-LONG ADAPTIVE FILTER

Event	Azimuth	Computation Gate		Power Reduction (dB)	
		Start Time	Stop Time	$\mu = 0.007$	$\mu = 0.5$
Panama	113°	20:33:00	20:40:00	1.151	15.515
Kamchatka	273°	21:07:30	21:15:00	1.508	7.748
Panama	113°	21:20:00	21:28:00	9.663	19.743
Kamchatka	273°	22:07:00	22:14:00	3.644	17.046
Andreanof Islands	237°	23:25:00	23:35:00	5.355	10.976

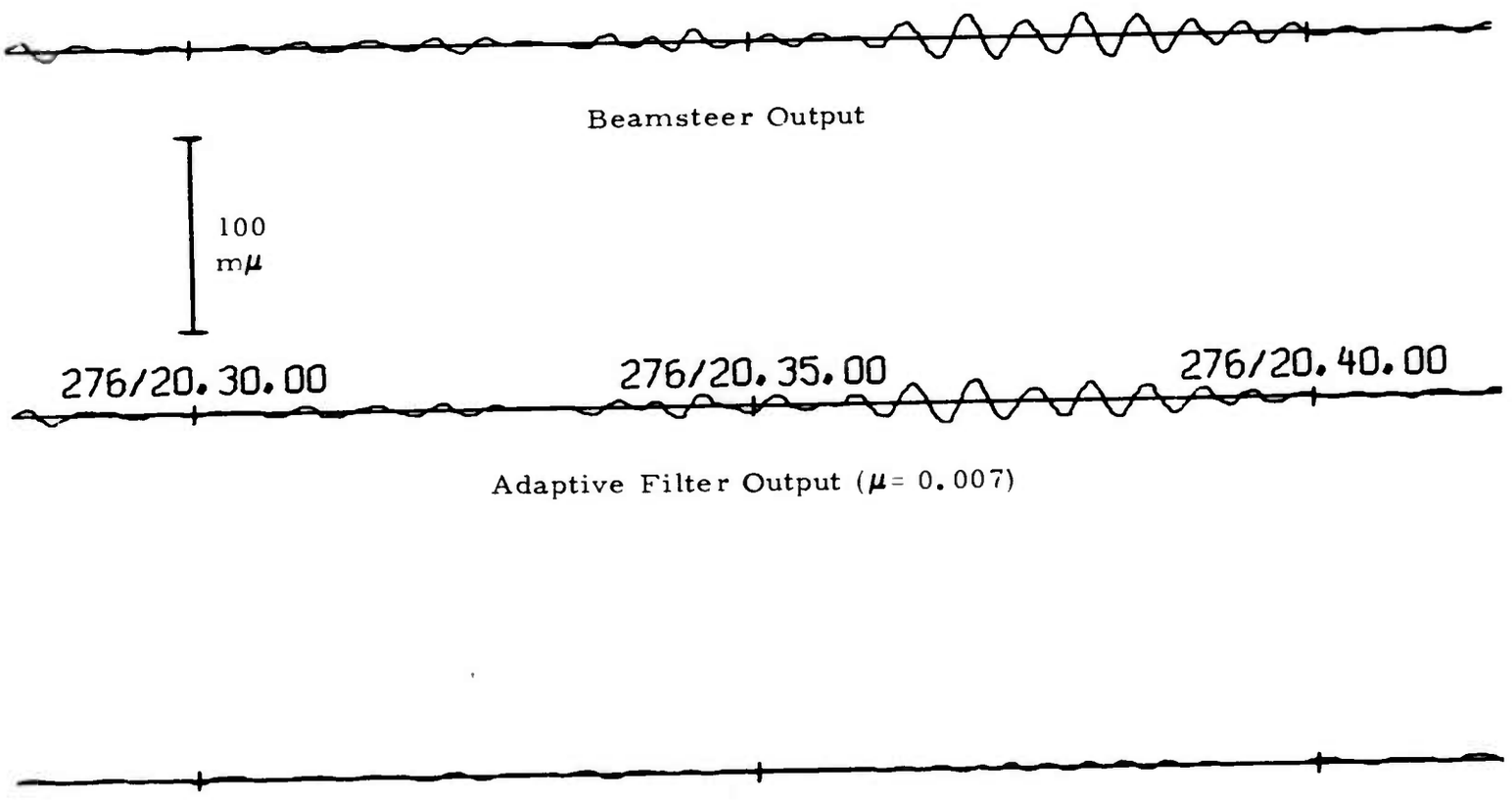

FIGURE II-83

BEAMS FOR MAGNITUDE 3.6 PANAMA EVENT WITH 15-POINT-LONG ADAPTIVE FILTER (DAY 276 1971, STEER DIRECTION 302.5°)

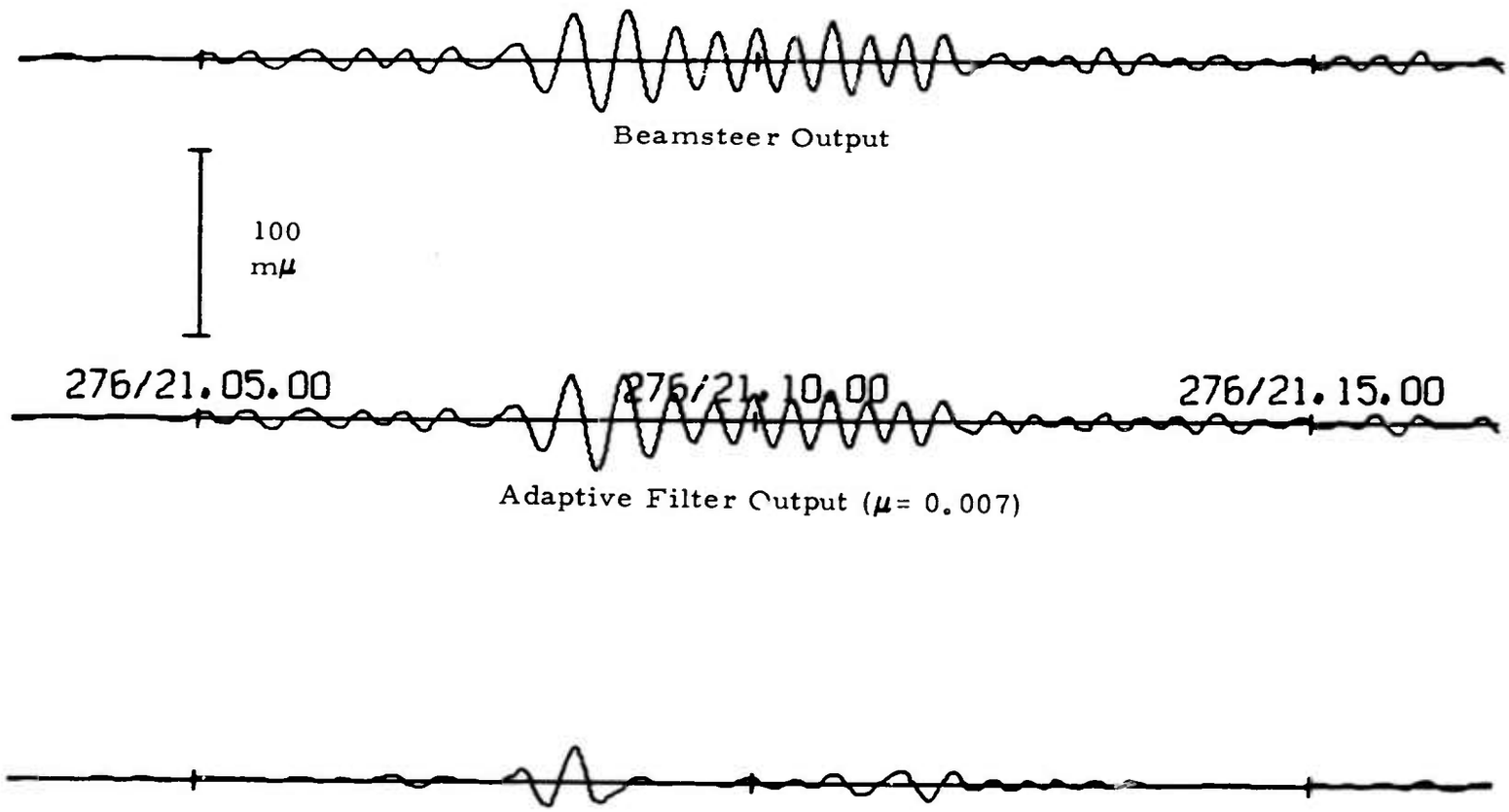

FIGURE II-84

BEAMS FOR MAGNITUDE 4.5 KAMCHATKA EVENT WITH 15-POINT-LONG ADAPTIVE FILTER (DAY 276 1971, STEER DIRECTION 302.5°)

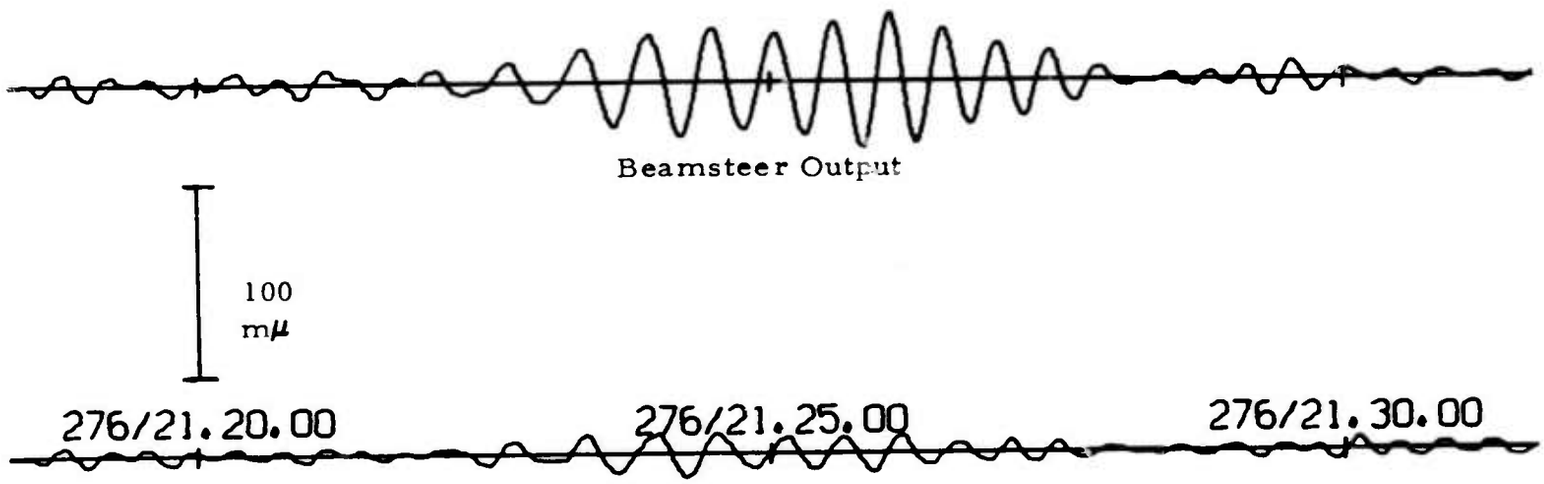

Adaptive Filter Output (μ= 0.007)

Adaptive Filter Output (μ= 0.5)

FIGURE II-85

BEAMS FOR MAGNITUDE 4.7 PANAMA EVENT WITH 15-POINT-LONG ADAPTIVE FILTER (DAY 276 1971, STEER DIRECTION 302.5°)

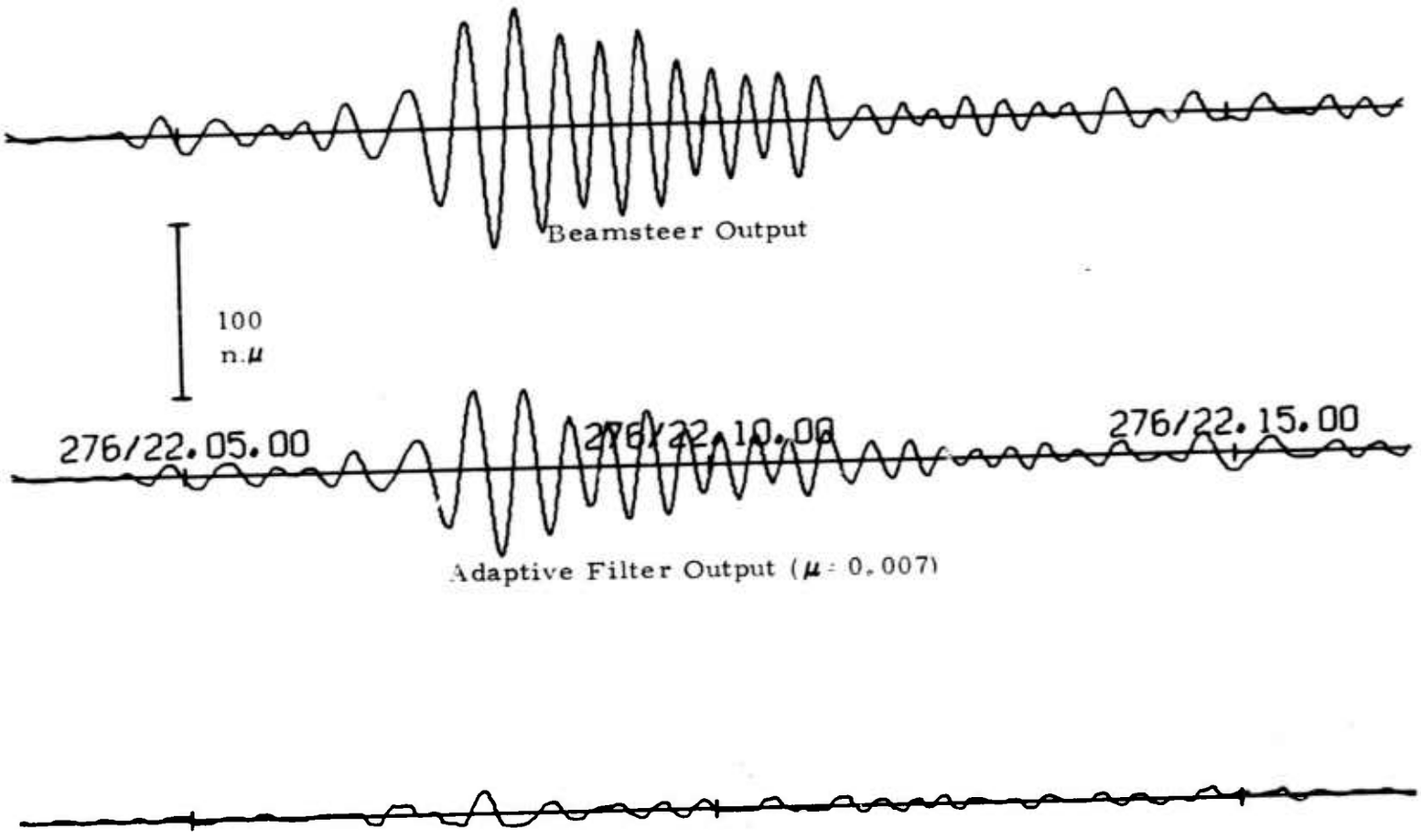

FIGURE II-86

BEAMS FOR MAGNITUDE 4.9 KAMCHATKA EVENT WITH 15-POINT-LONG ADAPTIVE FILTER (DAY 276 1971, STEER DIRECTION 302.5°)

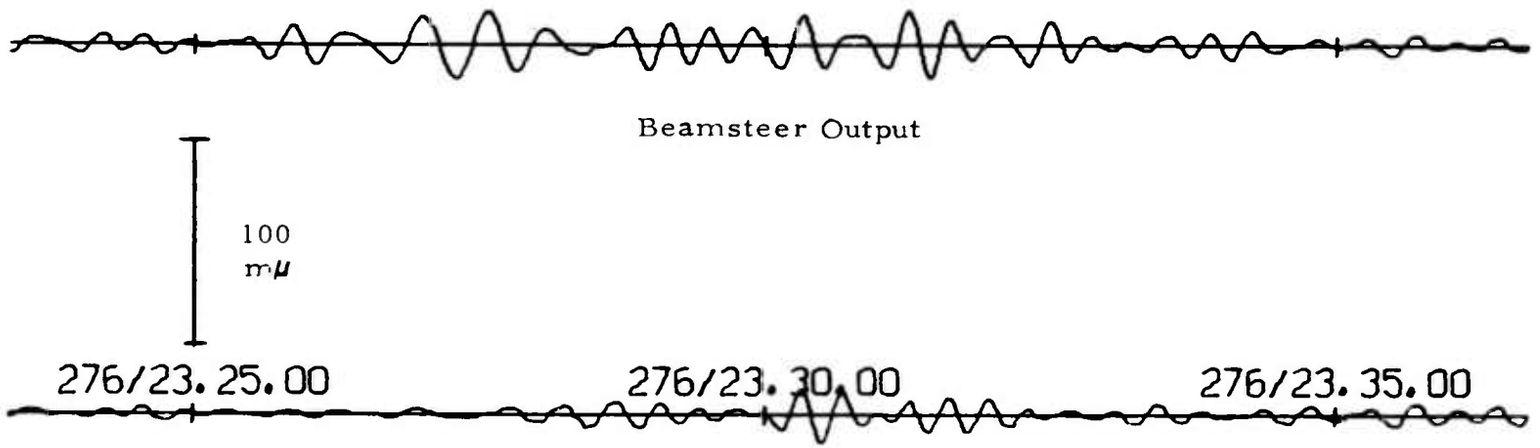

FIGURE II-87

BEAMS FOR ANDREANOF ISLANDS EVENT WITH 15-POINT-LONG ADAPTIVE FILTER (DAY 276 1971, STEER DIRECTION 302.5°)

TABLE II-44

SIGNAL DEGRADATION VERSUS CONVERGENCE RATE WITH 15-POINT-LONG ADAPTIVE FILTER FOR A STRONG SIGNAL FROM KAMCHATKA (ALPA, 16 SITES, 1971 DAY 276 21.07.18-21.11.33)

Convergence Rate (μ)	Signal Degradation (dB)
0.0010	0.084
0.0015	0.121
0.0020	0.154
0.0030	0.216
0.0040	0.271
0.0050	0.321
0.0070	0.411
0.0100	0.529
0.0150	0.694
0.0200	0.828
0.0300	1.036
0.0400	1.191
0.0500	1.310
0.0700	1.476
0.1000	1.619
0.1500	1.728
0.2000	1.784
0.3000	1.857
0.4000	1.887
0.5000	1.857

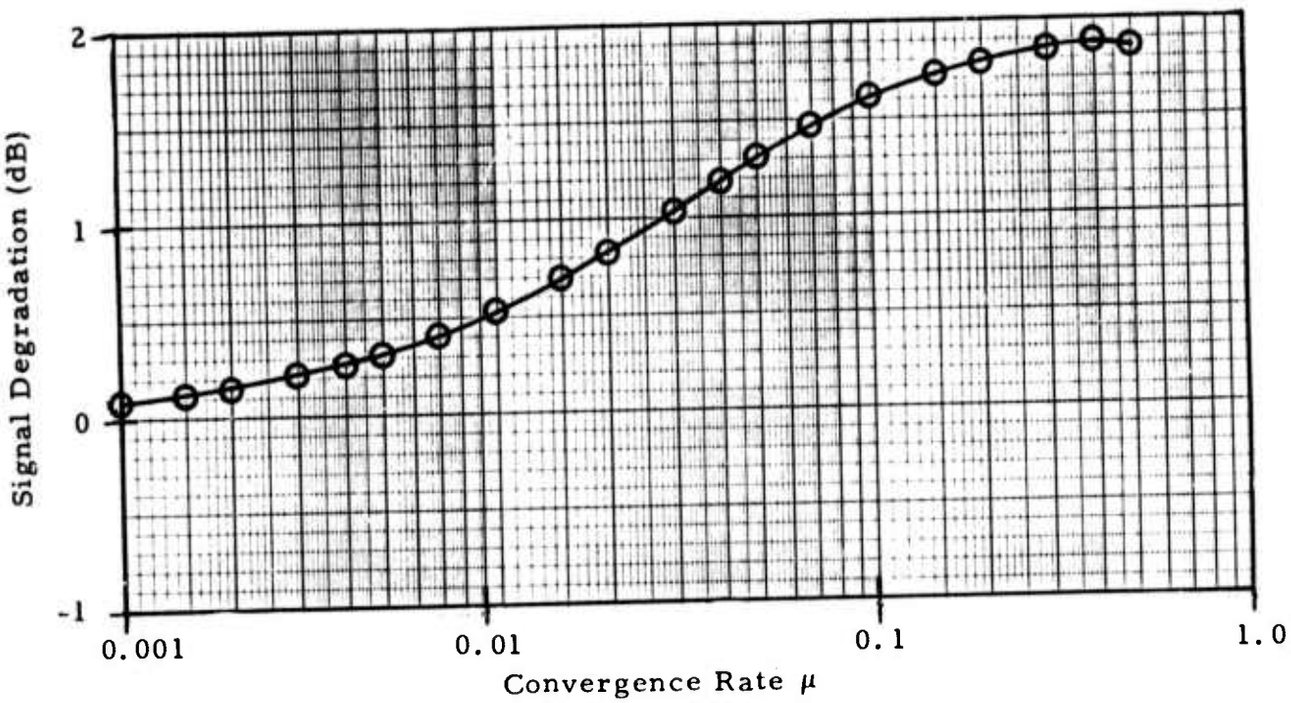

FIGURE II-88

SIGNAL DEGRADATION AS A FUNCTION OF CONVERGENCE RATE WITH 15-POINT-LONG ADAPTIVE FILTER FOR A STRONG SIGNAL FROM KAMCHATKA (ALPA, 16 SITES, 1971 DAY 276 21.07.18-21.11.33)

TABLE II-45

SIGNAL-TO-NOISE GAIN VERSUS CONVERGENCE RATE WITH 15-POINT-LONG ADAPTIVE FILTER FOR A STRONG SIGNAL FROM KAMCHATKA (ALPA, FULL ARRAY, 1971 DAY 276 21.07.18-21.11.33, USING NOISE FROM 1972 DAY 335 0415-0815)

Convergence Rate (μ)	Signal-to-Noise Gain (dB)
0.0010	0.511
0.0015	0.668
0.0020	0.792
0.0030	0.977
0.0040	1.112
0.0050	1.218
0.0070	1.376
0.0100	1.535
0.0150	1.700
0.0200	1.810
0.0300	1.971
0.0400	2.106
0.0500	2.237
0.0700	2.498
0.1000	2.892
0.1500	3.520
0.2000	4.069
0.3000	4.923
0.4000	5.543
0.5000	6.019

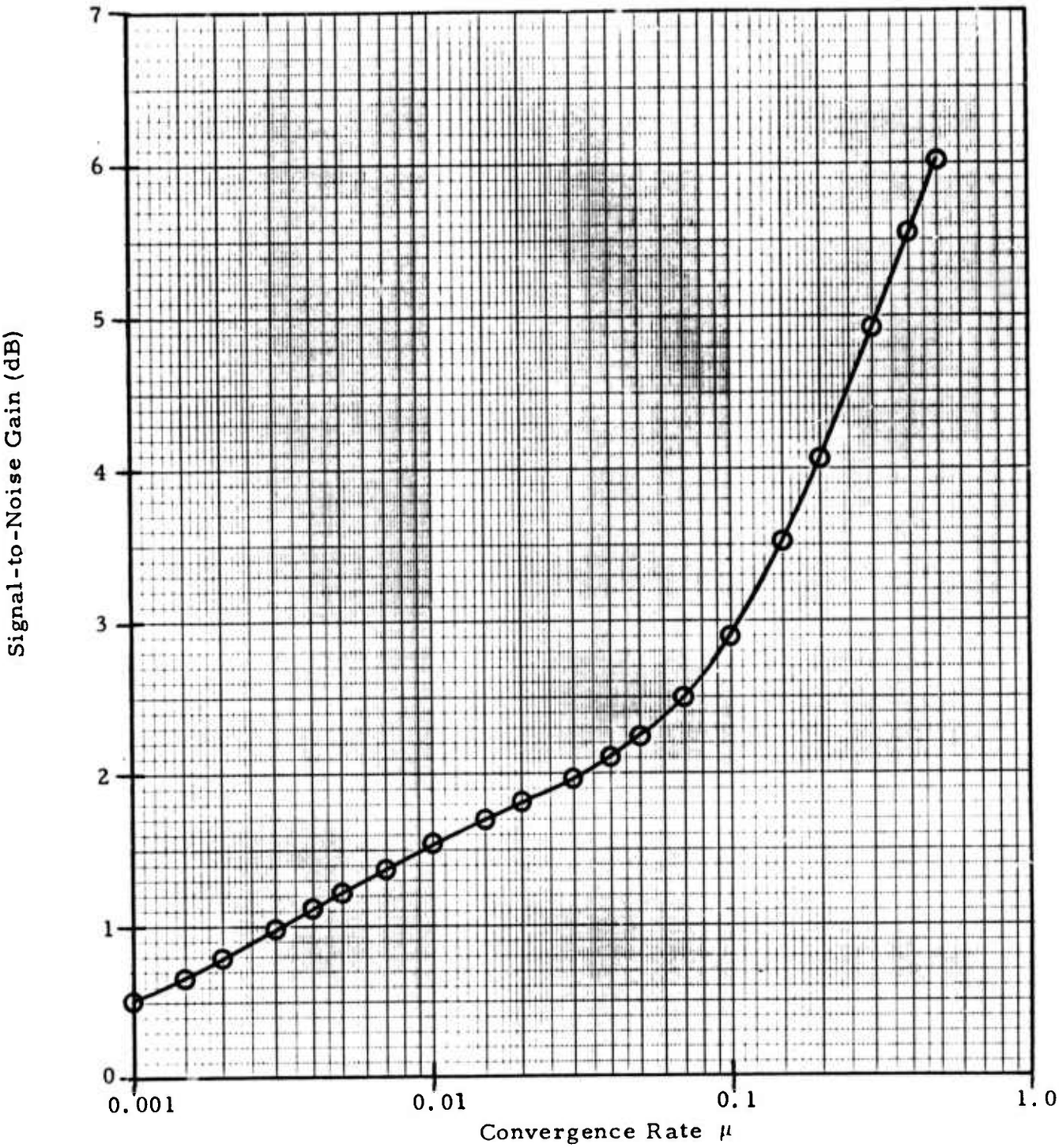

FIGURE II-89

SIGNAL-TO-NOISE GAIN AS A FUNCTION OF CONVERGENCE RATE WITH 15-POINT-LONG ADAPTIVE FILTER FOR A STRONG SIGNAL FROM KAMCHATKA (ALPA, FULL ARRAY, 1971 DAY 276 21.07.18-21.11.33, USING NOISE FROM 1972 DAY 335 0415-0815)

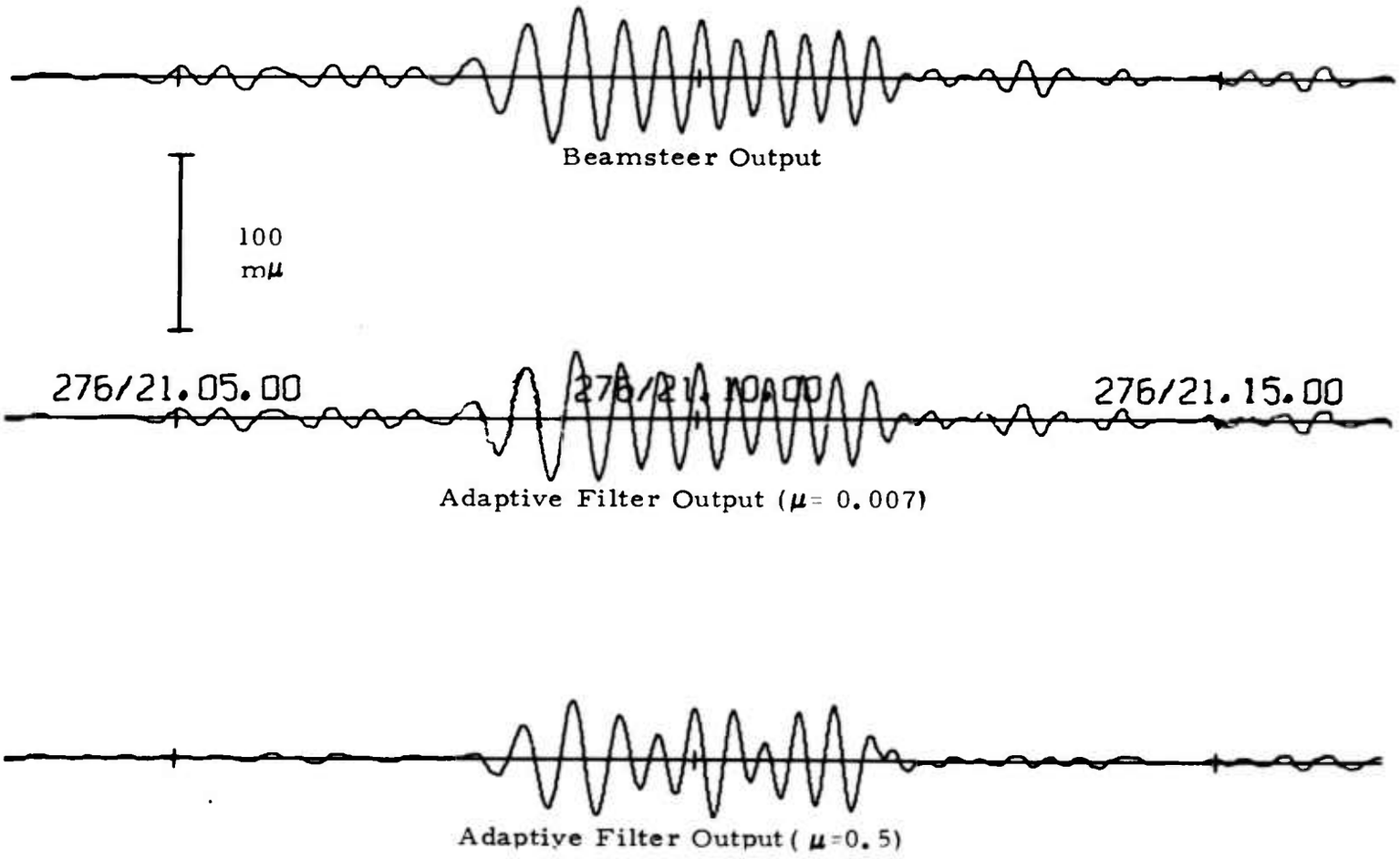

FIGURE II-90

BEAMS FOR MAGNITUDE 4.5 KAMCHATKA EVENT WITH 15-POINT-LONG ADAPTIVE FILTER (DAY 276 1971, STEER DIRECTION 273°)

visible in the ABF output for $\mu = 0.5$ at the bottom. For the second Kamchatka event, which reached ALPA at approximately 2207, signal degradation with the 15-point filter length is shown in Table II-46 and Figure II-91. This event has the best signal similarity across channels of any event in the sample from day 276 of 1971. Table II-47 and Figure II-92 indicate the estimated signal-to-noise gain for the second Kamchatka event. As in the case of the earlier Kamchatka event, the use of the shorter filter length reduces the improvement relative to beamsteering by 0.3 to 0.4 dB (see Table II-38). Figure II-93 pictures the beam outputs for this event. Signal distortion and degradation are considerably less than for the first Kamchatka event in Figure II-90.

Table II-48 lists the power reduction relative to beamsteering at $\mu = 0.007$ and $\mu = 0.5$ with the 15-point-long adaptive filter for four events away from the 273° steer azimuth of the two Kamchatka events. With the exception of the first Panama event at $\mu = 0.007$ and the weak event from 300°-305° at $\mu = 0.5$, event suppression is greater for the shorter filter length than the 31-point filter length (Table II-39). At the 273° steer direction, off-azimuth event suppression again is not degraded by the shorter filter length. Figure II-94 exhibits the beam outputs for the weak event from 300°-305°. Interestingly, some energy is visible on the adaptive filter output for $\mu = 0.5$ at the time where signal degradation is worst for the 302.5° steer azimuth (Figure II-82). Perhaps the apparent arrival azimuth of this event drifts significantly with time. Figure II-95 is the corresponding beam-output display for the Andreanof Islands event. In the adaptive filter output for $\mu = 0.5$ at the bottom, a cycle or so of this event (36° from the look azimuth) escapes suppression.

When the new prefilter is applied to the site vertical-component data before input to the beamforming process, the New Britain event becomes strong enough on the beam outputs to provide reasonably reliable signal degradation measurements. This fact provides an opportunity to determine

TABLE II-46

SIGNAL DEGRADATION VERSUS CONVERGENCE RATE WITH 15-POINT-LONG ADAPTIVE FILTER FOR A VERY STRONG SIGNAL FROM KAMCHATKA (ALPA, 16 SITES, 1971 DAY 276 22.07.02-22.11.17)

Convergence Rate (μ)	Signal Degradation (dB)
0.0010	0.105
0.0015	0.150
0.0020	0.191
0.0030	0.264
0.0040	0.328
0.0050	0.386
0.0070	0.484
0.0100	0.600
0.0150	0.742
0.0200	0.841
0.0300	0.962
0.0400	1.024
0.0500	1.056
0.0700	1.088
0.1000	1.107
0.1500	1.090
0.2000	1.019
0.3000	0.782
0.4000	0.486
0.5000	0.175

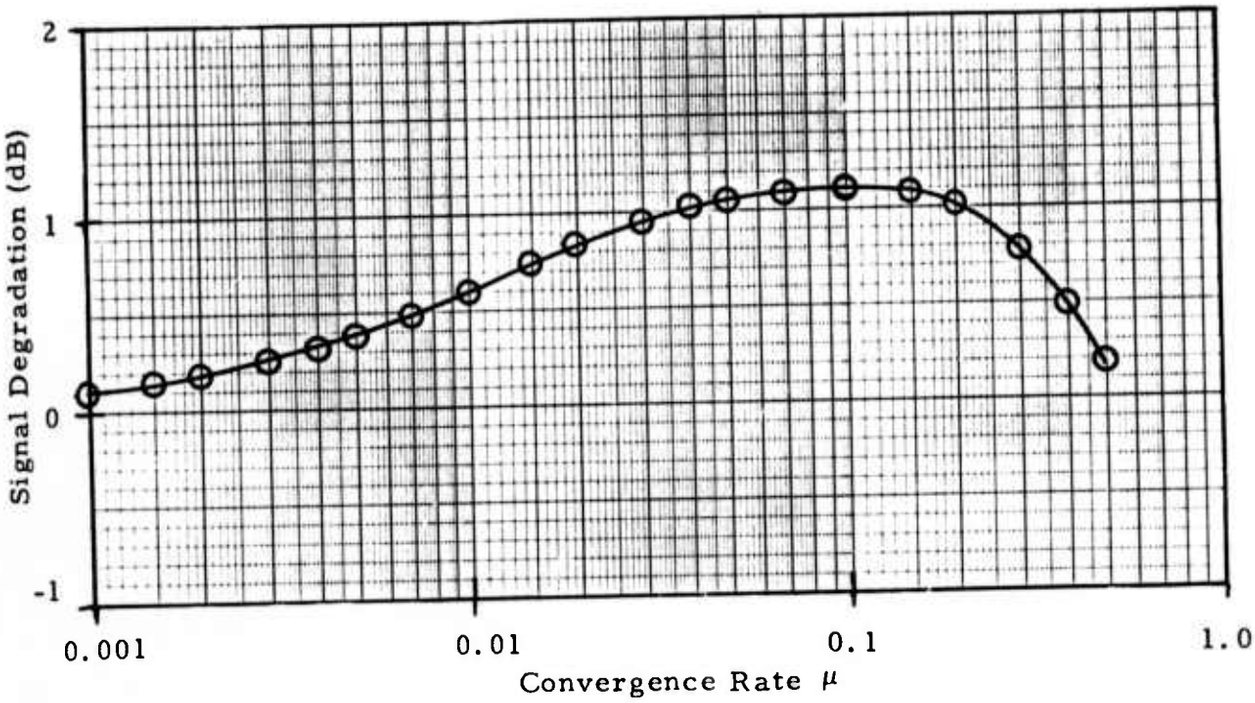

FIGURE II-91

SIGNAL DEGRADATION AS A FUNCTION OF CONVERGENCE RATE WITH 15-POINT-LONG ADAPTIVE FILTER FOR A VERY STRONG SIGNAL FROM KAMCHATKA (ALPA, 16 SITES, 1971 DAY 276 22.07.02-22.11.17)

TABLE II-47

SIGNAL-TO-NOISE GAIN VERSUS CONVERGENCE RATE WITH 15-POINT-LONG ADAPTIVE FILTER FOR A VERY STRONG SIGNAL FROM KAMCHATKA (ALPA, FULL ARRAY, 1971 DAY 276 22.07.02-22.11.17, USING NOISE FROM 1972 DAY 335 0415-0815)

Comvergence Rate (μ)	Signal-to-Noise Gain (dB)
0.0010	0.490
0.0015	0.639
0.0020	0.755
0.0030	0.929
0.0040	1.055
0.0050	1.153
0.0070	1.303
0.0100	1.464
0.0150	1.652
0.0200	1.797
0.0300	2.045
0.0400	2.273
0.0500	2.491
0.0700	2.886
0.1000	3.404
0.1500	4.158
0.2000	4.834
0.3000	5.998
0.4000	6.944
0.5000	7.701

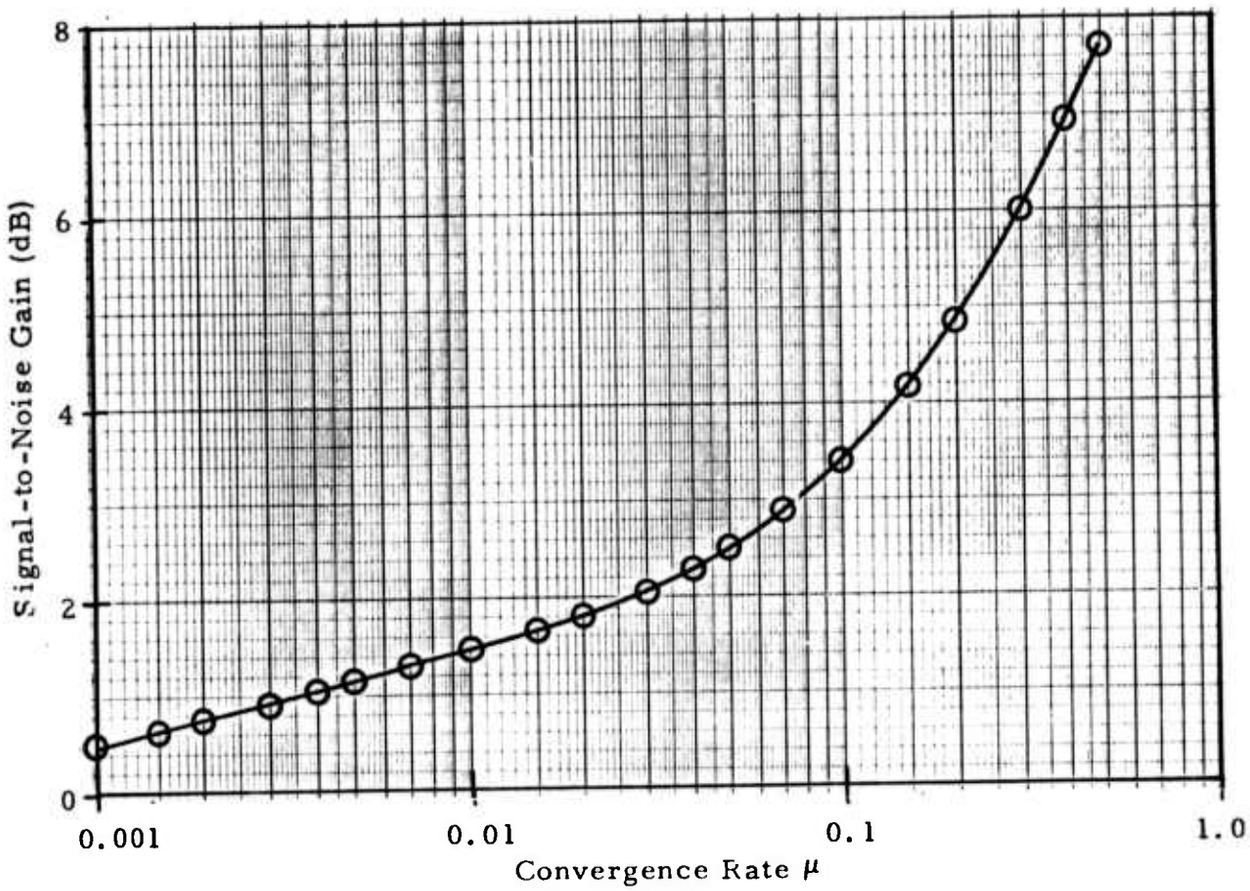

FIGURE II-92

SIGNAL-TO-NOISE GAIN AS A FUNCTION OF CONVERGENCE RATE WITH 15-POINT-LONG ADAPTIVE FILTER FOR A VERY STRONG SIGNAL FROM KAMCHATKA (ALPA, FULL ARRAY, 1971 DAY 276 22.07.02-22.11.17, USING NOISE FROM 1972 DAY 335 0415-0815)

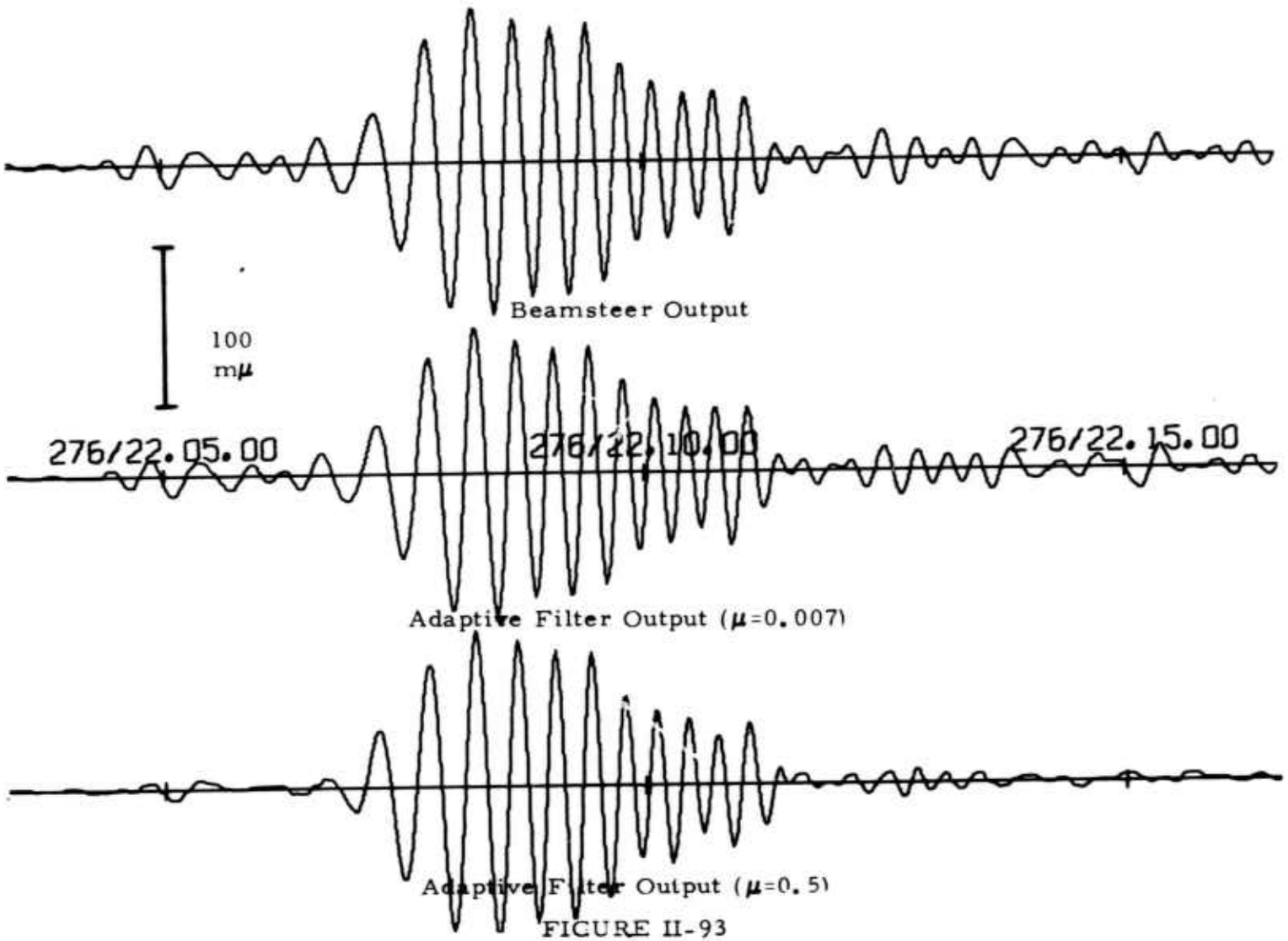

FICURE II-93

BEAMS FOR MAGNITUDE 4.9 KAMCHATKA EVENT WITH 15-POINT-LONG ADAPTIVE FILTER (DAY 276 1971, STEER DIRECTION 273°)

TABLE II-48

OFF-AZIMUTH EVENT SUPPRESSION
FOR 273° STEER DIRECTION
WITH 15-POINT-LONG ADAPTIVE FILTER

Event	Azimuth	Computation Gate		Power Reduction (dB)	
		Start Time	Stop Time	$\mu = 0.007$	$\mu = 0.5$
Panama	113°	20:33:00	20:40:00	-1.051	14.523
Panama	113°	21:20:00	21:28:00	8.211	15.587
Weak Event	302.5°	21:38:00	21:43:00	2.024	9.991
Andreanof Islands	237°	23:25:00	23:35:00	4.875	13.987

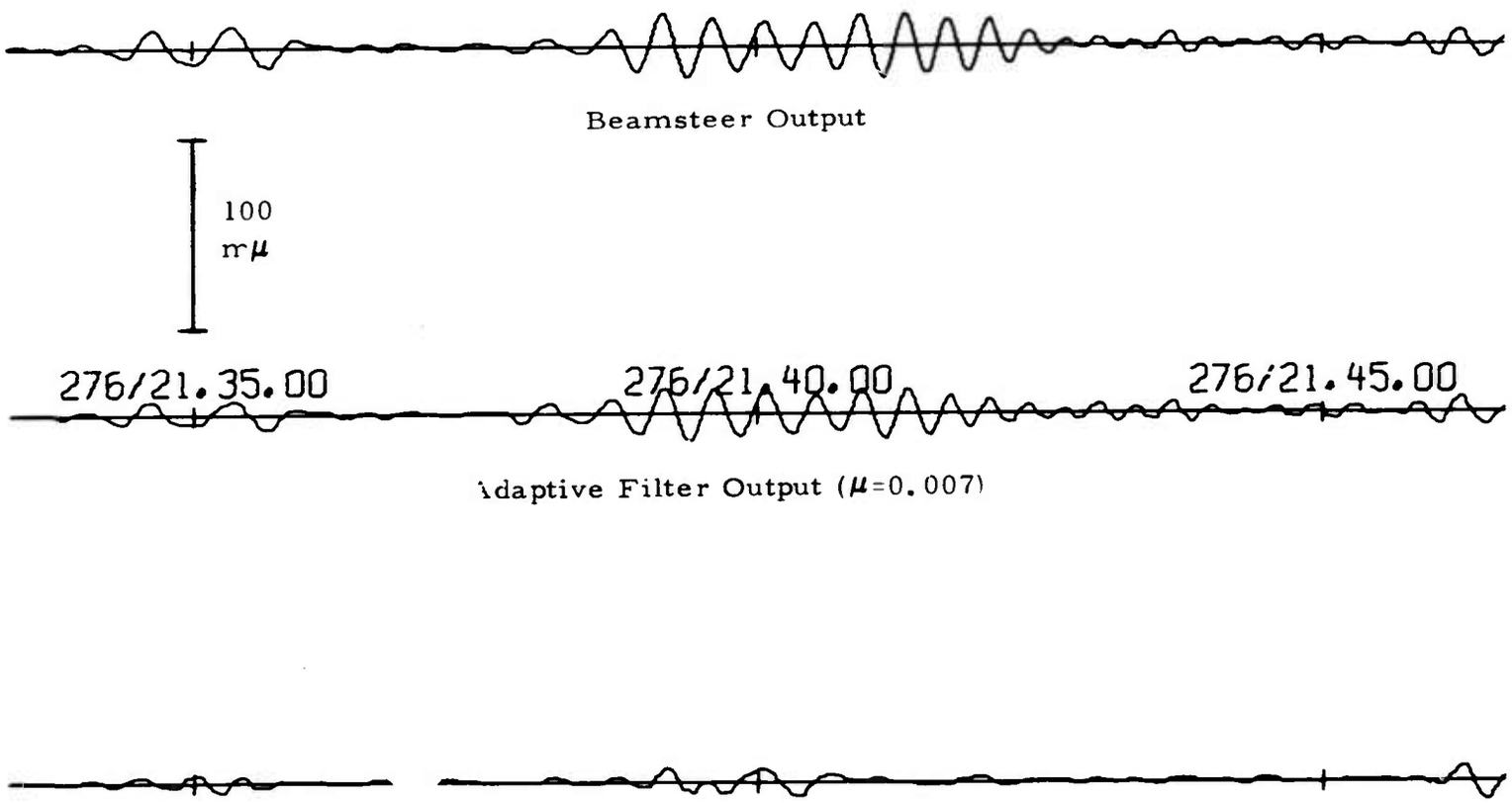

FIGURE II-94

BEAMS FOR A WEAK EVENT FROM 300°-305° WITH 15-POINT-LONG ADAPTIVE FILTER (DAY 276 1971, STEER DIRECTION 273°)

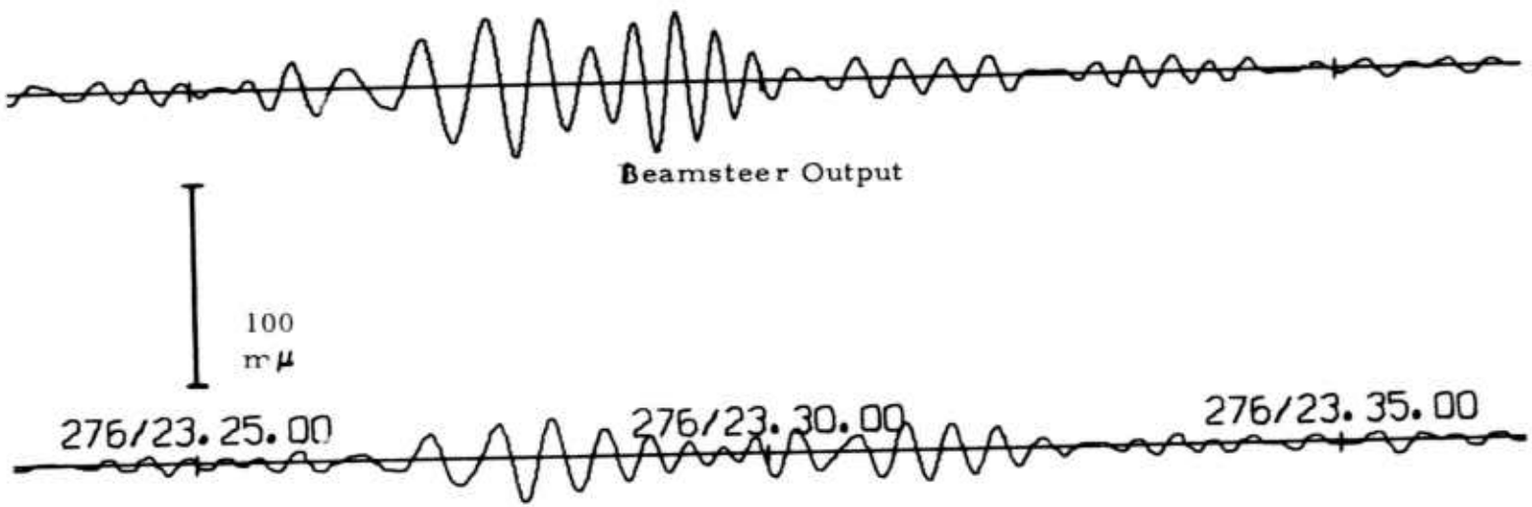

Adaptive Filter Output (μ=0.007)

Adaptive Filter Output (μ=0.5)

FIGURE II-95

BEAMS FOR ANDREANOF ISLANDS EVENT WITH 15-POINT-LONG ADAPTIVE FILTER (DAY 276 1971, STEER DIRECTION 273°)

whether the inferior signal-to-noise gain for the weak event from 300°-305° is due to poor signal similarity or low signal-to-noise ratio. Table II-49 and Figure II-96 portray signal degradation for the New Britain event as a function of the convergence parameter μ . The degradation is significantly lower than for the weak event from 300°-305°, so that poor signal similarity is the apparent reason for the results with that event. Table II-50 and Figure II-97 present the estimated signal-to-noise gain for the New Britain event using the noise sample from day 335 of 1972. The 6.6 dB gain at $\mu = 0.5$ is even higher than the corresponding 6.0 dB gain for the first Kamchatka event, which is considerably stronger. Figure II-98 displays the beamsteer output and adaptive beam outputs at $\mu = 0.007$ and $\mu = 0.5$ for the New Britain event with the new prefilter and an adaptive-filter length of fifteen points. A clear detection is evident on the adaptive beam output for $\mu = 0.5$ in the bottom trace. To demonstrate the effectiveness of the new prefilter relative to the old prefilter in detecting signals, Figure II-99 pictures the beamsteer outputs and ABF outputs at $\mu = 0.005$ and $\mu = 0.5$ for the New Britain event with the old prefilter. At the maximum convergence rate in the bottom trace, the event is barely visible. The difference in signal-to-noise ratio between the new prefilter and the old prefilter seems to be about 6 dB on the adaptive beams at $\mu = 0.5$.

Five events in the data sample from day 276 of 1971 arrive from azimuths away from the 240° azimuth of the New Britian event. Table II-51 records the power reduction relative to beamsteering with the new prefilter for these events. In general, the off-azimuth event suppression is considerably less at the 240° look azimuth than at the 302.5° and 273° steer directions. One contributing factor is the excellent 240° time-shift-and-sum beam pattern, which appears in Figure II-100. The potential for improvement with adaptive beamforming is substantially limited in this situation. Figure II-101 presents the beam outputs for the first Panama event. At $\mu = 0.007$, the adaptive beam is unable to suppress the event as well as the time-shift-and-sum beam in the

TABLE II-49

SIGNAL DEGRADATION VERSUS CONVERGENCE RATE WITH 15-POINT-LONG ADAPTIVE FILTER FOR A WEAK SIGNAL FROM NEW BRITAIN (ALPA, 16 SITES, 1971 DAY 276 23.10.30-23.18.00)

Convergence Rate (μ)	Signal Degradation (dB)
0.0010	0.079
0.0015	0.110
0.0020	0.134
0.0030	0.171
0.0040	0.195
0.0050	0.211
0.0070	0.228
0.0100	0.234
0.0150	0.226
0.0200	0.212
0.0300	0.187
0.0400	0.170
0.0500	0.161
0.0700	0.164
0.1000	0.206
0.1500	0.323
0.2000	0.454
0.3000	0.715
0.4000	0.993
0.5000	1.304

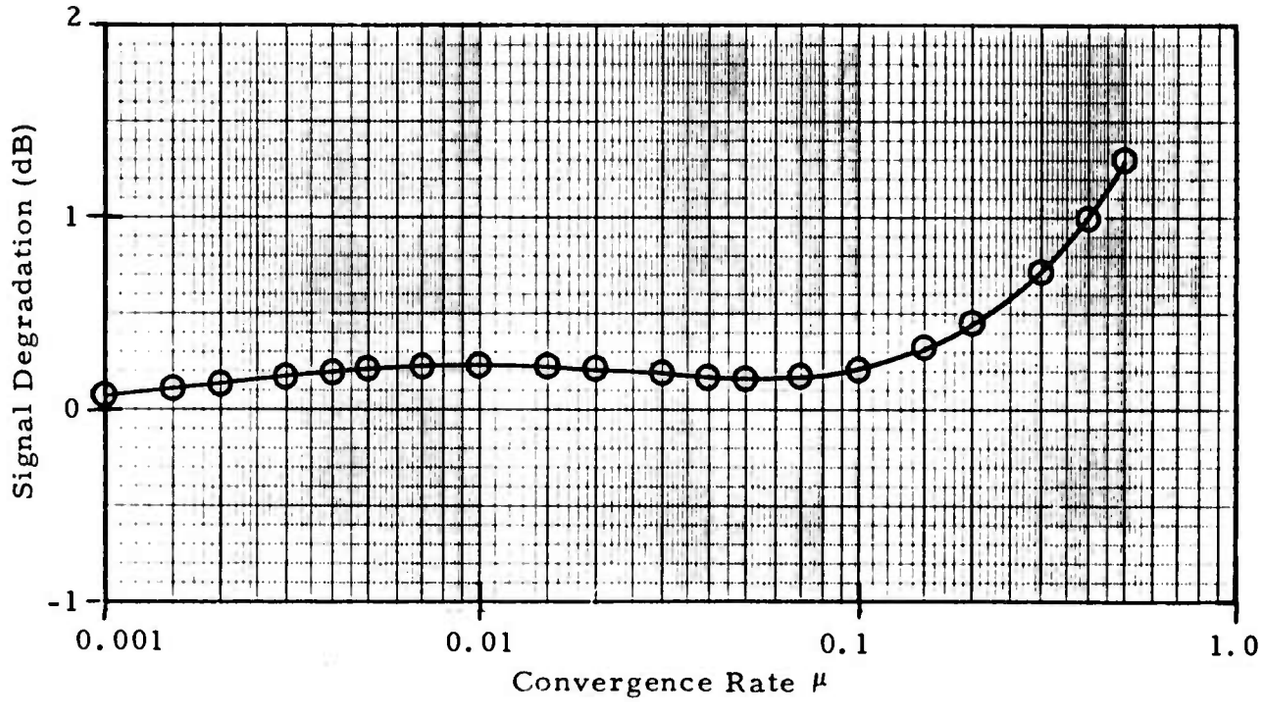

FIGURE II-96

SIGNAL DEGRADATION AS A FUNCTION OF CONVERGENCE RATE WITH 15-POINT-LONG ADAPTIVE FILTER FOR A WEAK SIGNAL FROM NEW BRITAIN (ALPA, 16 SITES, 1971 DAY 276 23.10.30-23.18.00)

TABLE II-50

SIGNAL-TO-NOISE GAIN VERSUS CONVERGENCE RATE WITH 15-POINT-LONG ADAPTIVE FILTER FOR A WEAK SIGNAL FROM NEW BRITAIN (ALPA, FULL ARRAY, 1971 DAY 276 23.10.30-23.18.00, USING NOISE FROM 1972 DAY 335 0415-0815)

Convergence Rate (μ)	Signal-to-Noise Gain (dB)
0.0010	0.516
0.0015	0.679
0.0020	0.812
0.0030	1.022
0.0040	1.188
0.0050	1.328
0.0070	1.559
0.0100	1.830
0.0150	2.168
0.0200	2.426
0.0300	2.820
0.0400	3.127
0.0500	3.386
0.0700	3.810
0.1000	4.305
0.1500	4.925
0.2000	5.399
0.3000	6.065
0.4000	6.437
0.5000	6.572

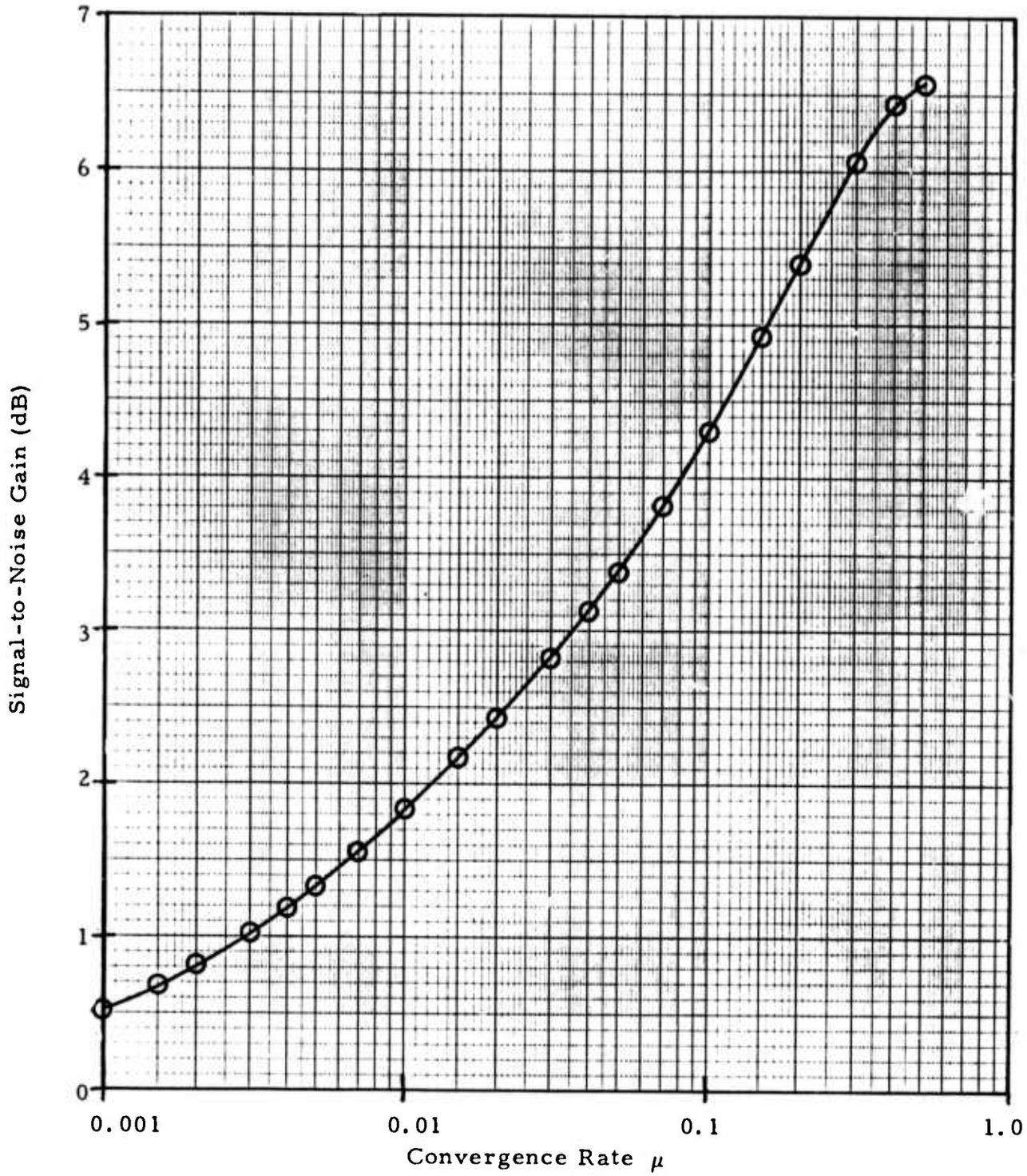

FIGURE II-97

SIGNAL-TO-NOISE GAIN AS A FUNCTION OF CONVERGENCE RATE WITH 15-POINT-LONG ADAPTIVE FILTER FOR A WEAK SIGNAL FROM NEW BRITAIN (ALPA, FULL ARRAY, 1971 DAY 276 23.10.30-23.18.00, USING NOISE FROM 1972 DAY 335 0415-0815)

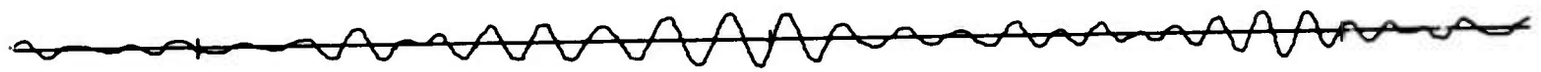

Beamsteer Output

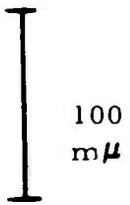

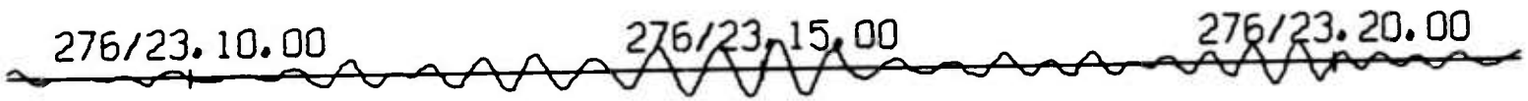

Adaptive Filter Output (μ=0.007)

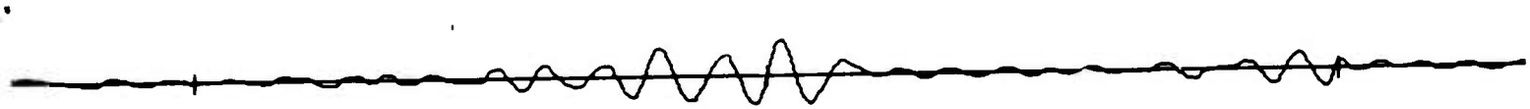

Adaptive Filter Output (μ=0.5)

FIGURE II-98

BEAMS FOR NEW BRITAIN EVENT WITH 15-POINT-LONG ADAPTIVE FILTER (DAY 27o 1971, STEER DIRECTION 240°)

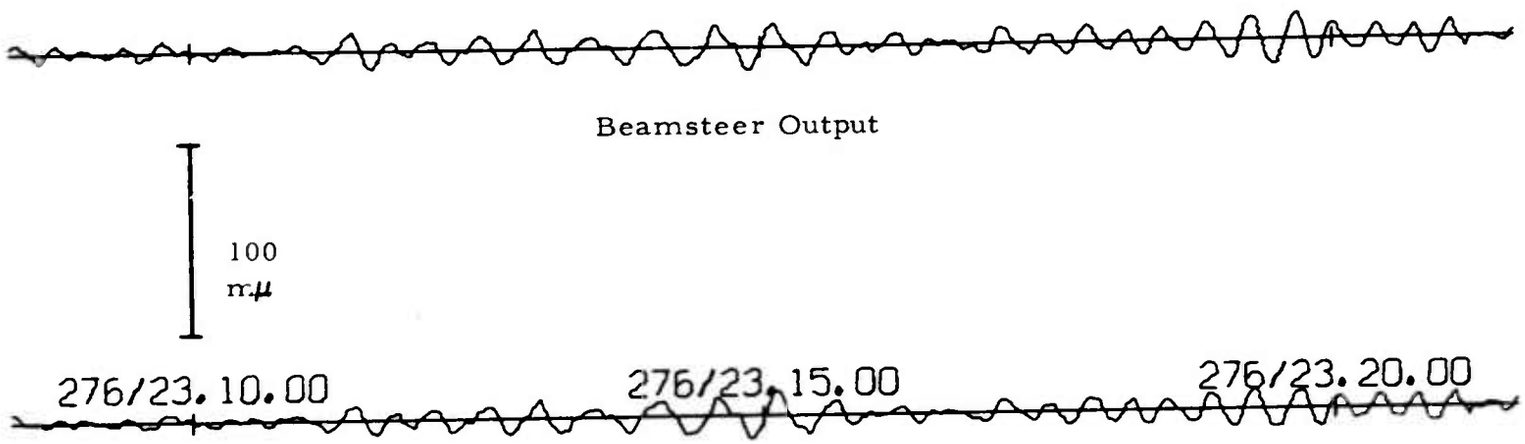

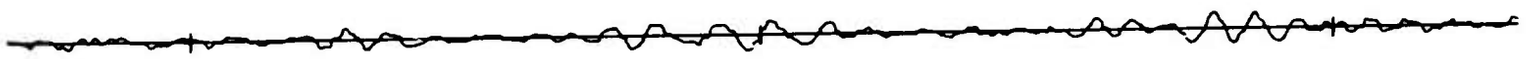

Adaptive Filter Output (μ=0.5)

FIGURE II-99

FULL-ARRAY BEAMS FOR NEW BRITAIN EVENT WITH OLD PREFILTER (DAY 276 1971, STEER DIRECTION 240°)

TABLE II-51

OFF-AZIMUTH EVENT SUPPRESSION
FOR 240° STEER DIRECTION
WITH 15-POINT-LONG ADAPTIVE FILTER

Event	Azimuth	Computation Gate		Power Reduction (dB)	
		Start Time	Stop Time	$\mu = 0.007$	$\mu = 0.5$
Panama	113°	20:33:00	20:40:00	-0.513	13.812
Kamchatka	273°	21:07:30	21:15:00	0.388	2.199
Panama	113°	21:20:00	21:28:00	5.347	16.408
Weak Event	302.5°	21:38:00	21:43:00	0.372	7.585
Kamchatka	273°	22:07:00	22:14:00	0.955	9.001

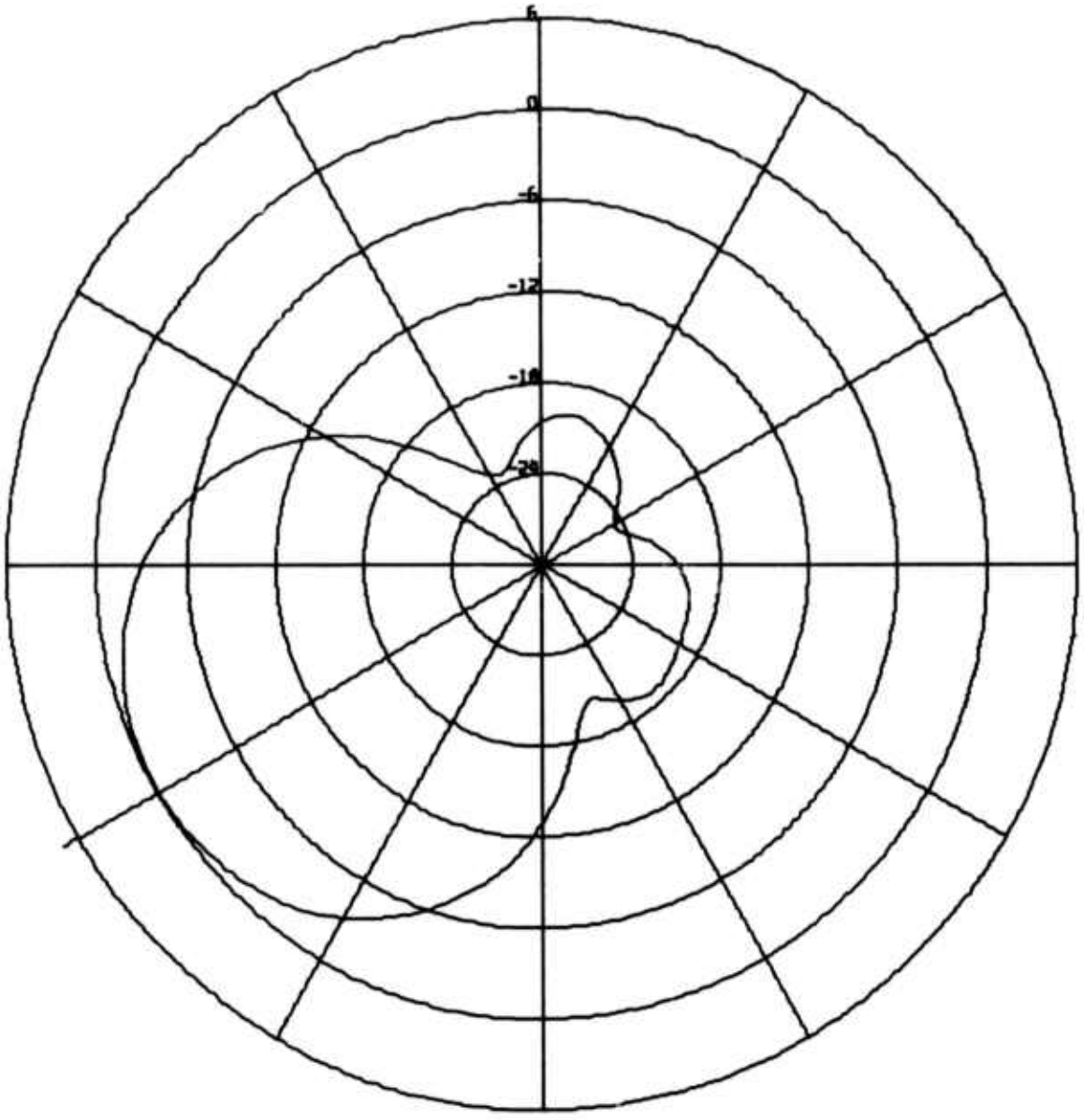

ALPA
TIME-SHIFT-AND-SUM BEAM PATTERN
BEAM LOOK VELOCITY IS 3.6, LOOK AZIMUTH 240.0
FREQUENCY IS 0.04000 HZ, PERIOD 25.0 SECONDS

FIGURE II-100

BEAMSTEER RESPONSE FOR FULL-ARRAY
DATA SAMPLE FROM DAY 276 OF 1971

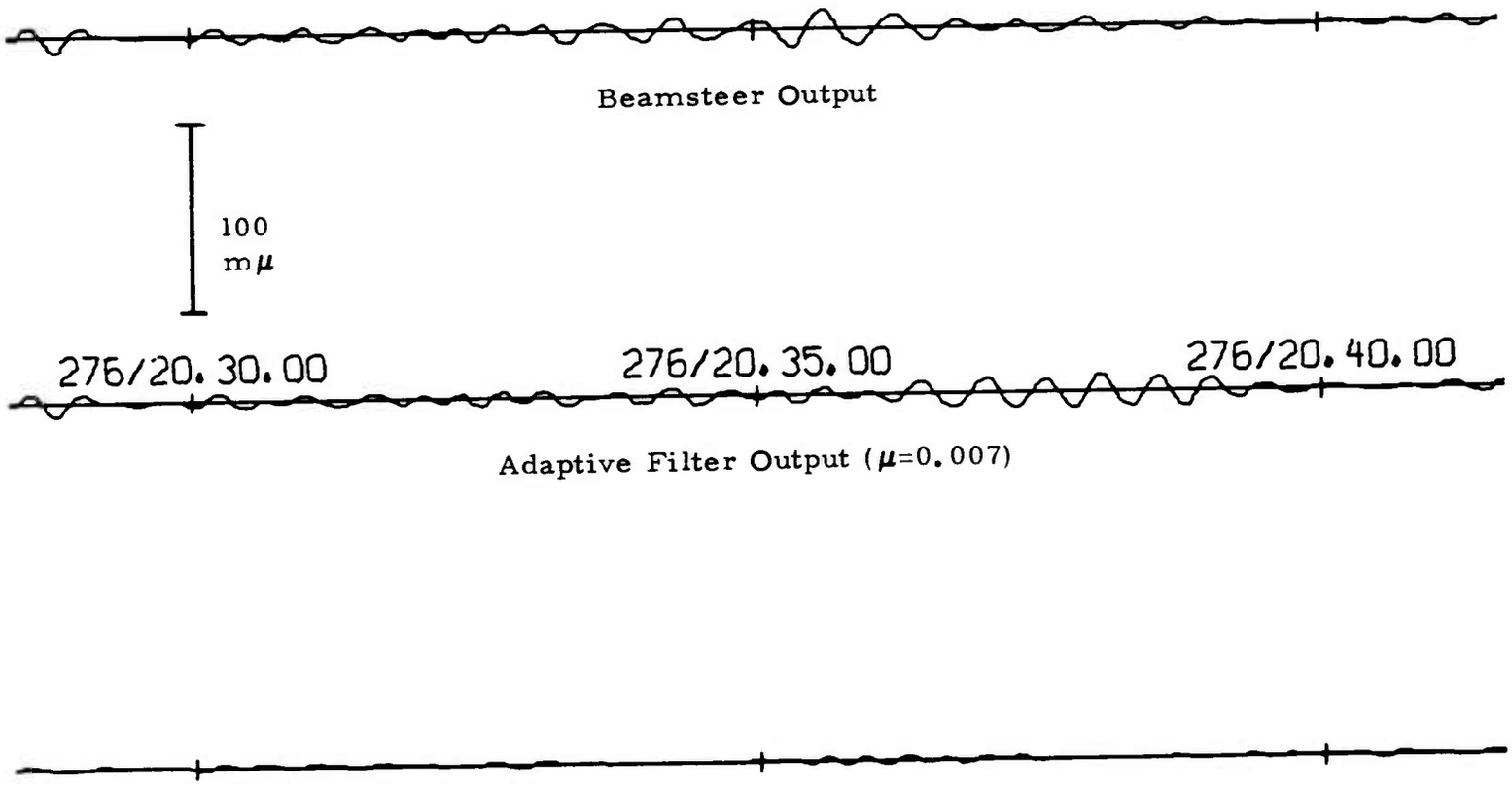

FIGURE II-101

BEAMS FOR A MAGNITUDE 3.6 PANAMA EVENT WITH 15-POINT-LONG ADAPTIVE FILTER (DAY 276 1971, STEER DIRECTION 240°)

time interval 2036-2039. Figures II-102 through II-104 show the ABF beam patterns at 2033, 2036 1/2, and 2040. The ABF response for 113° at 25 seconds is initially greater than the beamsteer response and does not drop until 2040. Unlike the adaptive beam for $\mu = 0.007$, the adaptive beam for $\mu = 0.5$ virtually annihilates the first Panama event. Figures II-105 through II-108 display the remaining four off-azimuth events. In the case of the two Kamchatka events 33° from the steer direction, considerable low-frequency energy at the beginning of the events leaks into the adaptive beams at the highest convergence rate. The beam outputs for the second Panama event are similar to those for the first Panama event, although event suppression is better for the second. After the event has subsided on the beamsteer output, it persists on the adaptive beam output for a short time after 2125 at the slower convergence rate. For the weak event from 300°-305°, event suppression relative to beamsteering is worse at the 240° steer direction than at the 273° steer direction. The probable explanation is the improved ability of the time-shift-and-sum beamformer to attenuate the event when the look azimuth is 240°. Compared with the ABF outputs at the 273° steer azimuth (Figure II-94), the adaptive beams at 240° seem to be slightly weaker for this event.

The Andreanof Islands event from 237° is only three degrees from the 240° steer direction. Figure II-109 is a Calcomp plot of the beamsteer and ABF outputs at $\mu = 0.007$ and $\mu = 0.5$ for this event. At the slower convergence rate, the adaptive beam output closely resembles the beamsteer output. At the maximum convergence rate, however, the ABF output is 3.4 dB weaker than the beamsteer output in the top trace. Since a three-degree shift in azimuth has only a minimal effect on the steer delays, it is extremely unlikely that the 3.4 dB attenuation is due to the high resolution of adaptive beamforming. More likely explanations are poor signal similarity across the array and an apparent arrival azimuth different from the true 237° azimuth of the event. A visual examination of the site vertical-component data reveals that the

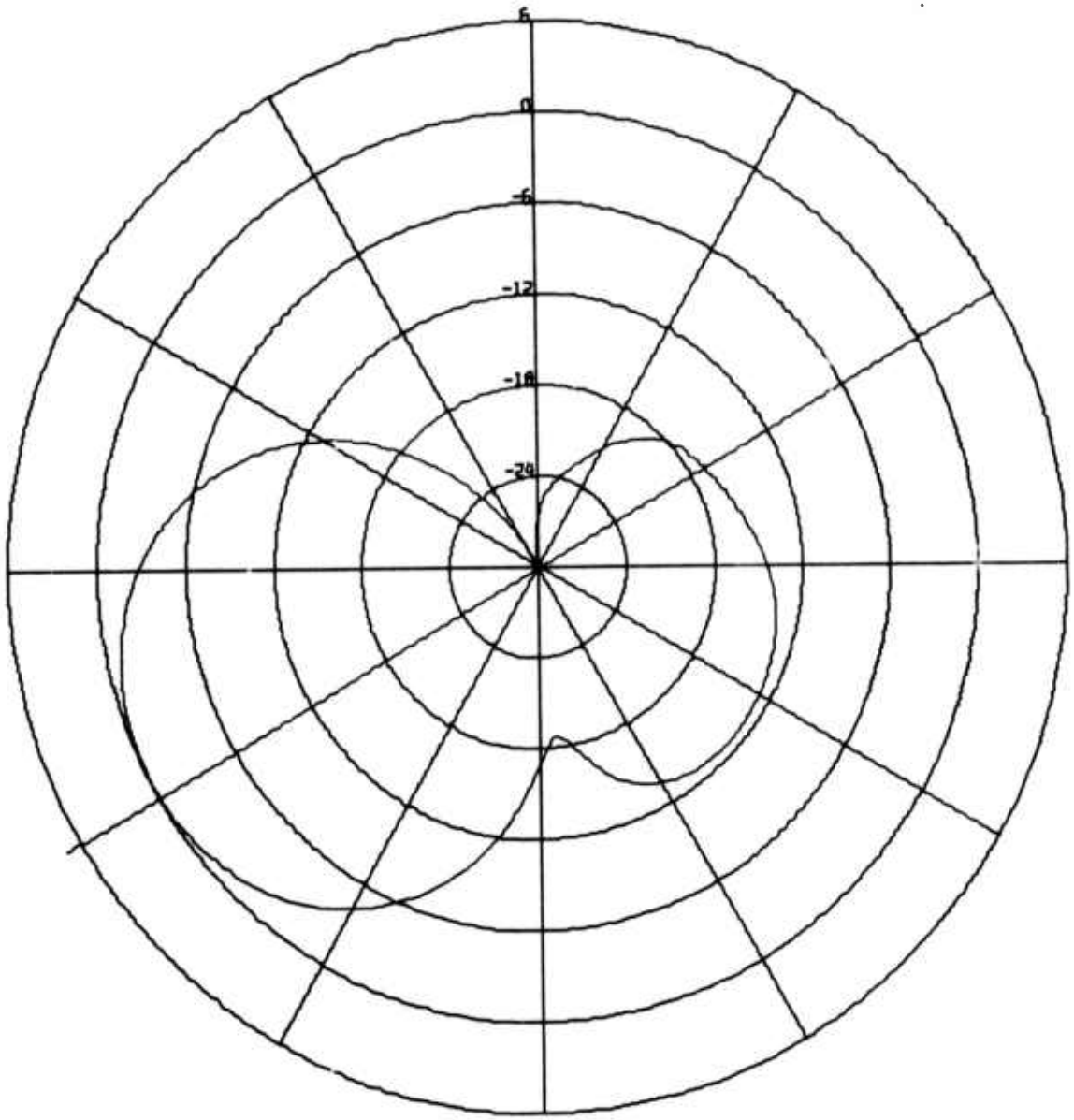

ALPA
ABF BEAM PATTERN AT 276/20.33.00
CONVERGENCE RATE IS 0.0070
BEAM LOOK VELOCITY IS 3.6, LOOK AZIMUTH 240.0
FREQUENCY IS 0.04000 HZ, PERIOD 25.0 SECONDS

FIGURE II-102

FULL-ARRAY ABF RESPONSE FOR MAGNITUDE
3.6 PANAMA EVENT AT 2033 ON DAY 276 OF 1971

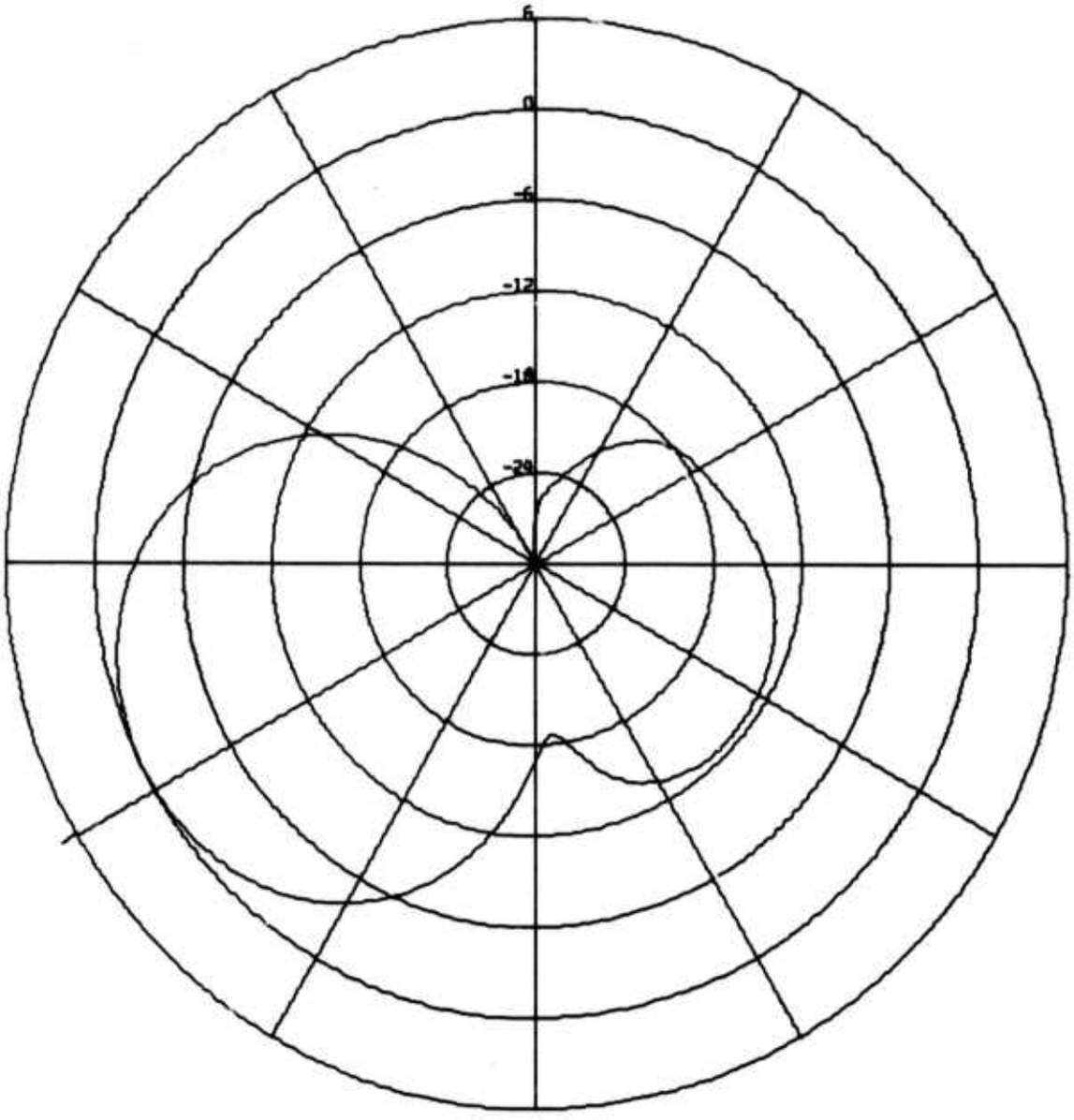

ALPA
ABF BEAM PATTERN AT 276/20.36.30
CONVERGENCE RATE IS 0.0070
BEAM LOOK VELOCITY IS 3.6, LOOK AZIMUTH 240.0
FREQUENCY IS 0.04000 HZ, PERIOD 25.0 SECONDS

FIGURE II-103

FULL-ARRAY ABF RESPONSE FOR MAGNITUDE
3.6 PANAMA EVENT AT 2036 1/2 ON DAY 276 OF 1971

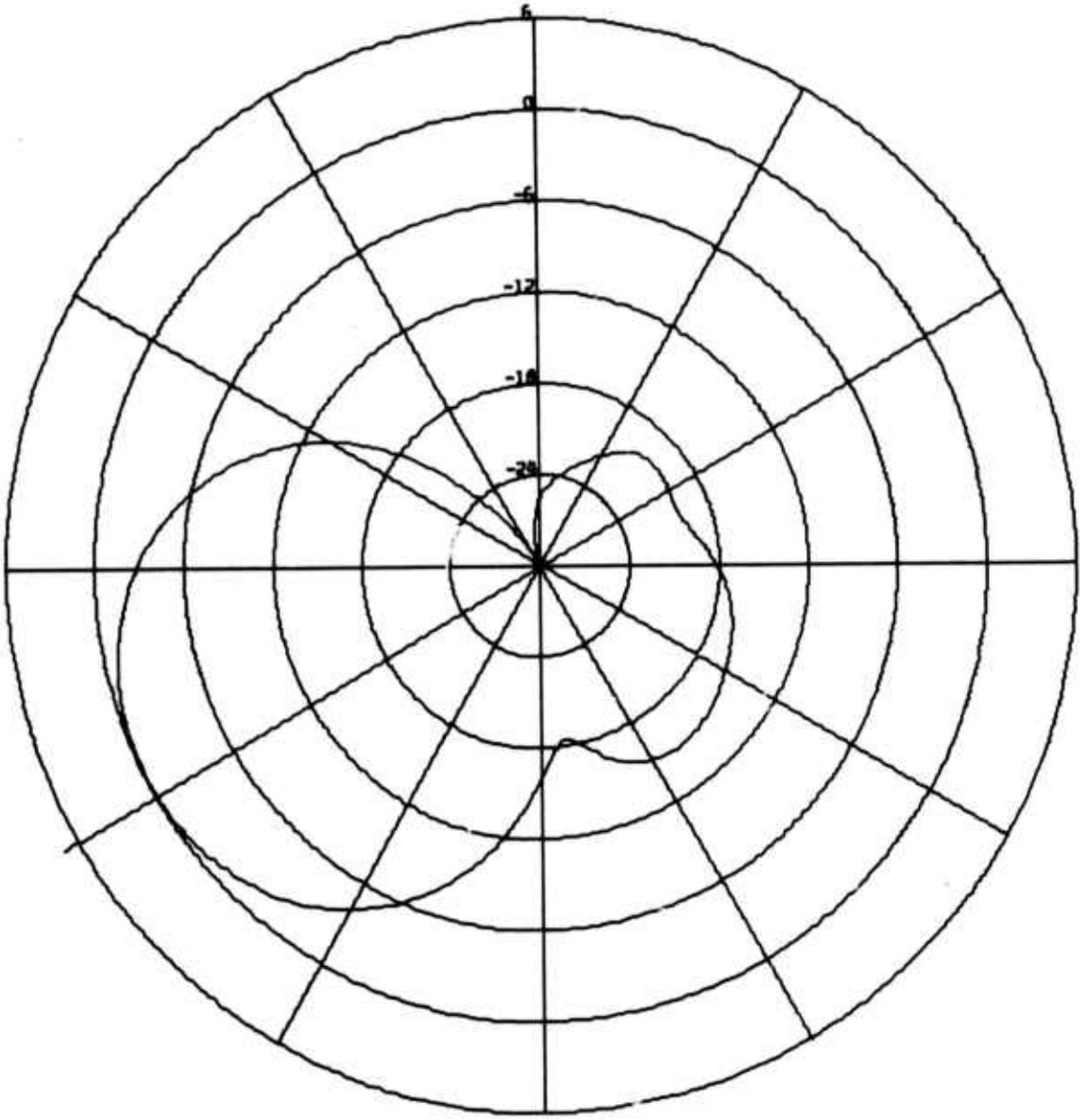

FIGURE II-104

FULL-ARRAY ABF RESPONSE FOR MAGNITUDE 3.6 PANAMA EVENT AT 2040 ON DAY 276 OF 1971

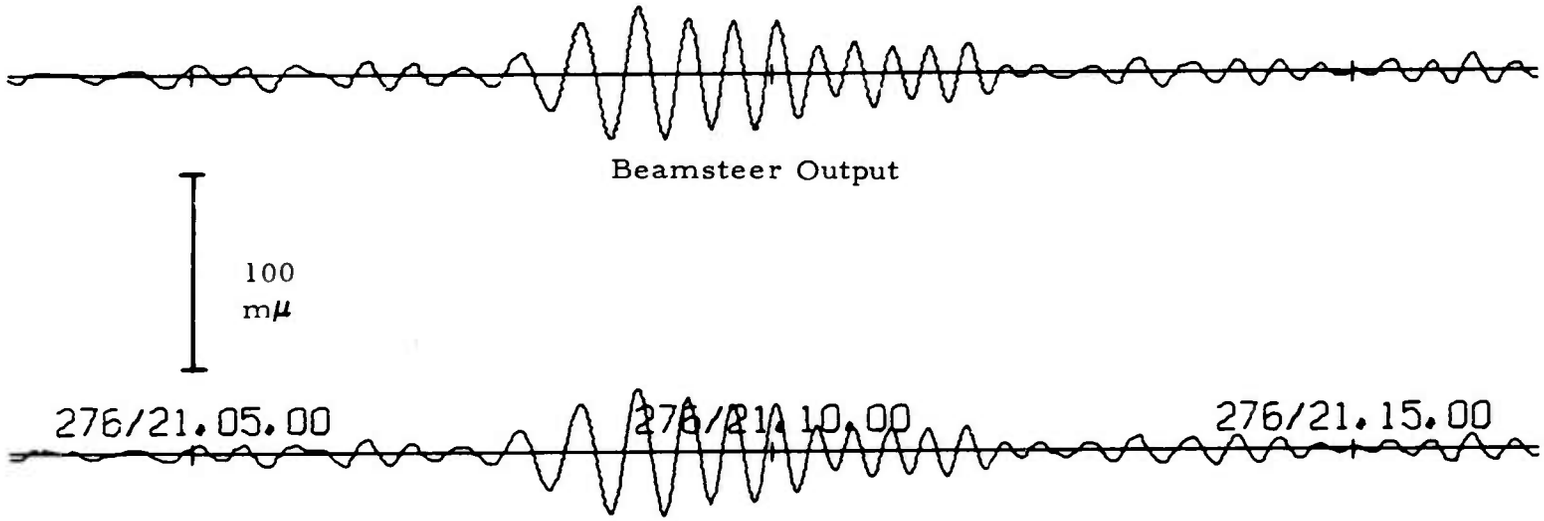

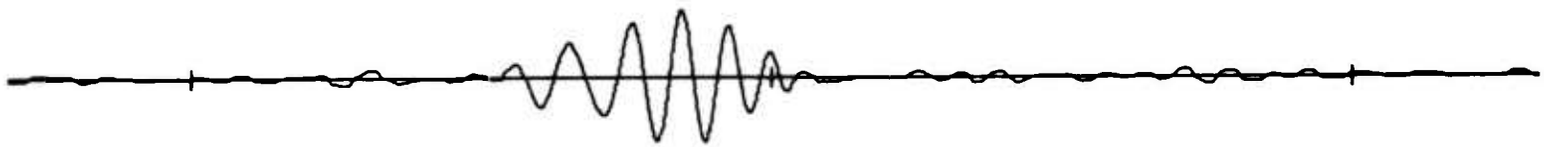

FIGURE II-105

BEAMS FOR MAGNITUDE 4.5 KAMCHATKA EVENT WITH 15-POINT-LONG ADAPTIVE FILTER (DAY 276 1971, STEER DIRECTION 240°)

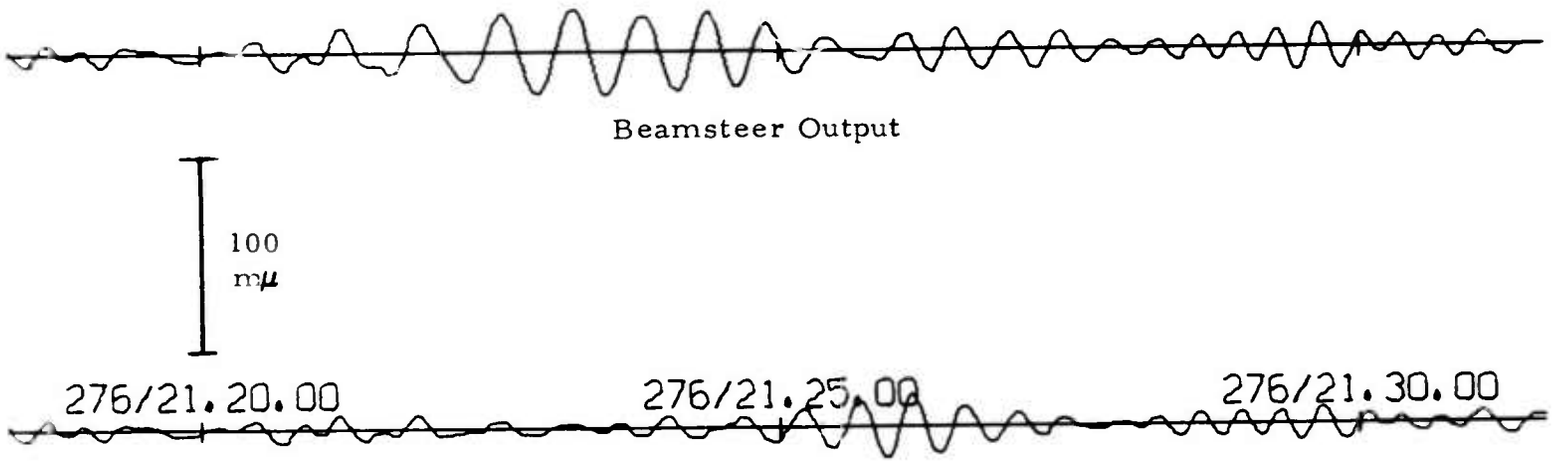

FIGURE II-106

BEAMS FOR MAGNITUDE 4.7 PANAMA EVENT WITH 15-POINT-LONG ADAPTIVE FILTER (DAY 276 1971, STEER DIRECTION 240°)

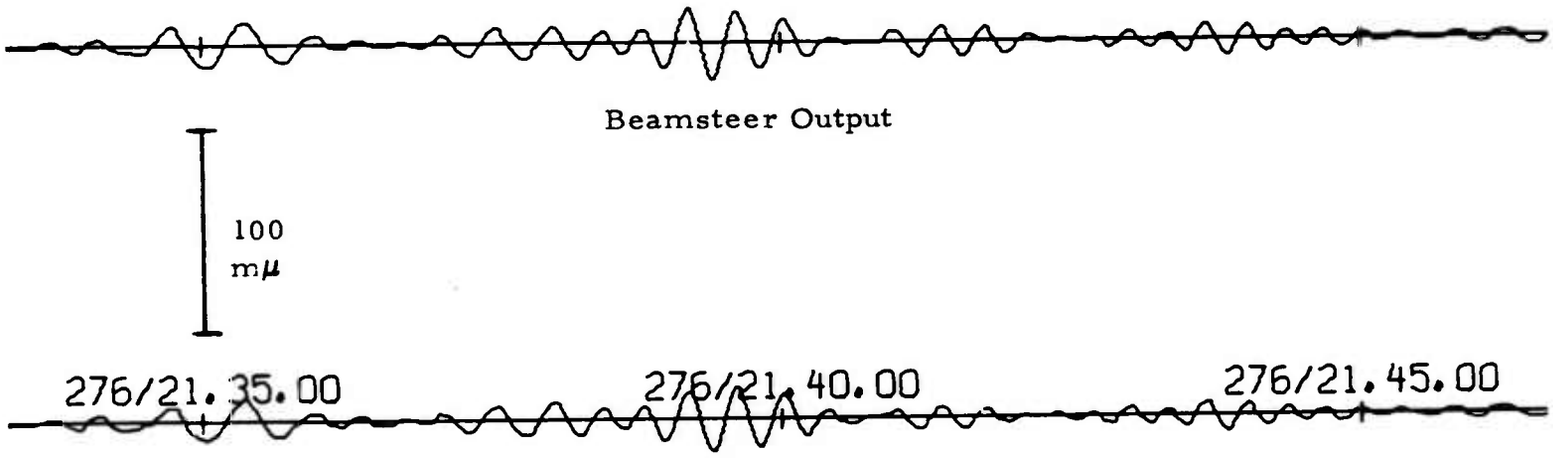

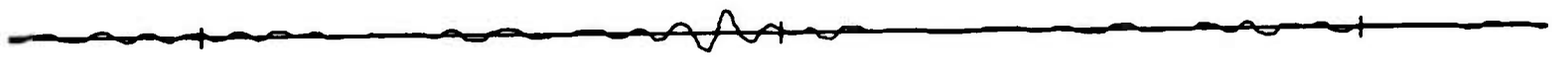

Adaptive Filter Output (μ=0.5)

FIGURE II-107

BEAMS FOR A WEAK EVENT FROM 300°-305° WITH 15-POINT-LONG ADAPTIVE FILTER (DAY 276 1971, STEER DIRECTION 240°)

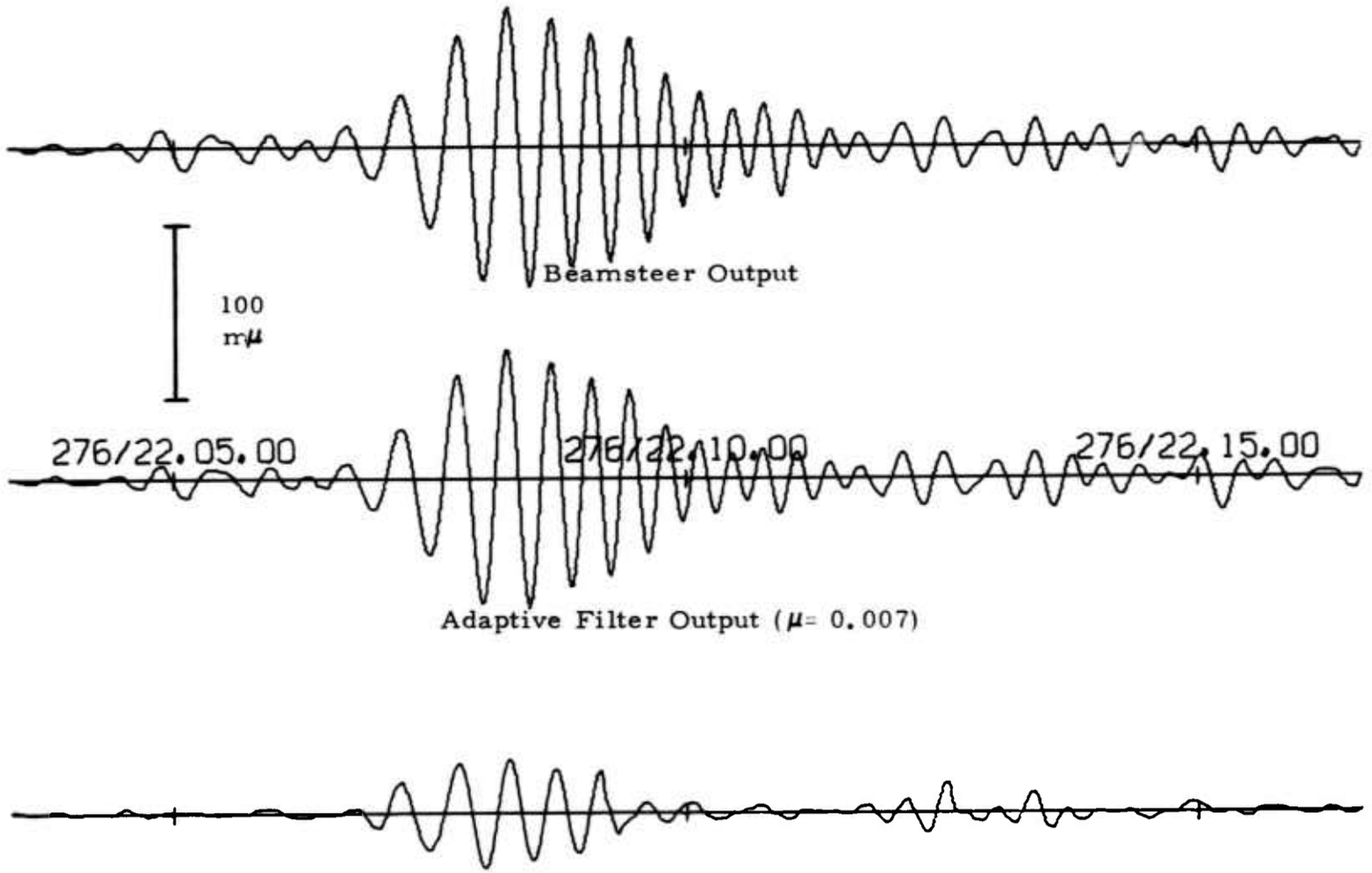

FIGURE II-108

BEAMS FOR MAGNITUDE 4.9 KAMCHATKA EVENT WITH 15-POINT-LONG ADAPTIVE FILTER (DAY 276 1971, STEER DIRECTION 240°)

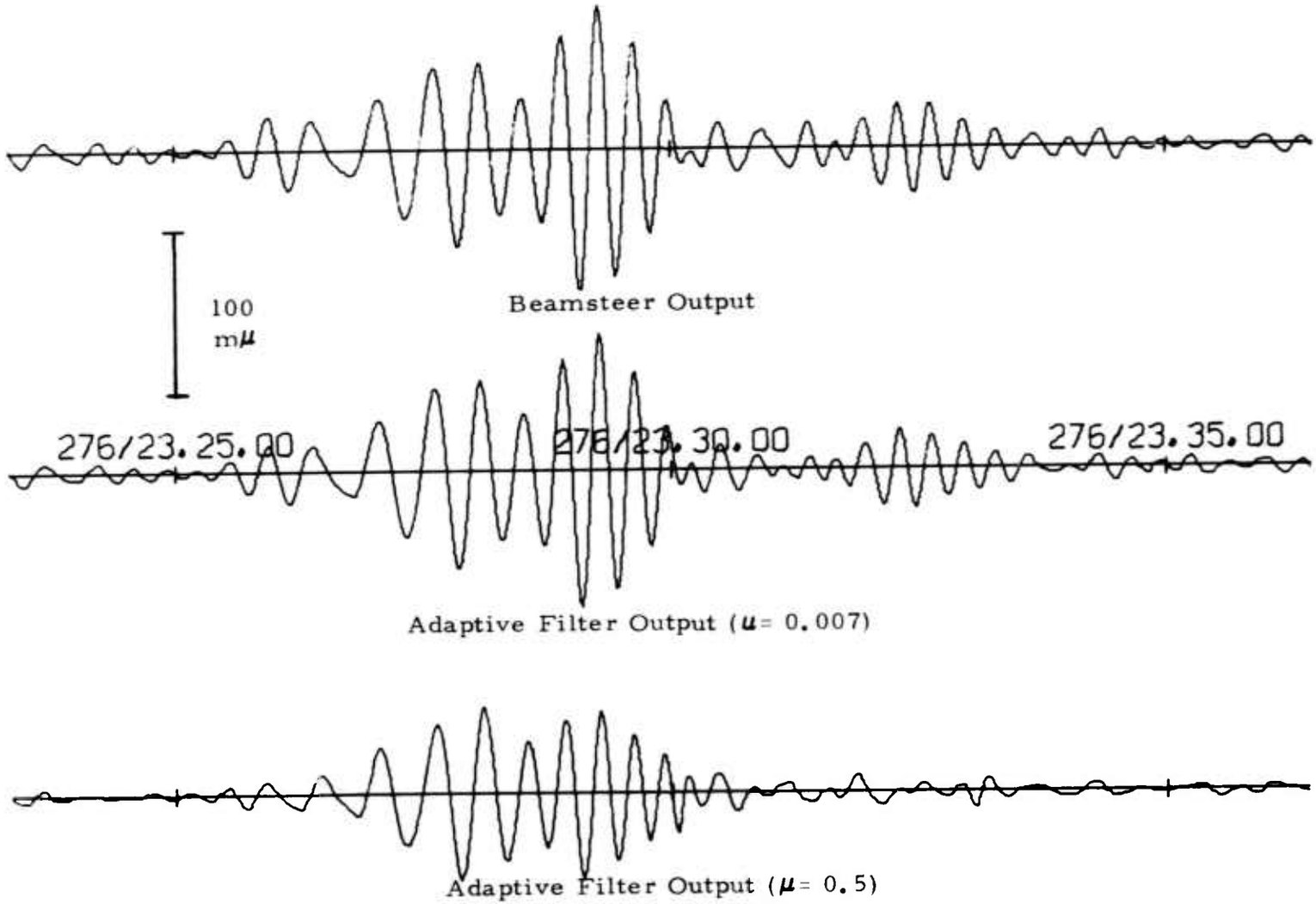

FIGURE II-109

BEAMS FOR ANDREANOF ISLANDS EVENT WITH 15-POINT-LONG ADAPTIVE FILTER (DAY 276 1971, STEER DIRECTION 240°)

signal similarity is not perfect, but not much worse than that of the two Kamchatka events. Perhaps a combination of less-than-perfect signal similarity and a discrepancy between the source azimuth and arrival azimuth can account for the partial suppression of this event.

The results of this subsection clearly demonstrate the effectiveness of the new prefilter depicted in Figure II-71. Detection improvement from the new prefilter is not limited to that achieved by frequency filtering. The new prefilter's emphasis on the more coherent energy at low frequencies raises adaptive filtering noise reduction relative to beamsteering by more than 3 dB compared with the old prefilter of Figure II-1. This additional noise reduction occurs when vertical-component data passed through the new prefilter are input to an adaptive beamformer having either 31 or 15 points per channel. The difference in noise reduction for the two adaptive filter lengths is between 0.3 and 0.4 dB with the new prefilter. Signal degradation for the weak event from 300°-305°, however, is more than 2.1 dB less with the shorter filter length. For this event, which has poor signal similarity, the signal-to-noise gain is more than 1.8 dB greater with the shorter adaptive filter length. For the two Kamchatka events with good similarity, the difference in signal degradation between the two adaptive filter lengths is less than 0.1 dB. The loss in estimated signal-to-noise gain is between 0.3 and 0.4 dB with the shorter filter length. The significantly reduced computation load associated with the shorter adaptive-filter length probably justifies the use of the 15-point-long filter in any on-line implementation of adaptive beamforming. Estimated signal-to-noise gain relative to beamsteering for the New Britain event is 6.6 dB at the maximum convergence rate with the new prefilter and the 15-point-long adaptive filter. The highest signal-to-noise gains were obtained at $\mu = 0.5$ for the New Britain event and the other three events used for signal degradation measurements with the new prefilter. Using the 15-point-long adaptive filter, the estimated signal-to-noise gains were 3.3 dB, 6.0 dB, and 7.7 dB, respectively, for the weak

event from 300°-305°, the first Kamchatka event, and the second Kamchatka event. Thus the signal-to-noise ratio improvement relative to beamsteering ranged from 3 to 8 dB for the four events examined. An improvement of 6 dB can apparently be expected under ordinary conditions. This 6 dB improvement over beamsteering occurs in addition to detection gains obtained from the frequency response of the new prefilter.

G. SUMMARY

The new adaptive algorithm

$$A(t+\Delta t) = A + \frac{2\mu X^T A(\bar{X}-X)}{X^T X}$$

yields dramatic signal-to-noise ratio improvement relative to the old adaptive algorithm

$$A(t+\Delta t) = A + \frac{2\mu X^T A(\bar{X}-X)}{(\bar{X}-X)^T(\bar{X}-X)}$$

employed in the previous adaptive-processing study. With the old adaptive algorithm, signal degradation increases as the signal-to-noise ratio increases and the maximum likelihood constraints do not guarantee preservation of the signal. With the new adaptive algorithm, on the other hand, signal degradation seems to depend more on signal similarity across the array than on signal-to-noise ratio, so that the two Kamchatka events are well-preserved, although in distorted form, even at the maximum convergence rate. For the weak event from 300°-305°, which has poor signal similarity between sites, the estimated signal-to-noise gain based on the noise sample from day 238 of 1970 is never much more than one dB higher with the new adaptive algorithm than with the old algorithm when six sites and the old prefilter of Figure II-1 are employed in the beamforming process. In the case of the weak event from 300°-305°, highest

signal-to-noise improvement relative to beamsteering occurs with both adaptive algorithms at slow convergence rates near $\mu = 0.004$ and $\mu = 0.005$. The essential difference between the two adaptive algorithms emerges in the processing results for the two Kamchatka events. With the old adaptive algorithm, the greatest signal-to-noise gains of 0.965 dB and 0.136 dB arise at $\mu = 0.004$ and $\mu = 0.002$, respectively, for the first and second Kamchatka events. At $\mu = 0.25$, processing gains relative to beamsteering are either minor (for the first Kamchatka event) or negative (for the second Kamchatka event). With the new adaptive algorithm, however, the best signal-to-noise gains for the two Kamchatka events are at the maximum convergence rate. At $\mu = 0.5$, the estimated signal-to-noise ratio improvements based on the noise sample from day 238 of 1970 are 5.75 dB and 7.5 dB, respectively, for the first and second Kamchatka events with six sites and the old prefilter. In detection processing, where signal distortion is a relatively minor consideration, these sharply improved gains demonstrate that significantly improved detection capability for events with good signal similarity is possible at rapid convergence rates. Another effect of operating at high convergence rates is a narrowing of the adaptive processor beamwidth, as indicated by the greater suppression of off-azimuth events at $\mu = 0.5$ than at lower values of the convergence parameter. The effectiveness of the new adaptive algorithm hinges on slowing the effective adaptation rate in the presence of on-azimuth signals. In the extreme case of an ideal signal (where $\overline{X} = X$), the filter vector A stops completely with the new algorithm, whereas the step size $|A(t + \Delta t) - A(t)|$ becomes infinite with the old algorithm. Consequently, replacing the old adaptive algorithm with the new adaptive algorithm reduces signal degradation, particularly for events with good signal similarity.

When beams are formed from data passed through the old prefilter, the estimated signal-to-noise gain of adaptive beamforming relative to beamsteering is normally lower with the full array than with six channels. Differences

in measured signal degradation between the full array and the closely-spaced six-channel array are highly variable, particularly at the higher convergence rates, where 2 dB differences occur for the weak event from 300°-305° and the second Kamchatka event. The main reason for the reduced improvement relative to beamsteering with the full array, however, is not the change in measured signal degradation but instead the measured noise reduction for the data sample from day 335 of 1972: at all convergence rates, the noise reduction is lower with the full array than with six channels. One of the reasons for the lower full-array noise reduction is that the more widely-spaced sensors of the full array have less coherence between sensor pairs than the closely packed elements of the array used for the six-channel measurements. Another reason is that, for the arrays used in the noise reduction measurements, the ratio of the beamsteer directivity index for the fifteen-channel array to that for the six-channel array is greater than 15/6 ($\simeq$4 dB). Thus the ratio of coherent energy to spatially uncorrelated energy in the beamsteer output is less for the fifteen-channel array than for the six-channel array (assuming coherent energy is equally likely at all azimuths). As a result, the potential noise reduction of adaptive beamforming relative to beamsteering is less for fifteen channels than for six channels.

The new signal-enhancement prefilter shown in Figure II-71 is a definite improvement over the old prefilter. Not only is detection gain achieved by the frequency response of the new prefilter, but also the new prefilter's emphasis on the more coherent energy at low frequencies increases ABF noise reduction relative to beamsteering by more than 3 dB compared with the old prefilter. This additional noise reduction occurs with both the 31-point and 15-point adaptive filter lengths. The difference in noise reduction with the new prefilter is only 0.3 - 0.4 dB for the two adaptive-filter lengths. For the two Kamchatka events with good signal similarity, the difference in signal degradation is less than 0.1 dB, so that the loss in estimated signal-to-noise gain due to reduced

noise reduction is 0.3 - 0.4 dB with the shorter filter length. On the other hand, signal degradation for the weak event from 300°-305°, which has poor signal similarity, is more than 2.1 dB lower with the 15-point-long adaptive-filter length, so that the estimated signal-to-noise gain is actually more than 1.8 dB higher with the shorter filter length. Estimated signal-to-noise gain relative to beamsteering for the New Britain event is almost 6.6 dB at the maximum convergence rate with the new prefilter and the 15-point-long adaptive filter.

Table II-52 summarizes the estimated signal-to-noise gains relative to beamsteering for on-azimuth events processed with the new adaptive algorithm. Noise reduction estimates for this summary table are based in all cases on the noise sample from 0415 to 0815 on day 335 of 1972. Both of the blocks showing results for the new prefilter apply to ALPA data in which all available sites were processed. With the exception of the weak event from 300°-305° when processed with the old prefilter using six sites, the best signal-to-noise ratio improvement relative to beamsteering occurs at the most rapid convergence rate. Evidently the adaptive processor can take advantage of transient correlation between successive data vectors X in such a way that noise reduction increases more than signal degradation as the convergence parameter μ approaches its maximum value 0.5. When vertical-component data passed through the old prefilter form the beam inputs, signal-to-noise gain is normally less with the full array than with six channels because of the lower noise reduction obtained with the more widely-spaced sites of the full array. The new prefilter provides increased signal-to-noise ratio improvement relative to beamsteering over and above any detection gain from its frequency response. The use of a 15-point-long adaptive filter instead of a 31-point-long adaptive filter increases the signal-to-noise ratio for the weak event from 300°-305° more than 1.8 dB by reducing the signal degradation for this event, which has poor signal similarity between sites. At the same time, however, the lower noise reduction

TABLE II-52

SUMMARY OF ESTIMATED SIGNAL-TO-NOISE RATIO IMPROVEMENT RELATIVE TO BEAMSTEERING AT SELECTED CONVERGENCE PARAMETERS μ UNDER VARIOUS CONDITIONS

Signal-to-Noise Gain in dB with 6 Sites and Old Prefilter			
Event	$\mu = 0.004$	$\mu = 0.007$	$\mu = 0.5$
Weak Event from 300°-305°	1.488	1.538	-1.120
First Kamchatka Event	1.254	1.522	4.079
Second Kamchatka Event	1.208	1.502	5.874

Signal-to-Noise Gain in dB with Full Array and Old Prefilter			
Event	$\mu = 0.004$	$\mu = 0.007$	$\mu = 0.5$
Weak Event from 300°-305°	0.263	0.245	1.149
First Kamchatka Event	0.804	1.013	4.646
Second Kamchatka Event	0.570	0.681	3.846

Signal-to-Noise Gain in dB with New Prefilter and 31-Point ABF		
Event	$\mu = 0.007$	$\mu = 0.5$
Weak Event from 300°-305°	0.903	1.512
First Kamchatka Event	1.464	6.358
Second Kamchatka Event	1.350	8.067

Signal-to-Noise Gain in dB with New Prefilter and 15-Point ABF		
Event	$\mu = 0.007$	$\mu = 0.5$
Weak Event from 300°-305°	1.026	3.338
First Kamchatka Event	1.376	6.019
Second Kamchatka Event	1.303	7.701
New Britain Event	1.559	6.572

with the shorter filter length results in decreased signal-to-noise gain for the two Kamchatka events, which have good signal similarity. The significantly diminished computational load for the shorter adaptive-filter length probably justifies the use of the 15-point-long filter in any on-line implementation of adaptive beamforming. In any event, the signal-to-noise ratio improvement for the full array with the new prefilter and an adaptive-filter length of 15 points per channel falls within a range of 3 to 8 dB. Normally, a gain of 6 dB might be expected in this mode of operation. Thus adaptive beamforming could conceivably lower the Rayleigh-wave detection threshold at ALPA by 0.3 magnitude units.

Off-azimuth events are strongly suppressed by adaptive beamforming at the maximum convergence rate, where the greatest improvement over time-shift-and-sum beamforming is achieved for on-azimuth events. Some off-azimuths signals are almost completely annihilated. Ordinarily, the strongest off-azimuth events are attenuated the most. For some signals 30° to 60° from the steer direction, however, considerable energy leaks into the adaptive beams, even in the case of the strongest events. The use of the new signal-enhancement prefilter produces some reduction in off-azimuth event suppression. The apparent explanation for this result is the emphasis given to low-frequency energy by the new prefilter. This feature not only increases the effective beamwidth of the adaptive processor but also concentrates more energy near the beginning of events, so that the adaptive filter set cannot react as effectively to the presence of off-azimuth events. Even with the new prefilter, however, the attenuation of off-azimuth events is considerable. This fact demonstrates that greater directional resolution at ALPA and other similar long-period arrays is possible through the beam-narrowing capability of adaptive processing. Such arrays, in effect, become superdirective antennas when adaptive beamforming is employed.

SECTION III
INTERFERING-EVENT RESULTS

A. DISCUSSION

The previous section of this report focused on the ability of adaptive beamforming to detect individual unmixed seismic events in the presence of background noise. This section presents adaptive processing results for mixed events in which both an on-azimuth signal and an off-azimuth interfering event are present in time-overlapped form on the data traces. With data as actually recorded, there is no reliable method to isolate the contribution from each separate event on the beam output. The most realistic method for evaluating the effect of adaptive multichannel filtering on mixed events seems to be a simulation where two data samples, each containing one signal, are summed to create a composite sample containing an interfering event. Such a simulation technique permits considerable variety in the situations which can be examined. The relative strength of the events, the time interval between their arrivals, and their azimuthal separation are all subject to control with the procedure described. In assessing the potential detection gains of adaptive beamforming over conventional time-shift-and-sum processing, the beam outputs for the composite data sample are the most important performance criterion. As long as something closely resembling a seismic event appears on the composite sample beam output during the time period when the on-azimuth signal is present, a detection can be declared. Since only the composite-sample beam is available in practice, phenomena on the beam outputs for the two individual samples can only shed light on the processes involved in adaptive beamforming, but cannot serve as the deciding factor in its evaluation. The relative on-azimuth to off-azimuth event strength at which a detection is

possible on the beamsteer or ABF output for the composite sample determines the detection gain of adaptive multichannel filtering over time-shift-and-sum beamforming. A second but still important consideration in adaptive processing performance, once a signal is detected, is the accuracy with which the peak-to-peak amplitude of the composite-sample beam reflects the peak-to-peak amplitude of the on-azimuth event. Measurement of this amplitude furnishes a surface-wave magnitude estimate for the detected on-azimuth event.

As mentioned earlier, the basic mixed-event simulation procedure sums two data samples, one with an on-azimuth signal and another with an off-azimuth event, to create a composite data sample containing an interfering event. Figure III-1 is a schematic diagram of the interfering-event simulation procedure. Before the summation which creates the composite data sample used in designing the adaptive filter set, individual sites of the sample with the on-azimuth signal are individually scaled, passed through a zero-phase prefilter identical for all sites, and individually time-shifted to time-align the on-azimuth signal at all sites. In the case of the sample with the off-azimuth event, preprocessing of the individual sites is the same except that, before the on-azimuth signal-alignment time delays are applied, the off-azimuth event can be time-shifted from its true direction so as to appear to come from a different direction. Thus the individual sites of the off-azimuth event sample seem to be time-shifted so that the time delays for the on-azimuth signal are applied to an event coming from the specified fictitious arrival direction. Immediately before the adaptive-filter update, the two data samples are summed so that the new adaptive filter update algorithm

$$A(t + \Delta t) = A + \frac{2\mu X^T A(\bar{X}-X)}{X^T X}$$

utilizes the composite data sample for adaptive filter design. To eliminate redundant computations, the computer program used in this study can simultaneously update twenty adaptive filter sets, each corresponding to one particular

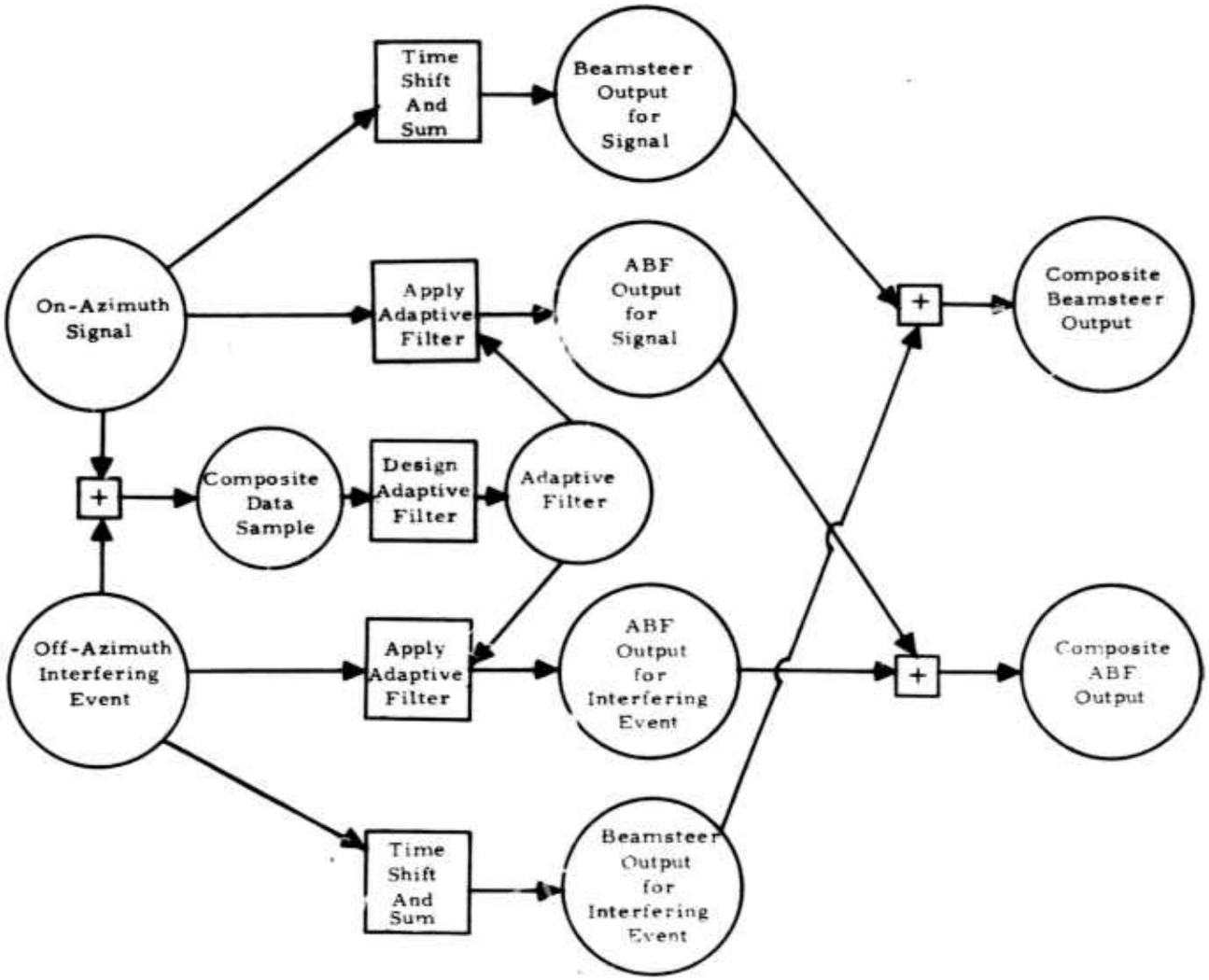

FIGURE III-1

BLOCK DIAGRAM OF INTERFERING-EVENT SIMULATION PROCEDURE

value of the convergence parameter μ. To observe the effect of adaptive beamforming on each of the two data samples used to form the composite sample, the adaptive filter sets are applied separately to each sample. Subsequently, the beam outputs for both samples are summed to create the composite-sample beam output for each adaptive filter set. Similarly, time-shift-and-sum outputs are computed for both data samples and later added to produce the composite-sample beamsteer output. The composite-sample beam output, for beamsteering or for any adaptive filter set, represents the only beam output available in the simulated real-world situation. However, to facilitate an understanding of the processes involved in adaptive beamforming (or in beamsteering), Calcomp plots of the individual-sample beam outputs are displayed along with the composite-sample beam output for any selected time-shift-and-sum or adaptive beamformer. The series of three-trace plots produced in this way form the principal basis for evaluating adaptive-processing performance relative to beamsteering.

The results presented in this section are preliminary and encompass only a limited range of the situations possible in practice. Subsection B discusses adaptive-processing results obtained using long-period data from ALPA. This subsection employs three different pairs of interfering events to compare the relative performance of adaptive beamforming and time-shift-and-sum processing. In one case, the data sample with the off-azimuth event is formed from the on-azimuth event sample by shifting the apparent arrival azimuth of the on-azimuth signal by 180°. The other two event combinations utilize two distinct data samples. Subsection C is a brief discussion of interfering event results based on data from the Korean short-period array. Subsection D summarizes the tentative long-period interfering-event results given in Subsection B.

B. ADAPTIVE BEAMFORMING APPLIED TO LONG-PERIOD INTERFERING EVENTS AT ALPA

The principal goal of this subsection is to examine the detection improvement of adaptive beamforming relative to beamsteering for long-period interfering events simulated by adding two suitably preprocessed data samples from the Alaska Long-Period Array. A secondary objective is to evaluate the reliability of the peak-to-peak amplitude on the composite-sample adaptive filter output as an estimate of the on-azimuth signal's peak-to-peak amplitude. Throughout this subsection, the vertical components for the individual sites pass through the new prefilter shown in Figure II-71 before input to the new adaptive update algorithm. In all cases, the adaptive-filter length is 15 points per channel. At various points in this subsection, four events (all recorded during 1972) are used to simulate mixed events. Table III-1 lists the pertinent data for these events. Each of these events is considerably stronger than the background noise level and has good signal similarity across ALPA. As in Section II, the sites at ALPA are referenced in terms of their transmission order. Figure I-1 and Table 1-1 in the introductory section give the array geometry at ALPA.

To simulate the first mixed event, the data samples for the two Tonga Islands events are summed. The event from day 296 serves as the on-azimuth signal, while the event from day 335 serves as the off-azimuth interfering event. Start times for the two data samples were chosen so that the on-azimuth event from day 296 arrives about three minutes later than the interfering event from day 335. The interfering-event azimuth was shifted from 206° to 25° to achieve 180° azimuthal separation between the two events used in the simulation. Likewise, the event from day 335 was scaled so that the peak-to-peak amplitude of the on-azimuth event from day 296 is 18 dB less than the corresponding amplitude of the interfering event at the single-sensor level. Fourteen sites (all but sites 7, 16, 17, 18, and 19) constitute the channel inputs to the beamformers. In this first mixed-event simulation, the signal-to-noise ratio

TABLE III-1

LONG-PERIOD ALPA EVENTS USED IN INTERFERING-EVENT SIMULATION

Origin Time (Year Day/Hr. Min. Sec.)	Latitude (Degrees)	Longitude (Degrees)	Region	m_b	Azimuth (Degrees)
1972 007/06.25.48	2.1 S	139.0 E	New Guinea	5.9	253
1971 276/21.54.13	55.8 N	162.2 E	East Coast of Kamchatka	4.9	273
1972 296/06.08.08	15.8 S	173.7 W	Tonga Islands	5.3	205
1972 335/02.45.41	17.6 S	174.9 W	Tonga Islands	5.1	206

remains fixed at -18 dB and the convergence parameter μ for the adaptive-filter update varies in order to observe the effect of the convergence rate on adaptive processing detection gain relative to beamsteering.

Figure III-2 displays the 0.04 Hz beamsteer response corresponding to the 205° steer azimuth used to time-align the on-azimuth signal at the 14 sites processed. At the 25° azimuth of the interfering event, the beamsteer response is almost 21 dB lower than at the 205° look azimuth. The beamsteer output traces for the first interfering-event simulation appear in Figure III-3. The upper trace is the beamsteer output for the data sample from day 296 with the on-azimuth signal. The middle trace is the beamsteer output for the data sample from day 335 with the interfering event from 25°. The bottom trace is the composite-sample beamsteer output formed by summing the upper and middle traces. Even though the interfering event is attenuated by approximately 21 dB, no clear indication of the on-azimuth signal in the top trace is visible on the composite-sample beamsteer output. The ratio of the maximum peak-to-peak amplitude during the time gate where the on-azimuth signal is present to the maximum peak-to-peak amplitude before its arrival is a commonly used measure for the reliability of a detection. To avoid confusion with the term signal-to-noise ratio, which in a strict sense would apply to amplitude or power ratios of the on-azimuth signal in the top trace to the interfering event in the middle trace, the term amplitude rise is used in referring to the composite sample beam output. For the composite-sample beamsteer trace in Figure III-3, the amplitude rise is -2 dB, so that no detection is possible.

For a convergence parameter value of 0.007, Figure III-4 shows the ABF response at 0646 corresponding to the beamsteer response in Figure III-2. At the 25° azimuth of the interfering event, the ABF response is about 4 dB lower than the beamsteer response. The adaptive beam outputs for $\mu = 0.007$ appear in Figure III-5. At this slow convergence rate, the ABF traces are

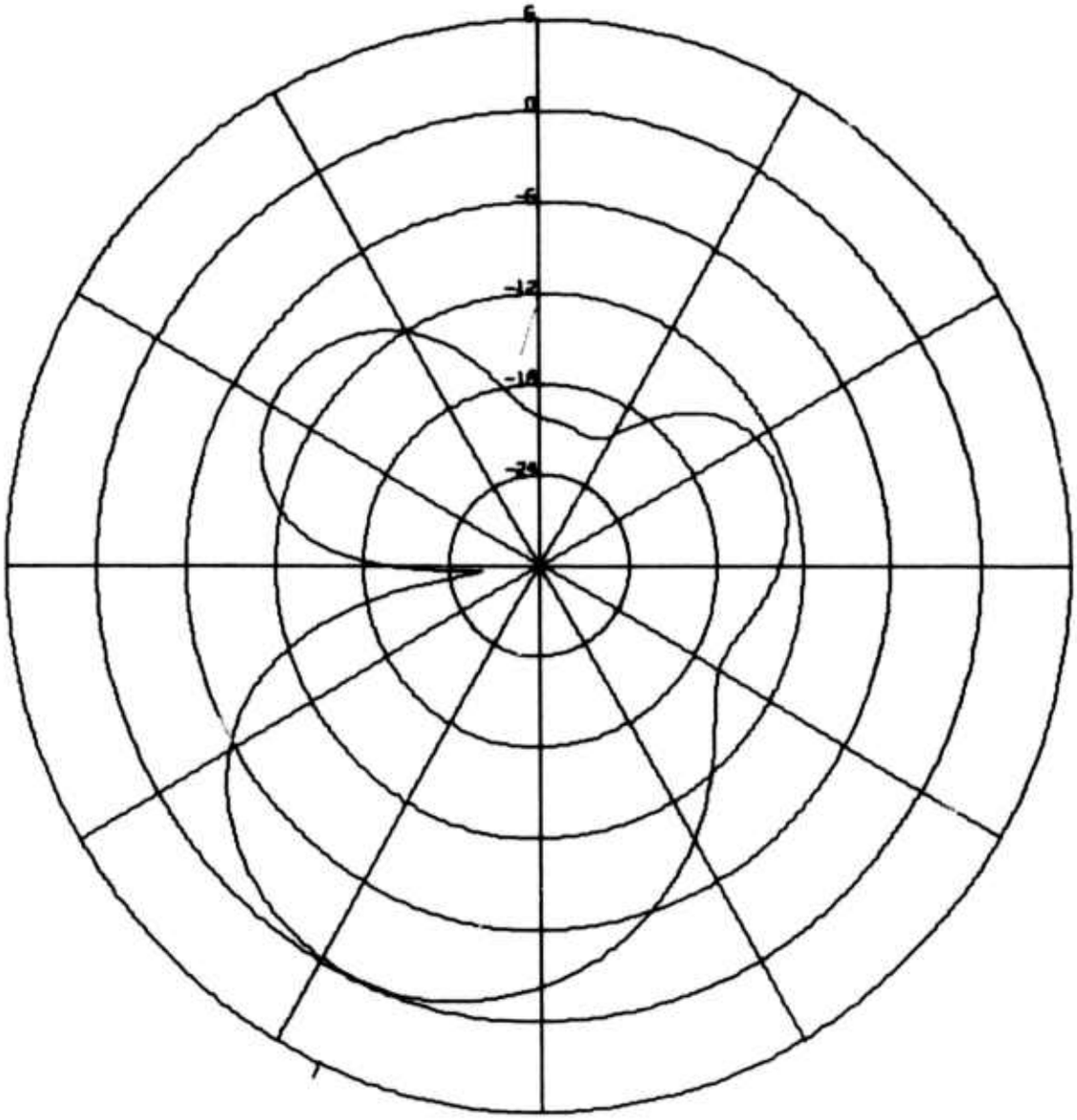

ALPA
TIME-SHIFT-AND-SUM BEAM PATTERN
BEAM LOOK VELOCITY IS 3.6, LOOK AZIMUTH 205.0
FREQUENCY IS 0.04000 HZ, PERIOD 25.0 SECONDS

FIGURE III-2

14-CHANNEL BEAMSTEER RESPONSE
FOR THE SIMULATED MIXED EVENT
FROM DAYS 296 AND 335 OF 1972
(INTERFERING EVENT AZIMUTH 25°)

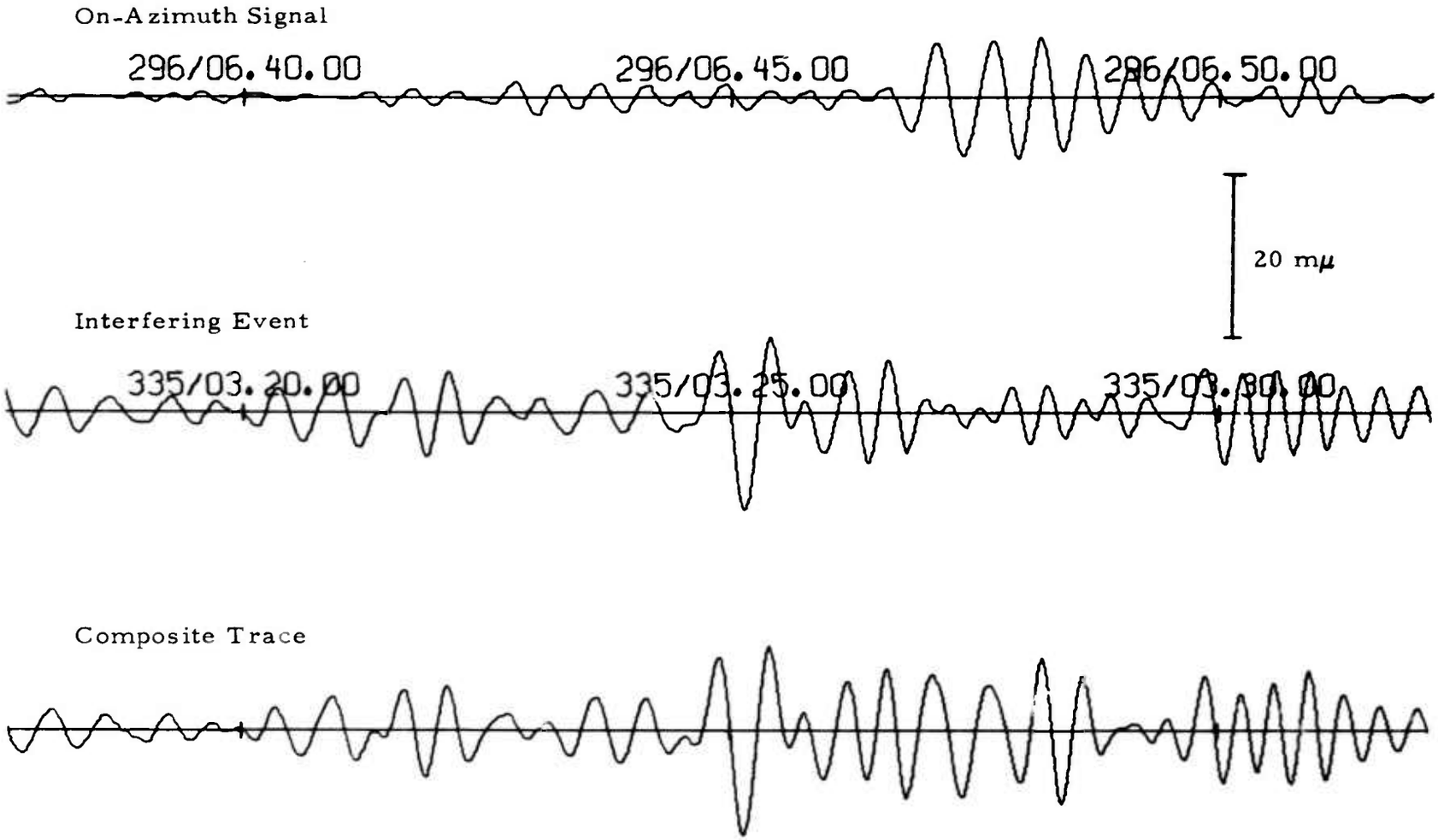

FIGURE III-3

BEAMSTEER OUTPUT FOR THE MIXED EVENT FROM DAYS 296 AND 335 OF 1972
(SIGNAL AZIMUTH 205°, INTERFERING EVENT AZIMUTH 25°, INTERFERING EVENT
18 dB ABOVE THE ON-AZIMUTH SIGNAL)

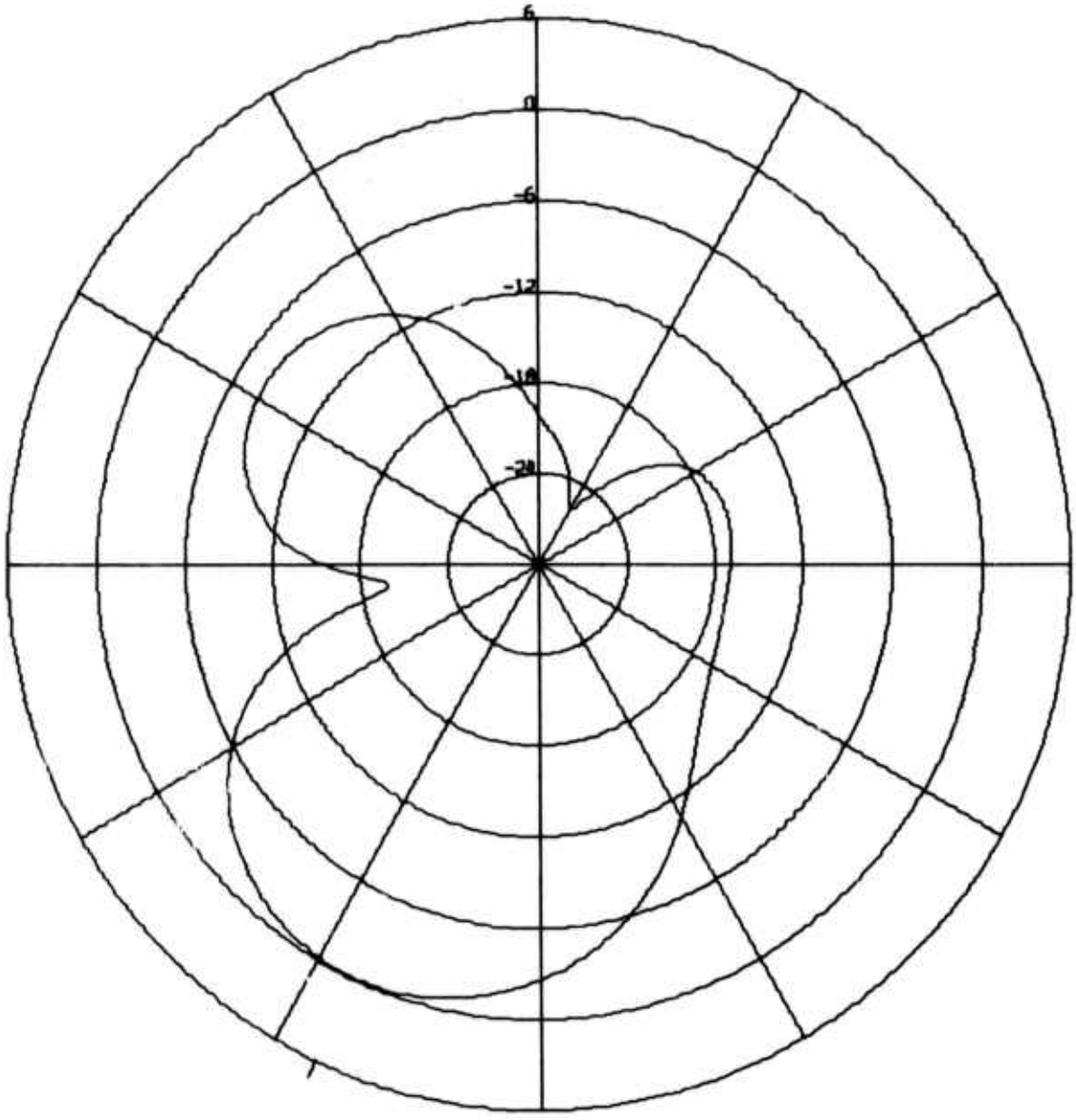

ALPA
ABF BEAM PATTERN AT 296/06.46.00
CONVERGENCE RATE IS 0.0070
BEAM LOOK VELOCITY IS 3.6, LOOK AZIMUTH 205.0
FREQUENCY IS 0.04000 HZ, PERIOD 25.0 SECONDS

FIGURE III-4

14-CHANNEL ABF RESPONSE AT 0646
FOR THE SIMULATED MIXED EVENT
FROM DAYS 296 AND 335 OF 1972
(INTERFERING EVENT AZIMUTH 25°)

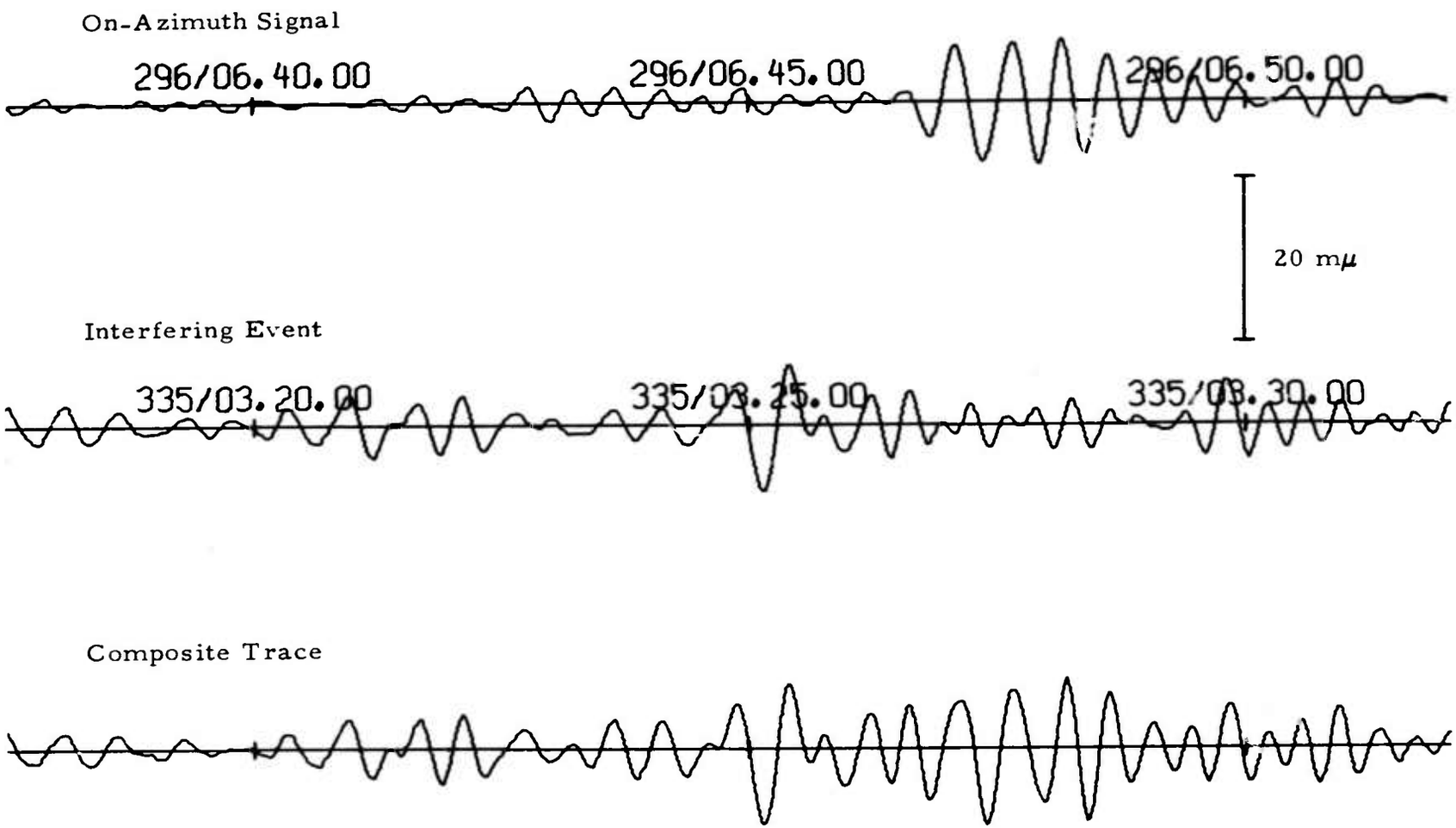

FIGURE III-5

ABF OUTPUT FOR THE MIXED EVENT FROM DAYS 296 AND 335 (μ = 0.007, SIGNAL AZIMUTH 205°, INTERFERING EVENT AZIMUTH 25°, INTERFERING EVENT 18dB ABOVE THE ON-AZIMUTH SIGNAL)

similar to the time-shift-and-sum traces. The principal difference is a slightly greater attenuation of the interfering event in the middle trace. As before, the composite-sample beam does not reflect the presence of the on-azimuth signal: the amplitude rise on the composite-sample trace is about 0 dB.

As the convergence rate increases, adaptive beamforming is able to suppress the interfering event more, and the measured amplitude rise on the composite trace is greater. Figure III-6 presents the adaptive beams at $\mu = 0.05$. The amplitude rise on the composite trace is approximately 4 dB, 6 dB higher than on the beamsteer output. The greatest amplitude rise occurred at a convergence rate of 0.2. Figure III-7 is a plot of the adaptive filter outputs at this rate. The amplitude rise on the composite trace is about 6 dB. Even though there is some signal distortion at this rapid convergence rate, a detection can definitely be made. In this case, adaptive processing produced an 8 dB detection gain over beamsteering. The maximum peak-to-peak amplitude on the composite trace at $\mu = 0.2$ is about 2 dB lower than the corresponding amplitude for the on-azimuth signal in the top trace. This difference is equivalent to 0.1 magnitude units.

An interesting aspect of Figure III-7 is that part of the interfering-event waveform in the middle trace closely resembles the negative of the on-azimuth signal in the top trace. In the maximum likelihood adaptive filter update algorithm, the adaptive processor attempts to create from the data sample containing the off-azimuth event a filter output 180° out of phase with the filter output from the data sample containing the on-azimuth event. Even though the on-azimuth event is passed virtually undistorted, the addition of the filtered off-azimuth event tends to produce mutual cancellation. This phenomenon is consistent with the maximum likelihood filter design specifications (minimization of the filter output power subject to unity-response constraints in the beam look direction). Even with partial cancellation, however, adaptive beamforming suppresses the interfering event so strongly that a detection gain of 8 dB is still achieved.

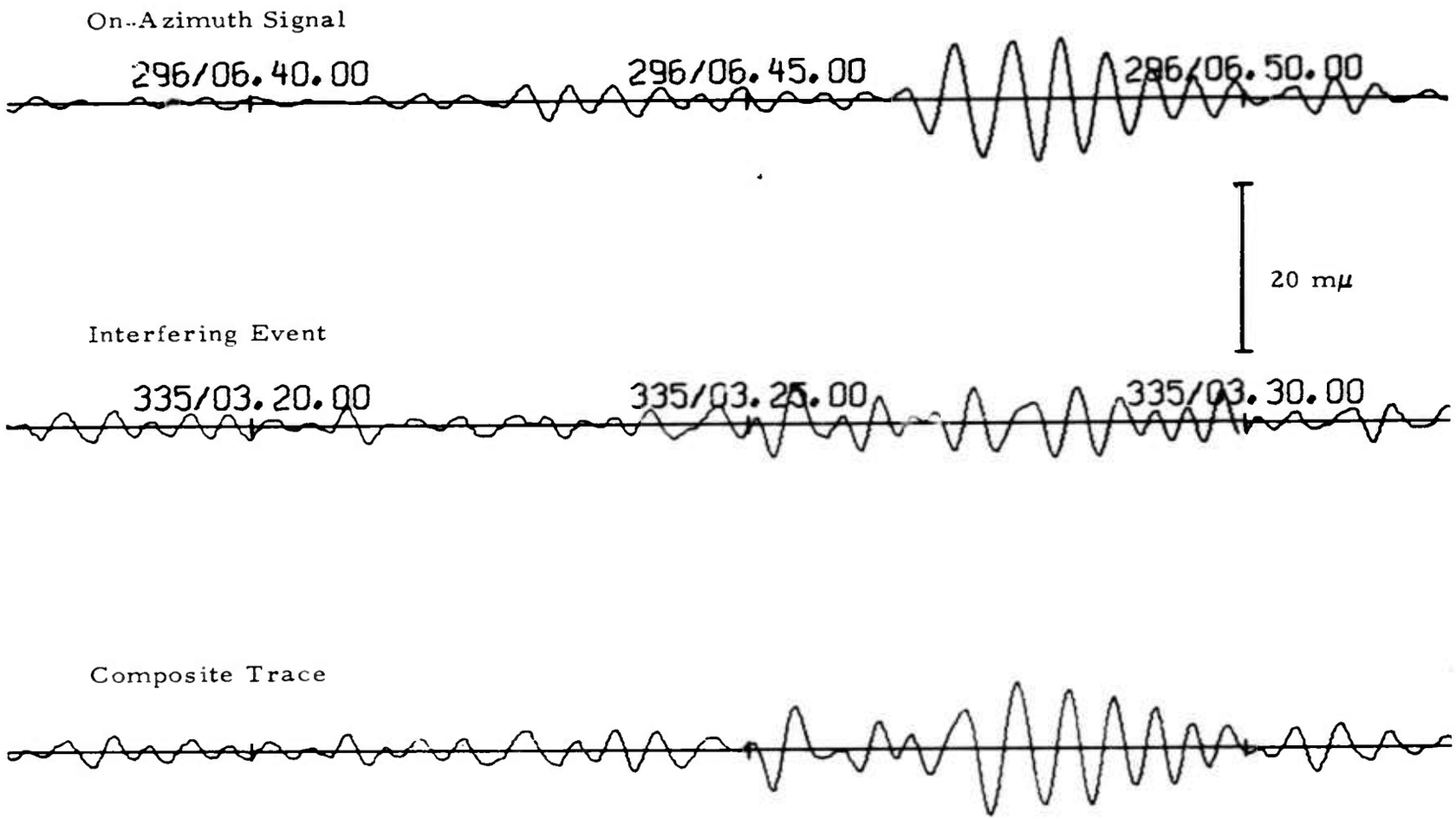

FIGURE III-6

ABF OUTPUT FOR THE MIXED EVENT FROM DAYS 296 AND 335 OF 1972 (μ = 0.05, SIGNAL AZIMUTH 205°, INTERFERING EVENT AZIMUTH 25°, INTERFERING EVENT 18dB ABOVE THE ON-AZIMUTH SIGNAL)

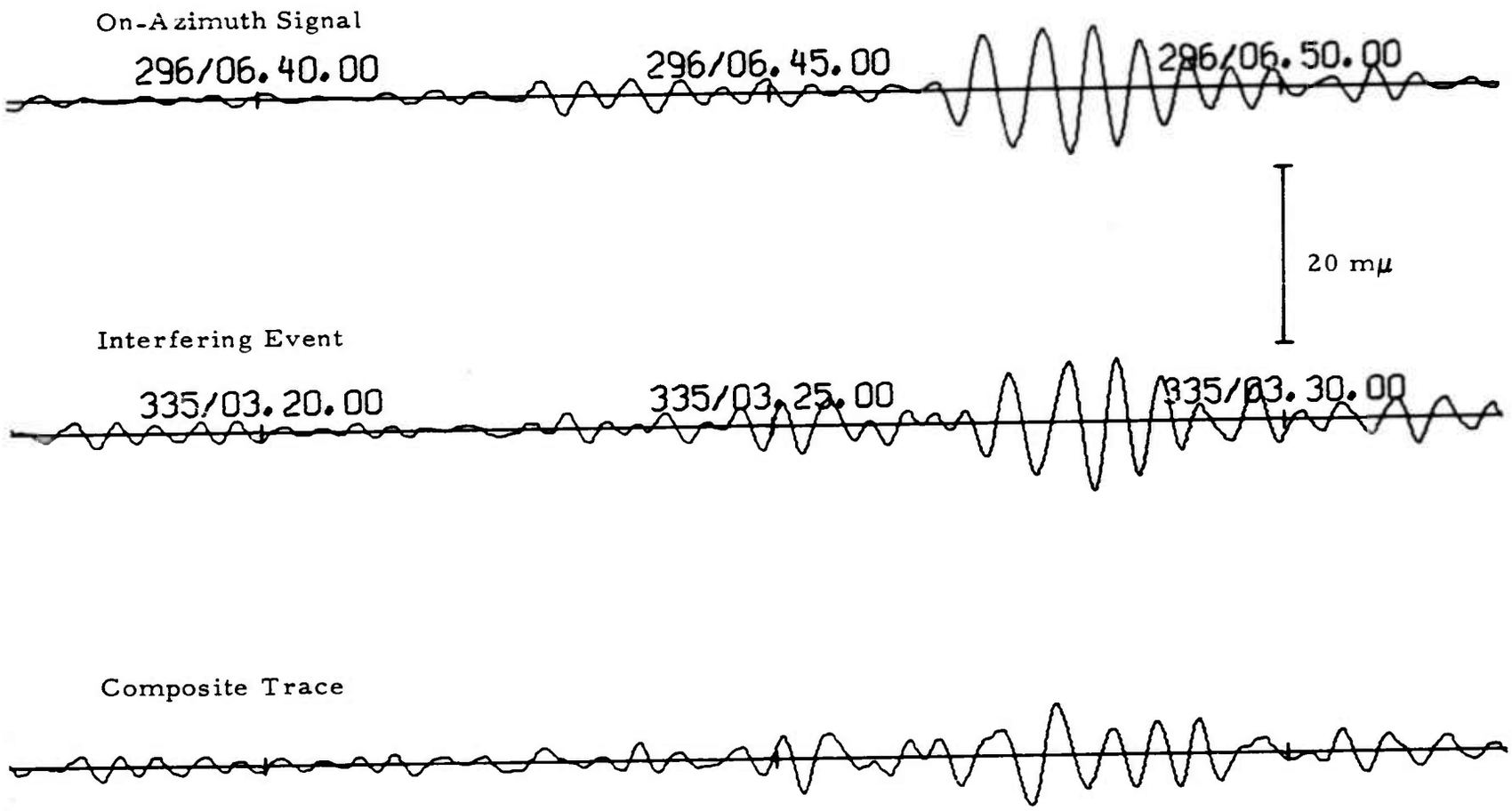

FIGURE III-7

ABF OUTPUT FOR THE MIXED EVENT FROM DAYS 296 AND 335 OF 1972 (μ= 0.2, SIGNAL AZIMUTH 205°, INTERFERING EVENT AZIMUTH 25°, INTERFERING EVENT 18dB ABOVE THE ON-AZIMUTH SIGNAL)

The second mixed-event simulation employs the Tonga Islands event from day 296 for both the on-azimuth signal and the off-azimuth interfering event. For the data sample with an on-azimuth signal, the simulation uses the data exactly as recorded. The apparent arrival azimuth of the event is shifted from 205° to 25° to form the data sample serving as the interfering event. Neither data sample is scaled, so that both events are equally strong at the single-sensor level. Likewise, the start times for both samples are identical, so that both events arrive simultaneously at site 8, the central site at ALPA. Fifteen sites (all but sites 7, 17, 18, and 19) are input to the beamforming process. Figure III-8 displays the adaptive filter outputs at $\mu = 0.5$. The beam output for the off-azimuth event is almost a perfect replica of the on-azimuth signal except for a 180° phase shift. The result on the composite sample trace is a near-zero output due to mutual cancallation of the events. Just to demonstrate that near-perfect cancellation does not happen at all convergence rates, Figure III-9 shows the corresponding adaptive beams at $\mu = 0.002$. This second mixed-event simulation is presented for illustrative purposes only. When the same event is used for both samples in simulating an interf[illegible] event situation, each channel is the sum of two perfectly correlated but time-shifted time series. In accordance with its design objective, the maximum likelihood adaptive beamformer easily reduces the composite sample energy to a bare minimum at high convergence rates. The perfect correlation between corresponding channels of the two data samples utilized makes this simulation extremely unrealistic. In practice, differences in event waveforms, dispersion characteristics, relative arrival times, and relative strengths combine to prevent such near-perfect cancellation of interfering events.

The last mixed-event simulation in this subsection sums the Kamchatka event from day 276 and the New Guinea event from day 007. The Kamchatka event, at an azimuth of 273° from ALPA, serves as the on-azimuth signal, while the New Guinea event serves at the off-azimuth interfering event. The

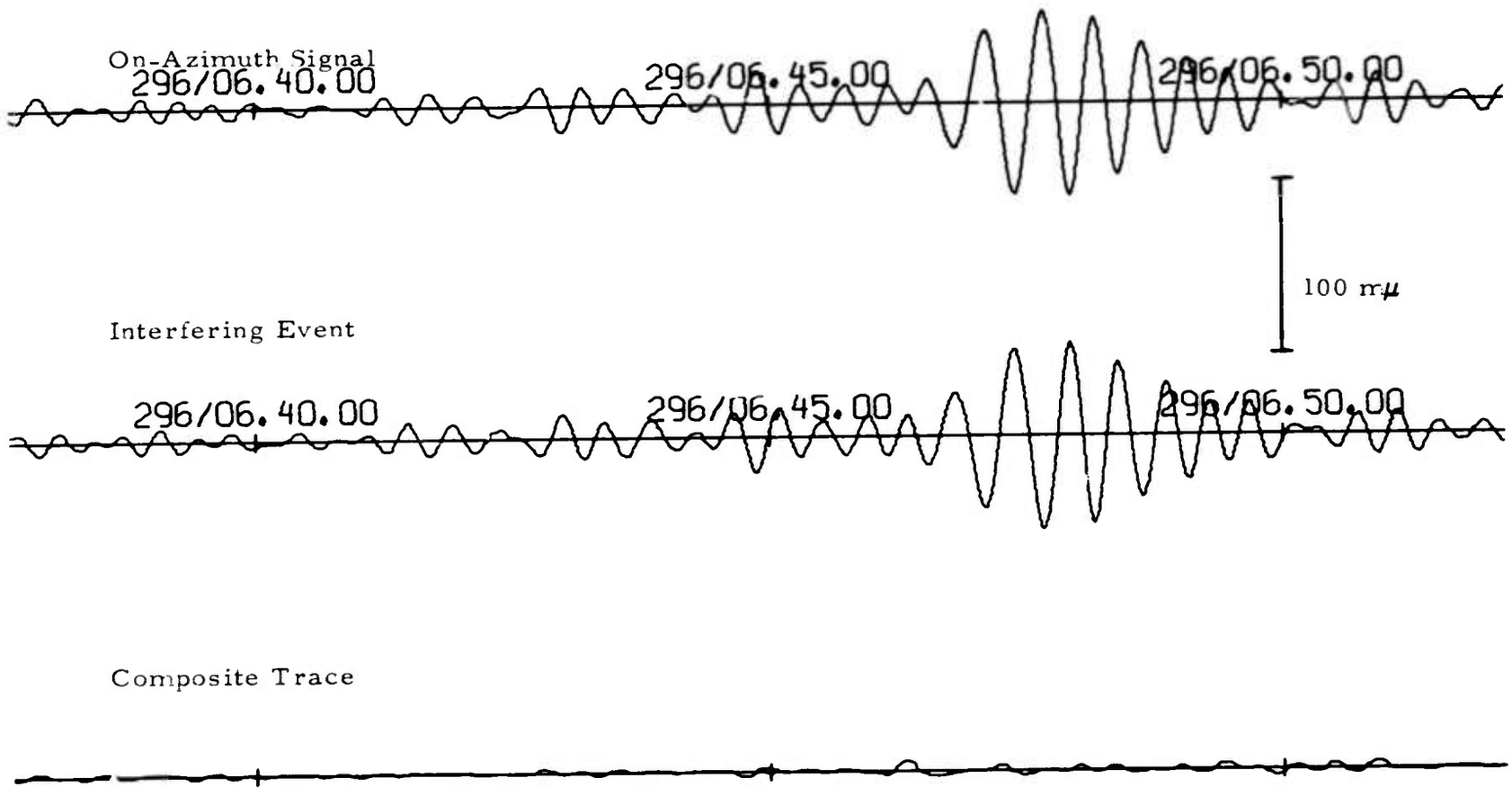

FIGURE III-8

ABF OUTPUT FOR THE EVENT FROM DAY 296 MIXED WITH ITSELF (μ = 0.5, SIGNAL AZIMUTH 205°, INTERFERING EVENT AZIMUTH 25°, INTERFERING EVENT EQUAL IN STRENGTH TO THE ON-AZIMUTH SIGNAL)

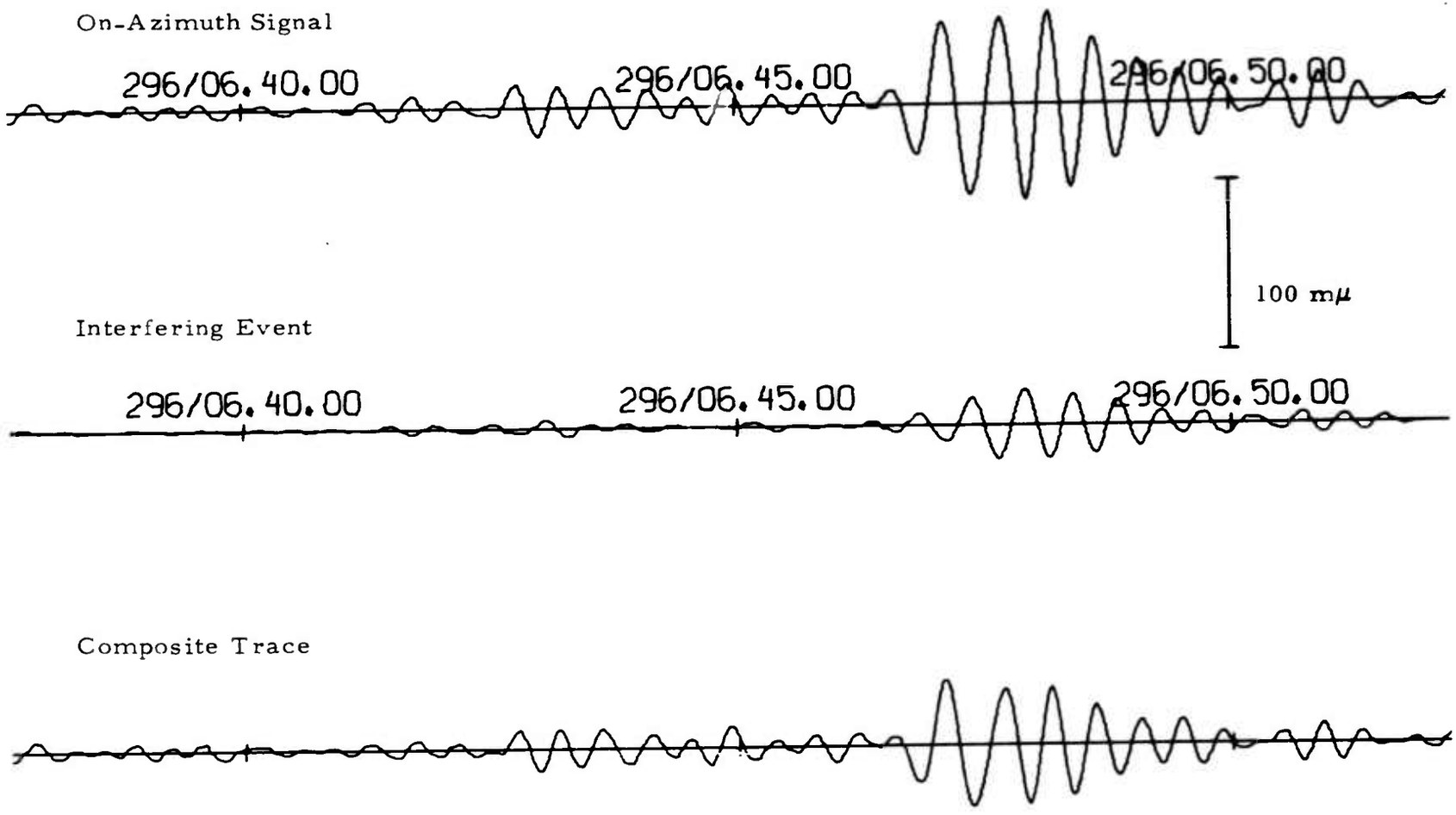

FIGURE III-9

ABF OUTPUT FOR THE EVENT FROM DAY 296 MIXED WITH ITSELF
(μ = 0.002, SIGNAL AZIMUTH 205°, INTERFERING EVENT AZIMUTH 25°,
INTERFERING EVENT EQUAL IN STRENGTH TO THE ON-AZIMUTH SIGNAL)

azimuth of the New Guinea event was shifted from 253° to 93° to obtain 180° separation between the two events. With the start times selected, the interfering event arrives eleven minutes before the on-azimuth signal. Twelve sites (all but 3, 4, 5, 6, 7, 11, and 18) are used in forming the beams. The beamsteer response corresponding to a steer azimuth of 273° appears in Figure III-10. At the 93° azimuth of the interfering event, the attenuation is 15 dB, close to the maximum for all azimuths. In this last mixed-event simulation, the relative strength of the two events is varied in order to observe its effect on adaptive-processing performance.

Initially, the interfering event is scaled so that it is 12 dB above the on-azimuth signal at the single-sensor level. Figure III-11 presents the beamsteer output traces for this case. The amplitude rise is approximately 8 dB on the composite-sample beam. A visual inspection of the bottom trace in Figure III-11 confirms that a detection is possible with time-shift-and-sum processing. Figure III-12 displays the corresponding adaptive beam outputs for $\mu = 0.2$. The amplitude rise on the composite sample trace is nearly 15 dB at this convergence rate. Thus the detection gain over beamsteering is approximately 7 dB. The drop in maximum peak-to-peak amplitude from the top trace to the bottom trace is slightly more than 2 dB, or 0.1 magnitude units.

When the off-azimuth event is scaled so that it is 18 dB above the on-azimuth signal at the single-sensor level, no detection is possible on the composite sample beamsteer trace. Figure III-13 pictures the beamsteer traces in this situation. The amplitude rise on the composite-sample beamsteer trace is only 2 dB. Figure III-14 is a plot of the corresponding adaptive beams for $\mu = 0.007$. At this convergence rate, the adaptive filter set attenuates the interfering event enough to produce a 6 dB amplitude rise on the composite beam. As the convergence rate increases, the composite-trace amplitude rise improves until it reaches a maximum of about 12 dB at $\mu = 0.2$. In this case, the ABF detection gain over beamsteering is 10 dB. The adaptive beam outputs

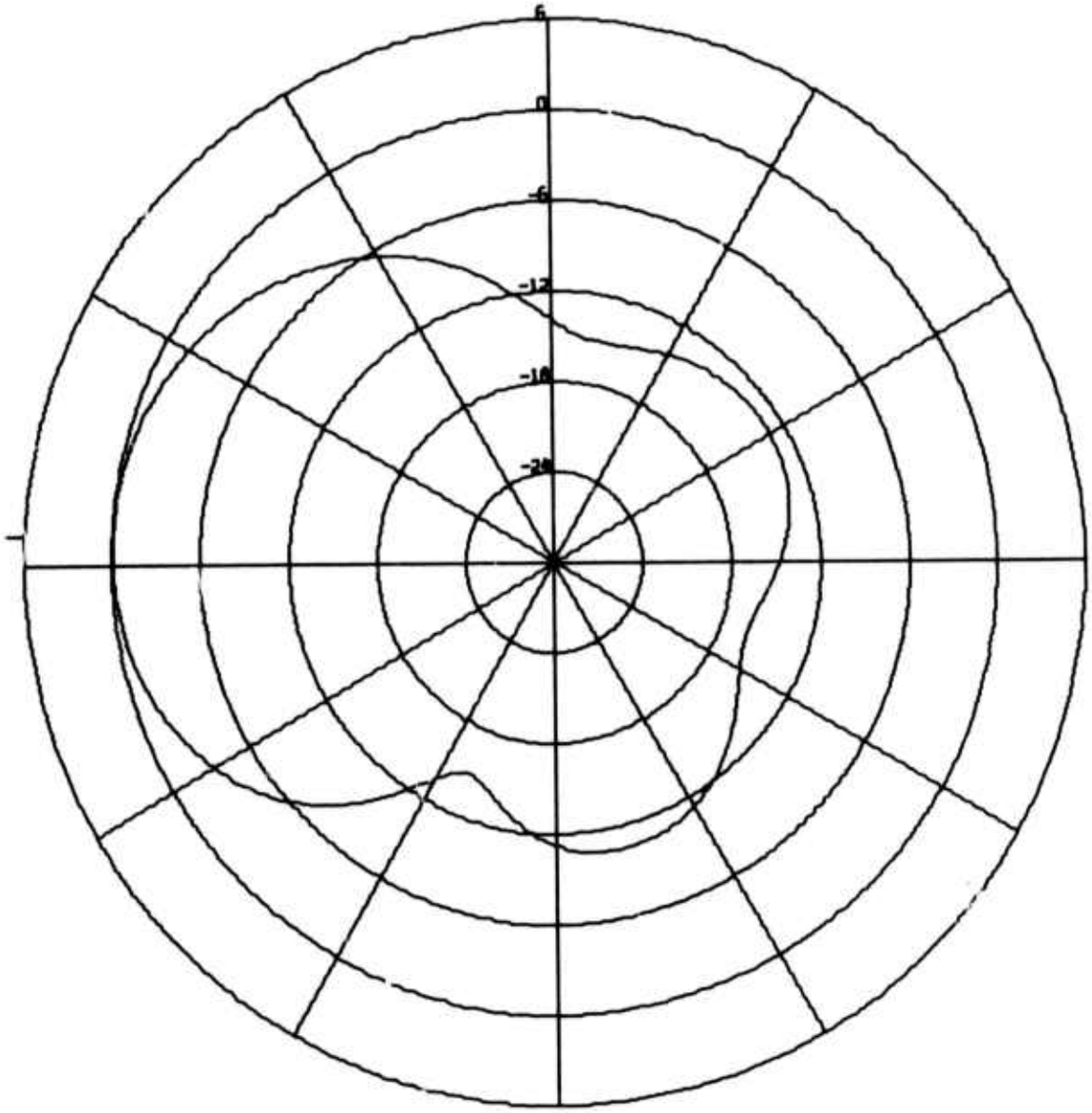

ALPA
TIME-SHIFT-AND-SUM BEAM PATTERN
BEAM LOOK VELOCITY IS 3.6, LOOK AZIMUTH 273.0
FREQUENCY IS 0.04000 HZ, PERIOD 25.0 SECONDS

FIGURE III-10

12-CHANNEL BEAMSTEER RESPONSE
FOR THE SIMULATED MIXED EVENT
FROM DAYS 276 AND 007
(INTERFERING EVENT AZIMUTH 93°)

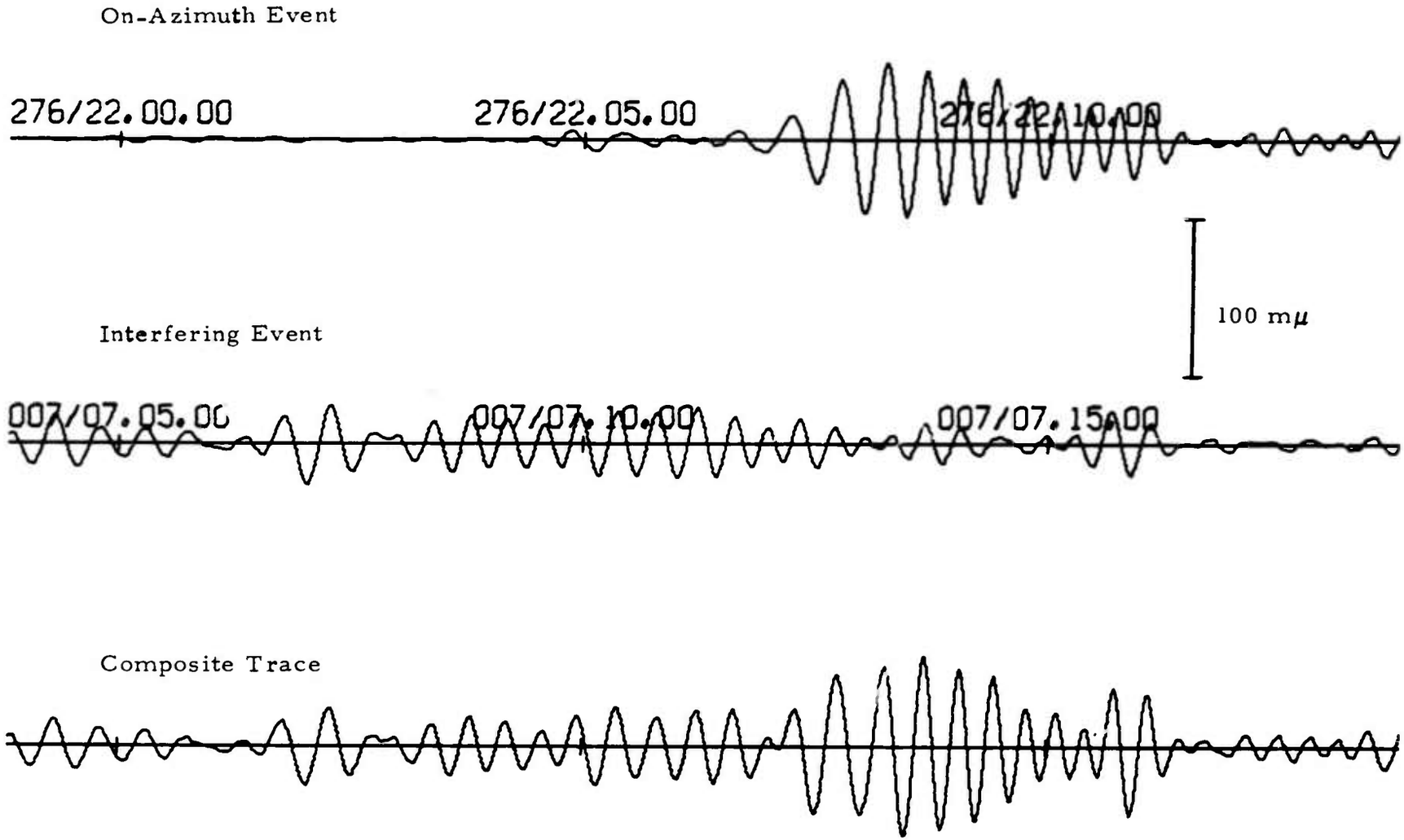

FIGURE III-11

BEAMSTEER OUTPUT FOR THE MIXED EVENT FROM DAYS 276 AND 007
(SIGNAL AZIMUTH 273°, INTERFERING EVENT AZIMUTH 93°, INTERFERING EVENT
12dB ABOVE THE ON-AZIMUTH SIGNAL)

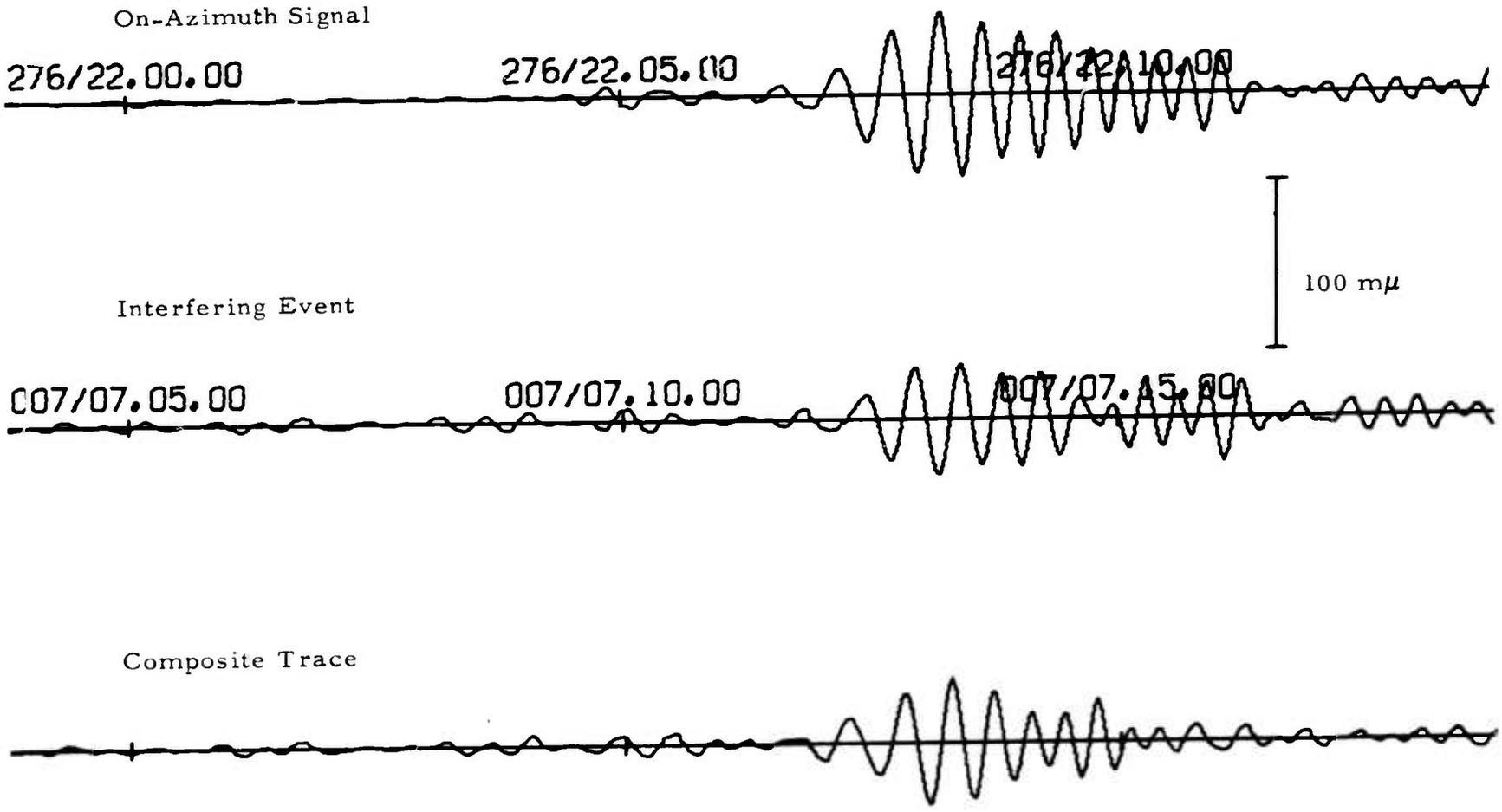

FIGURE III-12

ABF OUTPUT FOR THE MIXED EVENT FROM DAYS 276 AND 007 ($\mu = 0.2$, SIGNAL AZIMUTH 273°, INTERFERING EVENT AZIMUTH 93°, INTERFERING EVENT 12dB ABOVE THE ON-AZIMUTH SIGNAL)

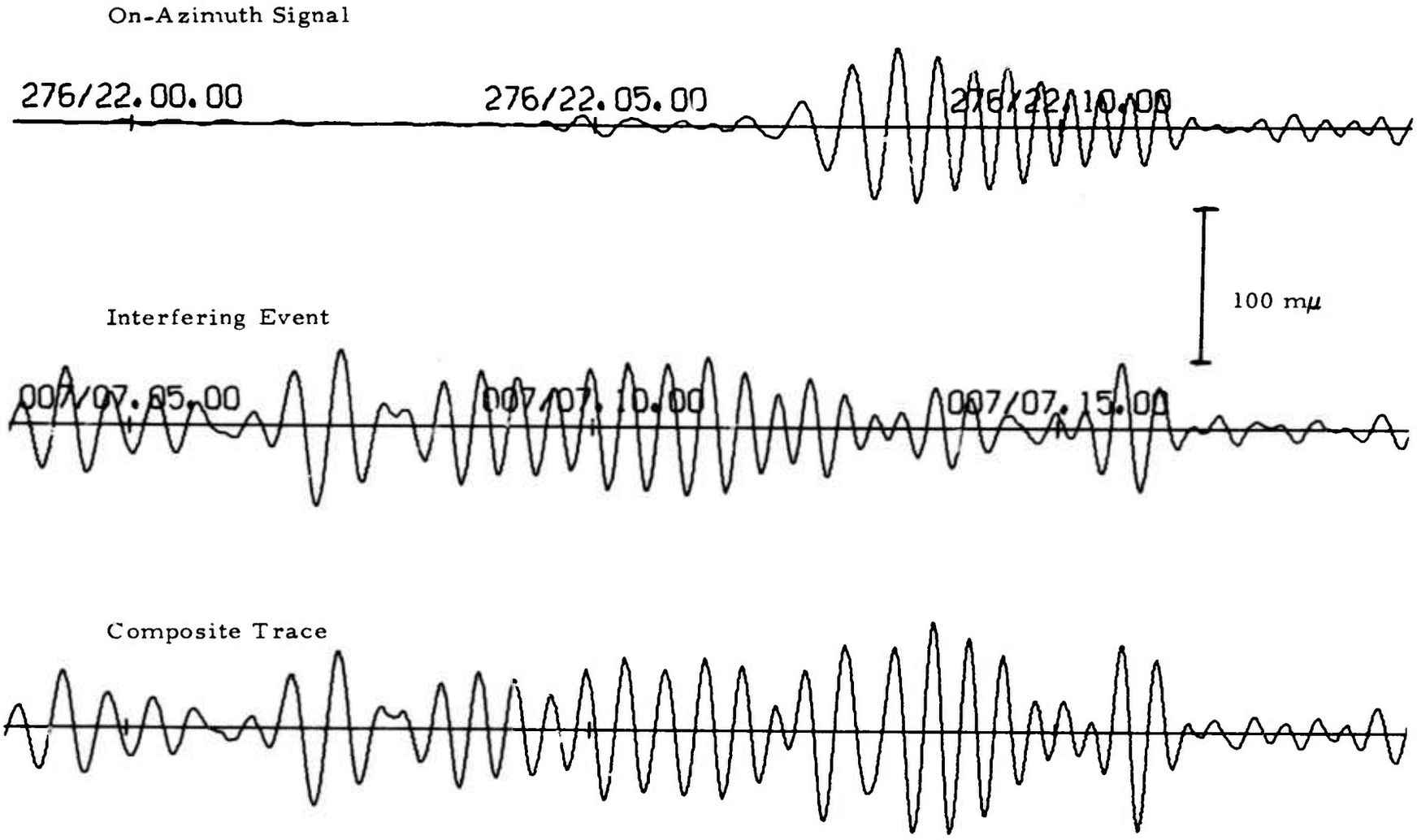

FIGURE III-13

BEAMSTEER OUTPUT FOR THE MIXED EVENT FROM DAYS 276 AND 007
(SIGNAL AZIMUTH 273°, INTERFERING EVENT AZIMUTH 93°, INTERFERING EVENT
18dB ABOVE THE ON-AZIMUTH SIGNAL)

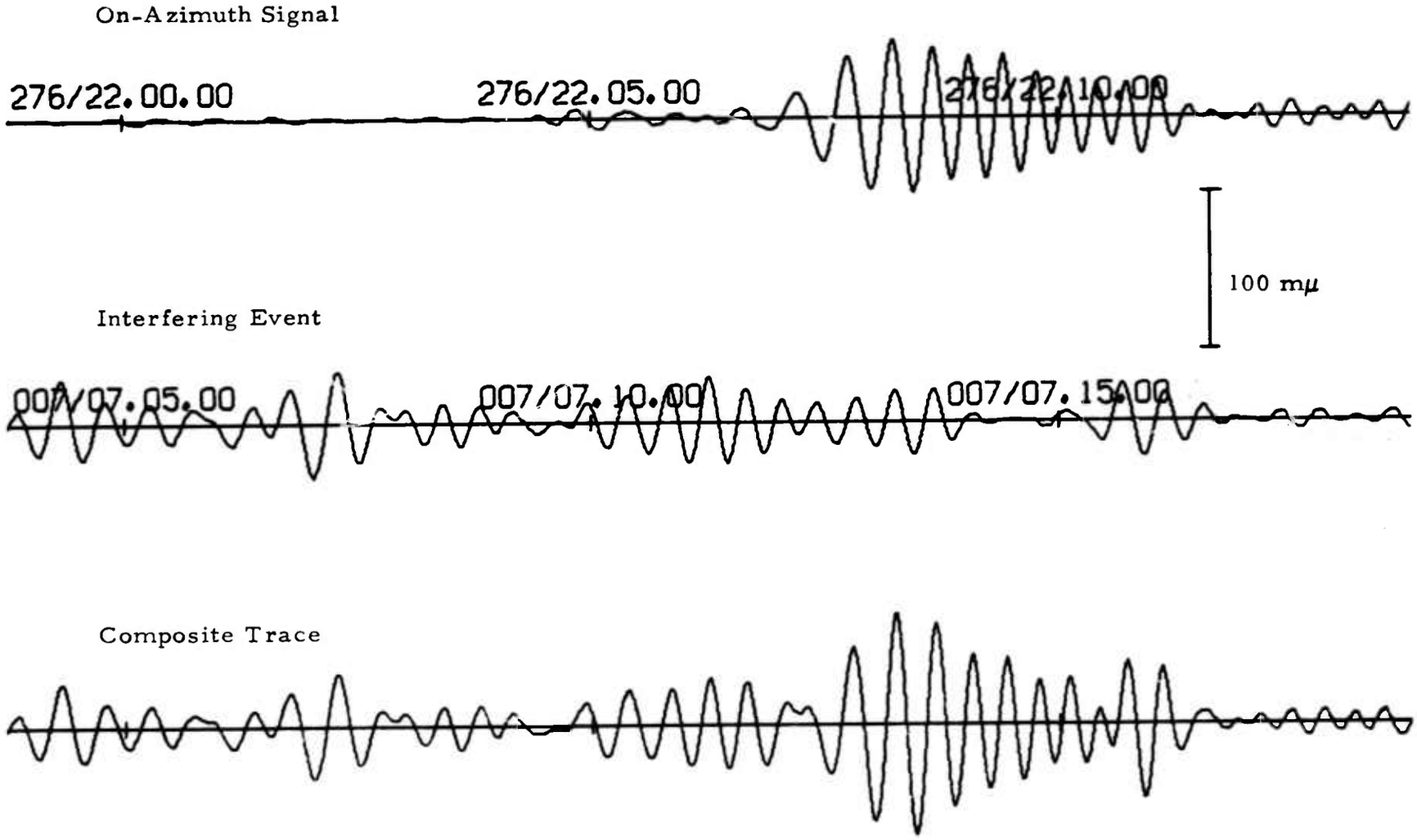

FIGURE III-14

ABF OUTPUT FOR THE MIXED EVENT FROM DAYS 276 AND 007 (μ= 0.00[illegible] SIGNAL AZIMUTH 273°, INTERFERING EVENT AZIMUTH 93°, INTERFERING EVENT 18dB ABOVE THE ON-AZIMUTH SIGNAL)

for this convergence rate appear in Figure III-15. A clear detection is possible in the bottom trace. Here the decrease in the maximum peak-to-peak amplitude from the on-azimuth signal beam to the composite sample beam is slightly less than 2 dB. The detection gains at high convergence rates are possible in the interfering-event situation chiefly through the dramatic suppression of the off-azimuth event before the arrival of the on-azimuth signal. Immediately after the arrival of the signal, the adaptive beamformer is unable, at least for a while, to effect mutual cancellation of the interfering events when the events are not highly correlated. The burst of energy on the composite sample beam at the arrival time of the on-azimuth signal permits the signal to be detected.

At an off-azimuth event strength 24 dB above the on-azimuth signal, time-shift-and-sum processing is even less effective than at the 18 dB level. For purposes of comparison, however, Figure III-16 presents the beamsteer outputs for the 24 dB case. The corresponding adaptive beams at $\mu = 0.2$ are shown in Figure III-17. On the composite sample beam, the amplitude rise is slightly more than 8 dB, the same as for the beamsteer processor at an off-azimuth event strength only 12 dB above the on-azimuth signal. Thus adaptive beamforming is able to produce detection results comparable to those obtained from beamsteering at a 12-dB-lower event separation. In the 24 dB case, the difference in maximum peak-to-peak amplitudes between the top trace and the composite trace is negligible for the ABF outputs at $\mu = 0.2$.

To determine the maximum event separation at which a detection is possible with adaptive beamforming, the event separation is increased to 30 dB and 36 dB, respectively, in the last two cases examined. Figures III-18 and III-19 display the ABF outputs at a convergence rate of 0.5 for the 30 dB and 36 dB event separation levels, respectively. At a 30 dB separation, the amplitude rise is about 6 dB. A borderline detection is possible here. At a 36 dB separation, the amplitude rise is only 4 dB, so that no detection could be declared without additional information. An example of such information could be the expected arrival time determined from a short-period event bulletin.

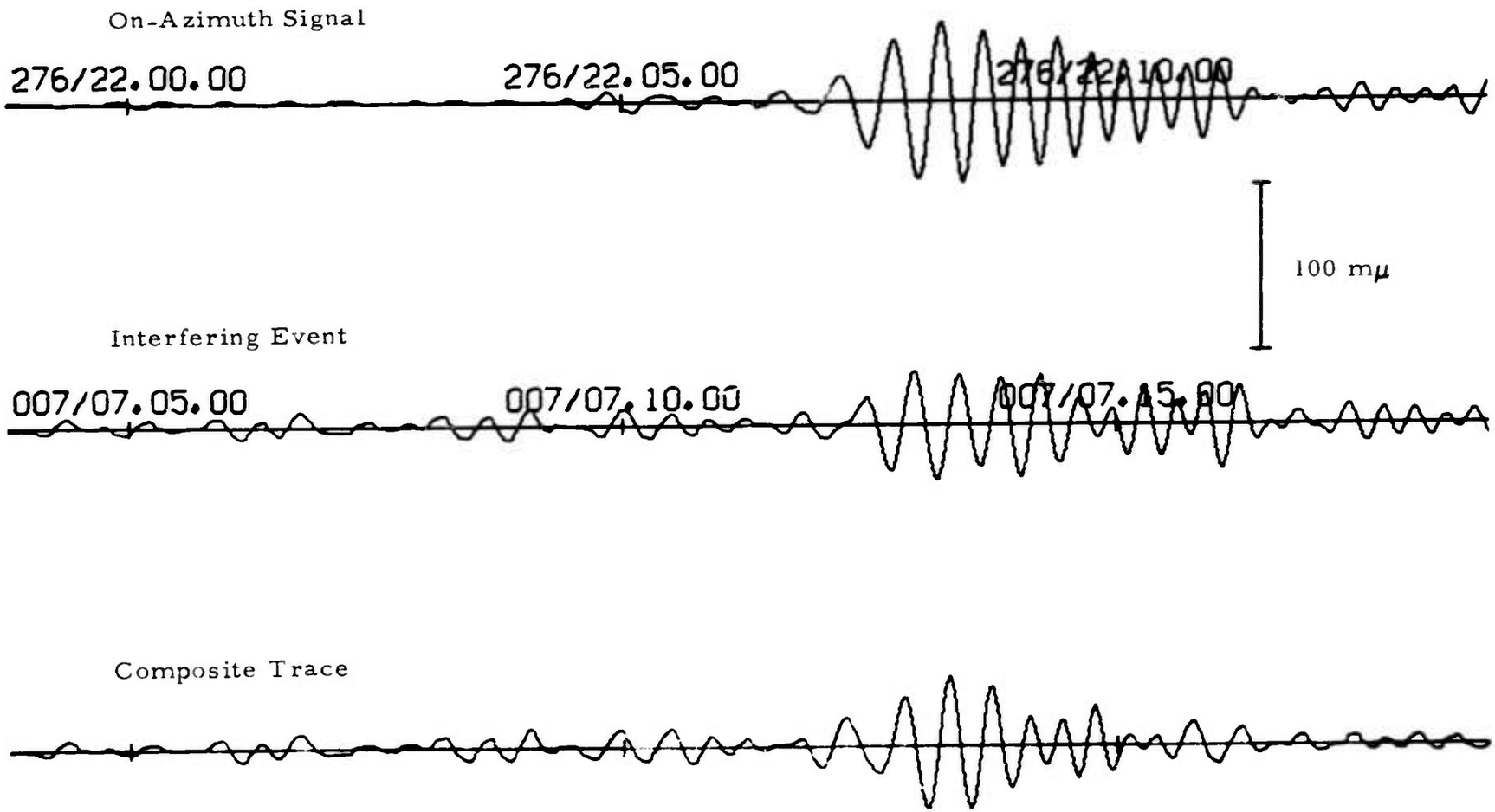

FIGURE III-15

ABF OUTPUT FOR THE MIXED EVENT FROM DAYS 276 AND 007 (μ = 0.2, SIGNAL AZIMUTH 273°, INTERFERING EVENT AZIMUTH 93°, INTERFERING EVENT 18dB ABOVE THE ON-AZIMUTH SIGNAL)

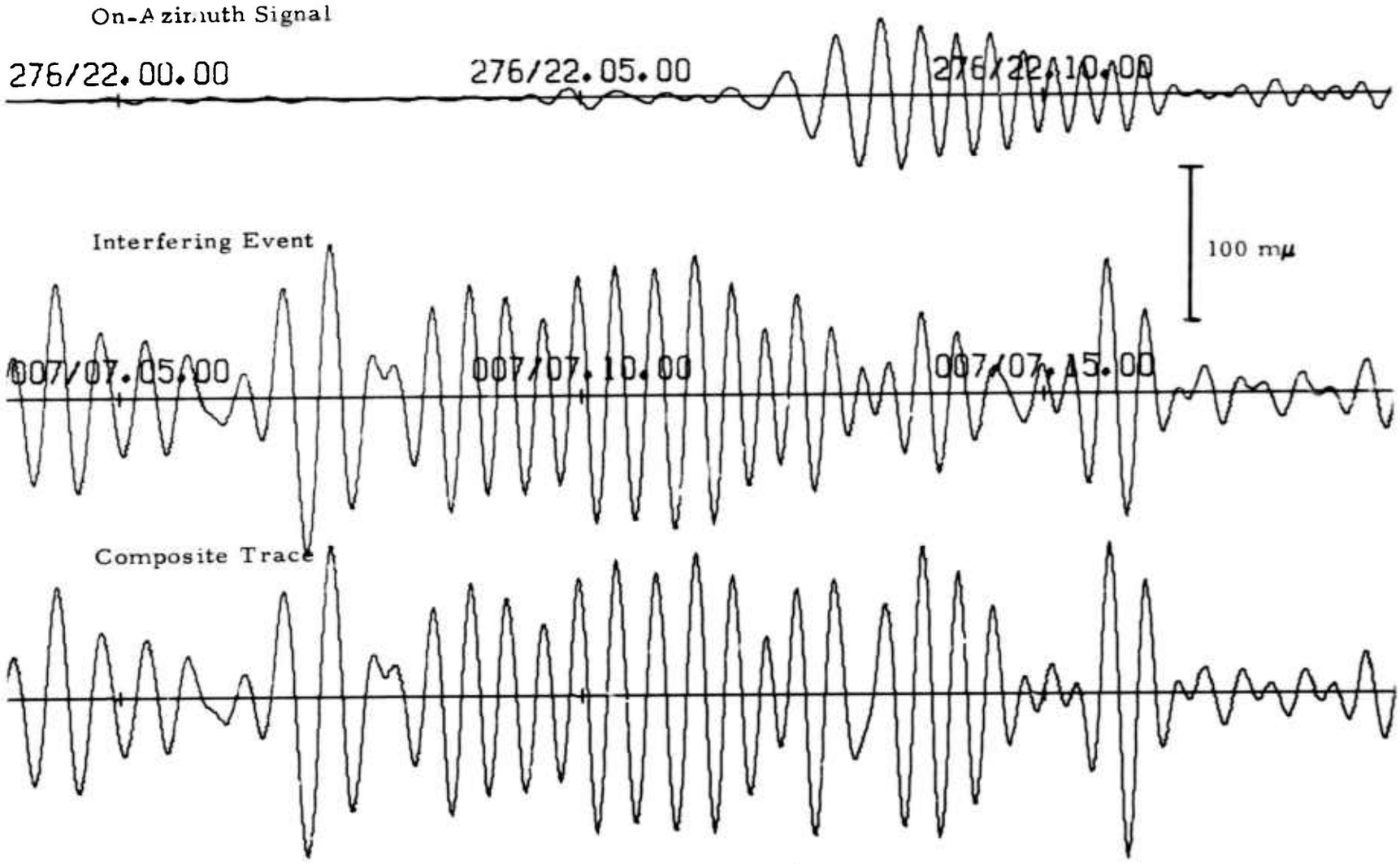

FIGURE III-16

BEAMSTEER OUTPUT FOR THE MIXED EVENT FROM DAYS 276 AND 007
(SIGNAL AZIMUTH 273°, INTERFERING EVENT AZIMUTH 93°, INTERFERING EVENT
24 dB ABOVE THE ON-AZIMUTH SIGNAL)

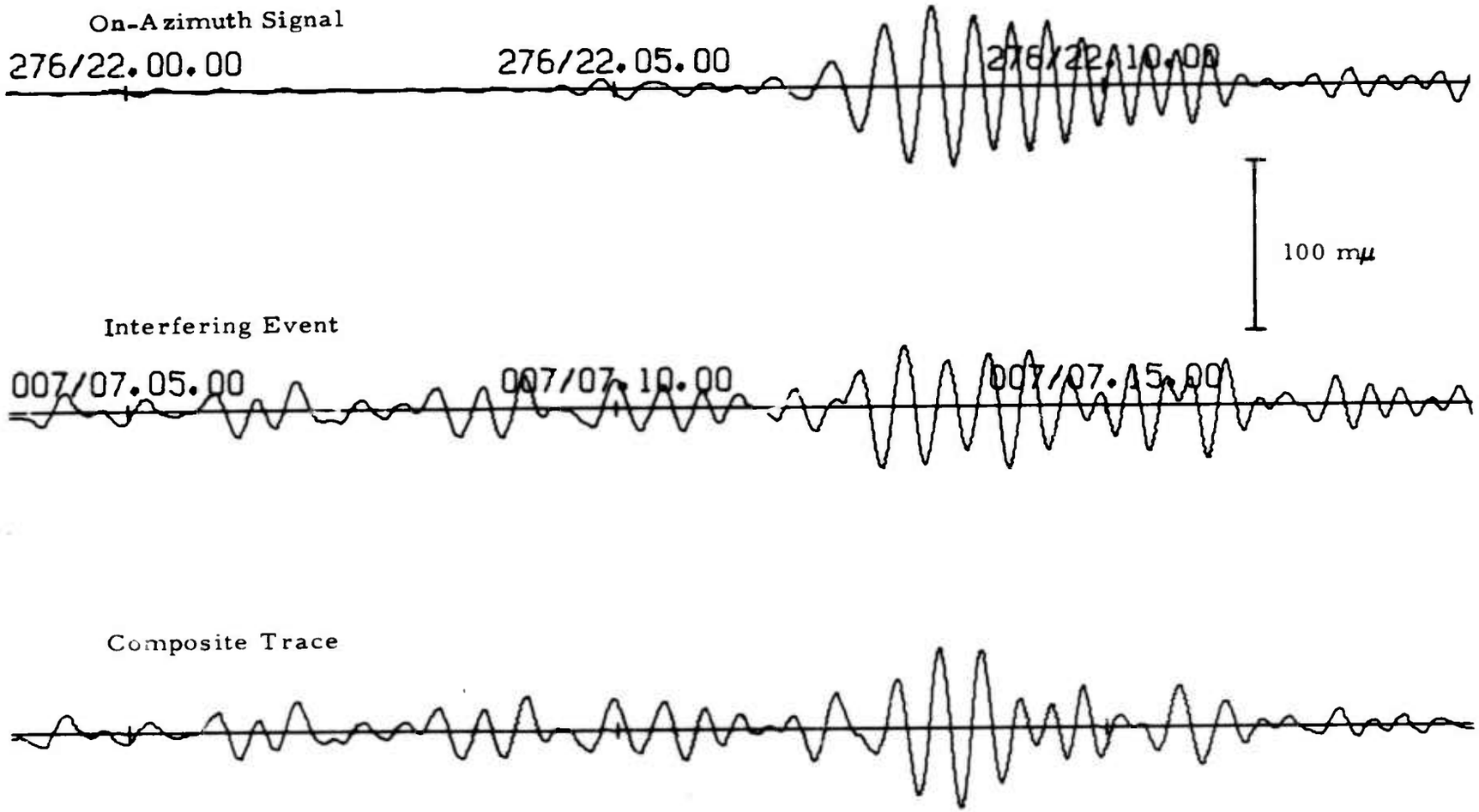

FIGURE III-17

ABF OUTPUT FOR THE MIXED EVENT FROM DAYS 276 AND 007 (μ = 0.2, SIGNAL AZIMUTH 273°, INTERFERING EVENT AZIMUTH 93°, INTERFERING EVENT 24 dB ABOVE THE ON-AZIMUTH SIGNAL)

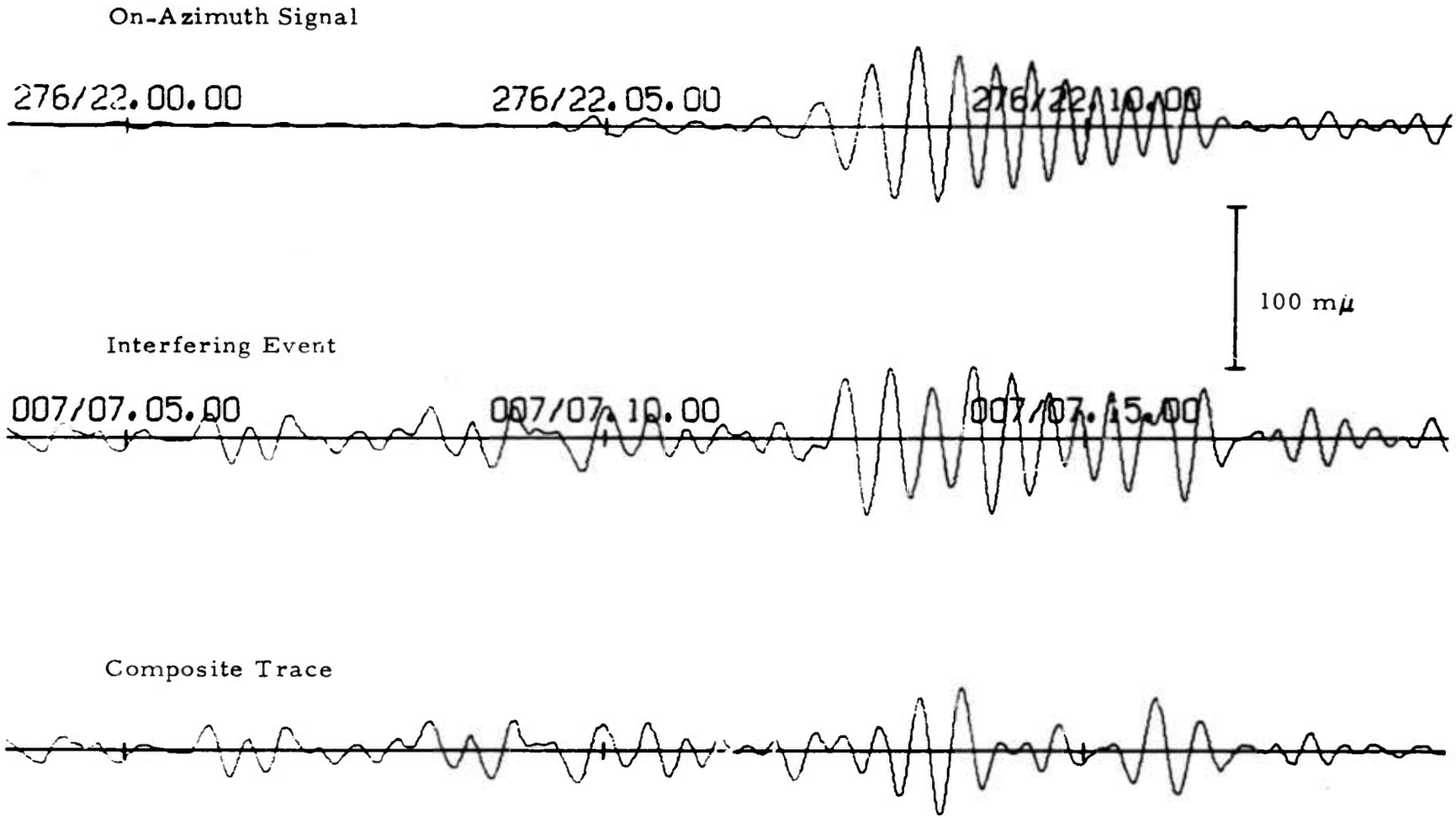

FIGURE III-18

ABF OUTPUT FOR THE MIXED EVENT FROM DAYS 276 AND 007 ($\mu = 0.5$, SIGNAL AZIMUTH 273°, INTERFERING EVENT AZIMUTH 93°, INTERFERING EVENT 30dB ABOVE THE ON-AZIMUTH SIGNAL)

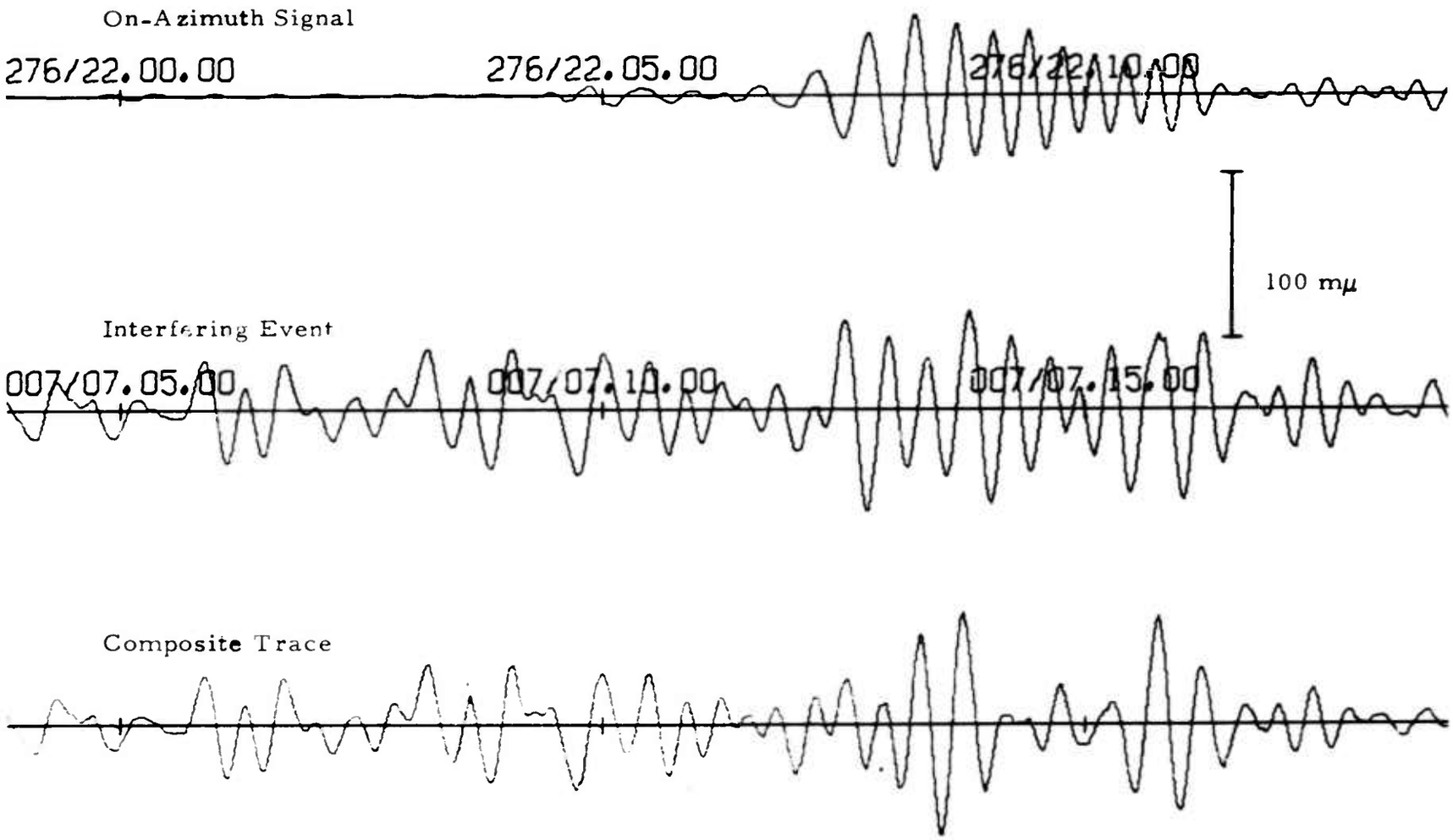

FIGURE III-19

ABF OUTPUT FOR THE MIXED EVENT FROM DAYS 276 AND 007 ($\mu = 0.5$, SIGNAL AZIMUTH 273°, INTERFERING EVENT AZIMUTH 93°, INTERFERING EVENT 36dB ABOVE THE ON-AZIMUTH SIGNAL)

An examination of the ABF outputs at various levels of separation reveals that adaptive beamforming is able to suppress the off-azimuth interfering event by about 33 dB maximum (1.65 magnitude units) before the arrival of the on-azimuth signal. Another interesting result is that the convergence rate corresponding to the greatest amplitude rise increases as the event separation level. At the 30 dB and 36 dB levels, the best convergence rate is 0.5, the same rate at which best signal-to-noise gain is achieved in the presence of background noise alone.

The results of this subsection demonstrate that adaptive processing produces significant detection gains over conventional time-shift-and-sum beamforming for mixed long-period events. The results at different levels of event separation for the interfering event simulated by summing the Kamchatka event from day 276 and the New Guinea event from day 007 indicate a detection gain over beamsteering of more than 12 dB.

C. ADAPTIVE BEAMFORMING APPLIED TO SHORT-PERIOD INTERFERING EVENTS AT KOREA

Some processing of simulated interfering events has been performed with data from the Korean short-period array. The preliminary results depend to a great extent on the frequency response of the prefilter applied to the data used as input to the beamformers. With a 1-to-3-Hz bandpass filter on the data from the individual sites at Korea, adaptive beamforming produced some detection gain over beamsteering. The replacement of that prefilter with a prefilter passing energy between 1 and 2 Hz improved the detection performance of adaptive processing relative to beamsteering. To what extent the improvement is due to the lowered frequency band or to the reduced bandwidth of the prefilter is unknown at this time. Until it is possible to specify an appropriate frequency response for the prefilter applied to the individual sensor outputs, a presentation of results is not likely to provide a reliable indication

of the potential processing gains of adaptive filtering over time-shift-and-sum processing. For this reason, no detailed short-period interfering-event results appear in this report. In future work, a better understanding of the factors influencing short-period adaptive-beamforming performance will be a major topic of investigation.

D. SUMMARY

The results of Subsection B demonstrate, for the two cases where mixed events are simulated by summing two distinct data samples, the adaptive beamforming produces significant detection gains over beamsteering for mixed long-period events. These gains, which occur at high convergence rates, are achieved in a roundabout way. Before the arrival of the on-azimuth signal, attenuation of the off-azimuth interfering event is pronounced. Immediately after the signal arrival, adaptive beamforming is unable, at least for a while, to produce mutual cancellation of the interfering events. The burst of energy on the composite-sample beam at the same time as the arrival of the on-azimuth signal permits a signal detection.

In the first mixed-event simulation, where the Tonga Islands events from days 296 and 335 are summed, the beamsteer response at a 25-second period in the direction of the interfering event is -21 dB, considerably lower than normal. When the off-azimuth event is scaled so that it is 18 dB stronger than the on-azimuth signal at the single-sensor level, the amplitude rise on the composite sample adaptive beam at $\mu = 0.2$ is 6 dB as compared with -2 dB on the corresponding time-shift-and-sum beam.

For the final mixed event, simulated by adding the Kamchatka event from day 276 to the New Guinea event from day 007, the 0.04 Hz beamsteer response in the direction of the off-azimuth event is -15 dB. At an off-azimuth event strength 18 dB above the on-azimuth signal, the amplitude rise on the

composite-sample ABF output is 12 dB, 10 dB higher than the 2 dB rise on the corresponding beamsteer trace. At an event separation level of 12 dB, the amplitude rise on the time-shift-and-sum beam is 8 dB, and the on-azimuth signal is just detectable. At an event separation level of 24 dB, the amplitude rise on the composite-sample adaptive beam at $\mu = 0.2$ is also 8 dB. Thus, in the final mixed-event simulation, adaptive multichannel filtering exhibits the same detection capability as beamsteering when the event separation is 12 dB greater.

In those cases where detection is possible with adaptive processing, the maximum peak-to-peak amplitude on the composite-sample beam provides a reasonably accurate estimate of the on-azimuth signal's maximum peak-to-peak amplitude. The maximum amplitude on the composite-sample adaptive beam is never much more than 2 dB lower than that of the on-azimuth signal.

The results of this section show definite promise in lowering detection thresholds for Rayleigh-wave arrivals when off-azimuth interfering events are present. Time-shift-and-sum processing is seldom able to reduce the detection threshold more than 0.6 to 0.9 magnitude units (12 to 18 dB) below that of a single seismometer. Adaptive beamforming may further reduce the detection threshold more than 0.6 magnitude units (12 dB) below the beamsteer detection threshold. However, these preliminary results span only a limited range of the situations possible. Before a definitive assessment of adaptive-filtering gains over beamsteering can be made for the mixed-event problem, many additional simulations are needed to determine the factors influencing adaptive-beamforming performance in the interfering-event situation. In particular, the azimuthal separation, the waveform similarity, the relative arrival times, and the relative strengths of interfering events need to be studied to determine their effect on the mutual-cancellation phenomenon. For example, when the azimuthal separation is small enough that the off-azimuth events falls within the beamsteer-response main lobe, adaptive-processing performance

relative to beamsteering should improve. In addition, adaptive beamforming needs to be tested on smaller long-period arrays such as the Iran Long-Period Array.

A maximum likelihood adaptive-filtering algorithm produced all of the results in this section. The design goal of this algorithm is to minimize the filter output power subject to unity-response constraints in the beam look direction. Better detection performance might occur with a Wiener filter, where the design goal is to minimize the mean square difference between the filter output and the on-azimuth signal. In any case, the detection gains illustrated in this section furnish a useful baseline from which further attempts at improvement can be made.

SECTION IV
CONCLUSIONS

For unmixed long-period seismic events in the presence of background noise, the new adaptive algorithm

$$A(t+\Delta t) = A + \frac{2\mu X^T A(\bar{X}-X)}{X^T X}$$

produces much higher signal-to-noise ratio improvement than the old adaptive algorithm

$$A(t+\Delta t) = A + \frac{2\mu X^T A(\bar{X}-X)}{(\bar{X}-X)^T(\bar{X}-X)}$$

used in the previous adaptive-beamforming study. The improved results with the new adaptive algorithm are due to a slowing of the effective adaptation rate in the presence of on-azimuth signals. For events with good signal similarity between sites, signal degradation with the new adaptive algorithm is dramatically reduced at high convergence rates. Since noise reduction increases significantly as a function of convergence rate, the best signal-to-noise gains occur at high convergence rates with the new adaptive algorithm. In contrast, severe signal degradation at high convergence rates causes the maximum signal-to-noise gains for the old adaptive algorithm to occur at low convergence rates near $\mu = 0.005$.

When the full ALPA array is used as input to the beamformers instead of a closely-spaced six-channel array, the measured noise reduction relative to beamsteering is lower at all convergence rates. Differences in measured signal degradation, however, are highly variable. At rapid convergence rates,

signal degradation is 2 dB higher for one event and 2 dB lower for another event. In most cases, the estimated signal-to-noise gain relative to beamsteering is less with the full array because of the decreased noise reduction.

The new signal-enhancement prefilter shown in Figure II-71 is a definite improvement over the old prefilter pictured in Figure II-1. Not only is detection gain achieved by the frequency response of the new prefilter, but also the new prefilter's emphasis on the more coherent energy at low frequencies increases ABF noise reduction relative to beamsteering for the full array by more than 3 dB compared with the old prefilter. This additional noise reduction occurs with both 31-point and 15-point adaptive-filter lengths. The difference in noise reduction is only 0.3-0.4 dB for the two adaptive-filter lengths. For two events with good signal similarity, the difference in signal degradation is less than 0.1 dB, so that the loss in estimated signal-to-noise gain is 0.3-0.4 dB with the shorter filter length. On the other hand, signal degradation for one event with poor signal similarity is more than 2.1 dB lower with the 15-point-long adaptive filter, so that the estimated signal-to-noise gain is actually 1.8 dB higher. The significantly diminished computational load probably justifies the use of the shorter adaptive filter length in any on-line implementation of adaptive beamforming.

When vertical-component data from the full ALPA array are passed through the new prefilter, the signal-to-noise gain over beamsteering falls within a 3-to-8 dB range for an adaptive filter length of 15 points per channel. Normally, a 6 dB gain might be expected in this operational mode. Thus adaptive beamforming could conceivably lower the Rayleigh wave detection threshold at ALPA by 0.3 magnitude units.

Off-azimuth events are strongly suppressed by adaptive beamforming at $\mu = 0.5$, the same convergence rate where the maximum gain over beamsteering is achieved for on-azimuth events. Some off-azimuth events are almost totally annihilated. Ordinarily, the strongest off-azimuth events are

attenuated the most. For some signals 30^{o} to 60^{o} from the steer direction, however, considerable energy leaks into the adaptive beams, even for the strongest events. The new prefilter reduces off-azimuth event suppression somewhat. Even with the new prefilter, however, the attenuation of off-azimuth events is considerable. Thus the beam-narrowing capability of adaptive processing can provide greater directivity at ALPA and other similar long-period arrays.

Until now, this section has discussed adaptive-processing results for single seismic events in the presence of background noise. The remainder of this section deals with mixed-event simulations where two data samples, each containing a signal, are summed to create a composite sample containing an interfering event. The mixed-event results in this report are preliminary and extend over only a limited range of the situations possible.

For the two mixed-event simulations where two different data samples are added, adaptive beamforming achieves significant detection gains over beamsteering. These gains, which are realized at high convergence rates, occur in a peculiar way. Before the on-azimuth signal arrival, the off-azimuth interfering event is strongly attenuated. After the signal arrival, adaptive beamforming cannot produce immediate mutual interfering-event cancellation. The energy burst coinciding with the on-azimuth signal arrival permits a signal detection.

In the first mixed event simulation, the time-shift-and-sum beam pattern in the off-azimuth event direction is much lower than normal (-21 dB). The off-azimuth event is 18 dB stronger than the on-azimuth signal at the single sensor level. The beamsteer amplitude rise after signal onset is -2 dB. For the adaptive beam at a 0.2 convergence rate, the amplitude rise is 6 dB. This 8 dB difference occurs despite the excellent beamsteer response toward the off-azimuth event.

The beamsteer response toward the off-azimuth event is -15 dB in the final mixed-event simulation. At a 12 dB event separation level, the beamsteer amplitude rise is 8 dB, and the on-azimuth signal is just detectable. At a 24 dB event separation level, the amplitude rise on the composite-sample adaptive beam at $\mu = 0.2$ is also 8 dB. Thus adaptive beamforming produces the same detection results as beamsteering when the event separation is 12 dB greater.

In those cases where detections are made with adaptive beamforming, the maximum peak-to-peak amplitude on the composite-sample beam furnishes a good estimate of the on-azimuth signal's maximum peak-to-peak amplitude. The maximum amplitude on the composite-sample adaptive beam is never much more than 2 dB lower than that of the on-azimuth signal.

The mixed-event results show definite promise in lowering detection thresholds for Rayleigh-wave arrivals masked by off-azimuth events. Beamsteering seldom reduces the detection threshold more than 0.6 to 0.9 magnitude units (12 to 18 dB) below that of a single seismometer. Adaptive beamforming may further reduce the detection threshold more than 0.6 magnitude units (12 dB) below the beamsteer detection threshold. However, these results are quite limited in scope. Many additional simulations are needed to determine the factors affecting adaptive-processing performance in the mixed-event situation. Furthermore, adaptive beamforming needs to be tried at smaller long-period arrays such as the Iran Long-Period Array.

A Wiener filter, where the design goal is to minimize the mean square difference between the filter output and the on-azimuth signal, might provide better detection performance than the maximum likelihood adaptive algorithm, which sometimes produces mutual cancellation of the interfering events.

SECTION V

REFERENCES

Barnard, T.E., 1973, "Simulated On-Line Adaptive Processing Results Using Alaska Long-Period Array Data," Special Report No. 2, Extended Array Evaluation Program, Texas Instruments Incorporated.

Daniell, T.P., 1968, "Adaptive Estimation with Mutually Correlated Training Samples," Stanford Electronics Laboratories, Stanford, California, Document SEL-68-083. (Technical Report TR 6778-4).

Widrow, B., 1966, "Adaptive Filters I: Fundamentals," Stanford Electronics Laboratories, Stanford, California, Report SEL-66-126 (Technical Report 6764-6).